University of Strathclyde

Department of Naval Architecture, Ocean and Marine Engineering

Modelling the Roughness Effects of Marine Coatings and Biofouling on Ship Frictional Resistance

Yigit Kemal Demirel

A thesis presented in fulfilment of the requirements for the degree of Doctor of Philosophy

2015

This thesis is the result of the author's original research. It has been composed by the author and has not been previously submitted for examination which has led to the award of a degree.

Signed: Date:

Acknowledgements

I have spent the most challenging yet the most important and constructive period of my life during my PhD study in Glasgow. It has been a unique journey from one harbour to another, sometimes with sunshine and sometimes with storms. Without a doubt, to be able to reach the final destination safely has been the biggest prize. I would like to thank everyone who contributed to this journey.

First of all, I would like to express my deepest appreciation to my first supervisor, Professor Osman Turan, for giving me the opportunity to study for a PhD. I would like to thank him not only for supervising and mentoring me, but also for always showing me the bigger picture and for preparing me for the academic environment by giving me additional opportunities and responsibilities which I believe have remarkably improved my academic abilities. If he did not believe in me, it would not have been possible for me to achieve this. I would like to acknowledge the valuable support and help of my second supervisor, Professor Atilla Incecik. I have always been inspired by his wisdom and energy. He has been not only a second supervisor but also a very good friend to me.

I would like to express my appreciation to Professor Michael Schultz of the US Naval Academy for helping me from time to time via e-mail. I am indebted to him for his advice and support during my studies. His support shed light on some of the problems I experienced. Additionally, I would like to thank my colleague Dr. Mahdi Khorasanchi for his support on aspects of the CFD work. I would like to thank my friend Holly Yu for helping me with the final proofreading of this thesis and my papers.

Moreover, I gratefully acknowledge that the research presented in this thesis was partially generated as part of the EU funded FP7 project FOUL-X-SPEL (Environmentally Friendly Antifouling Technology to Optimise the Energy Efficiency of Ships, Project number 285552, FP7-SST-2011-RTD-1). Thanks are also due to project partners and funding from the EU FP7 FOUL-X-SPEL Project. I would also like to thank the University of Strathclyde Faculty of Engineering for

giving a PhD Scholarship to support my PhD research and for provision of the ARCHIE-WeSt high performance computing facilities. The CFD results were obtained using the EPSRC funded ARCHIE-WeSt High Performance Computer (www.archie-west.ac.uk). EPSRC grant no. EP/K000586/1.

Many thanks go to our department's research secretary, Mrs. Thelma Will, for genuinely assisting and supporting me with my administrative problems. Similarly, thanks are due to the staff at the Kelvin Hydrodynamics Laboratory of the University of Strathclyde, who made my experiments possible.

I would like to thank my colleagues and friends for their continuous support during my days in Glasgow, in alphabetical order: Dr. Charlotte Banks, Chris Gilmore, Elif Oguz, Haipeng Liu, Konstantinos Dikis, Kurt Mizzi, Marine Gilmore, Matthias Maasch, Dr. Paula Kellett, Saishuai Dai, S. Anil Gunbeyaz, Dr. Serkan Turkmen and Volkan Arslan. I would like to thank my colleague, my flatmate, my best friend and my fellow PhD student, Dr. Tahsin Tezdogan, for his support and encouragement during my PhD research. I also gratefully acknowledge his great cooking ability which has made life much easier for me. I am also very grateful to his mother, Gulsum Tezdogan Hanimefendi, for taking care of us by visiting us in Glasgow.

I would like to thank my family members one by one for always believing in me and supporting me: my father Ahmet Yener Demirel, my mother Huriye Acar, my grandmother Makbule Demirel and my aunt Hurriyet Serpil Demirel. Many thanks are also due to my cousin and friend Mert Agacan and my beloved friend Aylin Sakar for their support and for turning my visits to Istanbul into fantastic holidays.

Last, but certainly not least, I would like to thank the very understanding and supportive Tugce Kalaycioglu for all her encouragement and for being my motive force, for listening to details of my successes and difficulties, and for bringing joy to my life. I hope she can be awarded her PhD degree soon after me.

Contents

List of Figures

List of Tables

Abstract

The answers to the question, *"How might the roughness of coatings and biofouling be related to full-scale ship resistance and powering?"* were sought in this research, and novel contributions were made to the state-of-the-art knowledge.

The current techniques used for predicting the roughness effects of marine coatings and biofouling on the resistance of full-scale ships rely on assumptions from similarity law scaling and boundary layer theory. Although this is a reasonable method, it may be difficult for less experienced users to carry out such an analysis since similarity law scaling includes several numerical procedures which may cause numerical errors and requires deep knowledge of the subject. It would also be beneficial to propose alternative methods with which to accurately predict these effects using fully-nonlinear Computational Fluid Dynamics (CFD) models, since current technological advances offer computational power which can be utilised to perform simulations based on Reynolds-Averaged Navier-Stokes (RANS) approaches.

This work mainly aims to model the roughness effects of marine coatings and biofouling on ship resistance and powering, and to develop and propose alternative models for this purpose.

Firstly, drag characterisation of several marine coatings, including the novel paints developed within the EU FP7 FOUL-X-SPEL Project, as well as control surfaces, was made through towing tests of flat plates coated with such coatings. An in-house code based on the similarity law scaling was then developed. This was used to assess the roughness effects of different marine coatings, including FOUL-X-SPEL Paints, and different fouling conditions on the frictional resistances of flat plates of ship lengths. Added resistance diagrams were generated using these predictions.

Following this, two separate CFD models were developed and proposed for the prediction of the roughness effects of marine coatings and biofouling using flat plates

of both model-scale and full-scale. These models were validated against an experiment and compared with the similarity law scaling, respectively.

Afterwards, unsteady RANS CFD simulations of the roughness effects of marine coatings and biofouling on the full-scale KCS hull appended with a rudder were performed, using the roughness models proposed earlier, in order to arrive at a final conclusion.

Finally, some discussions and conclusions on the outcomes of the work performed within this thesis are presented.

This author believes that this study has shown the applicability of the CFD-based method to investigate the roughness effects of marine coatings and biofouling on ship frictional resistance. The CFD methods and added resistance diagrams proposed in this thesis stand as practical prediction methods for both academia and industry.

1 Introduction

"Models now in tanks we tow.
All of that to Froude we owe.
Will computers, fast and new,
Make us alter Euler's view?"

Marshall Tulin

1.1 Introduction

This chapter defines the general perspectives of the subjects covered in this thesis, presents the motivations behind this work, details the ultimate aims and specific objectives of the research and outlines the structure of this thesis.

1.2 General Perspectives

Shipping has been, and still is, one of the most important methods of transport, with more reliance and importance now being placed on this mode of transport as a consequence of advances in shipping technology and the ability of ships to store and transport increasing capacities of goods. However, these improvements bring some problems to the industry due to an increase in fuel consumption, which is detrimental to the environment and which erodes company revenues. Although other forms of fuel power exist, such as wind energy and solar power, carbon-based fuel is currently the only way for ships to run effectively. For this reason, minimising fuel consumption is crucial for shipping companies. Such companies have therefore attempted to determine the optimum operation and maintenance approaches to either decrease the cost of operations or to increase the profit of the company. The release of harmful gases due to the use of carbon-based fuel is another reason that shipping companies should aim to reduce the fuel consumption of their ships. Some regulations, such as the Energy Efficiency Design Index (EEDI) (IMO, 2014) and the Ship Energy Efficiency Management Plan (SEEMP) (IMO, 2012), and recommended practices such as the Energy Efficiency Operational Indicator (EEOI) (IMO, 2009a)

have been implemented in recent times to limit the quantities of harmful gases that are released into the environment as a result of the fuel consumed by ships.

The importance of being energy efficient and the widespread understanding of the detrimental impact which carbon dioxide emissions have on the environment has been brought to prominence since the Kyoto Protocol treaty. The Kyoto Protocol, which was set up to try to reduce emissions of the six Greenhouse Gases (GHG), was negotiated in December 1997 in Japan and legally ratified by the United Nations and entered into force on 16th February 2005 (UNFCCC). In this protocol, gas sources are categorised in different industrial sectors, one of which is transportation. Although shipping is marginally more environmentally friendly than other forms of transportation, such as aviation and land, it was reported that ships released 870 million tons of CO_2 in 2007, which is equivalent to 2.7% of the total CO_2 emissions that year (IMO, 2009b). The International Maritime Organization (IMO) has therefore been forced, due in part to an increase in public awareness, to devise and implement energy efficiency and GHG regulations. Consequently the marine industry needs to find solutions to reduce GHG and achieve more energy efficient shipping. There is a plethora of methods capable of making ships more energy efficient and reducing their CO_2 emissions. However, focusing specifically on ship voyage operations, ship maintenance and the implementation of new technologies have been highlighted as being the most effective ways of reducing CO_2 emissions and increasing energy efficiency. It is therefore important that the industry investigates solutions for how to reduce fuel consumption and carbon gas emissions by implementing new technologies such as new antifouling coatings. Carrying out an energy audit is therefore vital, as it serves as a platform in order to achieve optimum performance, an effective reduction in fuel consumption and associated future economic benefits.

Hull resistance is of paramount importance to ships since it directly affects their speed, power requirements and fuel consumption. For this reason, reducing a ship's resistance is a fundamental requirement for naval architects, in order to benefit ship owners. Ship resistance can be classified into two types; frictional resistance and residuary resistance. Frictional resistance can account for up to 80-85% of a ship's

total resistance, particularly for merchant ships sailing at low speeds (van Manen and van Oossanen, 1988). As 95% of the world's cargo is transported by sea (RAEng, 2013), a means of reducing the frictional resistance of ships would dramatically reduce their fuel consumption, leading to reduced carbon emissions worldwide. The best method to reduce frictional resistance is to apply a treatment to a ship's hull, to minimise its physical and biological roughness. Physical roughness can be minimised by applying some preventative measures, but biological roughness (fouling) is more difficult to control.

Marine biofouling is an increasing problem from both economic and environmental points of view in terms of increased resistance, increased fuel consumption, increased GHG emissions and transportation of harmful non-indigenous species (NIS). It should be kept in mind that even a small amount of fouling may lead to a significant increase in fuel consumption. In particular, hard shelled fouling can cause a considerable rise in ship frictional resistance, and hence a ship's fuel consumption. Hard shelled barnacles can also deteriorate the paint and cause other problems such as corrosion. It should be noted that the impact of fouling on ship performance is greatly dependent on the type and coverage of fouling (Schultz, 2007).

Transportation of invasive aquatic species is another important problem which occurs due to fouling. Some fouling species remain alive for a long time; thereby, they may be transferred to another ecosystem. These invasive species can be very harmful in terms of ecological and economic aspects. They may cause extinction of some species and may harm biodiversity and/or transport and dissipate various diseases (Okay, 2004).

Due to its negative effects on ship efficiency and the marine environment, it is very desirable to mitigate the accumulation of biofouling on ship hulls. Marine coatings are prevalently used to smooth the surfaces of hulls. An ideal marine coating should be smooth enough to improve the surface properties of a hull in the as applied condition and should be effective against marine biofouling which occurs over time. These two aspects markedly affect the frictional resistance and hence fuel consumption of a ship.

As can be understood from the current situation described above, two main areas of interest are of vital importance from an end-user and a naval architect's point of view, with regards to energy saving. These areas of interest concern being able to predict:

i. the as applied drag performances of coatings on ship hulls
ii. the time-dependent drag performances of coatings on ship hulls due to the growth of biofouling

The as applied drag performances of coatings on ship hulls are a direct translation of the roughness effects of such coatings on the ship frictional resistance. The time-dependent drag performance is directly related to the roughness effects of biofouling, which occurs over time, on the ship frictional resistance. The majority of the experimental studies in the literature focus on the effects of marine coatings and biofouling on the turbulent boundary layer and/or on the skin friction of lab-scale plates (e.g. Ünal et al. (2012), Candries and Atlar (2004), Schultz (2000)). These fundamental studies and the information they provide is of great importance for a hydrodynamicist or a scientist in order to gain a deeper understanding of the subject. However, from a naval architect or a ship owner's point of view, though this knowledge is required, it alone is not sufficient for them to be able to assess the potential added value of the new coating towards reducing a ship's fuel consumption and GHG emissions. Before deciding whether to apply a new coating system or technology to a new ship, or to retrofit an existing ship, a life cycle assessment of the ship in question both with and without the new technology must be performed. For this reason, the effects of such coatings and biofouling on the frictional resistance of full-scale ships must also be investigated, rather than only investigating these effects on the boundary layer and skin frictions of lab-scale plates. Unfortunately, little effort has been made to develop a tool or methodology with which to accurately predict the roughness effects of marine coatings and biofouling on full-scale ships. The available theoretical prediction methods mainly concentrate on the uniform sand roughness effect on the skin friction, rather than real engineering surfaces such as marine coatings and biofouling. Existing numerical prediction methods (e.g. Granville (1958), Grigson (1985a)) use boundary layer theory and are only able to

predict the skin friction of flat plates if some assumptions are made. Full-scale sea trial measurements and assessments (e.g. Corbett et al. (2011), Munk (2006)) regarding the effect of fouling on fuel consumption can only provide some indications for a specific operational condition of a ship, and they include significant uncertainties.

Having outlined the present situation, it would be timely to locate the present research within this general framework. As stated earlier, a major challenge is to relate technologies such as antifouling coatings, and the effect of biofouling, to full-scale ship resistance, in order to evaluate their effects on energy efficiency and hence CO_2 emissions. While retrofitting existing ships with new antifouling paints will improve their energy efficiency, it is equally important to model and predict the potential effects of biofouling on ship resistance and to demonstrate the importance of the mitigation of such effects by performing scientific research. However, at present, no complete method exists to predict the roughness effects of antifouling coatings and biofouling on a ship's frictional resistance. The ultimate aim of this study is therefore to fill this gap by developing a novel model for the prediction of the roughness effects of marine coatings and biofouling on ship frictional resistance. Each main chapter presents a novel study to fill the gaps in the literature and hence makes state-of-the-art contributions to the field.

This work focuses on the determination of the drag characteristics of several coatings and the predictions of the effects of a range of coatings and biofouling conditions on ship frictional resistance. The overall (towed plate) method was used to obtain the drag characteristics of coatings. Two different prediction methods were used in this research: similarity law scaling and Computational Fluid Dynamics (CFD)-based Unsteady Reynolds-Averaged Navier-Stokes (URANS) methods.

1.3 Motivations behind this Work

- It was recommended that researchers should generate an extensive database of the roughness functions of different antifouling coatings and biofouling (ITTC, 2011b). This is because the roughness functions of such coatings must be known in order to predict the roughness effect that antifouling coatings

have on ship resistance. The roughness functions of antifouling coatings in as applied conditions can be evaluated by means of an experimental determination. Therefore, the drag performances of newly developed antifouling coatings, such as the ones developed within the FOUL-X-SPEL Project, can only be assessed through the experimental determination of roughness functions (Chapter 4).

- To the best of this author's knowledge, no experimental study exists which compares the drag performances of different antifouling surfaces with that of an uncoated ship hull condition, rather than only a smooth surface (Chapter 4).

- The ITTC (2011b) recommends the use of a roughness allowance formula as detailed in the 19th ITTC (1990), as this is currently the best option available. However, the ITTC also warns of the possible inaccuracy of the formula and therefore recommends researchers to develop new formulae or methods, using experimental data, for the prediction of the effects of coatings and biofouling on ship resistance (Chapter 5, Chapter 6 and Chapter 7).

- Although a similarity law scaling procedure is a suitable technique with which to predict the effects of coatings and biofouling on frictional resistance, it may be difficult for less experienced users to carry out such an analysis since it includes numerical methods and requires a deep knowledge of the subject. Goal-based added resistance diagrams for predicting the effect of biofouling on ship frictional resistance would therefore be of great benefit. To the best of this author's knowledge, no specific added resistance diagram exists to predict the roughness effect of marine coatings and biofouling on ship frictional resistance (Chapter 5).

- The use of marine antifouling coatings is a common method used to smooth hull surfaces to reduce the frictional resistance and fuel consumption of a ship. However, such coatings will have an initial surface roughness which

will affect a ship's frictional resistance. A means of assessing the effect of such a coating on frictional resistance would therefore be of great benefit. However, at present, there is no accurate method available to predict the effect of ship roughness due to the use of antifouling coatings (ITTC, 2008b, 2011b). To the best of this author's knowledge, no specific CFD model exists to predict the effects of a marine antifouling coating's roughness on flow and frictional resistance (Chapter 6).

- While improving the energy efficiency of existing ships retrofitted with new antifouling paints, it is equally important to accurately model the potential effects of biofouling on ship resistance and to demonstrate the importance of the mitigation of such effects by carrying out scientific research. However, at present, there is no complete method available to predict the effect of biofouling on ship frictional resistance. Current numerical prediction methods are limited by the use of boundary layer similarity law analysis. Although this is a reasonable method, it is still worth investigating the phenomenon by means of CFD. To the best of this author's knowledge, no specific CFD model exists to predict the roughness effect of biofouling on ship frictional resistance (Chapter 7).

- It is critical to be able to relate the roughness effects of marine coatings and biofouling on the total resistance and effective power of full-scale 3D ship hulls. Current methods can only predict such effects on the frictional resistance of flat plates representing ships, or take these effects into consideration using 3-dimensional boundary layer theory. Although these are suitable methods, it would be beneficial to investigate the phenomenon by means of CFD. By using CFD, it is also possible to combine roughness effects with the nonlinear effects such as spatial distribution of fouling, ship motions in waves, and propulsion, on ship resistance. In addition, the effect of surface roughness on the pressure drag of a hull could also be taken into consideration. To the best of this author's knowledge, to date no specific

unsteady RANS CFD simulation of the roughness effects of marine coatings and biofouling on full-scale 3D hulls has been performed (Chapter 8).

1.4 Research Aims and Objectives

The main aim of this PhD thesis is to model the roughness effects of marine coatings and biofouling on ship frictional resistance. Specific objectives are listed below, with each detailing the novelty of each chapter based on the motivations given in the previous section:

- To review the literature on modelling the roughness effects of marine coatings and biofouling on frictional resistance and to define the gaps in the literature.

- To determine the roughness functions of several marine coatings, including the new FOUL-X-SPEL paints and control surfaces, using Granville's (1987) overall method.

- To compare the resistance characteristics of such coatings with an uncoated ship hull condition, rather than with only a smooth surface.

- To predict the effects of FOUL-X-SPEL paints on full-scale ship frictional resistance.

- To develop an in-house code based on the similarity law scaling for the prediction of the roughness effect on skin friction.

- To generate added resistance diagrams to predict the increases in the frictional resistance coefficients and effective powers of ships due to the use of marine coatings and biofouling conditions.

- To investigate and show the applicability of a CFD method for the simulation of surface roughness by means of employing modified wall-functions.

- To develop and propose a CFD model which enables the prediction of the effect of antifouling coatings on frictional resistance.

- To outline details of CFD simulations of resistance tests on coated plates in a towing tank.

- To develop and propose a CFD model which enables the prediction of the effect of biofouling on frictional resistance.

- To investigate the applicability of the wall function approach of CFD to simulate the surface roughness on ship hulls, rather than on flat plates, and to show that it is a suitable method with which to predict the roughness effects of marine coatings and biofouling on full-scale 3D ships.

- To perform unsteady RANS CFD simulations of the roughness effects of marine coatings and biofouling on the full-scale KCS hull, and hence investigate such effects on the total resistance and effective power of the KCS.

1.5 Structure of this Thesis

The structure of this thesis is summarised below:

- Chapter 2 presents brief theoretical information about the fundamentals of the subjects covered and presents a literature review from a critical point of view. The gaps in the literature are also clearly listed.

- Chapter 3 presents the general methodology followed in this thesis.

- Chapter 4 presents an experimental determination of the roughness functions of several marine coatings including newly developed, novel FOUL-X-SPEL paints. Details of the towing tests of flat plates coated with different coatings

and two control surfaces are given and the drag coefficients and roughness function values of each surface are presented along with the experimental uncertainty limits.

- Chapter 5 proposes added resistance diagrams for the predictions of the increases in the frictional resistance coefficients and effective powers of ships due to the use of different antifouling coatings and biofouling. Details of the developed in-house prediction code based on the similarity law scaling are provided. The effects of FOUL-X-SPEL paints and a range of coating and fouling conditions on the ship frictional resistance are predicted and presented. The added resistance diagrams are then plotted using the predictions. Finally, added resistances and powering penalties of the Kriso Container Ship (KCS) and an LNG carrier induced by different surface fouling conditions are estimated using the generated diagrams.

- Chapter 6 proposes a Computational Fluid Dynamics (CFD) model which enables the prediction of the effect of antifouling coatings on frictional resistance. It also outlines details of CFD simulations of resistance tests on coated plates in a towing tank. The validity of the model is demonstrated by comparing the results with the experimental data. The effects of antifouling coatings on the frictional resistance of a flat plate representing a tanker are predicted using the validated CFD model.

- Chapter 7 proposes a Computational Fluid Dynamics (CFD) model which enables the prediction of the effect of biofouling on frictional resistance. The effects of a range of representative coating and biofouling conditions on the frictional resistance of flat plates representing a tanker and the KCS are predicted for varying service speeds using the proposed CFD model. The results of the present study are then compared with the results obtained in Chapter 5. Finally, the increases in the effective power of the KCS are estimated.

- Chapter 8 presents unsteady RANS CFD simulations of the roughness effects of marine coatings and biofouling on the full-scale KCS hull. It also predicts the increase in frictional and total drag, and effective power due to different hull surface conditions at design and slow steaming speeds, using the CFD model proposed in Chapter 7. The resulting frictional resistance values are then compared with those of flat plates, representing the KCS, computed in Chapters 5 and 7.

- Chapter 9 presents a discussion on the outcomes of this thesis and on its state-of-the-art contributions, demonstrating how well the aims and objectives were achieved. The difficulties experienced are discussed clearly.

- Chapter 10 presents the concluding remarks. It also outlines some recommendations for future avenues of research.

1.6 Chapter Summary

The general perspectives, the motivations behind this work, the aims and objectives, and the structure of this thesis have all been presented in this chapter.

2 Critical Review

2.1 Introduction

When carrying out a study to make a contribution to the state-of-the art, it is equally important to understand the previous research into the dedicated subject and to be aware of the current state-of-the art. An extensive literature survey was therefore performed and the important cornerstones of the subject are provided in this chapter, from a critical point of view, in order to determine the literature gaps and research motivations. It should be noted that only the specific subjects which are required to assess and understand the topic are covered in this chapter. This chapter is organised as follows:

In Section 2.2, the problem of marine biofouling is introduced, and the available marine coatings to control and mitigate biofouling are briefly presented. In addition, a comparison is made between the Self-polishing copolymers (SPC) and foul-release coatings (FR).

In Section 2.3, brief theoretical information is given about the velocity profile in the turbulent boundary layer and about roughness effects on the velocity profile in the turbulent boundary layer, respectively. This is more of a review section, rather than a critical review, since this section aims to present the information and background used in the present study. Having said that, any important points are discussed in detail and conflicting studies are included in order to emphasise the main assumptions made in this study.

A historical overview of the research into ship frictional resistance with a focus on hull roughness is presented in Section 2.4. The historical stages of the development of skin friction prediction formulae are presented, together with the important cornerstones of the roughness allowance calculation methods within the framework of the work performed by the ITTC. Section 2.4 clearly highlights the current state-of-the-art and presents the motivations behind the work carried out in this study.

In Section 2.5, investigations into the effects of hull roughness on frictional resistance are presented. This section also includes studies investigating the rough wall turbulent boundary layer within a narrow framework of real engineering surfaces, especially coatings and biofouling. Efforts to predict the effects of coating roughness and biofouling on the frictional resistance of model-scale plates and full-scale plates/ships are also surveyed.

In Section 2.6, different methods for the determination of roughness functions are presented. The method used in this study is presented in more detail alongside discussions made in the literature. The rationale for the selection of the current method is clearly detailed, showing examples from the literature.

In Section 2.7, the concluding remarks of this critical review are listed such that the gaps in the literature are clearly defined.

2.2 Marine Coatings to Prevent Biofouling

The bio-accumulation of marine organisms on the surfaces of submerged, or semi-submerged, natural or artificial objects is termed marine biofouling (Lewis, 1998). This infestation is inevitable because the marine environment has a unique bio-diversity. It is estimated that the number of types of marine organisms that cause biofouling may exceed 2500 (Anderson et al., 2003). Some species have a tendency to attach on surfaces, settle and then grow on them. These marine organisms are termed marine foulers and may be mainly classified into micro and macro foulers as shown in Figure 2.1 (Taylan, 2010).

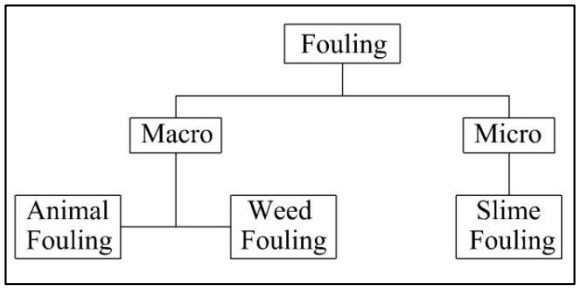

Figure 2.1: Fouling organisms, adapted from Taylan (2010)

A detailed classification of marine foulers is demonstrated in Figure 2.2 (Atlar, 2008).

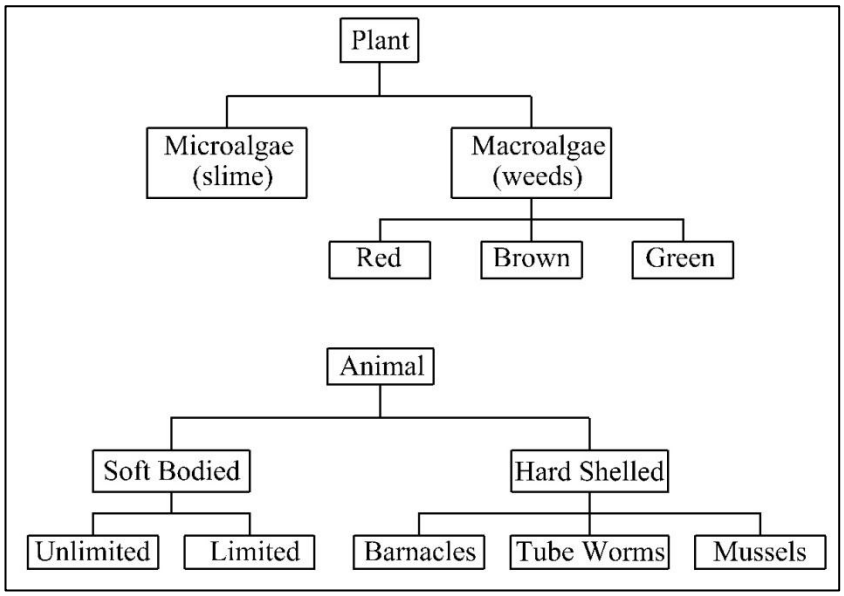

Figure 2.2: Classification of marine foulers, adapted from Atlar (2008)

Fouling begins to occur immediately after a ship is immersed in water, and will continue to occur throughout a ship's life at sea until a cleaning process is performed. Fouling is particularly likely to occur when a ship is stationary, such as when it is in a port. Fouling builds up more quickly in tropical waters and it also varies depending on a ship's operational geographical area (Candries et al., 2003a). The level of fouling depends on several factors, including the length of time spent at sea, the water temperature, the geographical location of the ship, surface conditions and the salinity of the sea. The longer the ship's immersion time, the greater the level of fouling. Such fouling is responsible for a dramatic increase in a ship's frictional resistance.

Fouling causes surface roughness, resulting in an increase in a ship's frictional resistance and fuel consumption (Kempf, 1937). Milne (1990) stated that the fuel consumption may increase by up to 40%, unless any precautions are taken to prevent fouling. According to Taylan (2010), the increase in resistance due to microorganism fouling is around 1-2%, whereas an accumulation of hard shelled organisms may cause an increase in resistance of up to 40%. Schultz (2007) investigated the effect of fouling on the required shaft power for a frigate at a speed of 15 knots. He found that the presence of slime alone caused a 21% increase in shaft power, compared to an otherwise identical slime-free frigate, whereas heavy calcareous fouling led to an 86% increase in shaft power requirements.

Fouling mitigation is therefore very desirable from a practical point of view. Fouling has been a challenging problem to solve for many years and efforts to find an effective protection method began long ago. The conventional antifouling method involves the application of antifouling paints, which contain toxic chemicals, on ships' hulls. These toxic chemicals, which are termed biocides, are gradually released into seawater due to exposure to water, and consequently a toxic layer is formed around the hull. This layer prevents fouling species from attaching to the hull. Several different methods have been trialled; it even seems that the toxic antifouling principle was in use as early as the 5th century BC. An Aramaic papyrus details the antifouling strategy of those days (ABS, 2011):

> *"...the arsenic and sulfur have been well mixed with the Chian oil that you brought back on your last voyage, and the mixture evenly applied to the vessel's sides, that she may speed through the blue waters freely and without impediment.''*

Christopher Columbus also suffered from fouling problems, with his fouling prevention method as follows (ABS, 2011):

> *"All ships' bottoms were covered with a mixture of tallow and pitch in the hope of discouraging barnacles and teredos, and every few months a vessel had to be hove-down and graved on some convenient beach. This was done by careening her alternately on each side, cleaning off the marine growth, re-pitching the bottom and paying the seams."*

Antifouling strategies have changed over time due to new technologies and legislations. The historical development of antifouling strategies is detailed in Table 2.1 (Dafforn et al., 2011).

Table 2.1: Historical development of antifouling strategies, adapted from Dafforn et al. (2011)

Timeline	Major events
1500-300 BC	Use of lead and copper sheets on wooden vessels
1800-1900s	Heavy metals (copper, arsenic, mercury) incorporated into coatings
1800s-present	Continued use of copper in AF coatings
1960s	Development of TBT conventional coatings
1974	Oyster farmers report abnormal shell growth
1977	First foul release AF patent
1980s	Development of TBT SPC coatings allowed control of biocide release rates
1980s	TBT linked to shell abnormalities in oysters (Crassostrea gigas) and imposex in dogwhelks (Nucella lapillus)
1987-90	TBT coatings prohibited on vessels <25 m in France, UK, USA, Canada, Australia, EU, NZ and Japan
1990s–present	Copper release rate restrictions introduced in Denmark and considered elsewhere e.g. California, USA
2000s	Research into environmentally friendly AF alternatives increases
2001	International Maritime Organization (IMO) adopts "AFS Convention" to eliminate TBT from AF coatings from vessels through: 2003 – prohibition of further application of TBT 2008 – prohibition of active TBT presence
2008	IMO "AFS Convention" comes into force

The most remarkable success against marine biofouling can be attributed to tributyltin (TBT) based antifouling paints. Self-polishing copolymer (SPC) TBT systems had been widely used from the 1960's until the 2000's due to their unbeatable antifouling ability. Unfortunately, research demonstrated that TBT exposure causes the malformation of oyster shells (Alzieu et al., 1986) and imposex of gastropod molluscs (Gibbs and Bryan, 1986). Moreover, TBT compounds persist in water, show toxic effects to marine organisms even with a low concentration, and they may accumulate in marine organisms and hence enter the food chain (Okay, 2004). As a consequence, IMO banned the application of antifouling coatings which contain TBT in 2003, and banned the operation of ships coated with TBT paints in 2008 (IMO (2001), Champ (2003)). Due to this ban, TBT has been replaced with other toxic biocides. These chemical systems release toxic compounds to the marine environment just like TBT, whereas they are not as effective as TBT.

Today, several types of coatings are used to mitigate fouling. They can be classified into two main categories based on their compositions; namely, biocidal and non-biocidal coatings. Biocidal coatings can be listed as Controlled Depletion Polymer (CDP), Self-Polishing Copolymer (SPC) and Hybrid SPC. Non-biocidal coatings are foul-release coatings (FR), which are also called non-stick coatings.

CDPs use a hydration process and release biocides into the marine environment. They are used for vessels which have short drydock intervals and are preferred for ships operating in low fouling regions (Atlar, 2008). Their effectiveness is said to be up to 3 years (Van Rompay, 2012). Self-Polishing Copolymers (SPC) have good initial hydrodynamic performance owing to their smooth surfaces and have better antifouling abilities due to controlled release of the biocide via hydrolysis. They are preferred for vessels which have longer drydock intervals (Taylan, 2010). SPCs can remain effective for up to 5 years (Van Rompay, 2012). Hybrid SPCs' biocide release method may be regarded as a hybrid of hydrolysis and hydration. The life span of Hybrid SPCs is between 3 and 5 years (Taylan, 2010). However, all biocidal antifouling coatings are under scrutiny regarding their toxic effects; hence, they all are affected by legislative issues and may still be banned in the near future.

Foul release (FR) coatings, on the other hand, prevent the attachment of marine species on hulls owing to their physical surface properties (Wahl, 1989), which act like a non-stick coating and prevent the build-up of fouling organisms. The term foul release is in fact misleading because FR coatings cannot release all of the slime on a hull. Additionally, they are only effective above a certain speed, since the release mechanism works by the creation of a shear force to detach the marine organisms. Because of this, FR coatings are not appropriate for slow ships and for ships spending a long time in ports (Candries et al., 2003a). Also, they are very expensive compared to other types of coatings and may be damaged easily by hard shelled fouling organisms or any mechanical effects such as cleaning. Some of the important properties of typical SPCs and FR coatings are shown in Table 2.2 (Van Rompay, 2012). Due to these limitations, a great deal of effort is being devoted towards developing a novel and environmentally friendly antifouling solution that can eliminate all of the drawbacks of the current antifouling coatings.

Table 2.2: Properties of existing hull coatings, adapted from Van Rompay (2012).

	Protection and longevity	**Fuel saving properties and conditions**	**Need to drydock for repainting**	**Environmental concerns**
Typical antifouling coatings (SPC)	Soft coating. Fairly easily damaged. 3-5 years before AF coating needs to be replaced. Full recoating down to bare steel 2 or 3 times in 25 years. Not suitable for aluminium hulls.	Unfouled hull roughness from AF coating gives 2-4% fuel penalty. Usually, sails with slime = up to 20% fuel penalty. Effectively reduces higher fuel penalties. Coating degradation increases fuel penalty over time.	5 - 8 drydockings required for paint alone during ship's service life including 1-3 full blasting and repainting. Multiple coats and length curing times can mean 2-3 weeks in drydock for a full repaint.	Contaminates marine environment with toxic biocides, harming marine life, the food chain and humans. Pulse release of biocides if cleaned in-water. High VOC content when applied. Limits fuel consumption and GHG emissions from effects of heavy fouling. Prevent some NIS but further others.
Typical FR coating system	Soft coating. Easily damaged. 3-5 years before FR coat needs repair/reapplication. Full recoating required 1-3 times in 25 years.	Smoothest tested surface when unfouled. Usually sails with slime = up to 20% fuel penalty. Can foul badly if vessel has long lay-ups. Coating degradation increases fuel penalty over time.	5 - 8 drydockings required for paint alone during ship's service life including 1-3 full blasting and repainting. Multiple coats and length curing times can mean as much as 2 – 3 weeks in drydock for a full repaint.	Does not contain biocides but leaches potentially harmful oils, alters enzymes in barnacle glue; some silicones catalysed by highly toxic dibutyltin dilaurate. Medium VOC. Some reduction in fuel consumption/GHG. Can help limit spread of NIS.

Several different aspects need to be considered when designing a new antifouling system. These aspects concern the environment, the coating and the substrate. Details of the main aspects are given in Figure 2.3 (Chambers et al., 2006). The main difficulty during the development of a novel antifouling system is to find a compromise among different and conflicting parameters. The requirements for an optimal antifouling coating are described in detail by Chambers et al. (2006) in Table 2.3.

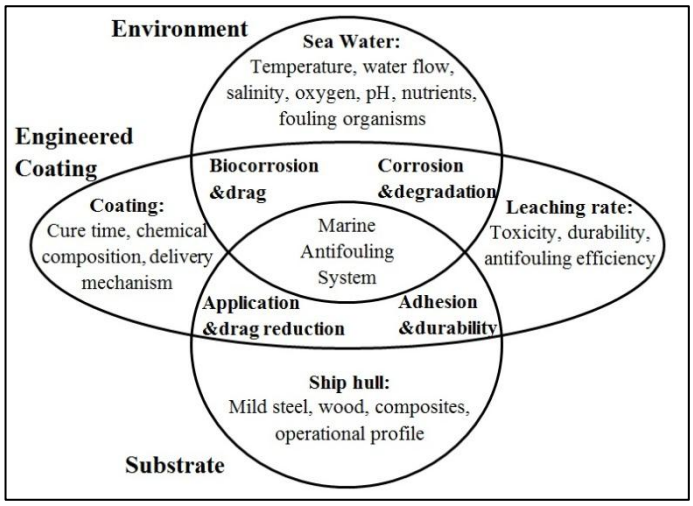

Figure 2.3: Key parameters for antifouling systems, adapted from Chambers et al. (2006).

Table 2.3: Requirements for an optimal antifouling coating, adapted from Chambers et al. (2006).

Must be	Must not be
Anticorrosive	Toxic to the environment
Antifouling	Persistent in the environment
Environmentally acceptable	Expensive
Economically viable	Chemically unstable
Long life	A target for non-specific species
Compatible with underlying system	
Resistant to abrasion/ biodegradation/erosion	
Capable of protecting regardless of operational profile	
Smooth	

Several attempts have been made to develop the optimum antifouling coating. An alternative strategy which is worth highlighting, is the use of an antifouling polymeric coating where a biocide is attached, in order to prevent the fouler microorganisms from attaching on the coated hull, without releasing the biocide (Charnley et al., 2011). These systems are called bioactive polymers. Reference may be made to Dafforn et al. (2011) for a comprehensive review on antifouling strategies.

One of the most recent antifouling projects is the EU funded FP7 Project FOUL-X-SPEL (Environmentally Friendly Antifouling Technology to Optimise the Energy Efficiency of Ships, Project number 285552, FP7-SST-2011-RTD-1). *"The basic idea concerns the modification of usual hulls by providing a new antifouling coating, by fixing bioactive molecules, which can provide biocide activity, in order to avoid leaching and to promote a long-term effect of surface protection"* (FOUL-X-SPEL, 2011).

Besides the direct impacts and product(s) of this FOUL-X-SPEL project, it has led to extensive research and has developed an increased understanding on the subject of fouling, antifouling technologies and fouling effects on ship resistance, fuel consumption and GHG emissions. It is believed that it will be a leap forward towards environmentally friendly antifouling systems. It is of note that the research performed in this thesis was partially generated as part of this FOUL-X-SPEL project. Examples of other recent EU funded research projects are AMBIO (2005), LEAF (2012), BYEFOULING (2013) and SEAFRONT (2014).

2.3 The Turbulent Boundary Layer

2.3.1 The Velocity Profile in the Turbulent Boundary Layer

The turbulent boundary layer concept is essential in order to understand and assess the flow around a ship, since a turbulent boundary layer occurs around a ship when she is in motion.

The boundary layer concept was first introduced by Ludwing Prandtl in 1904 as a thin region near the surface of an object in a fluid flow (Schlichting, 1979). He proposed that in a fluid flow around an object, the velocity of the fluid particle on the object is zero, in other words the fluid adheres to the object (termed the no-slip condition), whereas the velocity of the fluid flow after it reaches a particular distance away from the object is termed the free-stream velocity (Schultz, 1998). A velocity gradient therefore occurs in this region and is termed a boundary layer. The concept of a boundary layer is demonstrated in Figure 2.4 (Anderson, 2005).

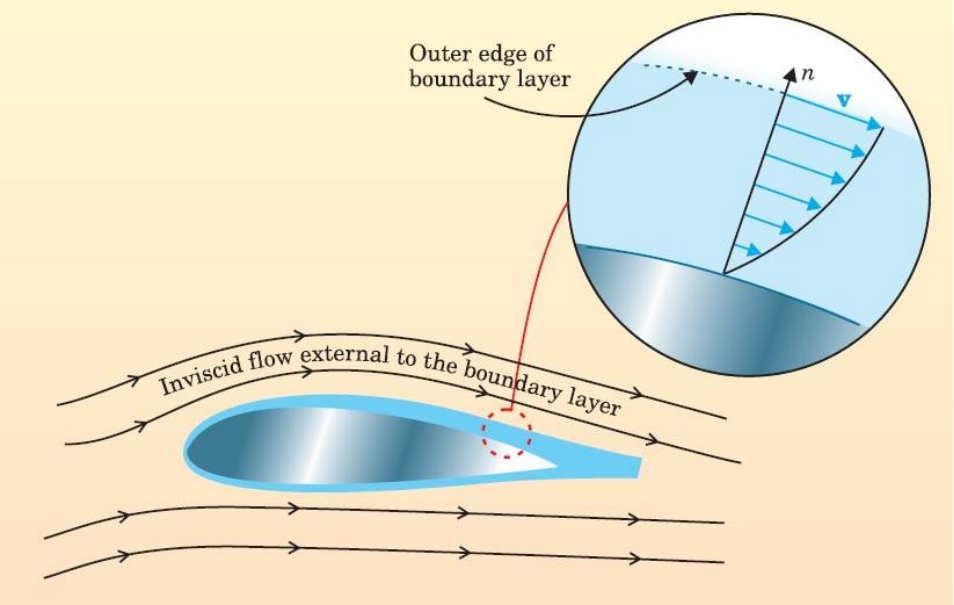

Figure 2.4: The boundary layer concept (Anderson, 2005).

Prandtl described the boundary layer concept as below (Anderson, 2005):

> *"A very satisfactory explanation of the physical process in the boundary layer [Grenzschicht] between a fluid and a solid body could be obtained by the hypothesis of an adhesion of the fluid to the walls, that is, by the hypothesis of a zero relative velocity between fluid and wall. If the viscosity was very small and the fluid path along the wall not too long, the fluid velocity ought to resume its normal value at a very short distance from the wall. In the thin transition layer [Übergangsschicht] however, the sharp changes of velocity, even with small coefficient of friction, produce marked results."*

If a flat plate is taken as an example, the flow is laminar at the first portion of the plate. As the flow continues across the plate, it becomes more and more turbulent in the transition region, until it eventually becomes a turbulent flow. The onset and the length of the transition region can vary due to several factors, including surface roughness, pressure and velocity fluctuations. The transition process is strongly dependent on the Reynolds number (Candries, 2001), which is the ratio of inertial forces to viscous forces and is defined as follows:

$$\mathrm{Re} = \frac{UL}{\nu} \tag{2.1}$$

where U is the mean velocity, L is a characteristic linear dimension and ν is the kinematic viscosity.

Figure 2.5 shows the typical development of a turbulent boundary layer over a flat surface (Cortana, 2013).

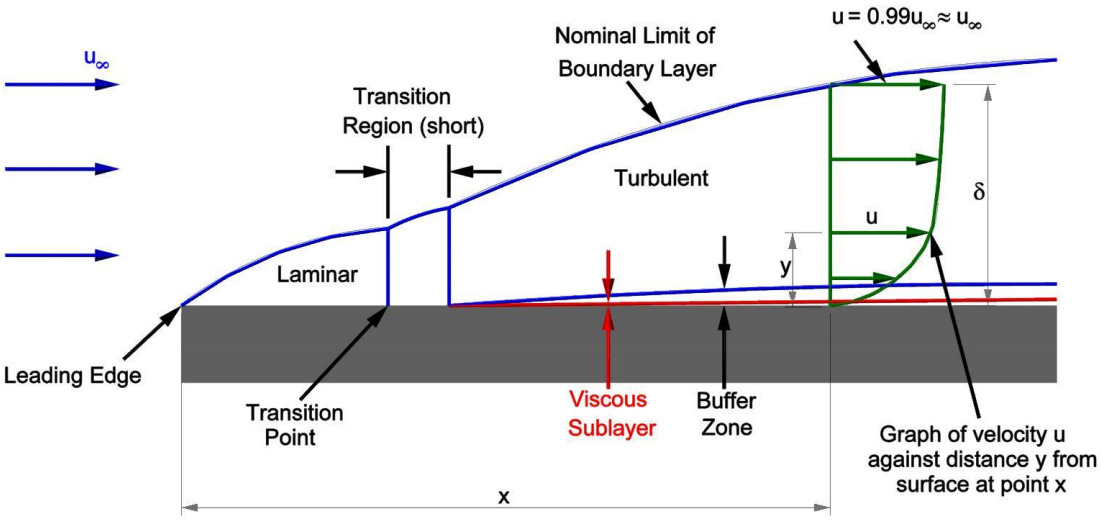

Figure 2.5: The development of a turbulent boundary layer over a flat surface (Cortana, 2013).

As was also demonstrated in Figure 2.5, the boundary layer thickness, δ, is described as the distance between the wall and the point where the velocity magnitude of the flow reaches the proportion of 0.99 of the free-stream velocity, $U_{e.}$

The turbulent boundary layer is assumed to consist of two main regions: an inner region and an outer region. The flow in the inner region is affected by surface conditions, such as roughness, whilst the flow in the outer region is not affected by such conditions. These are some of the main assumptions made in this study, which will be further discussed later.

The inner region is composed of a viscous sublayer and a log-law region. The mean average velocity in this region depends upon wall shear stress, the density of the fluid, kinematic viscosity and the distance from the wall.

The non-dimensional mean velocity profile can be expressed by the law of the wall, given by (2.2)

$$U^+ = f(y^+) \tag{2.2}$$

where U^+ is the non-dimensional velocity in the boundary layer and y^+ is the non-dimensional normal distance from the boundary. These terms are further defined in (2.3) and (2.4), respectively

$$U^+ = \frac{U}{U_\tau} \tag{2.3}$$

$$y^+ = \frac{yU_\tau}{\nu} \tag{2.4}$$

where U is the mean velocity, U_τ is the friction velocity defined as $\sqrt{\tau_w/\rho}$, y is the normal distance from the boundary, ν is the kinematic viscosity, τ_w is the shear stress magnitude and ρ is the density of the fluid.

The viscous sublayer consists of a linear sublayer and a buffer layer. In this sublayer, the viscosity, together with the wall boundary conditions, dominates the mean and turbulent motions of the flow (Schultz, 1998). The linear sublayer is assumed to constitute a very small portion of the boundary layer, i.e. $y^+ < 7$. As the name suggests, the velocity profile is linear in the linear sublayer, given by (2.5).

$$U^+ = y^+ \tag{2.5}$$

In the buffer layer ($7 < y^+ < 30$), the velocity profile begins to deflect from linearity. The region just outside the viscous sublayer, $30 < y^+$ and $y/\delta < 0.2$ according to Candries (2001), and $30 < y^+ < 300$ according to Schultz (1998), is called the log-law region. The shear stress in this region is significantly affected by the fluctuating velocity component whereas the viscous effect becomes negligible on the shear stress. In this region, a velocity profile for smooth surfaces was suggested as shown in (2.6) (Millikan, 1938),

$$U^+ = \frac{1}{\kappa} \ln y^+ + B \qquad \textbf{(2.6)}$$

where κ is the von Karman constant and B is the smooth wall log-law intercept. The velocity profile in a typical turbulent boundary layer is shown in Figure 2.6 (Schultz and Swain, 2000).

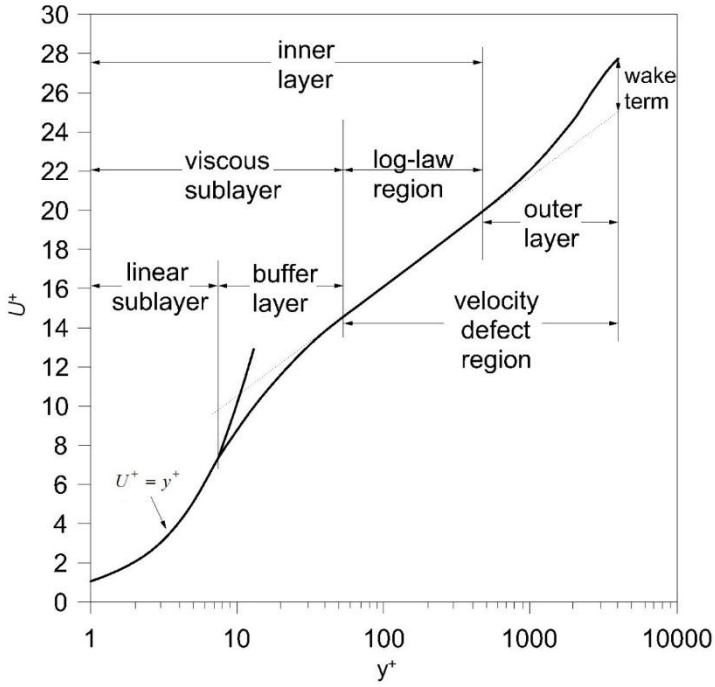

Figure 2.6: Velocity profile in a turbulent boundary layer, adapted from Schultz and Swain (2000).

The existence of a log-law region of the boundary layer has been proved by several studies such as Clauser (1954) and Klebanoff and Diehl (1951). The values of κ and B, on the other hand, are still under debate (George, 2007). Clauser (1954) employed κ=0.41 and B=4.9 while these values altered to 0.40 and 5.1, respectively according to Coles (1956). Cebeci and Bradshaw (1977) and Cebeci and Chang (1978) used κ=0.41 and B=5.2 while Zagarola and Smits (1998) proposed κ as 0.436 and B as 6.15 for fully developed turbulent pipe flow, whereas McKeon et al. (2004) determined κ to be 0.421 and B to be 5.60 for fully developed pipe flow. As cited in George (2007), κ was assumed to be 0.38 by Nagib et al. (2004).

The fluid motions in the outer region of the turbulent boundary layer ($y/\delta > 0.1$ to 0.2) are assumed to be independent of the fluid viscosity as stated in Yaglom (1979).

That is to say, the mean velocity and the turbulence intensity in this region is assumed not to be affected by the surface conditions (Townsend, 1976). This is called Townsend's Reynolds number similarity hypothesis. The velocity defect law can be expressed as follows:

$$\frac{U_e - U}{U_\tau} = f\left(\frac{y}{\delta}\right) \tag{2.7}$$

where U_e is the velocity at the outer edge of the boundary layer. It is worth noting that the velocity defect law is assumed to be valid for both smooth and rough surfaces.

The range of the applicability of the log-law and the velocity defect law was extended by the Coles (1956) wake function. Equation (2.8) shows the law of the wake

$$U^+ = \frac{1}{\kappa}\ln y^+ + B + \frac{2\Pi}{\kappa}\sin^2\left(\frac{\pi}{2}\frac{y}{\delta}\right) \tag{2.8}$$

where Π is the wake parameter, which can be assumed to be 0.55 for low free-stream turbulence and zero pressure gradient.

2.3.2 The Effect of Roughness on the Velocity Profile in the Turbulent Boundary Layer

Surface roughness leads to an increase in turbulence, which means that the turbulent stress and wall shear stress increase. Ultimately, the velocity in the turbulent boundary layer decreases.

Generally, roughness is classified into two types: k-type and d-type. This classification is related to the roughness functions, which will be explained later in this section. Roughness functions of k-type roughness scale on the roughness height, k, while roughness functions of d-type roughness scale on the pipe diameter, d (Perry et al., 1969). Nikuradse (1933), Hama (1954), Perry et al. (1969), Antonia and Luxton (1971), Antonia and Luxton (1972), Ligrani and Moffat (1986), Bandyopadhyay (1987), Krogstad et al. (1992), Shockling et al. (2006) and Schultz

and Flack (2007) are some examples of studies on rough wall turbulent boundary layers. Reference may be made to Jiménez (2004) for a comprehensive review on rough wall turbulent boundary layers.

K-type roughness is of interest in this study since hull roughness has been shown to be k-type (Schultz, 1998). The term roughness therefore stands for k-type roughness from this point onward.

Although roughness can be described using various parameters, the key parameter is thought to be the roughness height, k, or equivalent sand roughness height, k_s. The roughness height can be normalised and termed the roughness Reynolds number, given by (2.9).

$$k^+ = \frac{kU_\tau}{\nu} \tag{2.9}$$

The flow over a surface is generally classified with respect to the roughness Reynolds number, i.e. as a hydraulically smooth regime, a transitionally rough regime or a fully rough regime. According to Schlichting (1979), if the roughness height is so small that it does not extend into the laminar sub-layer, the flow regime is referred to as hydraulically smooth. In this case, the flow and the velocity profile in the turbulent boundary layer are assumed to be unaffected by the roughness. He added that if the protrusions are partly outside the laminar-sublayer, the flow is then in the transitionally rough regime and it generates an added resistance due to the form drag compared to an otherwise smooth surface. If all the protrusions are outside the laminar-sublayer, the flow reaches the fully rough regime and the law of the resistance is quadratic.

However, it should be noted that different roughness types may generate different flow regimes on surfaces even if the same roughness Reynolds number is recorded (Schultz, 2007). For example, Schlichting (1979) stated that the flow on a uniform sand roughness can be classified as hydraulically smooth when $k_s^+ < 5$, it can be classified as transitionally rough when $5 \leq k_s^+ \leq 70$, and it can be classified as fully rough when $k_s^+ > 70$. However, the onset of roughness effects (the upper limits for the hydraulically smooth regime), $k_{s,smooth}^+$, and the beginning of the fully rough

regime (the upper limit for the transitionally rough regime), k_s^+,rough on three dimensional rough surfaces of Schultz and Flack (2007) representing real engineering surfaces, rather than a uniform sand roughened surface, became 3 and 25, respectively (Schultz, 2007).

The law of the wall in the inner region changes in the presence of surface roughness. The velocity in the inner region of the turbulent boundary layer over a rough surface becomes a function of y^+ and k^+, given by (2.10) (Schubauer and Tchen, 1961).

$$U^+ = f\left(y^+, k^+\right) \tag{2.10}$$

Schlichting (1979) extended the work of Nikuradse (1933) in 1936 and represented the velocity profile in the turbulent boundary layer of a rough pipe by equations (2.11) or (2.12)

$$U^+ = \frac{1}{\kappa}\ln(y^+) + B_1 \tag{2.11}$$

$$U^+ = \frac{1}{\kappa}\ln\left(\frac{y}{k_s}\right) + B_2 \tag{2.12}$$

where κ=0.4 and B_1, B_2 have different values for the different flow regimes. The values of B_2 are given in (2.13) for the hydraulically smooth regime and the fully rough regime. B_2 values for the transitionally rough regime are demonstrated in Figure 2.7 (Schlichting, 1979).

$$B_2 = \begin{cases} 5.5 + \frac{1}{\kappa}\ln\left(k_s^+\right) & \rightarrow \text{ hydraulically smooth regime} \\ 8.5 & \rightarrow \text{ fully rough regime} \end{cases} \tag{2.13}$$

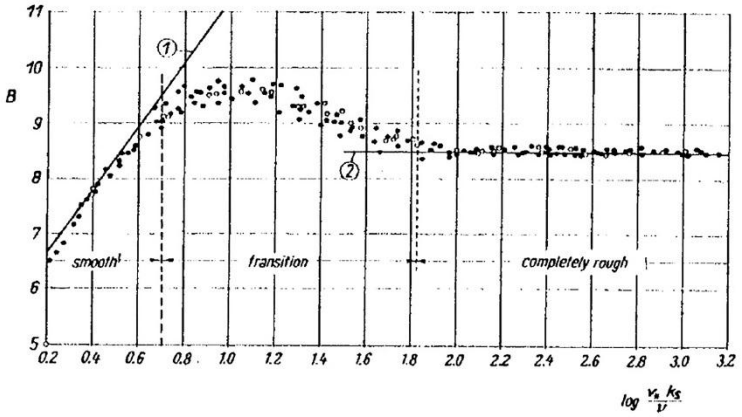

Figure 2.7: B_2 values for sand roughness by Nikuradse (1933) (Schlichting, 1979).

If (2.12) is rearranged using the B_2 value in (2.13), equation (2.14) is evaluated for hydraulically smooth regimes, in a similar form to (2.6) and (2.11).

$$U^+ = \frac{1}{\kappa}\ln(y^+) + 5.5 \qquad \textbf{(2.14)}$$

Schlichting (1979) then rearranged the equation for the fully rough regime and came up with equation (2.15) for the velocity profile of the fully rough regime.

$$U^+ = \frac{1}{\kappa}\ln(y^+) + 8.5 - \frac{1}{\kappa}\ln(k_s{}^+) \qquad \textbf{(2.15)}$$

It is of note that the smooth wall log-law intercept was taken to be 5.5 and κ was assumed to be 0.4 in his study.

Cebeci and Bradshaw (1977) also followed on from the experiments of Nikuradse (1933) and defined the velocity profile using equations (2.11) and (2.12). Nevertheless, they presented the analytical fit of Ioselevich and Pilipenko (1974) for B_1 values, given as:

$$B_1 = \begin{cases} B & \rightarrow \quad k_s^+ < 2.25 \\ B + \left[8.5 - B - \frac{1}{\kappa} \ln k_s^+ \right] \cdot \sin\left\{ 0.4258 \left(\ln k_s^+ - 0.811 \right) \right\} & \rightarrow \quad 2.25 > k_s^+ < 90 \\ 8.5 - \frac{1}{\kappa} \ln k_s^+ & \rightarrow \quad k_s^+ > 90 \end{cases} \qquad \textbf{(2.16)}$$

where κ was assumed to be 0.42 and B was assumed to be 5.2. $k_s^+{}_{,smooth}$ and $k_s^+{}_{,rough}$ were taken as 2.25 and 90, respectively, instead of 5 and 70 as proposed by Schlichting (1979).

As evidently shown, the effect of roughness on flow can be observed in the velocity profile (Schultz and Swain, 2000). Roughness causes a decrease in the log-law velocity profile (termed the roughness function) shown as ΔU^+. It should also be considered that the decrease in the velocity profile manifests itself as an increase in the frictional resistance (Demirel et al., 2013). The roughness function in the velocity profile due to roughness is depicted in Figure 2.8 (Schultz and Swain, 2000).

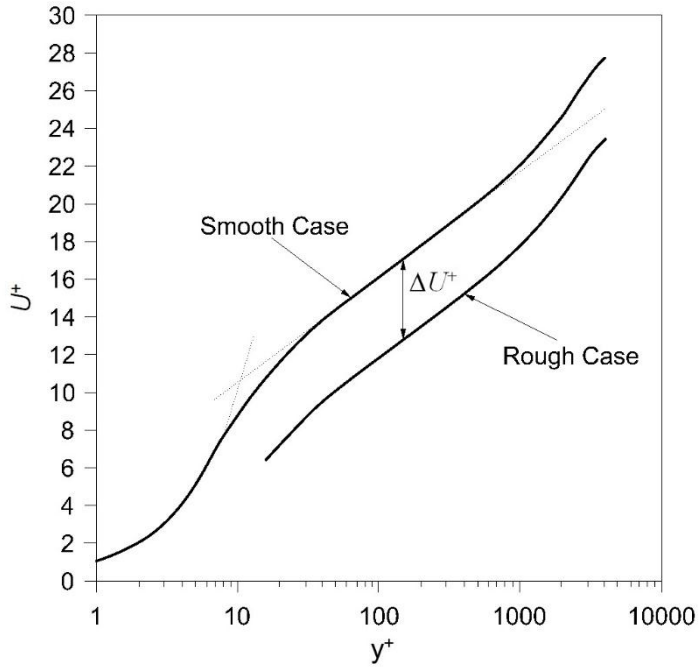

Figure 2.8: The roughness effect on a log-law velocity profile, adapted from Schultz and Swain (2000).

The log-law velocity profile for rough surfaces in the turbulent boundary layer is given by (2.17)

$$U^+ = \frac{1}{\kappa}\ln(y^+) + B - \Delta U^+ \quad \textbf{(2.17)}$$

in which ΔU^+ is the roughness function. By using (2.17), one can represent the change in the velocity profile due to roughness using ΔU^+, and the velocity profile can be defined by simply subtracting ΔU^+ from the smooth velocity profile given by (2.6). For this reason, (2.17) is used in this study to define the velocity profile. It should be borne in mind that ΔU^+ simply vanishes and equation (2.17) yields to become equation (2.6) in the case of a smooth condition. ΔU^+ values are typically obtained experimentally, since there is no universal roughness function model for every kind of roughness.

As mentioned earlier, the mean velocity of the outer region is assumed not to be affected by surface roughness and obeys the velocity defect law (Hama (1954), Clauser (1954)), as given by (2.7). Having said that, U_τ is affected by the existence of surface roughness and hence it suggests an indirect dependence on roughness (Granville, 1987). It should also be noted that the velocity-defect law is not applicable for the low Reynolds numbers due to the transition from laminar to turbulent flow (Granville, 1977). The velocity defect law is in agreement with the Reynolds number similarity hypothesis of Townsend (1976) and of Perry and Li (1990) which expresses that the turbulence outside the inner layer is not a function of surface roughness.

Although some studies, such as Krogstad et al. (1992), Tachie et al. (2000), Keirsbulck et al. (2002) and Acharya et al. (1986) showed the changes in the velocity defect law and that it is affected by surface roughness, the majority of the studies such as Bandyopadhyay (1987), Raupach et al. (1991), Krogstad and Antonia (1999), Antonia and Krogstad (2001), Schultz and Flack (2003), Schultz and Flack (2005), Flack et al. (2005), Kunkel and Marusic (2006), Schultz and Flack (2007) and Ünal et al. (2012) experimentally showed the validity of the velocity defect law on smooth and rough walls. A representative plot supporting the velocity-defect law using the results of Flack et al. (2007) is shown in Figure 2.9 (Flack and Schultz, 2010).

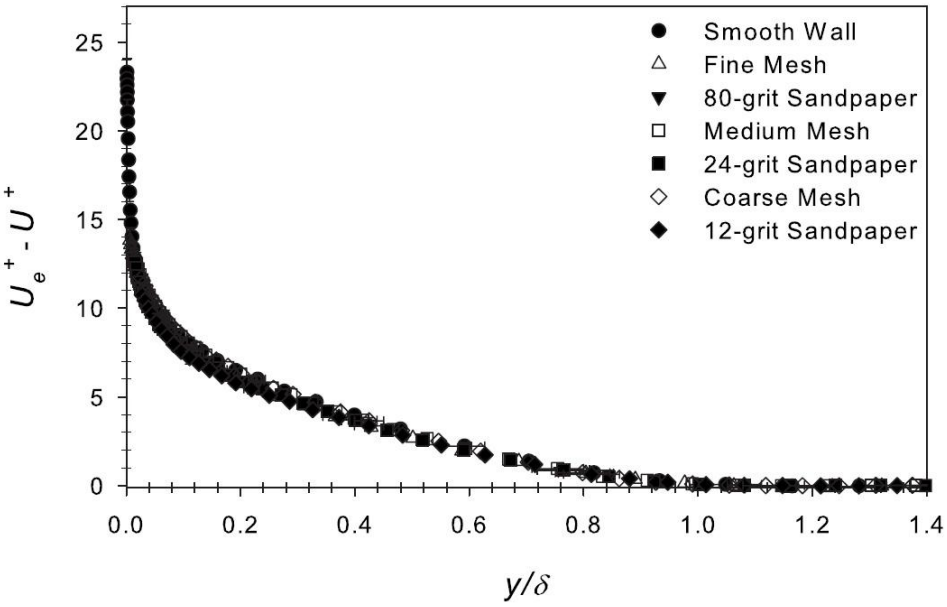

Figure 2.9: Mean velocity profiles in the velocity defect from Flack et al. (2007) (Flack and Schultz, 2010).

The very first application of this knowledge to engineering surfaces was performed by Colebrook and White (1937) and Colebrook (1939). Colebrook type roughness functions for galvanised, tar-coated, and wrought iron pipes with fully developed flow can be described by the following form (Schultz, 1998).

$$\Delta U^+ = A\log\left(1+k^+\right) \tag{2.18}$$

Although both Colebrook and Nikuradse roughness functions have an asymptote with the same slope at fully rough regimes, they show different behaviours in the transitionally rough regime. According to Schultz (2014), these roughness functions might be assumed to be the extreme cases, and the roughness functions of real surfaces are expected to show behaviour that is between the monotonic Colebrook and inflectional Nikuradse type roughness functions, such as those presented by Schultz and Flack (2007) and Shockling et al. (2006).

2.4 Historical Cornerstones of the Research into Ship Frictional Resistance with a Focus on Hull Roughness

The very first investigation on the skin friction of a ship was performed by William Froude (Froude, 1872, 1874), the 'father' of ship resistance prediction. He conducted towing tests of flat plates of different lengths up to 50 feet (15.2 m), in order to develop a general understanding on the frictional resistance component of a ship, as well as the effect of surface conditions on frictional resistance (van Manen and van Oossanen, 1988). The plates were fully immersed in order to eliminate as much residuary resistance as possible, so that the total measured resistance would only be the frictional resistance. He used different surface conditions along with smooth surfaces to investigate roughness effects. Finally, he came up with an empirical formula given in (2.19)

$$R_F = fSV^n \tag{2.19}$$

where R_F is the frictional resistance, S is the wetted surface area, V is the speed and f and n are parameters depending on the length and surface condition of the plates. Using this method, for the first time, the effect of different surface conditions on the frictional resistance were somehow addressed using an empirical formula. Frankly, Froude did not intend to evaluate roughness functions and so on. However, his attempt was very important and inspiring for later researchers in the field.

The skin friction coefficients of Froude had to be extrapolated to full-scale ship lengths and speeds in order to have a practical solution for ships. This was not an easy task to achieve, due to his observation suggesting that plates of different lengths have different resistance values per unit area, even if they are towed at the very same speed. He therefore suggested a practical way to perform an extrapolation: by his own words "*it is at once seen that, at a length of 50 feet, the decrease, with increasing length, of the friction per square foot of every additional length is so small that it will make no very great difference in our estimate of the total resistance of a surface 300 feet long whether we assume such decrease to continue at the same rate throughout the last 250 feet of the surface, or to cease entirely after 50 feet;*

while it is perfectly certain that the truth must lie somewhere between these assumptions." (van Manen and van Oossanen, 1988).

Froude (1874) also conducted towing tests of *HMS Greyhound*, a wooden ship of 52.28 m, and tried to validate his suggestions on the extrapolation. However, the actual ship resistance values were higher than those extrapolated from the model tests. He attributed this difference to the surface conditions and showed that this was a reasonable assumption (van Manen and van Oossanen, 1988).

Moreover, Froude (1874) explained his major assumption, which proposes that the skin friction of a hull is equal to that of a flat plate of the same length and area as the wetted surface of the ship, by his own words "*For this calculation the immersed skin was carefully measured, and the resistance due to it determined upon the hypothesis that it is equivalent to that of a rectangular surface of equal area, and of length (in the line of motion) equal to that of the model, moving at the same speed.*" (van Manen and van Oossanen, 1988).

As reported in van Manen and van Oossanen (1988), Blasius (1908) calculated the frictional resistance of a flat plate in laminar flow, as given by (2.20).

$$C_F = \frac{R_F}{\frac{1}{2}\rho S V^2} = 1.327\left(\frac{VL}{\nu}\right)^{-1/2} \tag{2.20}$$

Prandtl (1921) and von Karman, on the other hand, proposed equation (2.21) for the skin friction of a flat plate in turbulent flows, using the experimental results of Froude (1872, 1874) and Gebers (1919), as reported by van Manen and van Oossanen (1988).

$$C_F = \frac{R_F}{\frac{1}{2}\rho S V^2} = 0.072\left(\frac{VL}{\nu}\right)^{-1/5} \tag{2.21}$$

Equations (2.20) and (2.21) showed good agreement with the findings of Froude for laminar flow and turbulent flow, respectively (Date and Turnock, 1999).

Prandtl (1927, 1932) derived a theoretical skin friction formulation based on the universal logarithmic boundary layer velocity profile (Date and Turnock, 1999). The formula is given by

$$\frac{A}{\sqrt{C_F}} = \log(\mathrm{Re}\cdot C_F) + M \qquad \textbf{(2.22)}$$

where A and M are coefficients which can be obtained experimentally.

Kempf (1929) then measured the skin friction of plates installed on a 76.8 m towed pontoon, as reported by Schultz (1998). Following this, Schoenherr (1932) compiled all the available experimental data and added his own skin friction measurement at low Reynolds number and the results of Kempf (1929) at high Reynolds numbers, and proposed the Schoenherr friction line formulation, given by:

$$\frac{0.242}{\sqrt{C_F}} = \log(\mathrm{Re}\cdot C_F) \qquad \textbf{(2.23)}$$

It should be borne in mind that this formula is in the form of equation (2.22) and coefficients A and M were obtained by fitting the equation to the available experimental data.

The International Conference of Ship Tank Superintendents (ICSTS) discussed the subject of the skin friction of ships and the delegates came up with a frictional resistance prediction formula using the results of Froude in 1935 (Schultz, 1998). Although there was no consensus, in 1937 the ICSTS proposed that Nikuradse's sand grain roughness was the best method with which to take hull roughness into account (Schultz, 1998).

The American Towing Tank Conference (ATTC) proposed the use of the Schoenherr friction line given by (2.23) with a constant roughness allowance of 0.0004 for the prediction of the skin friction coefficients of clean new vessels. It is of note that the Schoenherr friction line was referred to as the 1947 ATTC line (van Manen and van Oossanen, 1988).

Hughes (1952, 1954) conducted several experiments using planks and very large pontoons. He came up with a two-dimensional skin friction formulation given by equation (2.24) (van Manen and van Oossanen, 1988).

$$C_F = \frac{0.066}{\left(\log \mathrm{Re} - 2.03\right)^2} \tag{2.24}$$

Due to the fact that the ATTC 1947 may not give accurate results for low Reynolds numbers for the ship models, the ITTC proposed the "ITTC 1957 model-ship correlation line" as "only an interim solution to this problem for engineering purposes" (van Manen and van Oossanen, 1988). The formulation is given by equation (2.25).

$$C_F = \frac{0.075}{(\log \mathrm{Re} - 2)^2} \tag{2.25}$$

It is of note that this is not an equation to represent the frictional resistance of a flat plate and it cannot be used for such purposes (van Manen and van Oossanen, 1988).

Granville (1977) derived a general formula for the calculation of the frictional resistance of two-dimensional flat plates in turbulent flow, given by equation (2.26):

$$C_F = \frac{a}{\left(\log \mathrm{Re} - b\right)^2} + \frac{c}{\mathrm{Re}} \tag{2.26}$$

where a=0.0776, b=1.88 and c=60. It is worth noting this equation has a similar form to the ITTC 1957 friction line given by equation (2.25). The aforementioned skin friction lines are given in Figure 2.10.

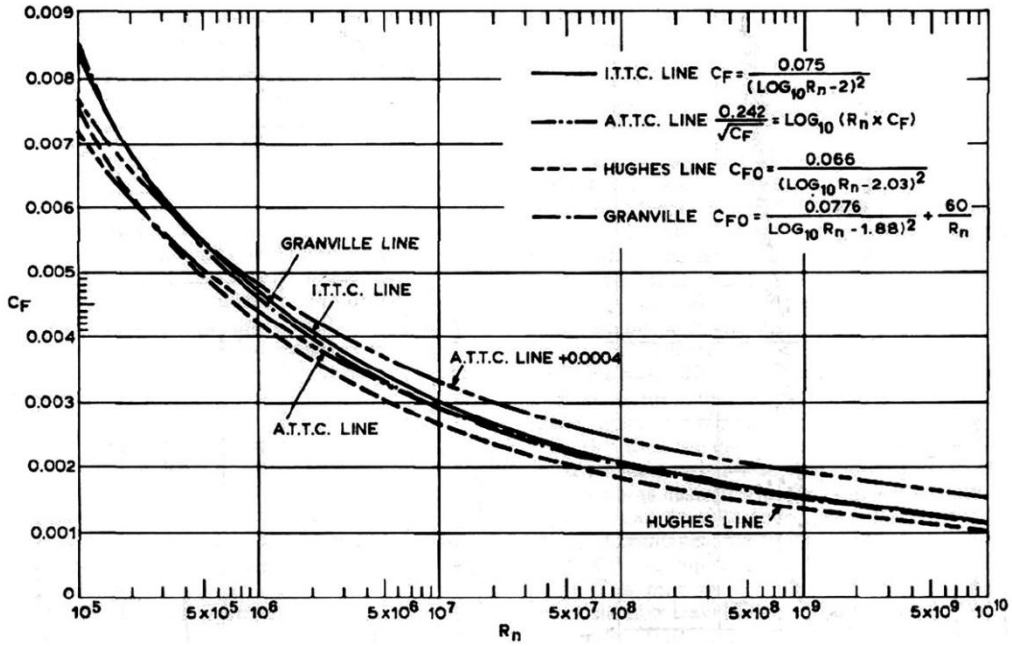

Figure 2.10: Skin friction lines (van Manen and van Oossanen, 1988).

The formula of Bowden and Davison (1974), given by equation (2.27), was adopted in 1978 by the ITTC as a correlation allowance which together accounts for the hull roughness, ΔC_F, and other model-ship correlation allowances, ΔC_R (ITTC, 1987):

$$C_A = \left(\Delta C_F + \Delta C_R\right) = 0.105\left(\frac{h}{L}\right)^{1/3} - 0.00064 \qquad \textbf{(2.27)}$$

where h is the average hull roughness height. This formula was criticised and questioned by several researchers just after its adoption (e.g. Musker and Lewkowicz (1978), Grigson (1983), Grigson (1985b), Okuno et al. (1985)), since it does not solely include the hull roughness and it does not reflect the effect of different ship speeds (ITTC, 1987).

Although several formulations were proposed by various researchers, the formula of Bowden and Davison (1974) was used by the ITTC until 1990. It was replaced by the formula of Townsin and Dey (1990) in the 19th ITTC (1990). This formula is given by equation (2.28).

$$\Delta C_F \times 10^3 = 44\left[\left(\frac{h}{L}\right)^{1/3} - 10\,\mathrm{Re}^{-1/3}\right] + 0.125 \qquad \textbf{(2.28)}$$

Since then, this subject was not considered extensively until 2002 (ITTC, 2002a). Some important discussion on the requirement of a new roughness allowance formula took place in the 23rd ITTC (2002a).

In the 25th ITTC (2008a) meeting, the use of the formula of Townsin and Dey (1990) for calculating the added resistance due to hull roughness was again referred to as a suitable method. Additionally, it was mentioned by the ITTC (2008b) that roughness and fouling effects should be accounted for the calculation of added power.

In the 26th ITTC (2011b) meeting, more attention was given to the roughness phenomenon by assembling a Special Committee on Surface Treatment. The generation of a skin friction database was proposed. The skin friction measurements of several surfaces, including coatings and biofouling, were therefore required. The lack of data on the drag-roughness correlation of coatings including the new-generation SPC and foul-release coatings was particularly emphasised. Although the ITTC (2011b) recommends the use of the roughness allowance formula accepted in the 19th ITTC (1990), since this is the best option for the time being, the committee strongly addressed the possible inaccuracy of the formula and recommended researchers to develop new formulae or methods using experimental data. It was stressed that the new formulae should also cover the potential effects of biofouling on ship resistance, rather than only predicting the coating roughness. Moreover, CFD was shown to be one of the best candidates for the calculation of a new prediction method.

In the 27th ITTC meeting, no discussion was made regarding the use of a formula for the roughness allowance; instead theoretical, experimental and numerical studies were proposed in order to precisely predict the effect of roughness on frictional resistance (ITTC, 2014a). Additionally, the numerical models, such as CFD-based models, were shown to be a reasonable method to account for the effect of coatings and fouling on ship resistance and powering (ITTC, 2014b).

2.5 Investigations into the Effects of Hull Roughness on Ship Resistance

Investigations into the effects of hull roughness on ship resistance can be classified into three groups; direct full-scale measurements and studies, experimental studies, and theoretical and numerical prediction studies.

Froude (1874) showed the effects of hull surface conditions on the resistance of HMS Greyhound by carrying out towing tests. His findings were consistent with his experiments (Froude, 1872, 1874), as reported by van Manen and van Oossanen (1988).

Todd (1951) performed a full scale study for the investigation into the roughness effect on skin friction. Surfaces were coated with several coatings and the added resistance coefficients due to surface roughness, ΔC_F, were obtained (Schultz, 1998). The frictional resistance values of Todd (1951) are given in Figure 2.11 (Schultz, 1998).

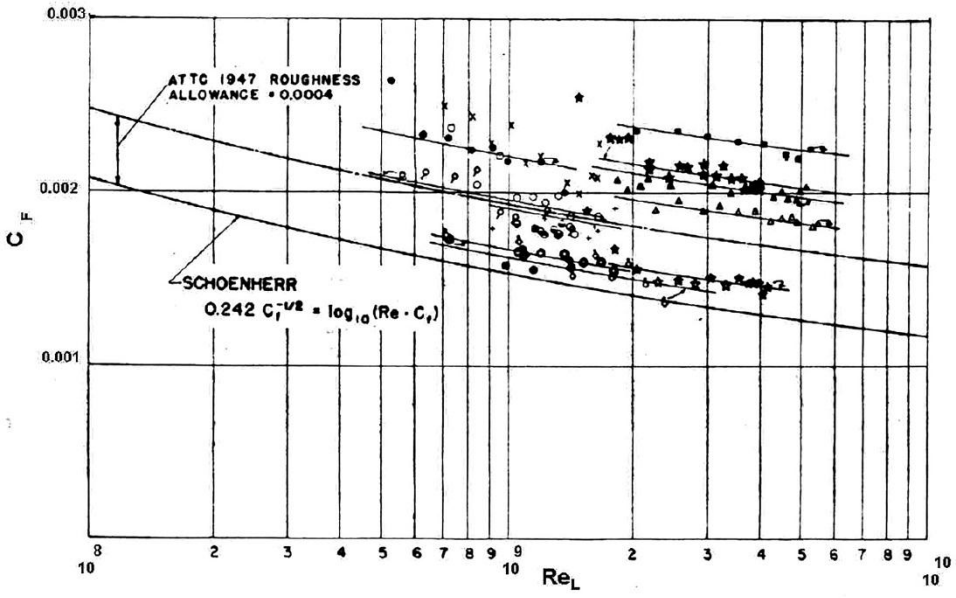

Figure 2.11: Frictional resistance values of Todd (1951), as reported by (Schultz, 1998).

BMT has performed some studies, including roughness measurements, on new ships, investigating the effects of hull roughness on ship resistance (Lackenby, 1962). In this study, the added resistance of a ship was found to be up to 20% compared to the sistership, with this difference attributed to the hull roughness (van Manen and van

Oossanen, 1988). According to Denny (1951), after 40 days of being stationary, the resistance of Lucy Ashton was reported to increase by 5% (Schultz and Swain, 2000). The details of these full-scale studies and the early works on the hull roughness effect on ship resistance can be found in Lackenby (1962).

Bowden and Davison (1974) proposed an equation, given by (2.27), for the calculation of the added frictional resistance coefficient, based on the sea trials of real ships (Schultz, 1998). As mentioned earlier, this added resistance coefficient was a correlation allowance which together accounts for the hull roughness, ΔC_F, and other model-ship correlation allowances, ΔC_R (ITTC, 1987). Townsin et al. (1981) suggested further adjustment to the formula given by (2.27) based on the measurements from containerships over one year's time. They suggested the following formula:

$$\Delta C_F \times 10^{-3} = 105\left(\frac{h}{L}\right)^{1/3} - 0.74 \qquad \textbf{(2.29)}$$

Later on, Townsin and Dey (1990) proposed equation (2.28) for the calculation of ΔC_F, as reported by Townsin (2003).

It is of note that equations, (2.27), (2.28) and (2.29) are proposed to calculate the added resistance due to clean, typical as applied coating conditions of ship hulls, rather than to predict the fouling effect on ship resistance.

Lewthwaite et al. (1985) and Haslbeck and Bohlander (1992) can be given as some examples of full-scale studies. According to Townsin (2003), Lewthwaite et al. (1985) reported an increase of 25% in the frictional resistance of a 23 m fleet tender after 240 days of operation around the South Coast of England. Haslbeck and Bohlander (1992) recorded the effect of hull cleaning of a frigate, after 22 months of being stationary in Hawaii, reporting that the required shaft power decreased by 18%. Recently, Yokoi (2004) showed the changes in speed, shaft power and fuel consumption of a training ship over 8 years, according to the ITTC (2011b). A 20% increase in the shaft power due to fouling was recorded. Munk (2006) demonstrated the increase in resistance of real ships in service. Additionally, the importance of hull

and propeller cleaning was highlighted, showing the decrease in resistance due to cleaning. Corbett et al. (2011) measured the fuel consumption data of a bulk carrier and tanker before and after the application of a foul release (FR) coating. The findings showed that the use of FR maintained a 10% and a 22% saving in fuel consumption for the tanker and the bulk carrier, respectively, compared to the use of TBT-free SPC. It is of note that these extreme savings might be claimed to be dubious when the findings of other researchers (e.g. Candries (2001), Schultz (2004)) are taken into consideration.

Although several existing studies have investigated the coating roughness and hull fouling effect on ship resistance and powering by conducting full-scale trials and measurements, the results include many uncertainties due to different operational conditions, routes, human factors and so on, as can be seen from the literature.

Experimental, lab-scale studies, on the other hand, provide more reliable data since the uncertainties can be estimated to a degree. Therefore, several experimental studies have been devoted towards investigating the roughness effect on the skin friction.

As mentioned earlier, the very first experimental investigation into the effect of hull roughness on frictional resistance can be attributed to Froude (1872, 1874). His findings were important as explained in detail in the previous section. According to Woods Hole Oceanographic Institution (1952), McEntee (1915) conducted the first extensive experimental study investigating the effect of fouling on frictional resistance. Flat plates were coated with anti-corrosive paints and kept in water for a given period of time. The plates were then towed with barnacles on them. The findings were remarkable since the resistance of the plates after 12 months of sea exposure increased to 4 times the resistance of an otherwise identical clean plate (Woods Hole Oceanographic Institution, 1952). As reported by Townsin (2003), Kempf (1937) conducted tests on pontoons covered with shell fouling and recorded an increase of 66% in the resistance, even with only 5% coverage. According to Schultz and Swain (2000), the increase in the frictional resistances of surfaces covered with slime was surveyed by conducting towing tests of flat plates by Benson et al. (1938), and performing experiments on cylinders, rotating disks and a model

ship by Watanabe et al. (1969). Lewkowicz and Das (1986) conducted towing tests of flat plates covered with artificial slime and the increase in the frictional resistance due to artificial slime was found to be 18% (Schultz and Swain, 2000). Loeb et al. (1984) conducted rotating disk experiments using disks covered with several different types of microbial slimes. It was observed that microbial slime led to an increase of 10% to 20% in the frictional resistance. Schultz and Swain (1999) and Schultz (2000) investigated the effects of biofilms and algae on the skin friction coefficients of flat plates using boundary layer measurements. Swain et al. (2007) surveyed the fouling growth on different types of coatings under static and dynamic conditions. Andrewartha et al. (2010) measured an increase of 99% in the drag coefficients of test plates due to biofilms in a recirculating water tunnel. The findings evidently demonstrated that the antifouling and hydrodynamic performances of coatings significantly vary depending upon operational conditions.

Grigson (1992) investigated the performances of hull finishes and proposed his very well-known Colebrook type roughness function model for the coatings. He also presented the early works performed to assess several types of coatings, suffice it to mention, Couch (1951), Yokoo et al. (1966), Lewkowicz and Musker (1978), Nakato et al. (1984), Kauczynski and Walderhaug (1983) and Okuno et al. (1985). In those studies, different experimental methods were used to determine the roughness functions (Grigson, 1992). Musker (1981), Townsin et al. (1981) and Granville (1987) are some of the studies which investigate the roughness effects of clean coatings, especially on SPC TBT systems, on the frictional resistance since SPC TBT was by far the most effective antifouling coating at that time.

Candries (2001) and Candries and Atlar (2004) compared the hydrodynamic characteristics of two different coatings, one being TBT-free SPC and the other being foul release silicone elastomer, using both boundary layer measurements and towing tests of flat plates. Candries et al. (2001a) and Candries et al. (2001b) presented towing tests of 2.55 m long plates and 6.3 m long plates, respectively, coated with TBT-free SPC and foul release coatings. The average advantage of the use of the foul release coatings over the use of the TBT-free SPC was measured to be 1.41% by Candries et al. (2001a) and 1.4% by Candries et al. (2001b). The difference can be

attributed to the difference in plate length. Candries et al. (2003b) examined the effect of antifouling coatings on cylindrical surfaces and flat plates.

Schultz (2002) carried out towing tests of flat painted plates smoothened by sanding. The results were interesting since the average roughness height was found to be sufficient to explain the majority of roughness functions for these surfaces using a Colebrook-type roughness function. Likewise, Schultz (2004) experimentally investigated the effects of the surface roughness of several coatings and biofouling on ship resistance and powering. Firstly, different coatings were applied to flat plates, and towing tests were conducted to obtain the frictional resistance and roughness functions of clean coatings. The flat plates bearing different coatings were then exposed to the sea for 287 days under static conditions. Afterwards, the fouling accumulation on the different coatings was recorded and the towing tests were repeated to correlate the fouling conditions to the roughness functions and hence frictional resistance. Additionally, Schultz (2004) conducted experiments after the cleaning of the flat plates to investigate the effect of cleaning on a ship hull. The results indicated that the roughness functions of sandpaper surfaces can be explained using a Nikuradse-type roughness function for uniform sand, given by Schlichting (1979). It was shown that the roughness functions of clean antifouling coatings may be represented by the Colebrook-type roughness function of Grigson (1992). Drag characteristics of a TBT SPC, a TBT-free SPC and a foul release coating were investigated by conducting rotating disk tests (Mirabedini et al., 2006). Lower frictional resistance characteristics of foul release coatings compared to the other SPCs were recorded, as expected. Examples of other rotary experimental studies are Weinell et al. (2003), Tanaka et al. (2003), Ghani et al. (2010) and Mieno (2012). Recently, Ünal et al. (2012) measured the turbulent boundary layer properties of flat plates coated with several types of coating, as well as two control surfaces, whereas boundary layer and frictional drag force measurements on an axisymmetric body apparatus coated with the same coatings were made by Atlar et al. (2012). Boundary layer measurements on surfaces coated with novel and state-of-the-art commercially in use coatings were made by Ünal (2012). Izaguirre-Alza et al. (2010) also conducted experiments with plates coated with two different coatings, namely a conventional and a silicone-based paint. According to the ITTC (2014a), Kawashima

et al. (2012) conducted towing tests of flat plates that have roughness due to the presence of paint.

Each type of roughness, including different types of paint, has its own unique surface properties and hence different effects on the frictional resistance. Therefore, experiments are required to identify such effects for the time being. Having said that, the theoretical and numerical models can then be employed to predict these effects on the frictional resistance of any body covered with the same roughness, once the roughness functions of such surfaces are obtained experimentally.

Theoretical and numerical studies exist in the literature to predict the roughness effects of coatings and biofouling on frictional resistance. Granville (1958) and Granville (1978) proposed a similarity law scaling procedure for the prediction of the roughness effects of a particular roughness on the frictional resistance of any arbitrary body covered with the same roughness, utilising the experimentally obtained roughness functions of such roughness. The only real assumption of the method is that the outer layer similarity holds in the mean velocity profiles for smooth and rough-wall boundary layers. That is to say, the velocity-defect profiles collapse to a single curve in the outer layer. Some examples of the use of this method are given by Loeb et al. (1984), Haslbeck and Bohlander (1992), Schultz (1998), Schultz (2002), Schultz (2004), Shapiro (2004), Schultz (2007), Flack and Schultz (2010) and Schultz et al. (2011). Grigson (1985a) proposed a method which is partly experimental and partly theoretical, just like the ones proposed by Granville (1958) and Granville (1978). Some numerical methods were also proposed for general rough surfaces rather than hull roughness, such as Christoph and Pletcher (1983), Lakehal (1999) and Grégoire et al. (2003).

When it comes to CFD-based models, there are fewer studies investigating the roughness effects of coatings and biofouling on ship resistance. Patel (1998) mentioned that the most complex problems for CFD are full scale Reynolds number flows and simulating surface roughness. Currently, physical modelling of the roughness sources, such as coatings or biofouling, in CFD is practically impossible due to their complex geometries. However, once the relation of $\Delta U^+ = f(k^+)$ is known, it can be employed in the wall-function or the turbulence models of the CFD

software, as discussed by Patel (1998). The use of CFD-based unsteady RANS models is of vital importance, since the phenomenon can be simulated by means of a fully non-linear method. For instance, one particular roughness Reynolds number value, k^+, and roughness function value, ΔU^+, are taken into consideration when a prediction is made for a specific condition in the similarity law scaling procedure of Granville (1958). However, the k^+ vs. ΔU^+ value is not uniform even on a flat plate due to differences in the friction velocity, u_τ, distribution. That is to say, u_τ varies along the flat plate. This effect, however, can be simulated using CFD-based models as u_τ is dynamically computed for each discretised cell. Therefore, the resulting frictional resistance can be more accurately computed using CFD methods.

Several studies exist which model the effects of a uniform sand-grain roughness, though not necessarily the hull roughness, either using wall-functions (e.g. Suga et al. (2006), Apsley (2007)) or using near-wall resolution (e.g. Krogstad (1991), Aupoix (2007)). Eça and Hoekstra (2011) showed that the effect of uniform sand-grain roughness on the frictional resistance of flat plates of full-scale ship lengths at full-scale ship speeds can be accurately simulated using either wall-functions or near-wall resolution. Date and Turnock (1999) demonstrated the required techniques to predict the skin friction of flat plates using RANS solvers and also showed that the effect of surface roughness on skin friction can be predicted using CFD software. They modified the wall-functions of a piece of commercial CFD software by modifying the wall function-coefficient (log-layer constant). Nevertheless, this method does not directly reflect the roughness effect on the frictional resistance and does not compute these effects dynamically. Leer-Andersen and Larsson (2003), on the other hand, employed roughness functions in a commercial CFD code and predicted the skin friction of full scale ships. However, they used a specific module of the software, which incorporates thin boundary layer methods with a potential flow solver, and the study does not include unsteady RANS calculations. Izaguirre-Alza et al. (2010) used the CFD software package STAR-CCM+ to simulate their experiments and validate the roughness feature of the software. Although the comparison shows a very good agreement between the experimental data and the evaluated results, there is no evidence of the use of a specific roughness function model, rather than the built-in roughness function. Khor and Xiao (2011)

investigated the effects of fouling and two antifouling coatings on the drag of a foil and a submarine by employing a CFD method. They used the equivalent sand grain roughness height and the built-in wall-function which considers the uniform sand-grain roughness function model proposed by Cebeci and Bradshaw (1977), based on Nikuradse's data (1933). Currently, the ITTC (2011a) is still questioning the validity of the roughness model and equivalent sand grain roughness used in CFD applications for hull roughness, since it is known that the built-in roughness function model is based on uniform, closely packed sand roughness, whereas the roughness functions of real engineering surfaces do not show this behaviour. Castro et al. (2011) carried out unsteady RANS CFD simulations of a full-scale KCS model with hull roughness using wall-functions. However, they used a constant roughness function without justifying the reasons for this, and they also used the dubious roughness allowance formulation proposed by the ITTC (1990). They also used the uniform sand-grain roughness approach, which is prevalently used by others, and did not attempt to employ a new type of roughness function model which is more appropriate for real engineering surfaces, especially for marine coatings or fouled surfaces.

2.6 Determination of Roughness Functions

Roughness functions are of practical importance, since the frictional resistance of any structure covered with a specific roughness can be predicted using a boundary layer method, once the roughness functions of such roughness are known (Granville, 1985, 1987). Due to the fact that there is no universal roughness function for all roughness types, the roughness functions and the behaviour of the roughness function model need to be determined for individual roughness types.

The determination of roughness functions can be realised by means of direct and indirect methods. The experimental measurement of the velocity profile in a boundary layer in a flow facility (the velocity profile method) is termed the direct method (Granville, 1987). The indirect methods are generally simpler and more appropriate compared to the direct methods in terms of economy. According to Granville (1987), Nikuradse (1933) reported the very first indirect method for the

determination of the roughness functions of a pipe with sand-grain roughness. He also used a direct method along with the aforementioned indirect method and the agreement between these was excellent.

Granville derived or rederived many indirect methods, including the local method with displacement thickness (Granville, 1987) based on the work of Hama (1954), the overall (towed plate) method (Granville, 1958), the rotating disk method (Granville, 1982), a local method without displacement thickness (Granville, 1987) and the indirect method for pipes.

The towed plate method of Granville (1958) was used to determine the roughness functions of the surfaces in question in this study (Chapter 4). For this reason, more detailed information and a review are given for the overall method at the end of this section.

The local method with displacement thickness involves measurements of the displacement thicknesses and skin friction coefficients, c_f, of both a smooth and rough surface. The roughness functions can then be obtained by subtracting U^+_{rough} from U^+_{smooth} at the same value of displacement thickness Reynolds number, $Re_{\delta*}$, as given by (2.30):

$$\Delta U^+ = \left(\sqrt{\frac{2}{c_f}}\right)_S - \left(\sqrt{\frac{2}{c_f}}\right)_R \qquad \textbf{(2.30)}$$

where the subscript *S* indicates a smooth condition, whereas the subscript *R* indicates a rough condition.

The local method without displacement thickness involves measurements of the skin friction coefficients and the Reynolds numbers of both a smooth and rough surface. The roughness functions can then be obtained by comparing the c_f values of smooth and rough surfaces at the same value of $R_{eL}c_f$, as given by (2.31).

$$\Delta U^+ = \left(\sqrt{\frac{2}{c_f}}\right)_S - \left(\sqrt{\frac{2}{c_f}}\right)_R - 19.7\left[\left(\sqrt{\frac{c_f}{2}}\right)_S - \left(\sqrt{\frac{c_f}{2}}\right)_R\right] \qquad \textbf{(2.31)}$$

The rotating disk method involves measurements of the torque and rotary speed of both a smooth and rough rotating disk. The roughness Reynolds numbers, k^+ and roughness functions, ΔU^+, can then be obtained by comparing the torque coefficients, $C_{m,}$ of smooth and rough surfaces at the same value of $R_{eR}(C_m)^{1/2}$, as given by (2.32) and (2.33), respectively,

$$k^+ = \left(\frac{k}{R}\right)\sqrt{\frac{5}{8\pi}}\,\mathrm{Re}_R\sqrt{C_m}\left\{1-\left[\frac{2}{\kappa}-\Delta U^{+'}\right]\left(\sqrt{\frac{C_m}{40\pi}}\right)_R\right\} \tag{2.32}$$

$$\Delta U^+ = \sqrt{\frac{8\pi}{5}}\left[\left(\frac{1}{\sqrt{C_m}}\right)_S-\left(\frac{1}{\sqrt{C_m}}\right)_R\right]+\frac{1}{5}+\Delta U^{+'} \tag{2.33}$$

where k is roughness length scale, R is the disk radius, R_{eR} is the disk Reynolds number and $\Delta U^{+'}$ is the roughness function slope, which is the slope of ΔU^+ as a function of $ln(k+)$. The reader should note that the roughness function slope, $\Delta U^{+'}$, is unknown in both equations (2.32) and (2.33). An iterative procedure is therefore performed to solve the equations.

The indirect method for pipes involves measurements of the pressure drop and the average velocity, V, of both a smooth and rough pipe. The roughness functions can then be obtained by comparing the Fanning friction factors, f, of smooth and rough surfaces at the same value of $R_e\sqrt{f}$, as given by (2.34),

$$\Delta U^+ = \left(\sqrt{\frac{2}{f}}\right)_S-\left(\sqrt{\frac{2}{f}}\right)_R \tag{2.34}$$

where

$$f = \frac{2\tau_\omega}{\rho V^2} \tag{2.35}$$

The details of the towed plate method was given by Granville (1987) following his earlier studies (Granville, 1958). The procedure involves towing tests of flat plates covered with any roughness. Once the C_F values of a surface are evaluated for a

range of speeds, the roughness functions can be computed iteratively. The most important point of the procedure is that the flat plate has to be exposed to a zero pressure gradient.

k^+ and ΔU^+ for the surfaces can be obtained iteratively using (2.36) and (2.37) (Granville, 1987) using the experimental data.

$$k^+ = \left(\frac{k}{L}\right)\left(\frac{\mathrm{R}_{eL}\, C_F}{2}\right)\left(\sqrt{\frac{2}{C_F}}\right)_R \left[1 - \frac{1}{\kappa}\left(\sqrt{\frac{C_F}{2}}\right)_R + \frac{1}{\kappa}\left(\frac{3}{2\kappa} - \Delta U^{+'}\right)\left(\frac{C_F}{2}\right)_R\right] \qquad \textbf{(2.36)}$$

$$\Delta U^+ = \left(\sqrt{\frac{2}{C_F}}\right)_S - \left(\sqrt{\frac{2}{C_F}}\right)_R - 19.7\left[\left(\sqrt{\frac{C_F}{2}}\right)_S - \left(\sqrt{\frac{C_F}{2}}\right)_R\right] - \frac{1}{\kappa}\Delta U^{+'}\left(\sqrt{\frac{C_F}{2}}\right)_R \qquad \textbf{(2.37)}$$

where L is the plate length, R_{eL} is the plate Reynolds number, C_F is the frictional drag coefficient, $\Delta U^{+'}$ is the roughness function slope, which is the slope of ΔU^+ as a function of $ln(k+)$, and the subscript S indicates a smooth condition whereas the subscript R indicates a rough condition. The C_F values of smooth and rough conditions are the values at the same value of $R_{eL}C_F$ as explained by Schultz (1998) and shown by Granville (1987) (Figure 2.12) using the data of Couch (1951).

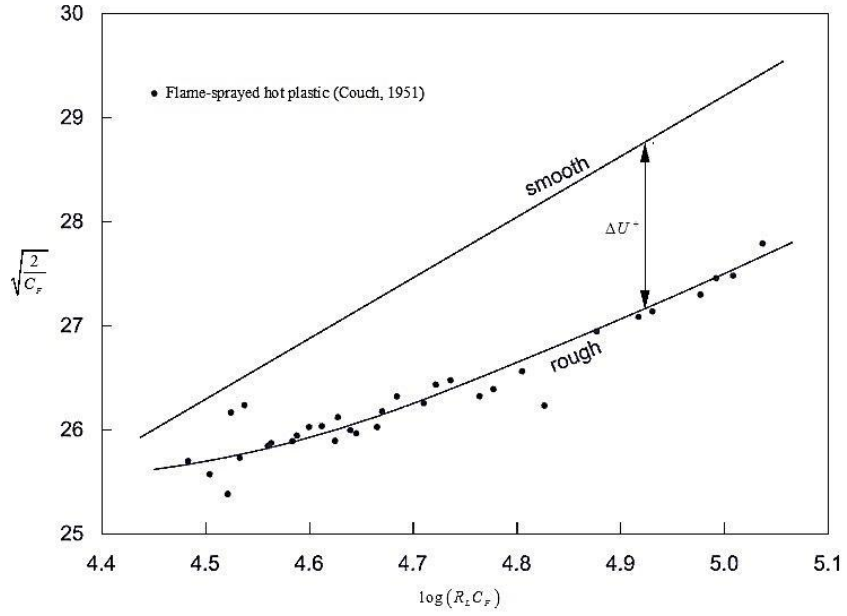

Figure 2.12: Overall method, adapted from Granville (1987).

The selection of the roughness length scale is critical to define a roughness function model, though the selected roughness height does not affect the roughness function value - it only affects the abscissa of the profile of roughness functions against roughness Reynolds numbers. For this reason, the roughness length scale can be selected such that the roughness function values fall on a pre-defined roughness function model, provided that the observed behaviours are still deemed appropriate relative to each other. Shown for comparison in Figure 2.13 are the roughness functions against roughness Reynolds numbers for the same surface, with values plotted for two different roughness length scales, namely k1 and k2 (Demirel et al., 2014a)

Schultz and Myers (2003) obtained the roughness function values of different surfaces using three different methods, namely the velocity profile, towed plate and rotating disk methods. They used $0.75R_t$ and $0.39R_a$ as roughness length scales for sandpaper surfaces and epoxy surfaces, respectively. The results of the study were given in Figure 2.14 together with the Nikuradse-type roughness function for uniform sand given by Schlichting (1979) and with the Colebrook-type roughness function of Grigson (1992). It is evidently seen from the results that there is a very good agreement between the overall method and velocity profile method. These results suggest that the indirect methods can be used in order to precisely evaluate the roughness functions. Additionally, the overall method is referred to as the best combination of accuracy and complexity by the ITTC (2011b).

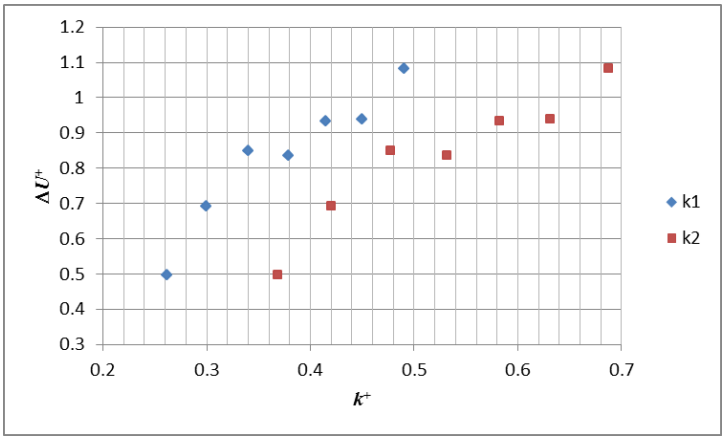

Figure 2.13: Roughness function vs. roughness Reynolds numbers for two different roughness height selections (Demirel et al., 2014a).

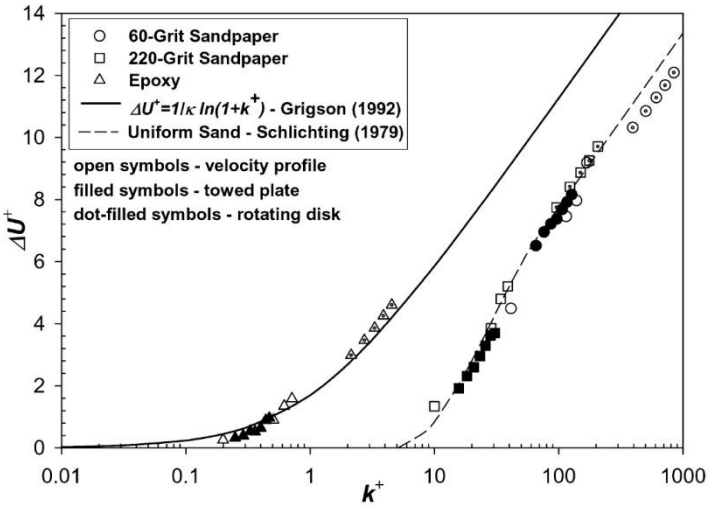

Figure 2.14: Roughness functions for the test surfaces obtained using the velocity profile, towed plate and rotating disk methods (Schultz and Myers, 2003).

It is important to note that the thickness of flat plate used for the towed plate method should be kept as small as possible since the pressure drag due to the thickness of the plate is generally assumed to be negligible (Candries (2001) and Schultz (2004)) and the calculations of the frictional resistance are made based on this assumption. Therefore, the thickness of the flat plate was chosen to be 3.2 mm by Schultz (2002, 2004) and Schultz and Myers (2003) whereas this was chosen to be 50 mm by Candries (2001) and Usta and Korkut (2013). This author believes that the assumption which proposes that the pressure drag of the plate is negligible may not be valid for the plates used by Candries (2001) and Usta and Korkut (2013) as the pressure drag arises due to the thickness of the plate.

Another point to be discussed is the selection of the plate length and towing speed. Longer plates or higher towing speeds enable higher Reynolds numbers to be achieved. A higher Reynolds number obtained at the model scale enables extrapolations to be made at a higher Reynolds number at full-scale.

Therefore, the length of the towing tank and maximum towing speed should be taken into account when choosing the length of the plate. In addition, the thickness of the flat plate is also determined by the length of the plate since a flat plate with a very high length to thickness ratio would be subjected to bending easily and this would cause experimental errors.

The dimensions of the flat plates used in Chapter 4 were therefore chosen considering all these conflicting parameters and a fair compromise was achieved.

2.7 Chapter Summary and Conclusions

The available literature on modelling the roughness effects of marine coatings and biofouling was reviewed and the gaps in the literature were determined. The important conclusions are listed below:

- The ITTC strongly recommends the development of new methods towards the accurate prediction of the added resistance due to coatings and hull fouling.

- Each kind of surface condition, such as coatings or fouled surfaces, has its own properties, the drag characterisation of which must be performed.

- No study exists which investigates the as applied drag performances of newly developed FOUL-X-SPEL coatings or compares the as applied drag performances of such coatings with uncoated hull surfaces.

- No specific diagram exists to predict the roughness effect of coatings and biofouling on ship frictional resistance.

- No specific CFD-based URANS models exist for the prediction of the roughness effects of marine coatings and biofouling on ship frictional resistance.

- No specific URANS CFD simulation has been performed to investigate the roughness effects of marine coatings or biofouling on the resistance of full-scale ship hulls.

3 Methodology

3.1 Introduction

This chapter depicts the methodology of this thesis.

3.2 Methodology

Although each chapter includes details of its own methodology, it would be beneficial to demonstrate the general methodology followed within this study, in order to demonstrate the bigger picture to the reader. The methodology followed in this thesis is therefore depicted in Figure 3.1.

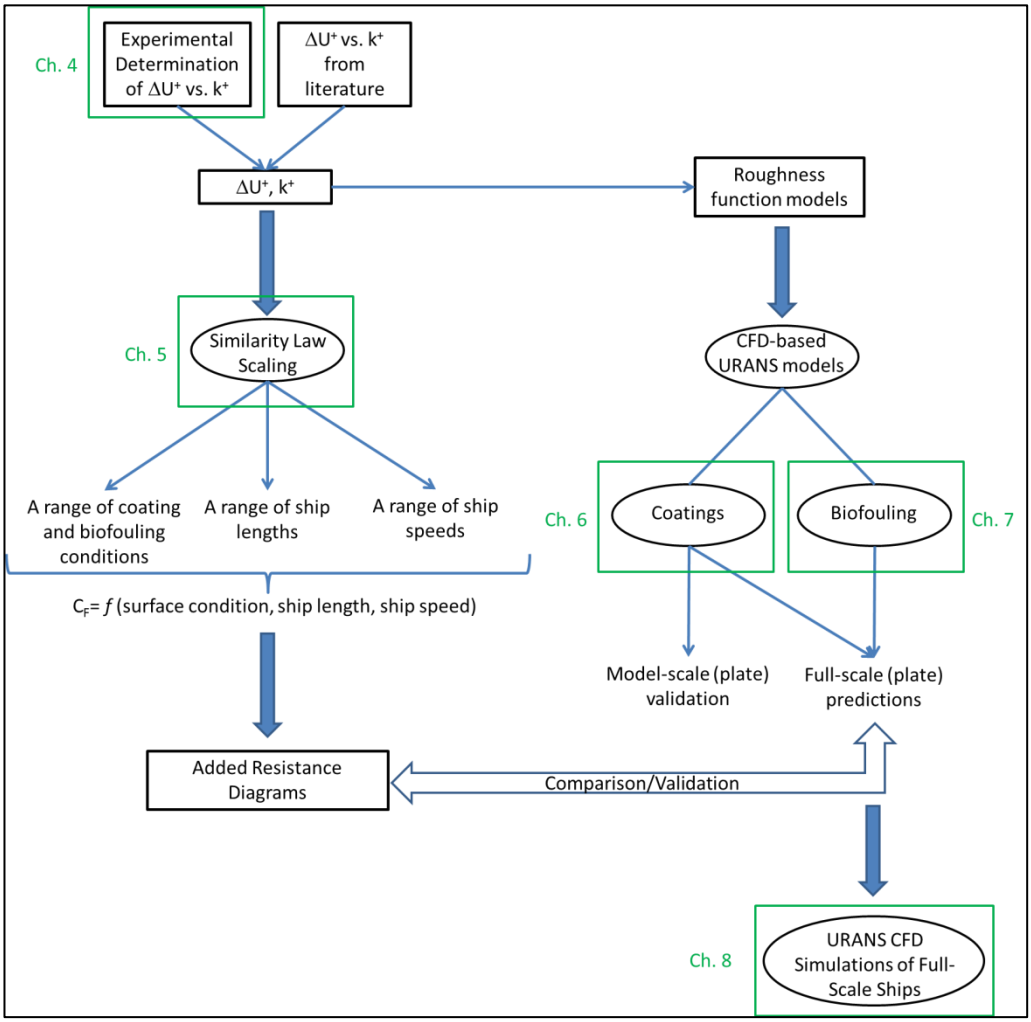

Figure 3.1: The methodology followed in this thesis.

The first requirement for the prediction of the effect of any roughness on the frictional resistance of any arbitrary body is to determine the roughness functions, ΔU^+, and roughness Reynolds numbers, k^+, of the surfaces in question.

In order to determine the roughness functions of several marine coatings, including the new FOUL-X-SPEL paints and control surfaces, towing tests of flat plates coated with these coatings are performed using Granville's (1987) overall method. This technique also enables the resistance characteristics of such coatings to be compared with an uncoated ship hull condition, rather than with only a smooth surface. The pairs of roughness functions and roughness Reynolds numbers for the novel paints developed within the FOUL-X-SPEL Project, and for the existing commercial paints are therefore experimentally obtained as presented in Chapter 4.

An in-house code based on the similarity law scaling procedure of Granville (1958) is developed and presented in Chapter 5, in order to enable predictions of the roughness effects of several coatings, including the novel FOUL-X-SPEL paints, and different fouling conditions on the frictional resistances of flat plates representing ships. The roughness function and roughness Reynolds numbers obtained in Chapter 4 using towing tests, for both the novel paints developed within the FOUL-X-SPEL Project and for existing commercial paints, are employed in the code. This enables the roughness effects of these coatings on full-scale ship frictional resistance to be predicted. Moreover, the roughness function and roughness Reynolds number pairs of Schultz and Flack (2007) representing a typical coating and different fouling conditions are employed in the code and predictions are made for various fouling conditions. Added frictional resistances of a range of flat plates at a range of ship speeds due to a variety of representative coating and fouling conditions are therefore obtained. Added resistance diagrams are then generated using these predictions. These diagrams are used for the validation of the CFD models proposed in Chapters 7 and 8.

The applicability of the CFD approach as an alternative technique with which to predict the roughness effects of coatings and biofouling on ship resistance is investigated using three steps, each of them presented in Chapter 6, Chapter 7 and Chapter 8, respectively. It is of note that the representative roughness function

models are used in the entire CFD work in this thesis, rather than using the roughness function and Roughness Reynolds number pairs directly.

In order to develop and propose a CFD model which enables the prediction of the effect of antifouling coatings on frictional resistance, a Colebrook type, monotonic roughness function model is chosen in Chapter 6 to represent the roughness functions and roughness Reynolds numbers of several coatings, which are taken from the literature. This roughness function model is employed in the CFD solver and a validation study is carried out by performing CFD simulations of towing tests of flat plates coated with several marine coatings. The obtained numerical results are then compared with the experimental data given in the literature. Predictions for flat plates of ship lengths are then made using the proposed CFD model and the results are compared with those obtained using similarity law scaling.

In order to develop and propose a CFD model which enables the prediction of the effect of biofouling on frictional resistance, a new inflectional roughness function model is proposed and employed in the solver in Chapter 7. The roughness function and roughness Reynolds number pairs of Schultz and Flack (2007) are used to develop a roughness function model to be employed in the CFD software to represent the coating and fouling conditions given by Schultz (2007). This is achieved by fitting an analytical equation to the roughness function and roughness Reynolds number pairs of Schultz and Flack (2007). Numerical simulations of towing tests of flat plates of ship lengths, hypothetically coated with a typical AF coating and covered with different fouling conditions, are performed using the proposed model. The results are compared with the results obtained in Chapter 5 to assess the applicability of the CFD approach.

Finally, in Chapter 8, the developed and proposed CFD approach is used, and CFD simulations of the roughness effects of marine coatings and biofouling on the resistance of a full-scale 3D KCS model are performed to assess the validity of the CFD approach on ship hulls, rather than on flat plates. The computed results are compared to the results obtained in Chapter 7 to investigate the applicability of the wall function approach to simulate the surface roughness on ship hulls, rather than on flat plates, since the pressure gradient varies significantly along ship hulls. In

addition, the results are compared to the results obtained in Chapter 5 using the similarity law scaling procedure to investigate the applicability of the CFD approach.

It can be seen from Figure 3.1 and the explanations above that each main chapter has interactions with the other chapters and they are all tied up within the general scope of the study, while each of them independently presents a novel study of its own.

3.3 Chapter Summary

The general methodology followed has been presented in this chapter.

4 Experimental Determination of the Roughness Functions of Marine Coatings

4.1 Introduction

The roughness of a hull's surface significantly affects the flow and frictional resistance of a ship. The main contribution to hull roughness can be attributed to marine biofouling. For this reason, several types of antifouling coating systems are in widespread use to mitigate marine biofouling, thus reducing ship resistance and power requirements. Having said that, an antifouling coating system itself has an initial surface roughness which affects a ship's frictional resistance; this initial roughness may ease the settlement of slime and subsequent marine organisms compared to an otherwise so-called smooth surface. A means of assessing the effect of the initial roughness of such a coating on resistance would therefore be of great benefit.

This study presents the results from resistance tests of flat plates coated with different marine coatings, including new paints developed within the FOUL-X-SPEL Project, two existing, commercial coatings, and two control surfaces. To the best of this author's knowledge, no experimental study exists which compares the drag performances of antifouling surfaces with that of an uncoated ship hull condition. One of the aims of the present study is also to compare the resistance characteristics of the coatings with the ship hull, rather than only with a smooth surface.

6 different surface conditions are considered in the experiments given below:

- Reference Plate (sanded and polished)
- Hempel's Antifouling Olympic+ 72950 (FoulXSpel 2)
- New FOUL-X-SPEL Polyurethane system with an immobilised biocide (F0037)

- New FOUL-X-SPEL Silicone system with an immobilised biocide (F0034)
- Hempasil X3 87500 (FoulXSpel 1)
- Grit-blasted surface (Hull)

Tests were carried out at the Kelvin Hydrodynamics Laboratory (KHL) of the University of Strathclyde.

It is important to note that the present experiments were conducted using flat plates, based on the major assumption of Froude, which proposes that the skin friction of a hull is equal to that of a flat plate of the same length and area as the wetted surface of the ship (Lackenby, 1962). It is therefore convenient to choose a flat plate, as the surface roughness affects only the skin friction of a ship.

Details of the experiments conducted in this study, namely experimental facilities, model details, roughness measurements, test methodology and repeatability and uncertainty estimates are outlined below. The results of the experiments then are given separately for the total and frictional resistance coefficients and discussed in detail. Afterwards, an evaluation of roughness functions and roughness Reynolds numbers of the test surfaces is presented.

4.2 Experimental Facilities

As mentioned earlier, the experiments were carried out at the Kelvin Hydrodynamics Laboratory (KHL) of the University of Strathclyde. The KHL test tank has dimensions of 76.0 m x 4.6 m x 2.5 m. The tank is equipped with a digitally-controlled towing carriage, state-of-the-art absorbing wavemaker, and a highly effective sloping beach. Figure 4.1 and Figure 4.2 show photos of the facility.

The carriage has a velocity range of 0 – 5 m/s, with the velocity range used in these experiments kept between 1.5 and 3.6 m/s. Fresh water was used in the experiments. The temperature of the water was monitored during the experiments in order to be able to evaluate drag coefficients according to the temperature.

Figure 4.1: The KHL tank.

Figure 4.2: The KHL towing carriage.

The overall drag values of each plate were measured using displacement transducers using the Linear Variable Differential Transformer (LVDT) principle. These brand new transducers were purchased to ensure sensitive measurements of the resistance values, as well as to minimise the cross coupling of drag and side forces, since the differences of the resistance values between different surfaces were expected to be very small. It is of note that two transducers were used in the experiments; one for measuring the overall drag of the plates and one for checking the side forces. The

intention was to keep the side forces effectively zero, to ensure the alignment of the plates.

Before the transducers were set on the plates, they were calibrated. This was performed by hanging weights of known magnitude from the gauges and recording the output voltages for each weight. Figure 4.3 shows the setup for this calibration.

Figure 4.3: Calibration of transducers.

These two transducers were calibrated separately across the expected load range. It should be noted that the expected loads were predicted using CFD simulations similar to those performed in Chapter 6. The calibration factors were evaluated by obtaining the relationship between the load and output voltage. The relation between the known loads and output voltages are seen in Figure 4.4 for the drag transducer and in Figure 4.5 for the side force transducer.

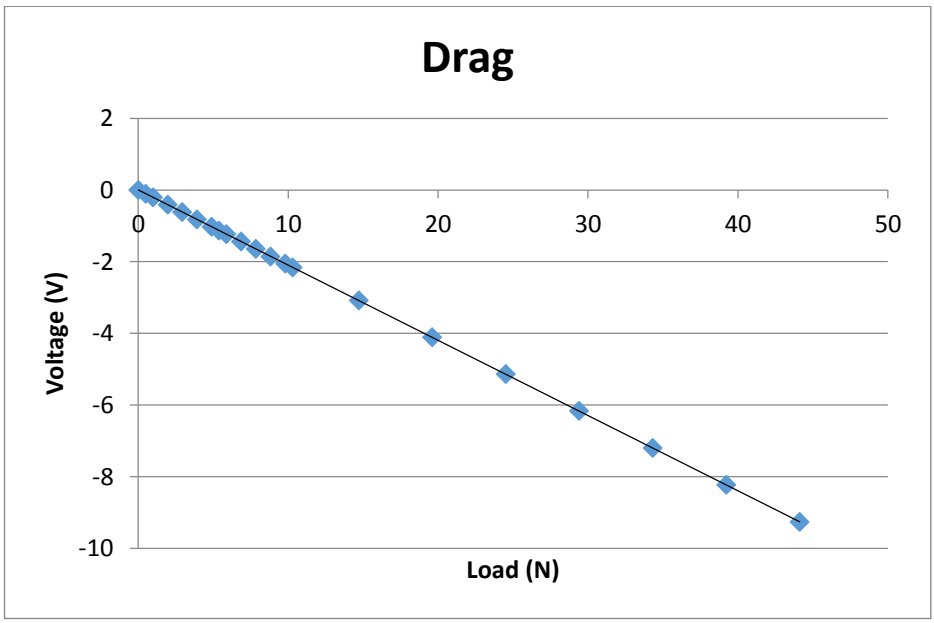

Figure 4.4: Calibration curve of the drag transducer.

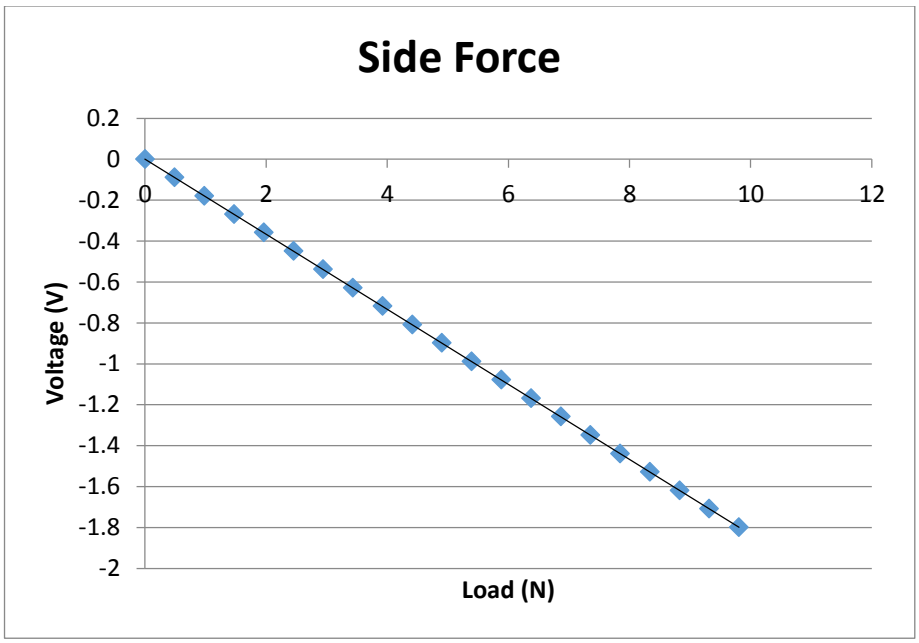

Figure 4.5: Calibration curve of the side force transducer.

4.3 Model Details and Preparations

The flat plates used for the tests were manufactured from 304 stainless steel sheet stock. Figure 4.6 depicts the dimensions of the flat plates. The leading edges of the plates were filleted to a radius of 2.5 mm while the trailing edge was kept sharp in order to mitigate the extra drag due to the separation as much as possible.

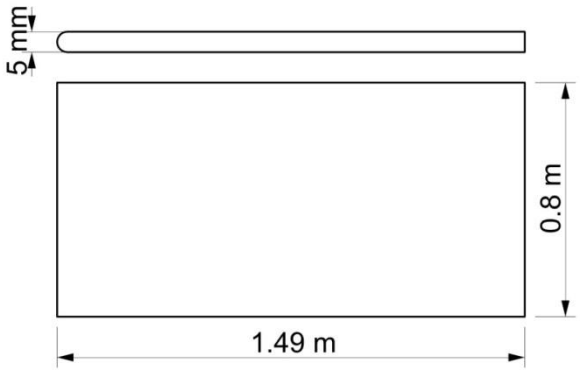

Figure 4.6: Dimensions of the flat plates.

The flatness of the plates, as well as their dimensions, were checked using a CNC machine. Figure 4.7 shows a view from one such flatness check.

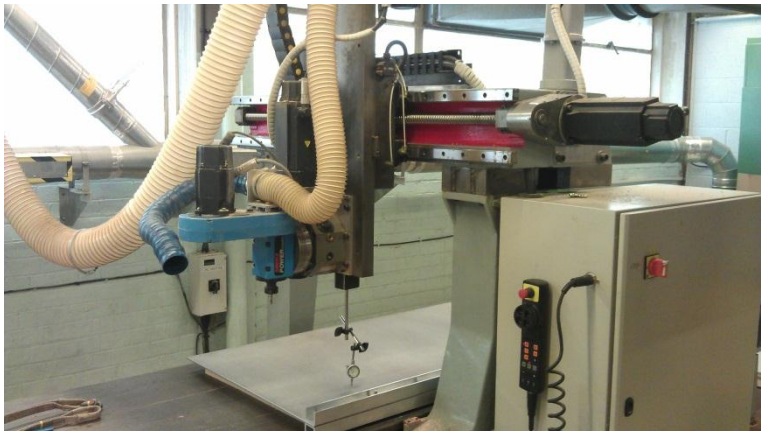

Figure 4.7: Checking the flatness of the plates.

In total, 6 plates were manufactured in order to test different surface conditions. The surface conditions of the plates used in the experiments are explained below:

The **Reference Plate** was sanded using an orbital sander with abrasive grit. 80 grit, 120 grit and 320 grit sandpapers were used, respectively, and the plate was then polished using a polishing compound. This was expected to serve as a smooth surface. The surface preparation of this plate was performed by staff at the KHL. Figure 4.8 shows the Reference Plate together with these staff members.

Figure 4.8: The Reference Plate.

The surface preparation and paint application for the remaining plates was performed according to the guidelines of HEMPEL by a professional paint company (Jerwin Coatings) based in Glasgow. Following a solvent wash to remove grease oil, the plates were grit blasted to Sa3 standard using aluminium oxide grit G17. Paints were then applied to each plate.

Plate 1 was coated with Hempel's Antifouling Olympic+ 72950 (FoulXSpel 2). From this point onward this plate is referred to as FoulXSpel 2. Figure 4.9 shows the preparation of FoulXSpel 2 for hanging.

Figure 4.9: Preparation of FoulXSpel 2.

Plate 2 was coated with a new FOUL-X-SPEL Polyurethane system with an immobilised biocide (F0037). From this point onward this plate is referred to as F0037 (Figure 4.10).

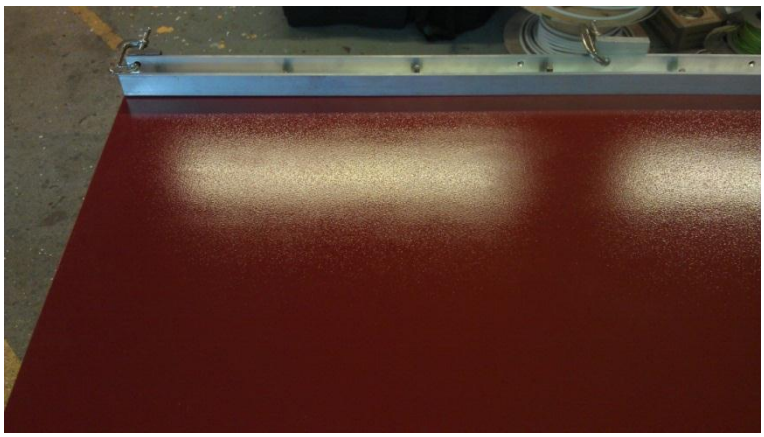

Figure 4.10: F0037.

Plate 3 was coated with a new FOUL-X-SPEL Silicone system with an immobilised biocide (F0034). From this point onward this plate is referred to as F0034.

Plate 4 was coated with Hempasil X3 87500 (FoulXSpel 1) which is a foul-release coating. From this point onward this plate is referred to as FoulXSpel 1.

Plate 5 was uncoated but grit blasted to Sa3. In other words, the surface preparation required for a coating application was performed, but it was left uncoated. This plate was used to replicate ship hulls without any paint. From this point onward this plate is referred to as Hull.

After the preparation of the plates, connection rigs were mounted at the top of the plates to hang them on the carriage. Figure 4.11 shows the connection holes in the top view of the plates.

Figure 4.11: Top view of the plates with connection holes.

Afterwards each plate was installed to the transducers rig on the towing carriage using nuts and bolts. Figure 4.12 shows the installation and Figure 4.13 shows the transducer of the Reference Plate. The ready to tow FoulXSpel 2 and Hull are shown

in Figure 4.14 and Figure 4.15. Figure 4.16 and Figure 4.17 show photos captured during the towing tests of FoulXSpel 2 at two different speeds.

Figure 4.12: Installation of the Reference Plate.

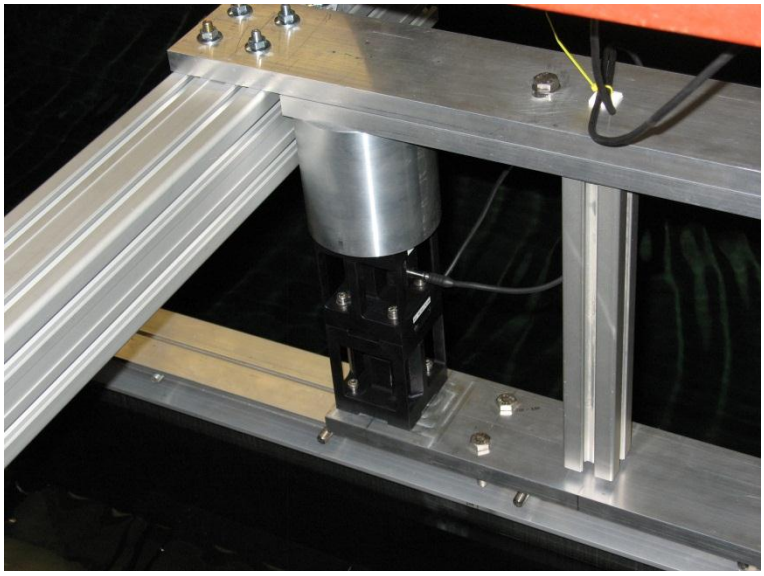

Figure 4.13: LDVT transducer on top of the Reference Plate.

Figure 4.14: FoulXSpel2 ready to tow.

Figure 4.15: Hull ready to tow.

Figure 4.16: FoulXSpel2 being towed at a low speed.

Figure 4.17: FoulXSpel2 being towed at a high speed.

4.4 Roughness Measurements

The average hull roughness (Rt_{50}) values of all test plates were measured before and after the towing procedure using a TQC Hull Roughness Gauge, which possesses a control unit and a sensor unit. The sensor unit has three non-slip wheels and a carbide tipped stylus (TQC, 2014). The sensor unit is moved horizontally over the plates. During this movement of the sensor unit, the maximum peak to trough roughness height over a 50 mm interval is measured. This is termed the Average Hull

Roughness (AHR) or Rt_{50}. The Rt_{50} range of the device is from 0 to 2500 μm with an accuracy of ±5μm or ±2% of the measured data, whichever is greater. A TQC Hull roughness Gauge is shown in Figure 4.18.

8 measurement lanes were selected on each side of the surfaces. 4 of them were from leading edge to trailing edge and the other 4 were from trailing edge to leading edge. Figure 4.19 shows the process of taking a roughness measurement of F0037.

Figure 4.18: TQC Hull Roughness Gauge.

Figure 4.19: Measurement of the roughness of F0037 using a TQC Hull Roughness Gauge.

The normalised histograms and probability density functions (pdf) of each surface were evaluated and are given below, from Figure 4.20 - Figure 4.31, respectively.

Figure 4.32 demonstrates the probability density functions (pdf) of the roughness data of all of the test surfaces.

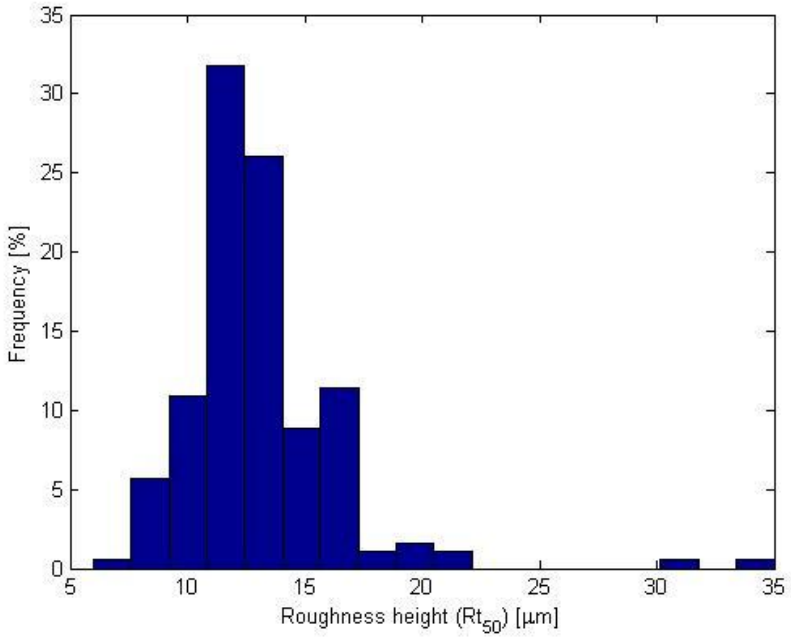

Figure 4.20: Normalised histogram of the roughness distribution of the Reference Plate.

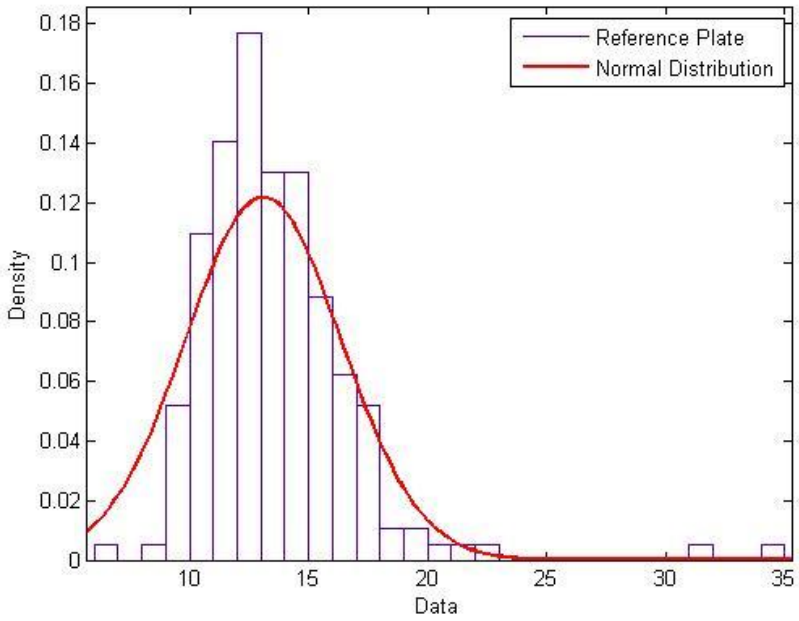

Figure 4.21: Probability density function (pdf) of the roughness data of the Reference Plate.

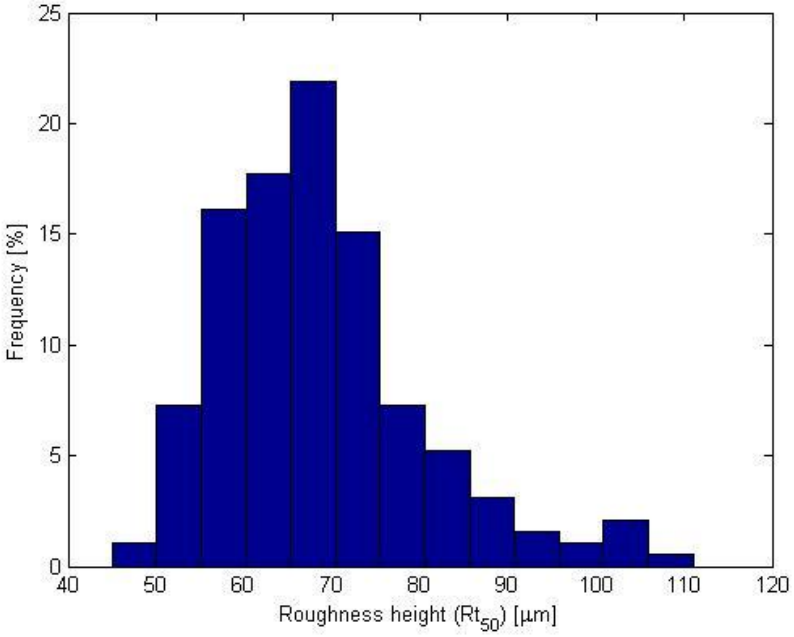

Figure 4.22: Normalised histogram of the roughness distribution of FoulXSpel 2.

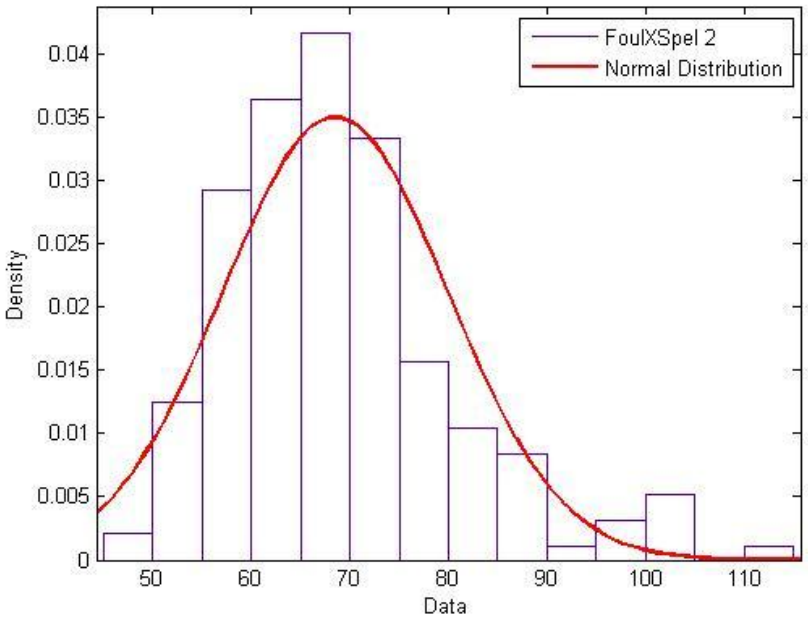

Figure 4.23: Probability density function (pdf) of the roughness data of FoulXSpel 2.

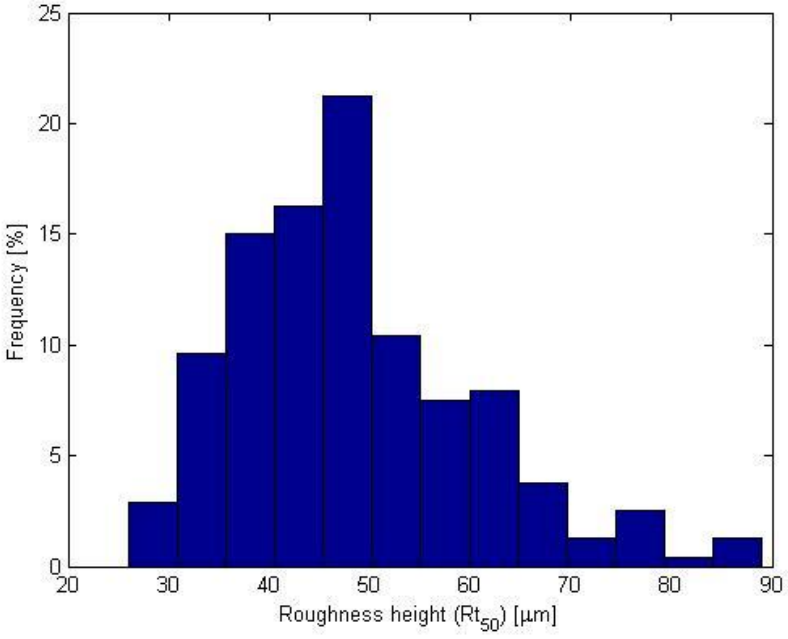

Figure 4.24: Normalised histogram of the roughness distribution of F0037.

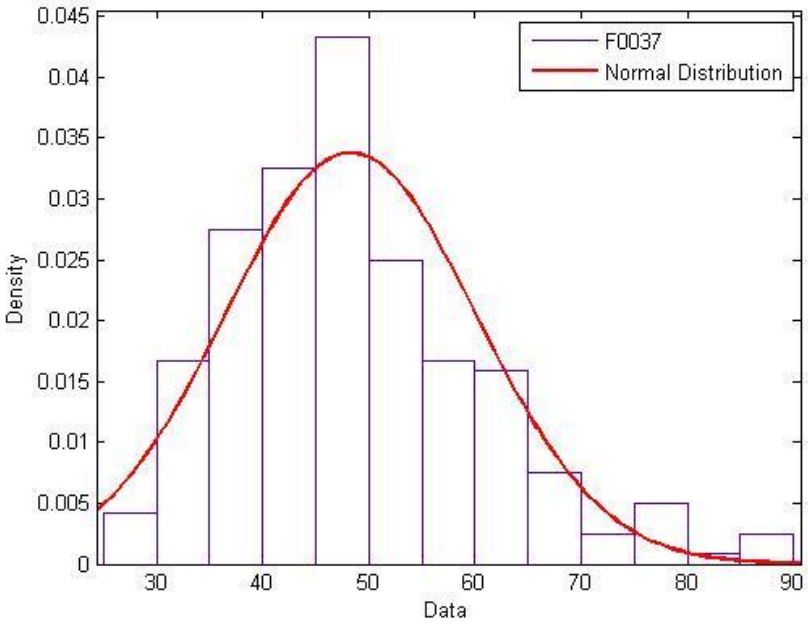

Figure 4.25: Probability density function (pdf) of the roughness data of F0037.

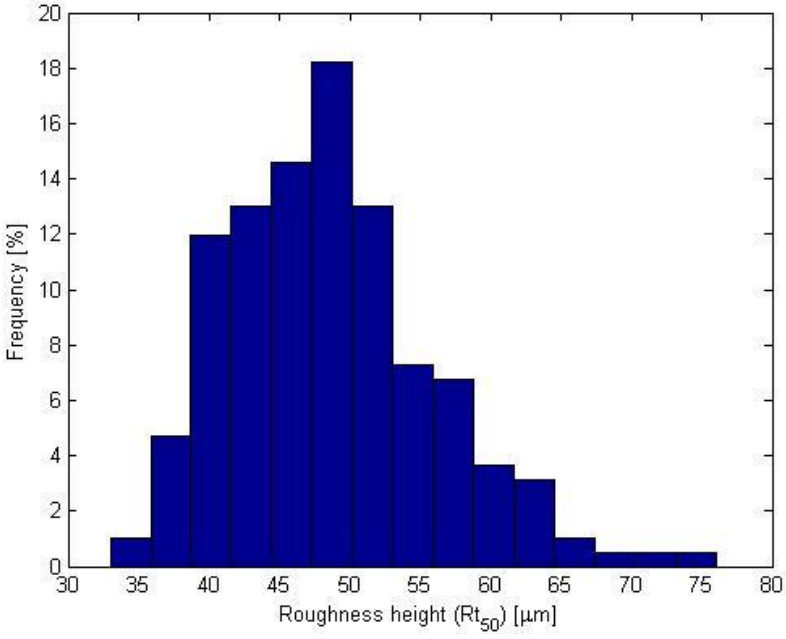

Figure 4.26: Normalised histogram of the roughness distribution of F0034.

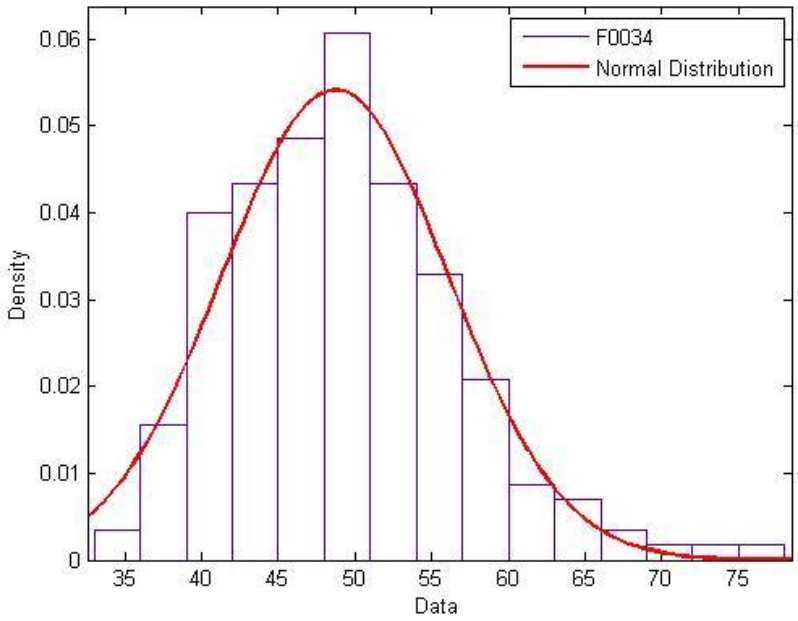

Figure 4.27: Probability density function (pdf) of the roughness data of F0034.

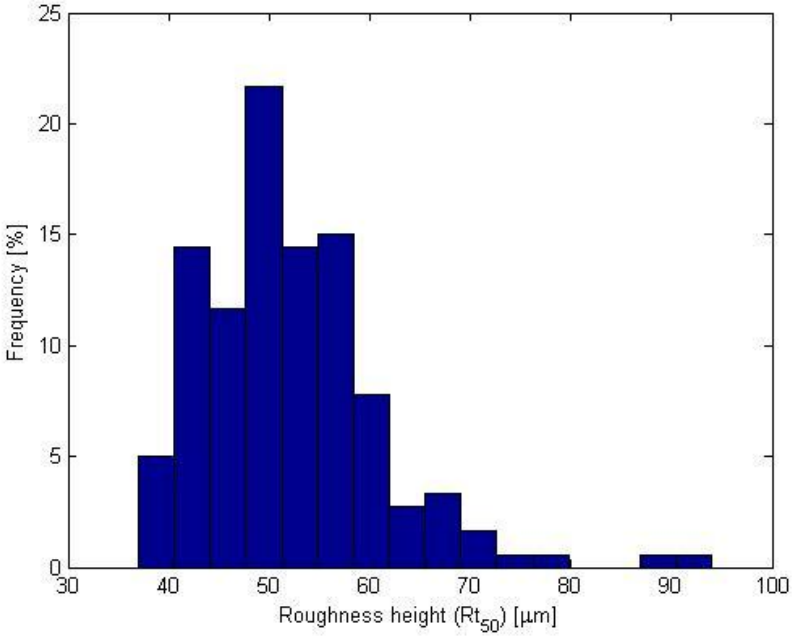

Figure 4.28: Normalised histogram of the roughness distribution of FoulXSpel 1.

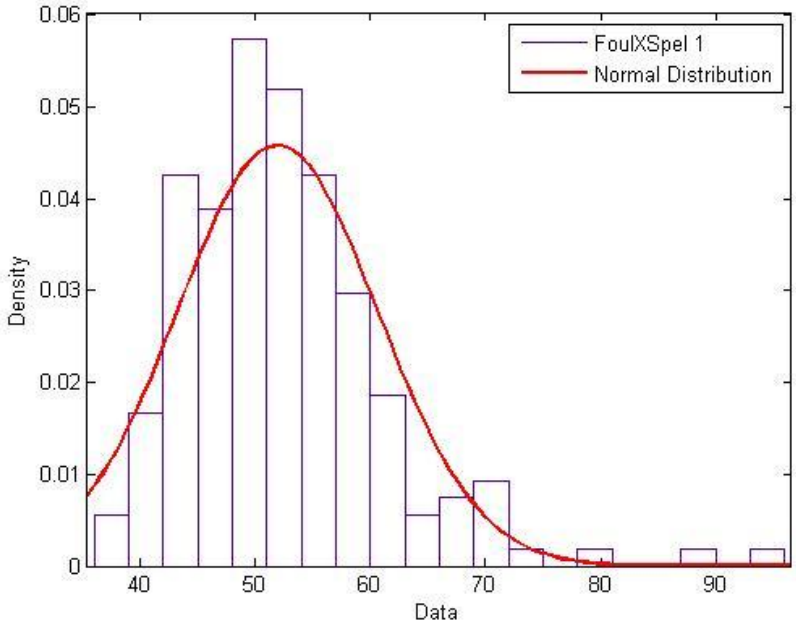

Figure 4.29: Probability density function (pdf) of the roughness data of FoulXSpel 1.

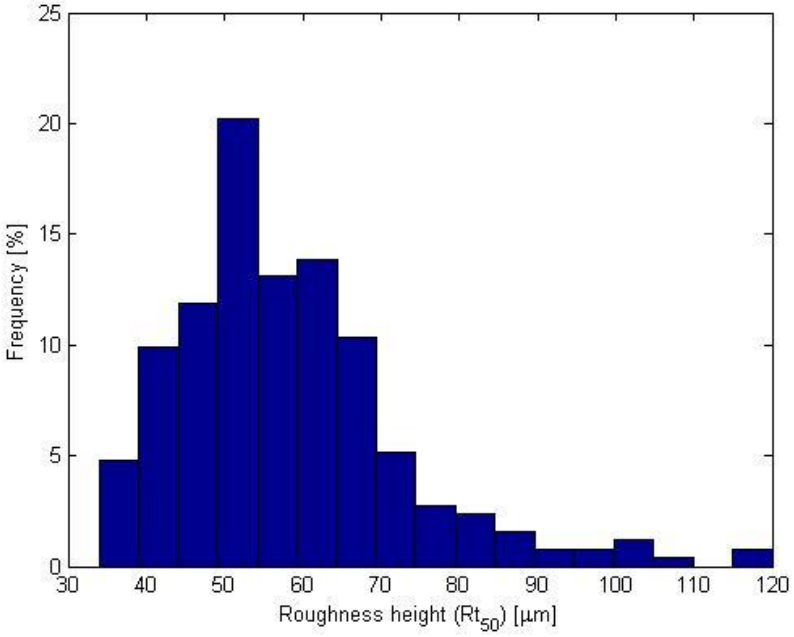

Figure 4.30: Normalised histogram of the roughness distribution of Hull.

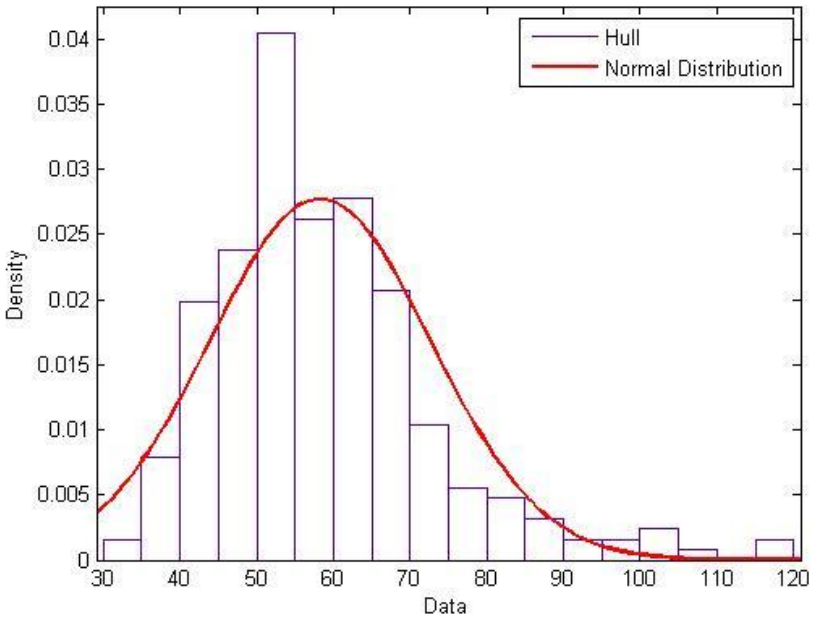

Figure 4.31: Probability density function (pdf) of the roughness data of Hull.

AHR values of each plate before towing are given in Table 4.1.

Table 4.1: Rt_{50} values of the plates.

Plate	Rt_{50} (μm)
Reference Plate	13±5
FoulXSpel 2	69±5
F0037	48±5
F0034	47±5
FoulXSpel 1	52±5
Hull	58±5

Normal distributions of the probability density functions of all of the test surfaces are shown together in Figure 4.32. As can be seen from Figure 4.32, the Reference Plate has a lower mean roughness height and the distribution of its roughness is narrower than that of the others. This is expected, since the Reference Plate was sanded using 320 grit sandpaper and then polished using a polishing compound. Hence, it was expected to be smooth, with a relatively homogenous roughness distribution.

FoulXSpel 2 has a higher mean roughness value than the other surfaces, which is in agreement with the higher resistance values given in Section 4.7.2. FoulXSpel 1, F0034 and F0037 have similar mean roughness values whereas the mean value of F0034 has the highest probability density. This can be attributed to a more homogenous roughness height distribution, and it supports the results given in Section 4.7.2. The mean roughness value of Hull falls into the region between FoulXSpel 2 and the other surfaces. It can be concluded from this that FoulXSpel 2 increases the mean surface roughness of a ship hull, while the other coatings reduce the mean roughness height compared to an otherwise uncoated ship hull.

It should be noted that the mean roughness height may not be the only parameter with which to assess the resistance characteristics of different surfaces, but it does provide a very useful means of assessing the differences between similar families of coatings, such as silicone based coatings.

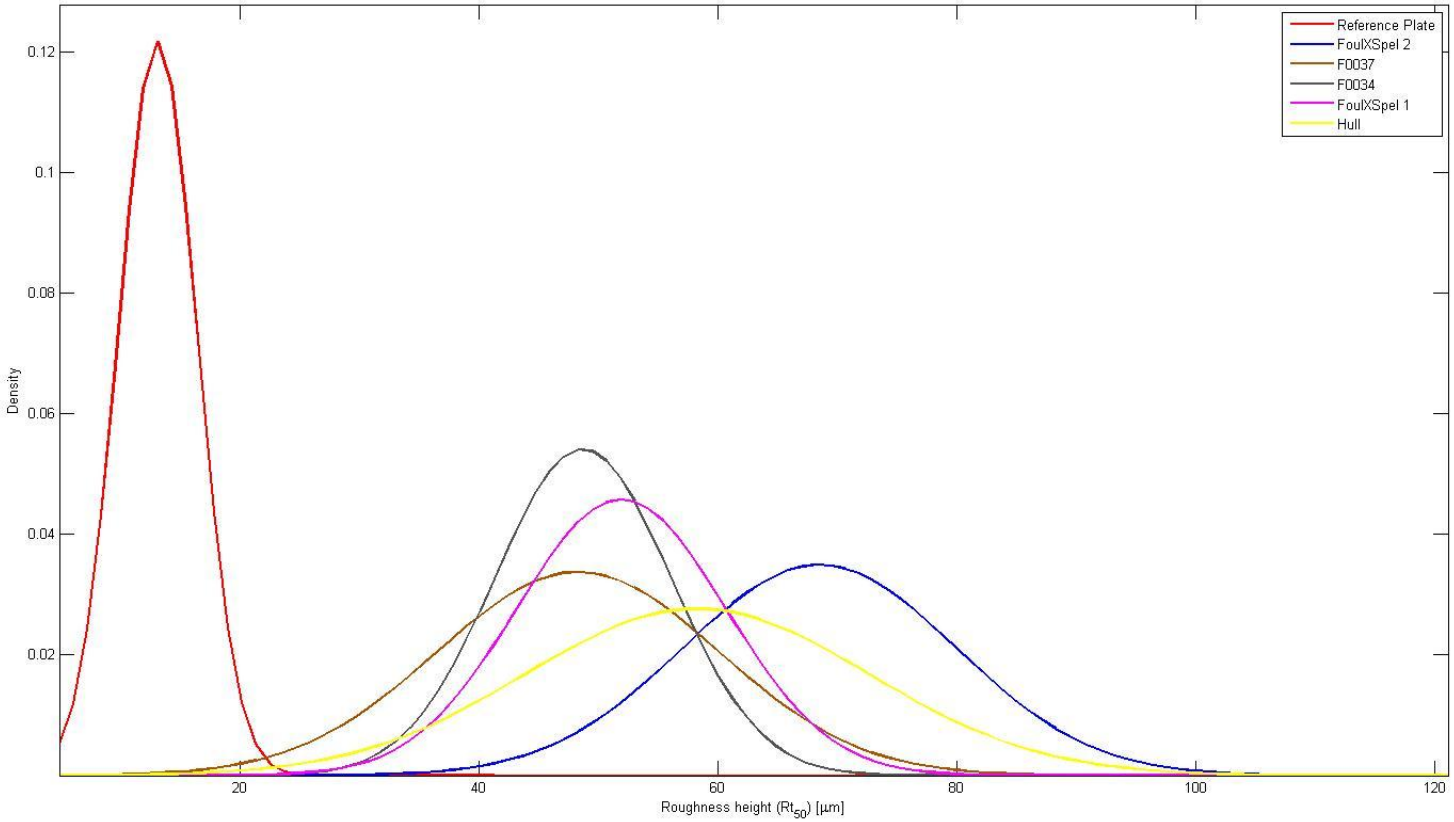

Figure 4.32: Probability density functions (pdf) of the roughness data of all of the test surfaces.

4.5 Test Methodology

The test methodology followed in this chapter is similar to that used by Schultz (2004). The Reference Plate was first towed repeatedly and the alignment of the plates adjusted until the side force was effectively zero. Once this was achieved, no further adjustments were made to the alignment over the course of the experiments. The side force of the plate was monitored for each run to ensure this alignment was maintained.

The total resistance (drag) of a flat plate, R_T, is mainly composed of two components; the residuary resistance, R_R, and the frictional resistance, R_F, as given by (4.1).

$$R_T = R_R + R_F \tag{4.1}$$

A more detailed decomposition of resistance is shown in Figure 4.33 (Larsson and Baba, 1996).

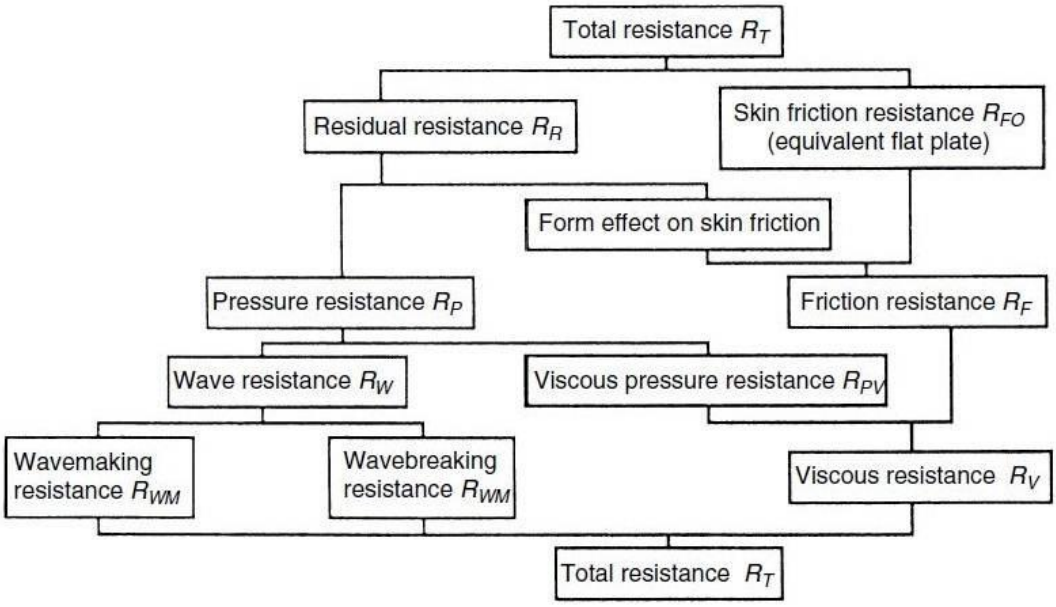

Figure 4.33: Resistance decomposition (Larsson and Baba, 1996).

The residuary resistance occurs due to the wavemaking resistance and pressure resistance of the plates, while the frictional resistance arises due to shear stresses on the plate surface. It is of note that in this case, the pressure drag is expected to be

negligible since the thickness of the plates is only 5mm. The surface roughness of antifouling coatings affects only skin friction resistance, which is equivalent to flat plate frictional resistance.

Once the total drag, R_T, values are obtained for each plate and related speeds, they were non-dimensionalised by dividing each term by the dynamic pressure and wetted surface area of the plates. The total drag coefficient, C_T, was therefore evaluated using the following equation (4.2)

$$R_T = \frac{1}{2}\rho S C_T V^2 \quad \textbf{(4.2)}$$

where ρ is the density of water, S is the wetted surface area, C_T is the total resistance coefficient and V is the speed.

Showing similarity to the resistance decomposition, the total resistance coefficient, C_T, is made up of the residuary resistance coefficient, C_R, and the frictional resistance coefficient, C_F. Given that the residuary resistance coefficient is a function of the Froude number, Fr, and the frictional resistance coefficient is a function of the Reynolds number, Re, the total resistance coefficient can, therefore, be written in the following form (Schultz, 2007):

$$C_T = C_R(Fr) + C_F(Re) \quad \textbf{(4.3)}$$

The frictional resistance coefficient, C_F, for both model and full-scale ships, can be estimated by using the ITTC 1957 formula, given by equation (2.25). However, this equation may not be used for the prediction of the frictional resistance of flat plates since it is "only an interim solution to this problem for engineering purposes" and it is not an equation to represent the frictional resistance of a flat plate so it cannot be used for such purposes (van Manen and van Oossanen, 1988).

The Karman-Schoenherr friction line (Schoenherr, 1932) given by (2.23) for a smooth plate can instead be used to predict the frictional resistance coefficients of a smooth flat plate. The C_F values of the reference smooth plate are therefore assumed to be equal to the C_F values obtained using (2.23). It is of note that Candries (2001)

and Schultz (2004) also showed that equation (2.23) can be used for the prediction of the frictional resistance of flat plates.

The differences between the C_T values obtained using the experimental data and the C_F values obtained using (2.23) were assumed to be the C_R values of the Reference Plate as shown by (4.4). The computed C_R values were taken to be the C_R values of all the test surfaces (eq. (4.5)), since the residuary resistances of the plates were not expected to be significantly affected by the surface roughness (Schultz, 2007). Hence, the C_F values of the test surfaces were computed by subtracting the C_R values of the Reference Plate from the C_T values of the test surfaces as shown by (4.6). The mathematical process for this is outlined below.

$$C_{R_s} = C_{T_s} - C_{F_s} \tag{4.4}$$

$$C_{R_s} = C_{R_r} \tag{4.5}$$

$$C_{F_r} = C_{T_r} - C_{R_r} \tag{4.6}$$

4.6 Repeatability and Uncertainty Estimates

Uncertainty estimates for the drag coefficients and roughness function calculations were made through repeatability tests using the procedure defined by the ITTC (2002b). The uncertainty estimates for any quantity can be defined as below (ITTC, 2002b):

$$(U_A)^2 = (B_A)^2 + (P_A)^2 \tag{4.7}$$

where U_A is the total uncertainty, B_A is the total bias limit and P_A is the precision limit for the quantity A. B_A can also be called systematic errors and occurs due to the errors of measurement devices; it can be calculated as:

$$(B_A)^2 = \left(\frac{\partial A}{\partial x} B_x\right)^2 + \left(\frac{\partial A}{\partial y} B_y\right)^2 + \left(\frac{\partial A}{\partial z} B_z\right)^2 + \ldots \quad \textbf{(4.8)}$$

where

$$A = f(x, y, z, \ldots) \quad \textbf{(4.9)}$$

P_A is caused by random errors with regards to the repeatability of the experiment and it can be calculated by (4.10) for multiple tests and (4.11) for a single run as follows:

$$P(M) = \frac{KSDev}{\sqrt{M}} \quad \textbf{(4.10)}$$

$$P(S) = KSDev \quad \textbf{(4.11)}$$

where *K* is the coverage factor (this may be assumed to be 2 according to the ITTC (2002b) for 95% confidence level), *M* is the number of runs and *SDev* is the standard deviation established by multiple runs, as given below.

$$SDev = \left[\frac{\sum_{k=1}^{M}\left(A_k - A_{average}\right)^2}{M-1}\right]^{\frac{1}{2}} \quad \textbf{(4.12)}$$

The details of the procedures to carry out an uncertainty analysis can be found in ITTC (2002b) and Coleman and Steele (1999).

In all of the tests, the combined bias uncertainty of the devices for C_T was lower than ±0.47%. This very low uncertainty level was achieved by the use of brand new displacement transducers which use the Linear Variable Differential Transformer (LVDT) principle. Additionally, precise calibration of the new transducers was performed.

The repeatability tests were performed at two speeds, namely 1.857 m/s and 3.591 m/s, which correspond to Reynolds numbers of ~$2.6x10^6$ and ~$5x10^6$, respectively. Details of the uncertainty limits at the two speeds are given in Table 4.2 for C_T, Table 4.3 for C_F and Table 4.4 for roughness functions, ΔU^+.

As can be seen from Table 4.2, the bias uncertainty in C_T ranged from ±0.473% at the lower Reynolds number to ±0.313% at the higher Reynolds number, while the precision uncertainty in C_T ranged from ±0.5% at the lower Reynolds number to ±0.007% at the higher Reynolds number. The overall uncertainty in C_T ranged from ±0.684% at the lower Reynolds number to ±0.313% at the higher Reynolds number.

The bias uncertainty in C_F ranged from ±0.708% at the lower Reynolds number to ±0.048% at the higher Reynolds number, while the precision uncertainty in C_F ranged from ±0.532% at the lower Reynolds number to ±0.008% at the higher Reynolds number. The overall uncertainty in C_F ranged from ±0.879% at the lower Reynolds number to ±0.058% at the higher Reynolds number.

The overall uncertainty levels of the drag coefficients are sufficient when compared to other experiments given in the literature such as Schultz (2004). The very small precision limits reveal the excellent repeatibility of the experiments.

The bias uncertainty in ΔU^+ ranged from ±66.81% to ±8% while the precision uncertainty in ΔU^+ ranged from ±0.01009% to ±0.00004%. The overall uncertainty in ΔU^+ ranged from ±66.81% to ±8%. The high uncertainty values for the ΔU^+ values were recorded since the present ΔU^+ values were around 0. It does not necessarily imply that the ΔU^+ values are not reliable. It is also due to the use of an indirect method, i.e. the overall method, which includes equation (2.36) involving the experimentally obtained parameters.

Table 4.2: Uncertainty limits in C_T.

		1.857 m/s		3.591 m/s	
	Term	**Value**	**% of C_T**	**Value**	**% of C_T**
Reference Plate	B_{CT}	1.8609E-05	0.473	1.13032E-05	0.315
	P_{CT}	2.85716E-06	0.073	1.07913E-06	0.030
	U_{CT}	**1.8827E-05**	**0.478**	**1.13546E-05**	**0.316**
FoulXSpel 2	B_{CT}	1.8978E-05	0.459	1.17936E-05	0.313
	P_{CT}	1.004E-05	0.243	2.73174E-07	0.007
	U_{CT}	**2.14701E-05**	**0.520**	**1.17968E-05**	**0.313**
F0037	B_{CT}	1.86706E-05	0.471	1.13522E-05	0.314
	P_{CT}	1.41991E-05	0.358	7.69085E-06	0.213
	U_{CT}	**2.34565E-05**	**0.591**	**1.37121E-05**	**0.380**
FoulXSpel 1	B_{CT}	1.88384E-05	0.465	1.124E-05	0.315
	P_{CT}	1.63152E-05	0.403	2.2329E-06	0.063
	U_{CT}	**2.49213E-05**	**0.615**	**1.14596E-05**	**0.322**
F0034	B_{CT}	1.87106E-05	0.466	1.11513E-05	0.316
	P_{CT}	2.01154E-05	0.501	5.5159E-07	0.016
	U_{CT}	**2.74721E-05**	**0.684**	**1.1165E-05**	**0.317**
Hull	B_{CT}	1.87337E-05	0.469	1.16855E-05	0.314
	P_{CT}	2.31965E-06	0.058	1.97847E-06	0.053
	U_{CT}	**1.88768E-05**	**0.472**	**1.18518E-05**	**0.318**

Table 4.3: Uncertainty limits in C_F.

		1.857 m/s		3.591 m/s	
	Term	**Value**	**% of C_F**	**Value**	**% of C_F**
Reference Plate	B_{CF}	1.85563E-06	0.050	1.57611E-06	0.048
	P_{CF}	2.85716E-06	0.077	1.07913E-06	0.030
	U_{CF}	**3.40686E-06**	**0.092**	**1.91014E-06**	**0.058**
FoulXSpel 2	B_{CF}	2.6644E-05	0.684	1.64115E-05	0.473
	P_{CF}	1.004E-05	0.258	2.73174E-07	0.008
	U_{CF}	**2.84729E-05**	**0.731**	**1.64138E-05**	**0.473**
F0037	B_{CF}	2.64259E-05	0.708	1.60972E-05	0.486
	P_{CF}	1.41991E-05	0.381	7.69085E-06	0.232
	U_{CF}	**2.99991E-05**	**0.804**	**1.78401E-05**	**0.539**
FoulXSpel 1	B_{CF}	2.65447E-05	0.696	1.60182E-05	0.490
	P_{CF}	1.63152E-05	0.427	2.2329E-06	0.068
	U_{CF}	**3.11578E-05**	**0.816**	**1.61731E-05**	**0.495**
F0034	B_{CF}	2.64542E-05	0.700	1.59562E-05	0.494
	P_{CF}	2.01154E-05	0.532	5.5159E-07	0.017
	U_{CF}	**3.32333E-05**	**0.879**	**1.59657E-05**	**0.495**
Hull	B_{CF}	2.64705E-05	0.704	1.6334E-05	0.477
	P_{CF}	2.31965E-06	0.062	1.97847E-06	0.058
	U_{CF}	**2.6572E-05**	**0.707**	**1.64533E-05**	**0.480**

Table 4.4: Uncertainty limits in ΔU^+.

		1.857 m/s		3.591 m/s	
	Term	**Value**	**% of ΔU^+**	**Value**	**% of ΔU^+**
FoulXSpel 2	$B_{\Delta U}{}^+$	0.080640952	11.59786	0.058979108	8.01770
	$P_{\Delta U}{}^+$	1.004E-05	0.00144	2.73174E-07	0.00004
	$U_{\Delta U}{}^+$	**0.080640952**	**11.59786**	**0.058979108**	**8.01770**
F0037	$B_{\Delta U}{}^+$	0.085220896	60.53541	0.061962044	66.81616
	$P_{\Delta U}{}^+$	1.41991E-05	0.01009	7.69085E-06	0.00829
	$U_{\Delta U}{}^+$	**0.085220897**	**60.53541**	**0.061962044**	**66.81616**
FoulXSpel 1	$B_{\Delta U}{}^+$	0.08283091	17.79572	0.062909885	51.21607
	$P_{\Delta U}{}^+$	1.63152E-05	0.00351	2.2329E-06	0.00182
	$U_{\Delta U}{}^+$	**0.082830912**	**17.79572**	**0.062909885**	**51.21607**
F0034	$B_{\Delta U}{}^+$	0.083676432	23.93294	0.063779458	21.95072
	$P_{\Delta U}{}^+$	2.01154E-05	0.00575	5.5159E-07	0.00019
	$U_{\Delta U}{}^+$	**0.083676434**	**23.93294**	**0.063779458**	**21.95072**
Hull	$B_{\Delta U}{}^+$	0.084402577	40.12117	0.059823686	10.47518
	$P_{\Delta U}{}^+$	2.31965E-06	0.00110	1.97847E-06	0.00035
	$U_{\Delta U}{}^+$	**0.084402577**	**40.12117**	**0.059823686**	**10.47518**

4.7 Results

Having presented the necessary uncertainty estimates, this section addresses the results of the resistance tests. Firstly, the total drag coefficients (C_T) obtained using the experimental data are presented in tabular form. Afterwards, the frictional resistance coefficient (C_F) values are calculated as explained in Section 4.5 and are presented and discussed in detail since the focus is on the frictional resistance.

4.7.1 Total Resistance Coefficients

C_T values of all of the test surfaces are shown in Table 4.5 and the changes in the C_T values of the test plates with respect to the Reference Plate and Hull are given in Table 4.6 and Table 4.7, respectively.

Table 4.5: C_T values of all of the test surfaces.

Speed	C_T					
m/s	Reference Plate	FoulXSpel 2	F0037	FoulXSpel 1	F0034	Hull
1.5	0.00402	0.00407	0.00406	0.00396	0.00396	0.00406
1.857	0.00394	0.00413	0.00397	0.00405	0.00402	0.00400
2.131	0.00384	0.00400	0.00388	0.00382	0.00378	0.00389
2.28	0.00383	0.00397	0.00384	0.00379	0.00376	0.00391
2.435	0.00378	0.00396	0.00381	0.00376	0.00371	0.00387
2.739	0.00372	0.00392	0.00387	0.00377	0.00381	0.00394
2.86	0.00368	0.00398	0.00388	0.00388	0.00387	0.00378
3.013	0.00364	0.00382	0.00369	0.00365	0.00366	0.00373
3.14	0.00360	0.00386	0.00364	0.00368	0.00358	0.00372
3.287	0.00358	0.00379	0.00363	0.00360	0.00357	0.00370
3.45	0.00358	0.00378	0.00360	0.00356	0.00355	0.00371
3.591	0.00359	0.00377	0.00361	0.00356	0.00353	0.00373

Table 4.6: Change in C_T values of the test plates with respect to the Reference Plate.

Speed	Change in C_T (%) with respect to the Reference Plate				
m/s	FoulXSpel 2	F0037	FoulXSpel 1	F0034	Hull
1.5	1.17	0.84	-1.71	-1.52	0.89
1.857	5.02	0.79	2.96	2.06	1.53
2.131	4.41	1.23	-0.35	-1.53	1.48
2.28	3.74	0.31	-0.97	-1.82	2.05
2.435	4.64	0.67	-0.65	-1.98	2.35
2.739	5.27	4.14	1.38	2.42	5.87
2.86	8.02	5.38	5.46	5.16	2.75
3.013	5.22	1.49	0.53	0.74	2.50
3.14	7.38	1.15	2.36	-0.34	3.31
3.287	6.10	1.51	0.76	-0.19	3.47
3.45	5.60	0.55	-0.37	-0.90	3.61
3.591	4.91	0.45	-0.81	-1.91	3.66

Table 4.7: Change in C_T values of the test plates with respect to Hull.

Speed	Change in C_T (%) with respect to Hull				
m/s	FoulXSpel 2	F0037	FoulXSpel 1	F0034	Reference Plate
1.5	0.28	-0.05	-2.58	-2.39	-0.88
1.857	3.43	-0.73	1.41	0.52	-1.51
2.131	2.89	-0.24	-1.81	-2.96	-1.46
2.28	1.66	-1.70	-2.96	-3.80	-2.01
2.435	2.24	-1.64	-2.93	-4.23	-2.30
2.739	-0.57	-1.64	-4.24	-3.26	-5.55
2.86	5.13	2.56	2.64	2.35	-2.68
3.013	2.65	-0.99	-1.92	-1.72	-2.44
3.14	3.94	-2.09	-0.92	-3.53	-3.21
3.287	2.54	-1.90	-2.62	-3.53	-3.35
3.45	1.93	-2.95	-3.84	-4.35	-3.48
3.591	1.21	-3.09	-4.31	-5.37	-3.53

4.7.2 Frictional Resistance Coefficients

The frictional resistance coefficients of the entire test surfaces were calculated as explained in Section 4.5. C_F values of all of the test surfaces are listed in Table 4.8, and the changes in the C_F values of the test plates with respect to the Reference Plate and Hull are given in Table 4.9 and Table 4.10, respectively.

Table 4.8: C_F values of all of the test surfaces.

Speed	C_F					
m/s	Reference Plate	FoulXSpel 2	F0037	FoulXSpel 1	F0034	Hull
1.5	0.00384	0.00389	0.00388	0.00378	0.00378	0.00388
1.857	0.00370	0.00390	0.00373	0.00382	0.00378	0.00376
2.131	0.00361	0.00378	0.00366	0.00360	0.00355	0.00367
2.28	0.00357	0.00371	0.00358	0.00353	0.00350	0.00365
2.435	0.00353	0.00370	0.00355	0.00350	0.00345	0.00361
2.739	0.00345	0.00365	0.00361	0.00351	0.00354	0.00367
2.86	0.00343	0.00372	0.00363	0.00363	0.00362	0.00353
3.013	0.00340	0.00359	0.00345	0.00342	0.00342	0.00349
3.14	0.00337	0.00364	0.00341	0.00346	0.00336	0.00349
3.287	0.00335	0.00356	0.00340	0.00337	0.00334	0.00347
3.45	0.00332	0.00352	0.00334	0.00331	0.00329	0.00345
3.591	0.00330	0.00347	0.00331	0.00327	0.00323	0.00343

Table 4.9: Change in C_F values of the test plates with respect to the Reference Plate.

Speed	Change in C_F (%) with respect to the Reference Plate				
m/s	FoulXSpel 2	F0037	FoulXSpel 1	F0034	Hull
1.5	1.22	0.88	-1.79	-1.59	0.93
1.857	5.34	0.84	3.15	2.19	1.63
2.131	4.68	1.31	-0.38	-1.62	1.57
2.28	4.02	0.34	-1.04	-1.96	2.20
2.435	4.98	0.72	-0.70	-2.13	2.52
2.739	5.67	4.46	1.48	2.60	6.32
2.86	8.62	5.78	5.87	5.55	2.96
3.013	5.59	1.59	0.57	0.79	2.68
3.14	7.87	1.23	2.52	-0.36	3.53
3.287	6.51	1.61	0.82	-0.20	3.71
3.45	6.04	0.59	-0.40	-0.97	3.89
3.591	5.35	0.49	-0.89	-2.08	3.99

Table 4.10: Change in C_F values of the test plates with respect to Hull.

Speed	Change in C_F (%) with respect to Hull				
m/s	FoulXSpel 2	F0037	FoulXSpel 1	F0034	Reference Plate
1.5	0.29	-0.05	-2.70	-2.50	-0.92
1.857	3.65	-0.78	1.49	0.55	-1.61
2.131	3.06	-0.26	-1.92	-3.14	-1.55
2.28	1.78	-1.82	-3.17	-4.07	-2.15
2.435	2.40	-1.75	-3.14	-4.53	-2.46
2.739	-0.61	-1.76	-4.55	-3.50	-5.95
2.86	5.49	2.74	2.83	2.51	-2.87
3.013	2.83	-1.06	-2.05	-1.84	-2.61
3.14	4.19	-2.22	-0.98	-3.76	-3.41
3.287	2.71	-2.02	-2.79	-3.77	-3.58
3.45	2.07	-3.17	-4.13	-4.67	-3.74
3.591	1.31	-3.36	-4.69	-5.83	-3.83

Figure 4.34 demonstrates the total drag coefficients of all of the test surfaces together with a Karman-Schoenherr friction line (Schoenherr, 1932) and the computed C_R values.

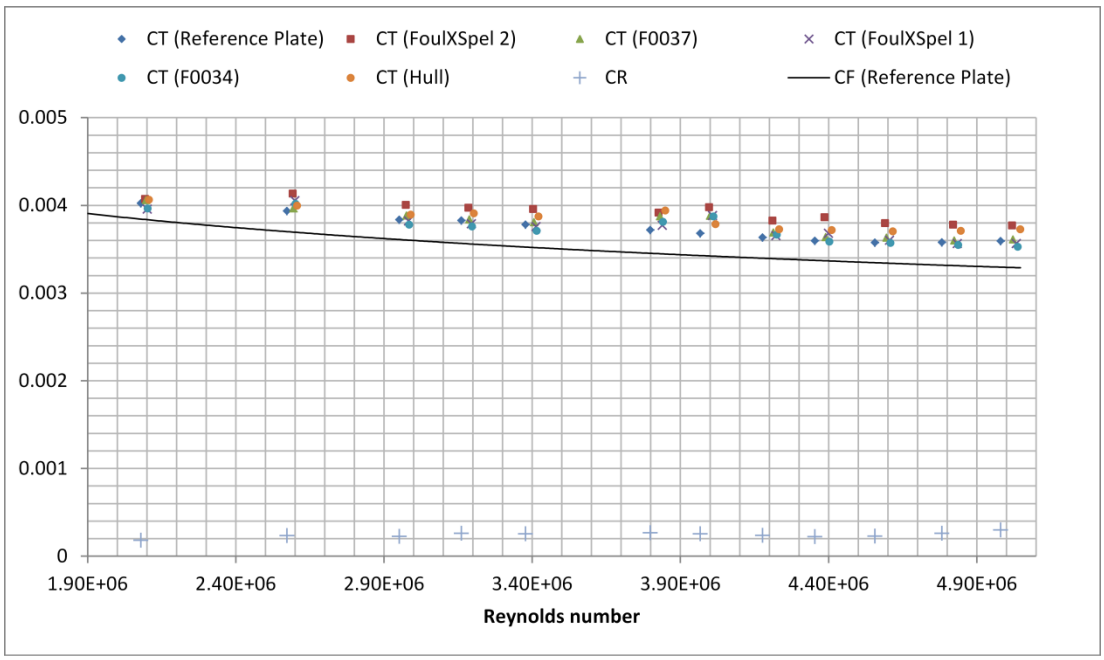

Figure 4.34: Total drag coefficients of all of the test surfaces together with a Karman-Schoenherr friction line and C_R values.

C_F values of the Reference Plate and Hull are shown together in Figure 4.35. As expected the C_F values of Hull are higher than those of the Reference Plate. For each test surface, the C_F values will be given together with those of the Reference Plate and Hull in order for a comparison to be made.

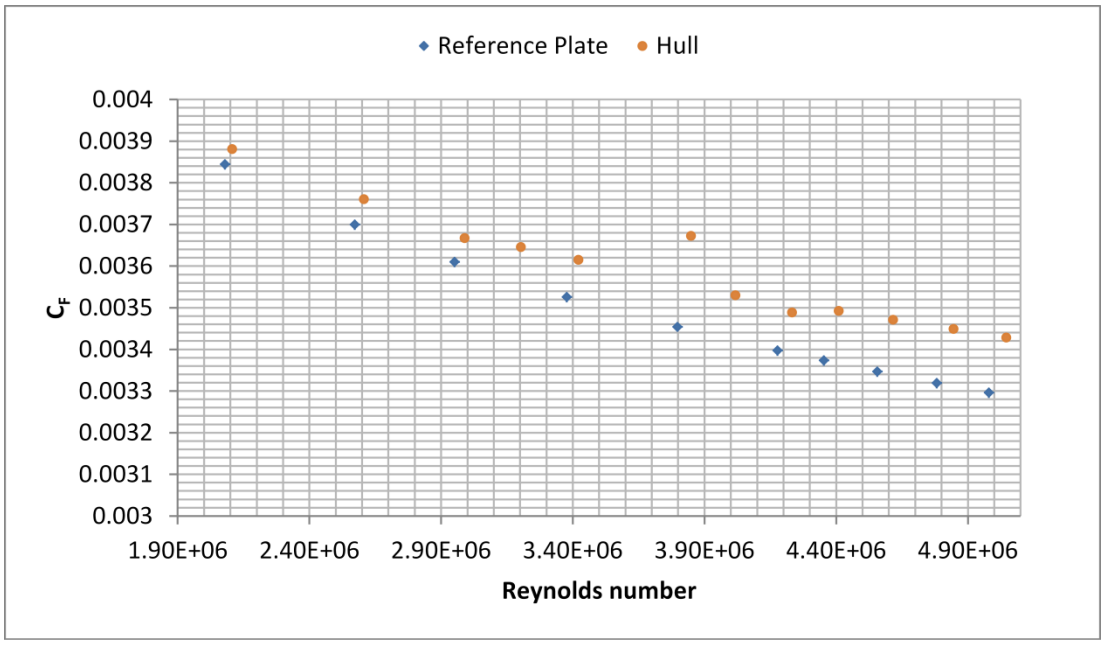

Figure 4.35: Frictional resistance coefficients of the Reference Plate and Hull.

It can be seen from Figure 4.36 that the C_F values of FoulXSpel 2 are higher than those of the Reference Plate and even the Hull surface. FoulXSpel 2 caused an increase of 1.22% at the lowest Reynolds number while it led to an increase of 5.35% at the highest Reynolds number, with an average increase of 5.16% compared to the Reference Plate. Surprisingly, it also caused an increase of 0.29% at the lowest Reynolds number and an increase of 1.31% at the highest Reynolds number, with an average increase of 2.43% compared to the Hull surface.

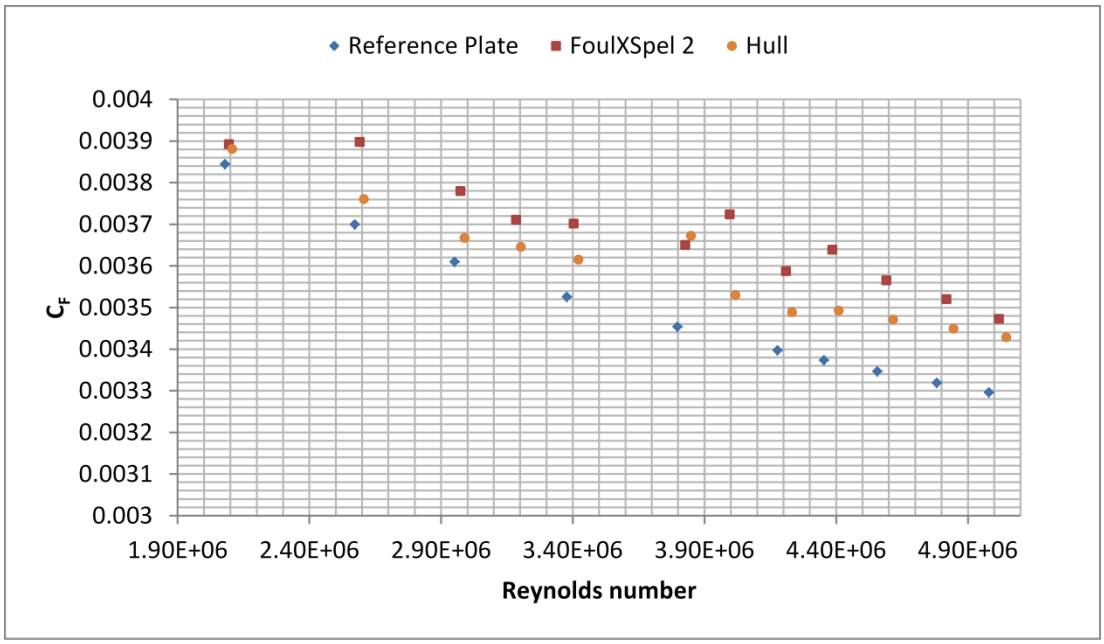

Figure 4.36: Frictional resistance coefficients of the Reference Plate, Hull and FoulXSpel 2.

It can be seen from Figure 4.37 that the C_F values of F0037 are slightly higher than those of the Reference Plate (on average 0.96% higher) and lower than those of the Hull surface (on average 1.65% lower). It is of note that although there is a significant difference in the Rt_{50} values of the Reference Plate and F0037, there are only very small differences between their C_F values.

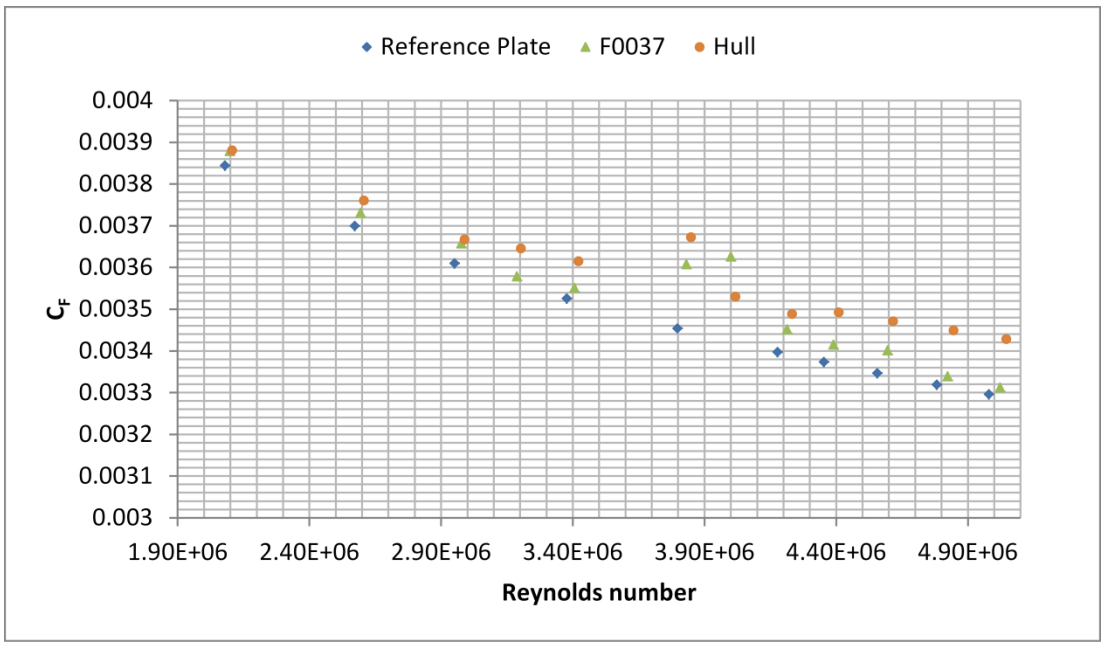

Figure 4.37: Frictional resistance coefficients of the Reference Plate, Hull and F0037.

The comparison between the newly developed F0037 and the existing FoulXSpel 2 is given in Figure 4.38. It is evident that the C_F values of F0037 are lower than those of FoulXSpel 2. The differences are in the range of 3.2% and 6.15%, except for the lowest Reynolds number. The average difference in C_F is recorded as 3.97%.

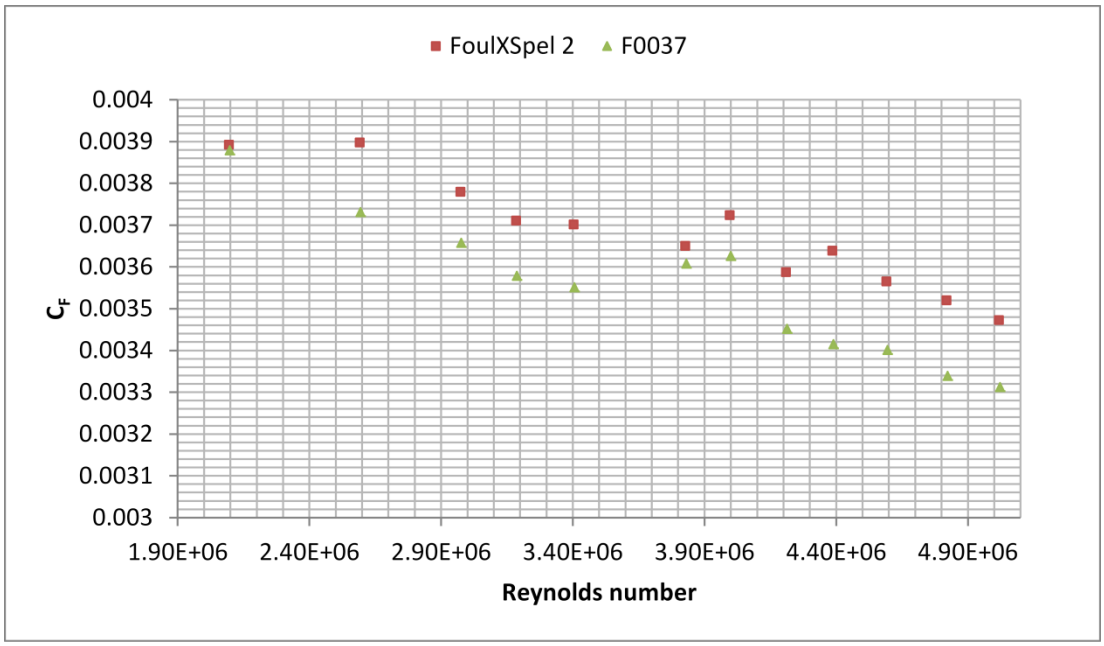

Figure 4.38: Comparison of the frictional resistance coefficients of FoulXSpel 2 and F0037.

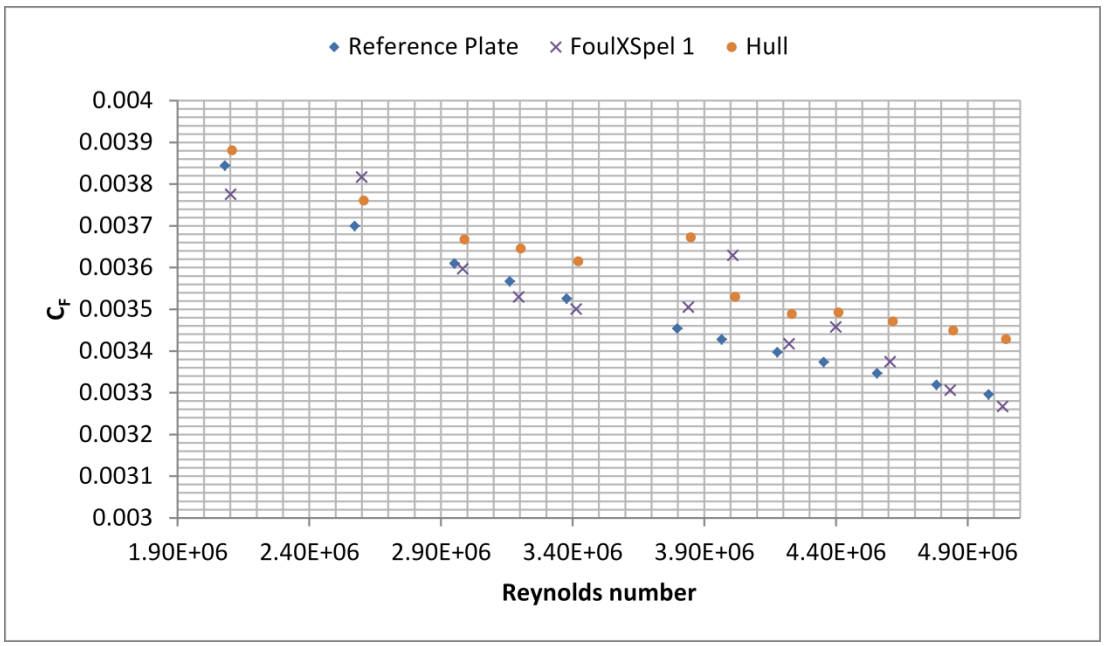

Figure 4.39: Frictional resistance coefficients of the Reference Plate, Hull and FoulXSpel 1.

Figure 4.39 demonstrates the C_F values of FoulXSpel 1. The C_F values of FoulXSpel 1 are slightly higher than those of the Reference Plate (on average 0.186% higher) and lower than those of Hull (on average 2.4% lower), with the exception of one speed.

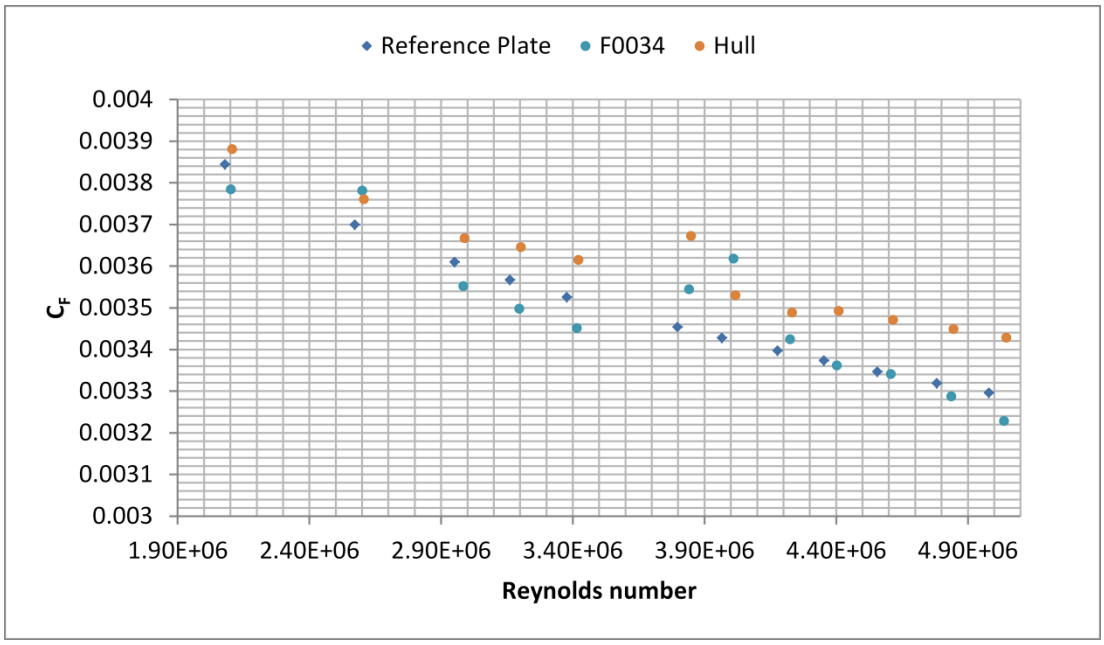

Figure 4.40: Frictional resistance coefficients of the Reference Plate, Hull and F0034.

Figure 4.40 shows the C_F values of F0034. It can be seen that the C_F values of F0034 are lower than those of both the Reference Plate (1.59% lower at the lowest speed

and 2.08% lower at the highest speed), with the exception of 1.857 m/s, and Hull (2.5% lower at the lowest speed and 5.83% lower at the highest speed). This leads to average decreases of 0.79% and 3.35% with respect to the Reference Plate and Hull, respectively.

Figure 4.41 compares the C_F values of F0034 and FoulXSpel 1. It can be seen that the C_F values of F0034 are slightly lower than those of FoulXSpel 1 (on average 0.97% lower). It was expected that the same C_F values would be obtained for these surfaces, given that they are both silicone based coatings. For this reason, the observed differences could be attributed to the slight differences between the roughness height values of these. Rt_{50} values can differ due to the quality of the surface preparation and/or the quality of the application, since it is almost impossible to have an identical surface preparation and paint application for two surfaces.

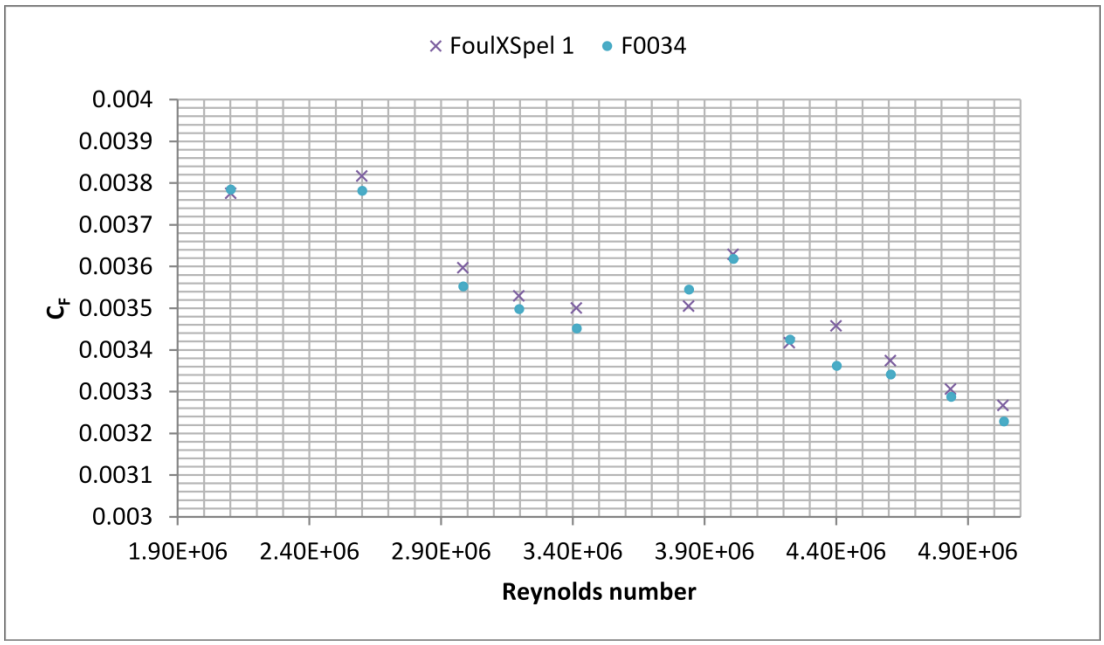

Figure 4.41: Comparison of the frictional resistance coefficients of FoulXSpel 1 and F0034.

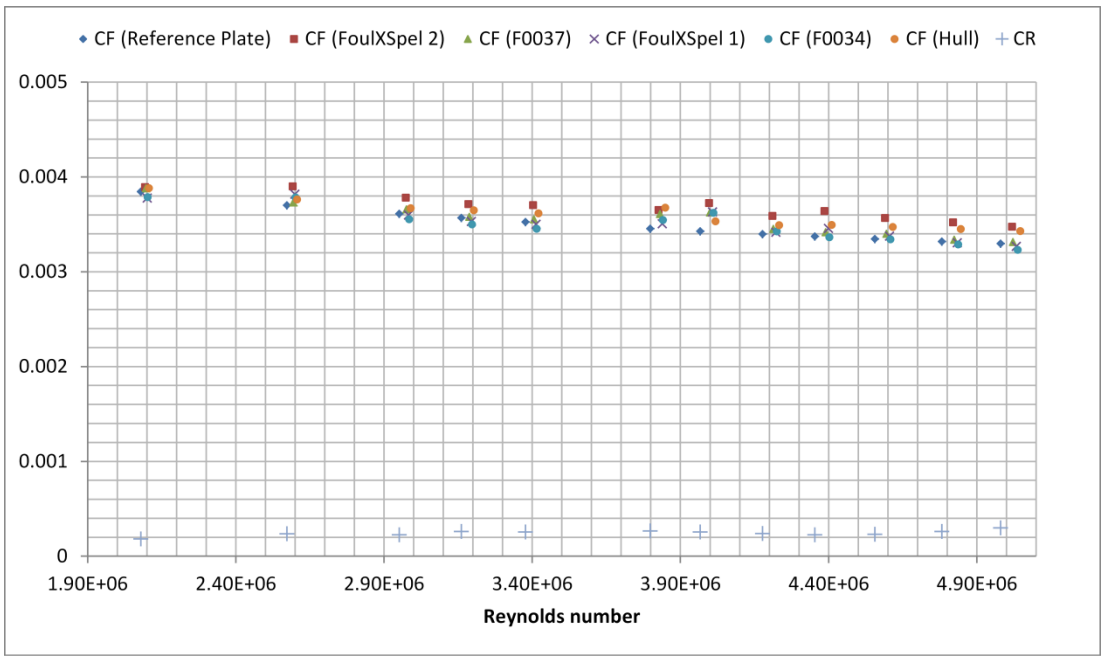

Figure 4.42: Frictional resistance coefficients of all test surfaces together with C_R values.

Figure 4.42 illustrates the frictional resistance coefficients of all of the test surfaces together with their C_R values. It is clearly seen that F0034 showed the best frictional resistance performance among all of the antifouling coatings, with an average decrease of 0.79% with respect to the Reference Plate. F0034 is the only one which led to a decrease compared to the Reference Plate. FoulXSpel 1 had the second best performance with an average increase of 0.186% with respect to the Reference Plate. It is followed by F0037 with an average increase of 0.96 % with respect to Reference Plate. It is also worthwhile to note that FoulXSpel 2 showed the worst frictional resistance performance among the entire set of test surfaces with an average increase of 5.16% with respect to the Reference Plate. This was also the only coating which led to an increase in C_F with respect to the Hull surface.

It should be noted that the average increases and decreases given in the discussions in this section were calculated by omitting the C_F values corresponding to speeds of 2.739 m/s and 2.86 m/s, since unexpected drag increases were recorded at these speeds due to wave reflection.

4.8 Determination of Roughness Functions

Roughness Reynolds numbers, k^+, and roughness function values, ΔU^+, for all of the surfaces were obtained iteratively using (2.36) and (2.37) following the overall procedure of Granville (1987) using the present experimental data. The details of this method are given in Chapter 2, Section 2.6.

The evaluated roughness functions against roughness Reynolds numbers using Rt_{50} as the roughness length scale are shown in Figure 4.43 and are given in Table 4.11. Shown for comparison in Figure 4.44 is the Colebrook type roughness function model of Grigson (1992) together with the roughness functions shown in Figure 4.43, using logarithmic scale in the x-axis. It is of note that some of the abnormal data due to wave reflection were not included in these figures. Additionally, the roughness functions for other antifouling coatings of Schultz (2004) are shown together with the present roughness functions in Figure 4.45. It should be borne in mind that the roughness Reynolds numbers of Schultz (2004) were recalculated using Rt_{50} as the roughness length scale instead of his original roughness length scale (0.17Ra) in order to enable a suitable comparison with the present findings.

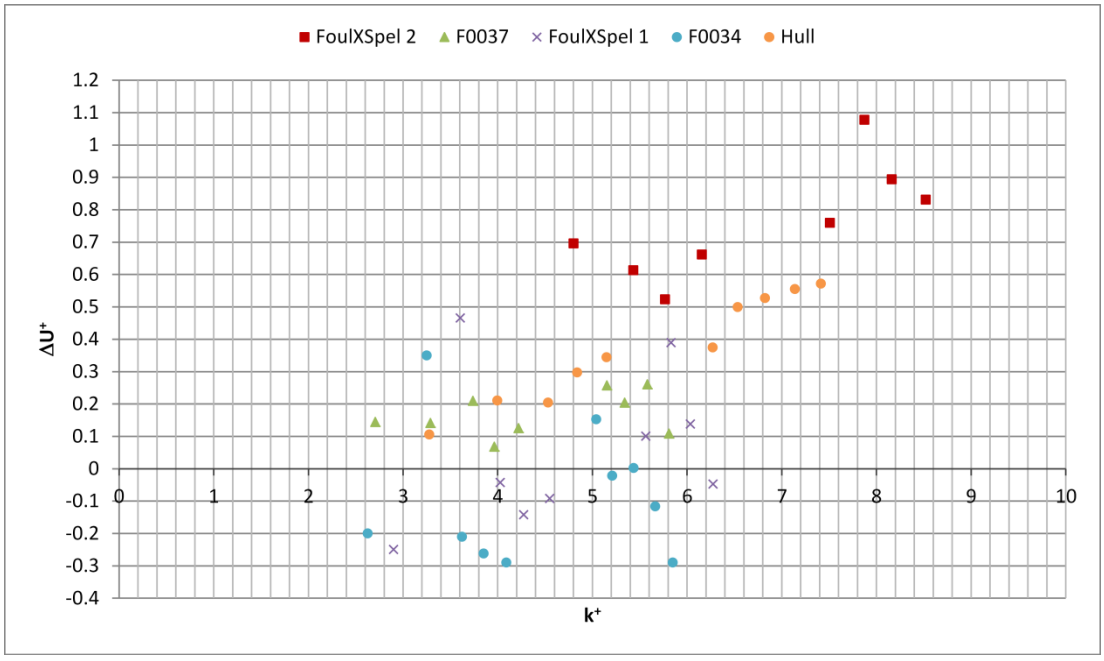

Figure 4.43: The roughness functions for all of the test surfaces.

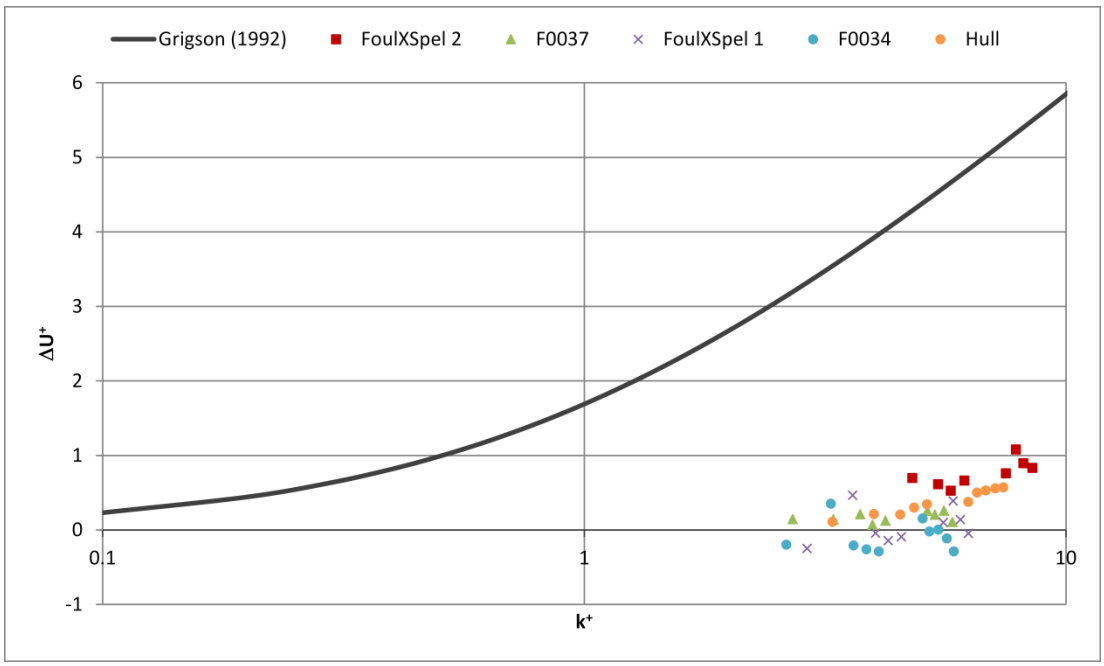

Figure 4.44: The roughness functions for all of the test surfaces together with the roughness function model of Grigson (1992).

As evident from Figure 4.43 and Figure 4.44, almost all of the roughness function values are below those of the Hull surface, except for FoulXSpel 2. This result suggests that all of the antifouling coatings, except for FoulXSpel 2, provide an improvement with respect to a bare ship hull, in terms of as applied frictional resistance performances. Another interesting result is that almost all of the roughness function values of F0034 are negative, which suggests the surface of F0034 is acting better than even the smooth surface similar to two nanostructured and fluorinated polymer coatings investigated by Atlar et al. (2012). Some roughness function values of FoulXSpel 1 are also negative. That is to say, the calculated frictional drag coefficients of these points are lower than those calculated using the theoretical Schoenherr (1932) friction line given by (2.23), as explained in Section 4.5. For these points, the velocity profile in the turbulent boundary layer would have an upward shift which manifests itself as a decrease in frictional resistance.

It should be noted that the roughness functions against roughness Reynolds numbers given in Figure 4.44 were calculated using Rt_{50} as the length scale as a reference and for consistency with the rest of the figures. Other length scales and roughness

function models should be further investigated in order to obtain an acceptable and meaningful correlation.

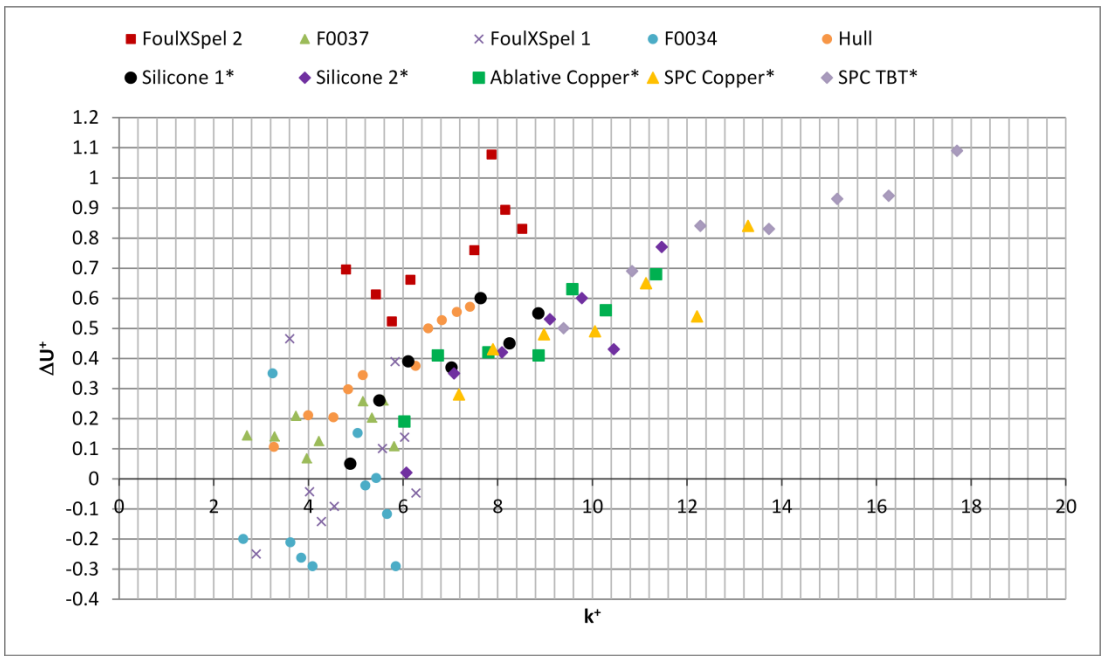

*Schultz (2004)

Figure 4.45: The roughness functions for all test surfaces together with the roughness functions of Schultz (2004).

It is seen from Figure 4.44 and Figure 4.45 that the roughness functions of FoulXSpel 2 and Hull show an increasing trend with increasing roughness Reynolds numbers which is in accordance with the roughness functions of Grigson (1992) and those obtained by Schultz (2004) for Silicone 1, Silicone 2, Ablative Copper, SPC Copper and SPC TBT. The roughness function values for F0034, F0037 and FoulXSpel 1, on the other hand, tend to decrease with increasing roughness Reynolds number above a certain speed. This can be attributed to the surface properties of new-generation silicone- and polyurethane-based coatings. This is in agreement with the findings of Candries (2001), Ünal et al. (2012) and Atlar et al. (2012).

Table 4.11: ΔU^+ and k^+ values.

k^+ FoulXSpel 2	ΔU^+ FoulXSpel 2	k^+ F0037	ΔU^+ F0037	k^+ FoulXSpel 1	ΔU^+ FoulXSpel 1	k^+ F0034	ΔU^+ F0034	k^+ Hull	ΔU^+ Hull
3.87838	0.11362	2.70674	0.14373	2.90126	-0.24992	2.62868	-0.20050	3.27765	0.10546
4.80214	0.69531	3.28889	0.14078	3.60611	0.46545	3.25067	0.34963	3.99724	0.21037
5.43312	0.61257	3.73879	0.20941	4.02667	-0.04266	3.62359	-0.21092	4.53298	0.20371
5.76896	0.52283	3.96470	0.06783	4.27558	-0.14232	3.85361	-0.26267	4.84208	0.29660
6.15809	0.66097	4.22081	0.12496	4.55047	-0.09183	4.09153	-0.29052	5.15225	0.34401
7.51023	0.75920	5.15383	0.25745	5.56602	0.10031	5.04371	0.15190	6.27175	0.37435
7.87535	1.07693	5.34293	0.20339	5.83181	0.38921	5.21032	-0.02237	6.53777	0.49918
8.16537	0.89316	5.58195	0.26047	6.03599	0.13775	5.43824	0.00204	6.82409	0.52663
8.52260	0.83036	5.80972	0.10809	6.27581	-0.04727	5.66566	-0.11695	7.14085	0.55448
8.81977	0.73561	6.02672	0.09274	6.49962	-0.12283	5.85192	-0.29056	7.41661	0.57110

4.9 Chapter Summary and Conclusions

An experimental study of the resistance of different marine coatings was performed. Six flat plates with different surfaces were towed at the Kelvin Hydrodynamics Laboratory (KHL) of the University of Strathclyde.

Firstly, flat plates were exposed to the required surface preparations and four of them were coated with different coatings, including new coatings developed within the FOUL-X-SPEL Project. Afterwards, the Rt_{50} values of all of the test surfaces were measured using a hull roughness gauge. Then, the plates were towed at a range of speeds and the total resistances of the surfaces were measured. The resistance values were then non-dimensionalised and presented in a comparative manner. The frictional resistance coefficients of all of the test surfaces were then computed using assumptions that suggest the frictional resistance coefficients of smooth surfaces obey the Karman-Schoenherr friction line (Schoenherr, 1932) and that the residuary resistances of flat plates are not affected by surface roughness. Uncertainty estimates were made through repeatability tests, with the uncertainty values found to be sufficient to ensure a reliable comparison.

Table 4.12 and Table 4.13 rank all of the paints in decreasing order from best to worst in terms of total and frictional resistance characteristics. They also show the changes in C_T and C_F values with respect to both the Reference Plate and Hull.

Table 4.12: Paint rankings and the change in total resistance coefficient with respect to the Reference Plate and Hull.

Paint	$\%\Delta C_T$ (WRT Reference Plate)	$\%\Delta C_T$ (WRT Hull)
F0034	-0.74	-3.14
FoulXSpel 1	0.175	-2.25
F0037	0.9	-1.54
FoulXSpel 2	4.82	2.275

Table 4.13: Paint rankings and the change in frictional resistance coefficient with respect to the Reference Plate and Hull.

Paint	$\%\Delta C_F$ (WRT Reference Plate)	$\%\Delta C_F$ (WRT Hull)
F0034	-0.79	-3.36
FoulXSpel 1	0.186	-2.4
F0037	0.96	-1.65
FoulXSpel 2	5.16	2.43

The as applied resistance characteristics of F0034 were found to be the best among the entire set of test surfaces, especially at high Reynolds numbers. F0034 showed lower frictional resistance coefficient values compared to even the smooth Reference Plate.

Afterwards, roughness function values of all of the test surfaces were calculated using an indirect method, following the overall method of Granville (1987). It was observed that above a certain speed, the roughness function values for F0034, F0037 and FoulXSpel 1 tend to decrease with increasing roughness Reynolds number, as opposed to those for FoulXSpel 2, Hull and other surfaces used by Schultz (2004). The descending behaviour of the roughness functions of F0034, F0037 and FoulXSpel 1 is in agreement with the findings of Candries (2001), Ünal et al. (2012) and Atlar et al. (2012).

The effects of the surface properties of the new-generation FR coatings and novel FOUL-X-SPEL coatings on the frictional resistance were experimentally shown in this chapter. This study evidently showed that as applied drag performances of marine coatings are of great importance for energy efficient shipping since they markedly affect the frictional resistance of flat plates.

The effect of FOUL-X-SPEL coatings on the frictional resistances of flat plates of several ship lengths will be predicted in Chapter 5, utilising the roughness functions obtained in this chapter.

5 An Implementation of a Traditional Method: Similarity Law Scaling Procedure

5.1 Introduction

Roughness of a ship's hull, which is often caused by marine coatings and biofouling, can dramatically increase a ship's frictional resistance and hence its fuel consumption and greenhouse gas emissions. Although a large body of research has been devoted to assess the effects of fouling on ship resistance and powering, little effort has been made to classify fouling conditions and relate them to full-scale ship frictional resistance, as can be seen in Chapter 2.

A well-known similarity law scaling procedure from Granville (1958) can be used to predict the effect of such roughness on the frictional resistance of flat plates of ship lengths, provided that the roughness function behaviour of such fouling is known (Schultz, 2007). Some examples of the use of this method are given by Schultz (2002), Schultz (2004), Shapiro (2004), Schultz (2007), Flack and Schultz (2010) and Schultz et al. (2011). Schultz (2007) proposed a methodology to predict the effects of a range of coating and biofouling conditions on ship frictional resistance, using his experimental data, by means of the similarity law scaling procedure of Granville (1958). However, it may be difficult for less experienced users to carry out such an analysis using this methodology. Goal-based, simple added resistance diagrams for predicting the effect of biofouling on ship frictional resistance would therefore be of great benefit.

To the best of this author's knowledge, no specific added resistance diagram exists to predict the roughness effects of coatings and biofouling on ship frictional resistance. The aim of the present chapter is therefore to fill this gap by generating such diagrams using an in-house code based on the similarity law scaling procedure

explained by Schultz (2007), for an extensive range of ship lengths and ship speeds. This chapter may therefore be considered as an extension of the study presented in Schultz (2007), in order for engineers to be able to make simple predictions. The proposed diagrams enable the prediction of the added frictional resistance coefficients due to a range of biofouling conditions for different ship lengths and speeds.

This chapter is organised as follows: The similarity law scaling procedure is explained in detail in Section 5.2. Predictions of the roughness effects of FOUL-X-SPEL paints on ship frictional resistance are made utilising the code and the results are presented in Section 5.3. In Section 5.4, an extensive database of added resistance coefficients is generated and added resistance diagrams are plotted. In addition, powering predictions of ships are made using the generated diagrams. Finally, the results of the study are discussed in Section 5.5, along with recommendations for future avenues of research.

5.2 Methodology

The prediction code was developed based on the similarity law scaling procedure of Granville (1958), which is explained in detail in Schultz (1998) and Schultz (2007).

The first step of the procedure is to obtain the smooth frictional resistance coefficients, $C_{Fsmooth}$, of flat plates for varying speeds solving (2.23) and to plot them against *log* (Re) as seen in Figure 5.1. It should be borne in mind that equation (2.23) was solved using the Newton-Raphson method.

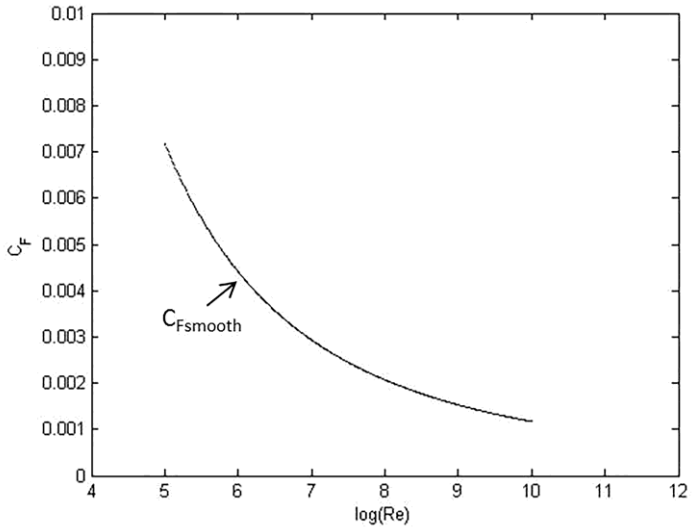

Figure 5.1: $C_{Fsmooth}$ versus log (Re).

The second step is to shift the $C_{Fsmooth}$ curve by $\Delta U^{+}\kappa[\ln(10)]^{-1}$ in the *log* (Re) direction. This new curve is referred to as C_{Frough}, as shown in Figure 5.2.

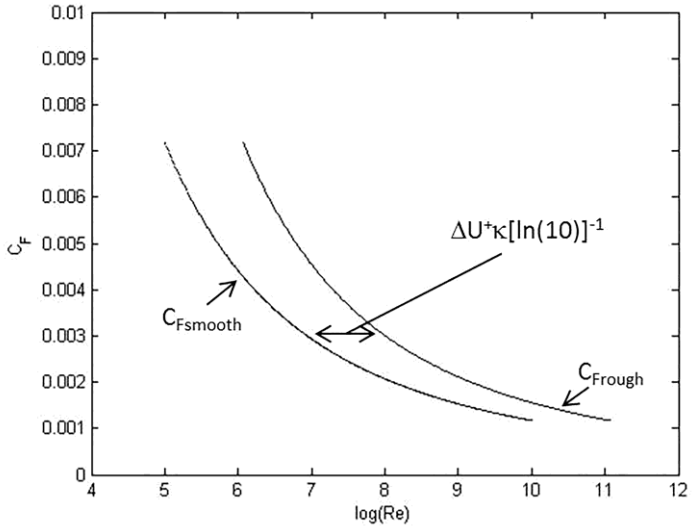

Figure 5.2: The second step of the Granville scale up.

The third step is to plot the line of the constant $L_{plate}+$ value, satisfying equation (5.1)

$$\mathrm{Re} = \frac{L_{plate}^{+}}{\sqrt{\frac{C_F}{2}}\left(1-\frac{1}{\kappa}\sqrt{\frac{C_F}{2}}\right)} \qquad \textbf{(5.1)}$$

where $L_{plate}+$ is defined by

$$L_{plate}{}^{+} = \frac{L_{plate} U_{\tau}}{\nu} \tag{5.2}$$

There are two methods of obtaining the $L_{plate}+$ value. The first is to obtain it using equation (5.1) and the laboratory scale C_F values evaluated by experiments, if there are any. The second method is to obtain it using equation (5.2), provided that the viscous length scale (ν/U_{τ}) is known. The viscous length scale (ν/U_{τ}) can be calculated by

$$\frac{\nu}{U_{\tau}} = \frac{k}{k^{+}} \tag{5.3}$$

and employed in (5.2). The third step is shown in Figure 5.3.

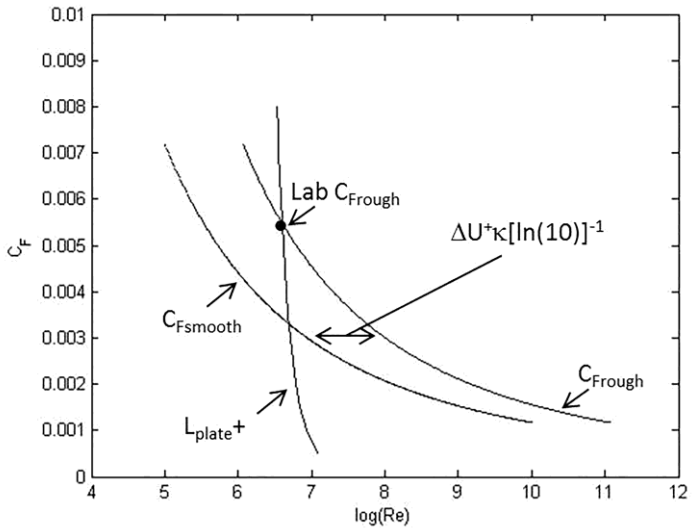

Figure 5.3: The third step of the Granville scale up.

The fourth step is to shift the line of constant $L_{plate}+$ a distance of *log* (L_{ship}/L_{plate}) in the *log* (Re) direction. This is then termed $L_{ship}+$. The intersection of $L_{ship}+$ and C_{Frough} gives the ship scale C_F value as shown in Figure 5.4.

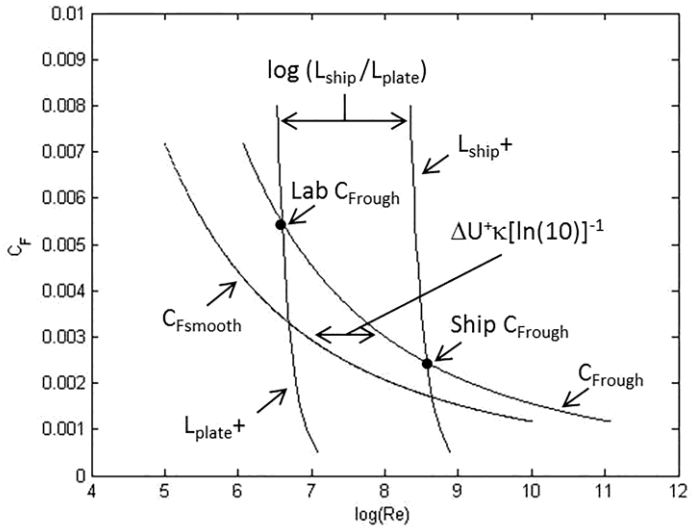

Figure 5.4: Granville scale-up procedure.

The difference between the evaluated C_{Frough} of the ship and the $C_{Fsmooth}$ of the ship (which can be calculated using equation (2.23)) for the same Reynolds number gives the added resistance coefficient, ΔC_F, of the ship due to roughness.

As seen from the above explanations, this procedure includes several numerical procedures which may cause numerical errors, should this be done manually for each case. A numerical in-house code, therefore, was developed in order to have a robust and fast solution.

The inputs of the said code are roughness height, roughness functions and corresponding roughness Reynolds numbers and the desired ship lengths. The code then calculates C_F values of ships for a given roughness on their hull for several ship speeds (depending on the number of ΔU^+ and k^+ pairs).

5.3 Prediction of the Roughness Effects of FOUL-X-SPEL Paints on Ship Frictional Resistance

The frictional resistance coefficients, C_F, and added resistance coefficients, ΔC_F, of flat plates representing a yacht of 10 m, a tugboat of 50 m, a cargo vessel of 100 m, a handymax tanker of 170 m, a containership of 232.5 m (KCS) and an LNG carrier of 270 m, hypothetically coated with FOUL-X-SPEL paints, were predicted by employing the roughness functions and roughness Reynolds numbers obtained in

Chapter 4 in the present developed code. It should be borne in mind that the predictions can only be made up to a certain ship speed due to the limited roughness functions. This is due to the limitations of the experiments carried out and presented in Chapter 4.

The added resistance diagrams were then generated using these predictions. The increases in the frictional resistances of ships were then calculated using the diagrams.

5.3.1 Added Resistance Diagrams

The added resistance coefficients, ΔC_F, due to the use of the FOUL-X-SPEL paints were plotted against the ship speeds. Either logarithmic or polynomial equations were then fitted to the ΔC_F values using the least squares method in order to evaluate added resistance diagrams. The diagrams (Figure 5.5 - Figure 5.8) are given separately for each surface condition.

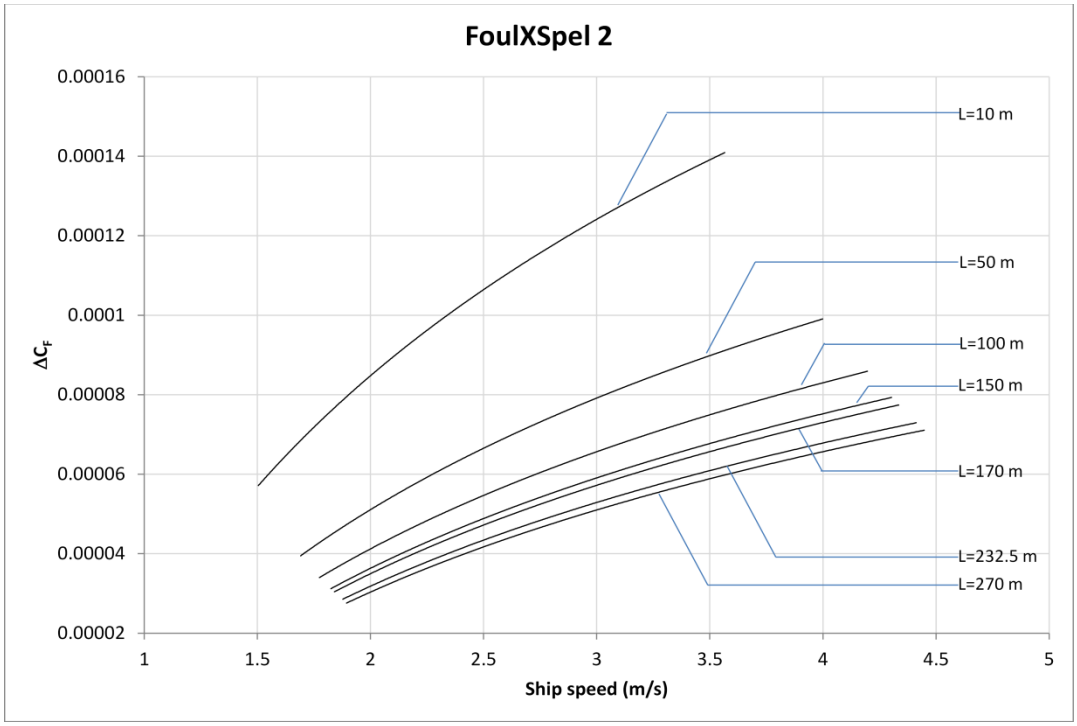

Figure 5.5: Added resistance diagram for ships bearing FoulXSpel 2.

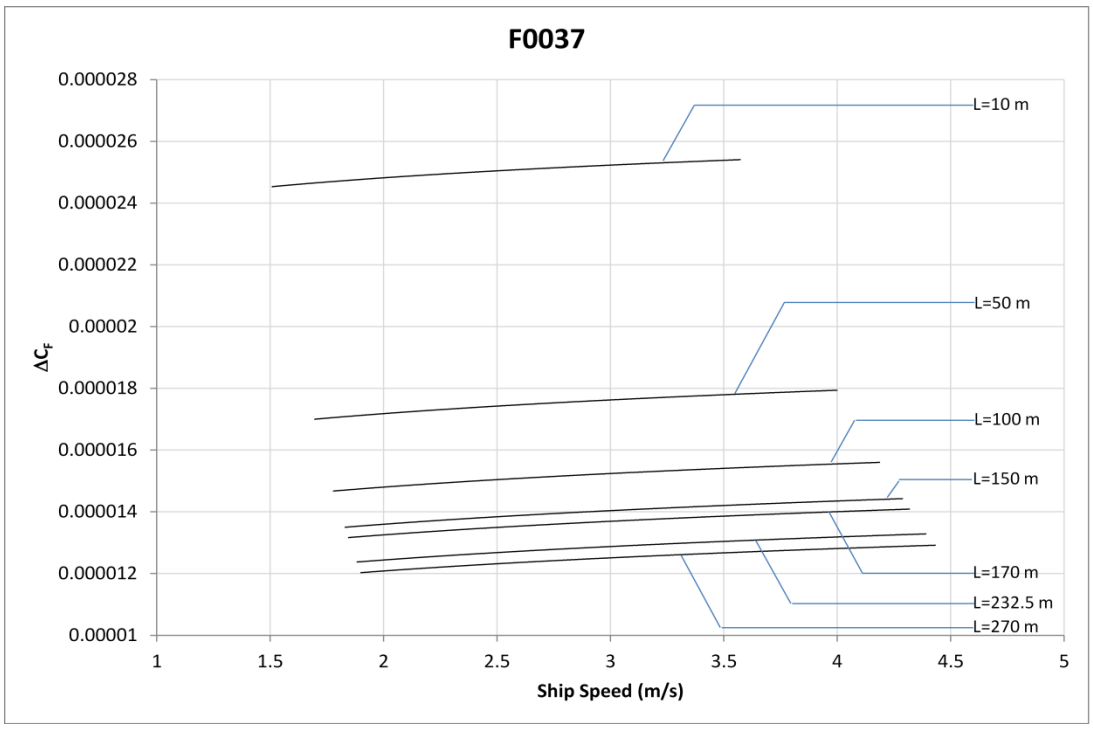

Figure 5.6: Added resistance diagram for ships bearing F0037.

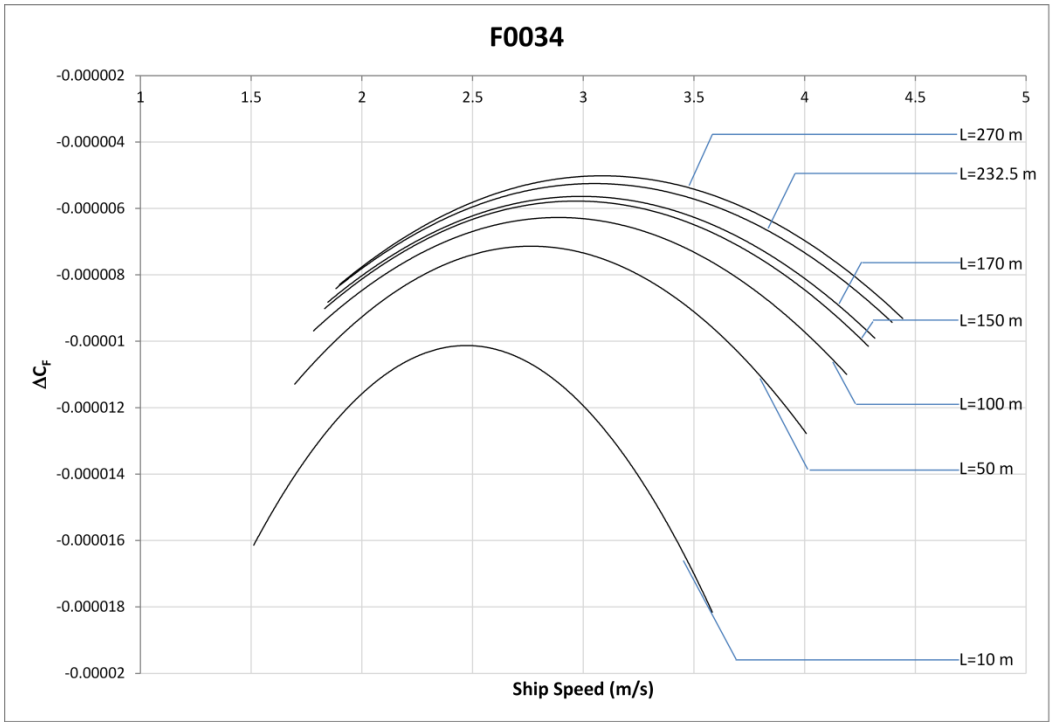

Figure 5.7: Added resistance diagram for ships bearing F0034.

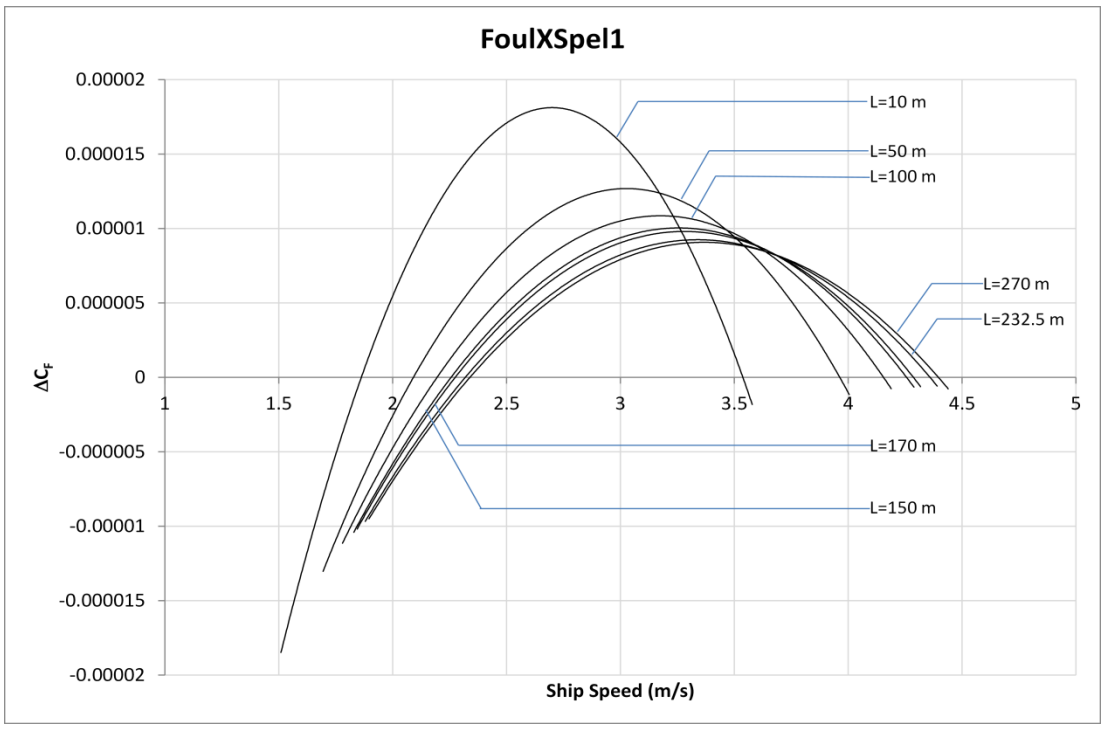

Figure 5.8: Added resistance diagram for ships bearing FoulXSpel 1.

5.3.2 Added Resistance of Ships

Table 5.1 - Table 5.6 display the C_F values of each surface and the percentage increases with respect to a smooth condition, for a yacht of 10 m, a tugboat of 50 m, a cargo vessel of 100 m, a handymax tanker of 170 m, a containership of 232.5 m (KCS) and an LNG carrier of 270 m, respectively. Only one representative ship speed is given in each table.

Table 5.1: The increases in the frictional resistance of the yacht at ~6.95 knots.

Surface	C_F	% ΔC_F
Reference Plate (Smooth)	0.002367473	-
FoulXSpel 2	0.002477123	4.6
F0037	0.002380275	0.5
F0034	0.002324431	-1.8
FoulXSpel 1	0.002348538	-0.8
Hull	0.002449781	3.5

Table 5.2: The increases in the frictional resistance of the tugboat at ~7.8 knots.

Surface	C_F	% ΔC_F
Reference Plate (Smooth)	0.001856350	-
FoulXSpel 2	0.001933563	4.2
F0037	0.001865815	0.5
F0034	0.001826549	-1.6
FoulXSpel 1	0.001843518	-0.7
Hull	0.001914482	3.1

Table 5.3: The increases in the frictional resistance of the cargo vessel at ~8.15 knots.

Surface	C_F	% ΔC_F
Reference Plate (Smooth)	0.001684358	-
FoulXSpel 2	0.001751440	4.0
F0037	0.001693137	0.5
F0034	0.001659258	-1.5
FoulXSpel 1	0.001673907	-0.6
Hull	0.001735038	3.0

Table 5.4: The increases in the frictional resistance of the handymax tanker at ~8.5 knots.

Surface	C_F	% ΔC_F
Reference Plate (Smooth)	0.001568635	-
FoulXSpel 2	0.001629147	3.9
F0037	0.001576875	0.5
F0034	0.001546451	-1.4
FoulXSpel 1	0.001559611	-0.6
Hull	0.001614454	2.9

Table 5.5: The increases in the frictional resistance of the KCS at ~8.5 knots.

Surface	C_F	% ΔC_F
Reference Plate (Smooth)	0.001505943	-
FoulXSpel 2	0.001562980	3.8
F0037	0.001513866	0.5
F0034	0.001484930	-1.4
FoulXSpel 1	0.001497581	-0.6
Hull	0.001549180	2.9

Table 5.6: The increases in the frictional resistance of the LNG carrier at ~8.5 knots.

Surface	C_F	% ΔC_F
Reference Plate (Smooth)	0.001477161	-
FoulXSpel 2	0.001532808	3.8
F0037	0.001484782	0.5
F0034	0.001456399	-1.4
FoulXSpel 1	0.001468675	-0.6
Hull	0.001519409	2.9

The results of the study evidently suggest that the use of the new FOUL-X-SPEL F0034 has significant advantages over the use of both the existing reference paints, i.e. FoulXSpel 1 and FoulXSpel 2, and the use of the new FOUL-X-SPEL F0037. In addition, it improves the surface conditions of the hull and it even shows better performance than the theoretical smooth surface. Table 5.7 is a summary table

showing the reduction in C_F (%) due to the use of F0034 with respect to the other surfaces at ship speeds given in Table 5.1 - Table 5.6.

Table 5.7: The reduction in C_F (%) due to the use of F0034 for all ships.

	Reduction (%) in C_F due to the use of F0034 with respect to:				
Ship	**Smooth**	**FoulXSpel 2**	**F0037**	**FoulXSpel 1**	**Hull**
Yacht	1.82	6.16	2.35	1.03	5.12
Tugboat	1.61	5.53	2.10	0.92	4.59
Cargo vessel	1.49	5.26	2.00	0.87	4.37
Handymax tanker	1.42	5.07	1.93	0.84	4.21
Containership	1.39	4.99	1.91	0.85	4.15
LNG carrier	1.41	4.98	1.91	0.84	4.42

Table 5.7 demonstrates the advantage of F0034 over the other test surfaces. It is worth noting that the use of the newly developed F0034 on a ship hull reduces the C_F by up to ~6% with respect to the C_F of the hull coated with a TBT-free antifouling coating, i.e. FoulXSpel 2. This can be translated into a significant decrease in fuel consumption, greenhouse gas emissions and therefore money when the life-cycle of a ship is taken into account. These results can be used to calculate the increases in the effective powers, provided that the towing test data of the ship models are in hand.

5.4 Prediction of the Roughness Effects of Biofouling on Ship Resistance and Powering

The roughness functions and roughness Reynolds numbers given in the following section were employed in the code and predictions were made for varying fouling conditions. Approximately 7000 predictions were made for ship lengths from 10 m to 300 m with 10 m increments. The added resistance diagrams were then generated using this database. The increases in the frictional resistances as well as the effective power of ships were calculated using the diagrams.

5.4.1 Roughness Functions and Fouling Conditions

Schultz and Flack (2007) determined the roughness functions for three dimensional rough surfaces similar to those used by Shockling et al. (2006). Schultz (2007) proposed that the roughness function behaviour of a range of fouling conditions

follow the roughness functions of Schultz and Flack (2007) and Shockling et al. (2006), based on his previous work presented in Schultz (2004). This is a reasonable assumption, since the roughness functions of real surfaces are expected to show behaviour that is between the monotonic Colebrook and inflectional Nikuradse type roughness functions, such as those presented by Schultz and Flack (2007) and Shockling et al. (2006), as shown in Figure 5.9. In addition, Schultz (2007) presented the equivalent sand roughness heights for a range of coating and fouling conditions together with the NSTM (Naval Ships' Technical Manual) rating and average coating roughness (Rt_{50}) based on his extensive experiments including Schultz (2004) (Table 5.8).

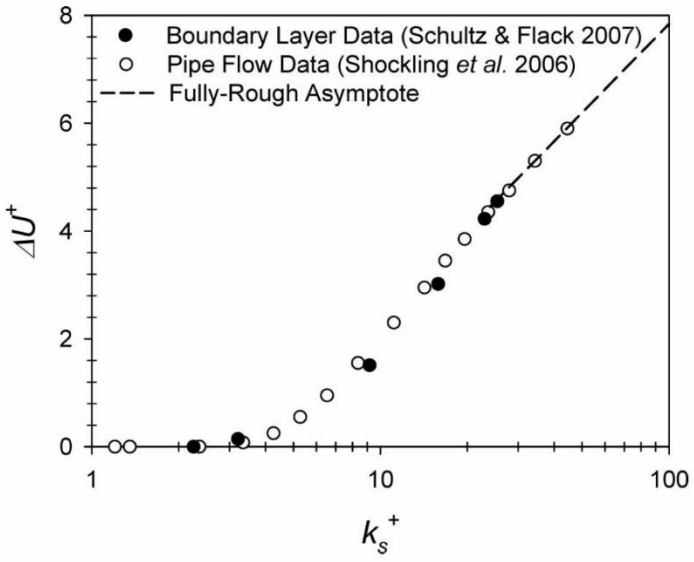

Figure 5.9: Roughness function vs. roughness Reynolds numbers (Schultz, 2007).

Table 5.8: A range of representative coating and fouling conditions. (Schultz, 2007).

Description of condition	NSTM rating*	k_s (μm)	Rt_{50} (μm)
Hydraulically smooth surface	0	0	0
Typical as applied AF coating	0	30	150
Deteriorated coating or light slime	10-20	100	300
Heavy slime	30	300	600
Small calcareous fouling or weed	40-60	1000	1000
Medium calcareous fouling	70-80	3000	3000
Heavy calcareous fouling	90-100	10000	10000

*NSTM (2002)

The present predictions were made based on the assumptions that the given fouling conditions can be represented by these roughness functions and roughness length scales. Schultz (2007) validated these assumptions and this method by comparing his

results with other studies such as Hundley and Tate (1980) and Haslbeck and Bohlander (1992), documenting the effects of coatings and biofouling on ship powering through full-scale trials.

5.4.2 Added Resistance Diagrams

The added resistance coefficients, ΔC_F, due to a typical coating and different fouling conditions were plotted against the ship speeds. Either logarithmic or polynomial equations were then fitted to the ΔC_F values using the least squares method in order to evaluate added resistance diagrams. The diagrams are given separately for each surface condition. In addition, the diagrams of each condition are split into three, with each diagram showing a certain range of plate lengths, for visual convenience. These diagrams (Figure 5.10 - Figure 5.27) can be used directly to predict the added effective power requirements of ships due to hull fouling.

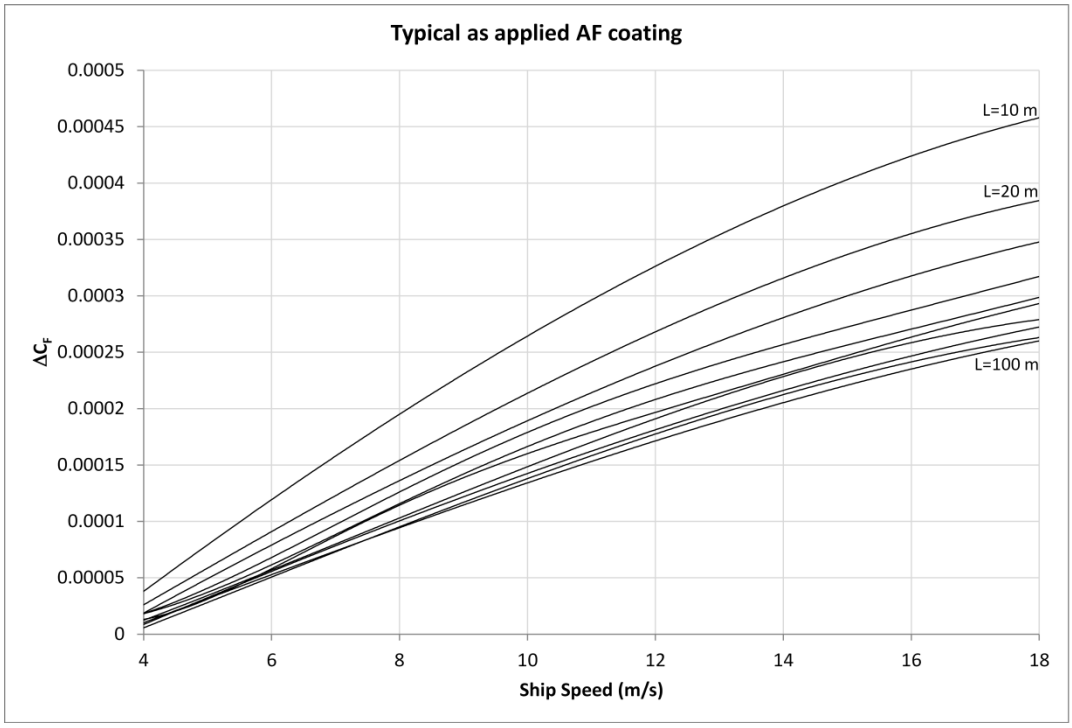

Figure 5.10: Added resistance diagram for ships with a typical as applied AF coating (L=10-100 m, 10 m increments).

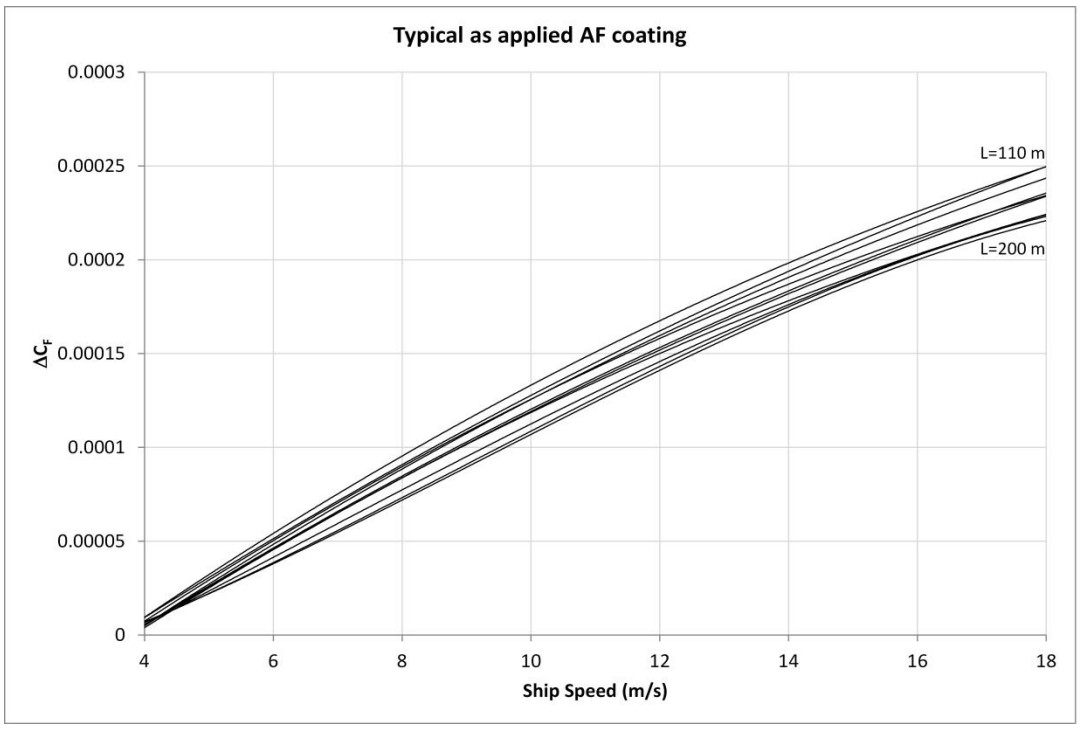

Figure 5.11: Added resistance diagram for ships with a typical as applied AF coating (L=110-200 m, 10 m increments).

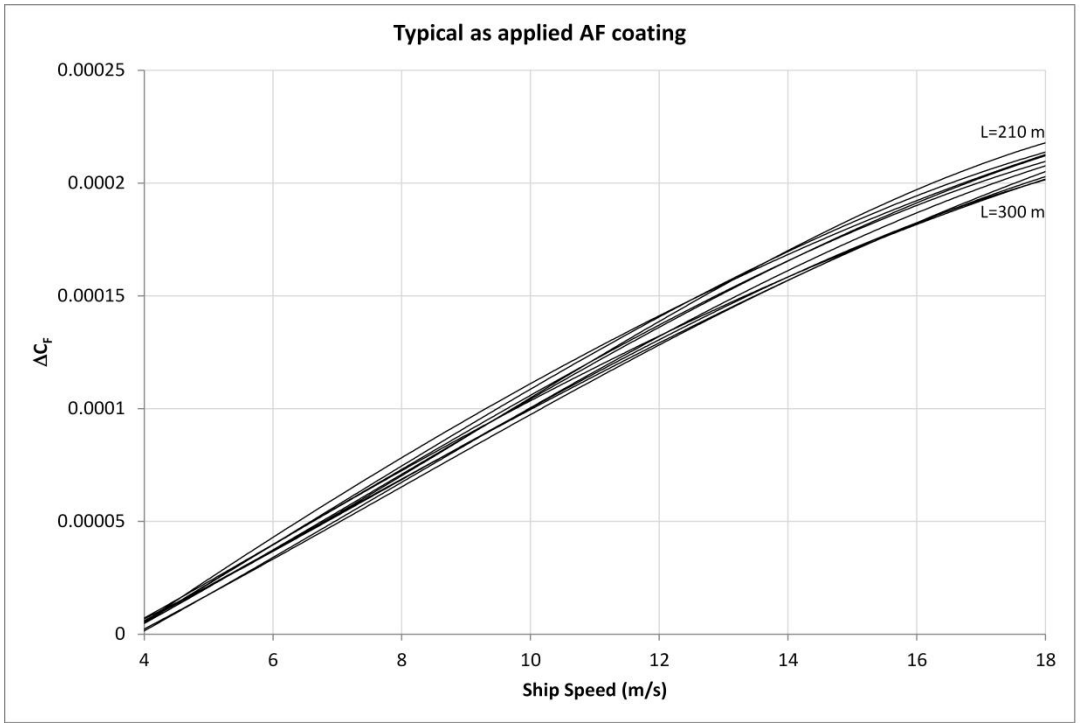

Figure 5.12: Added resistance diagram for ships with a typical as applied AF coating (L=210-300 m, 10 m increments).

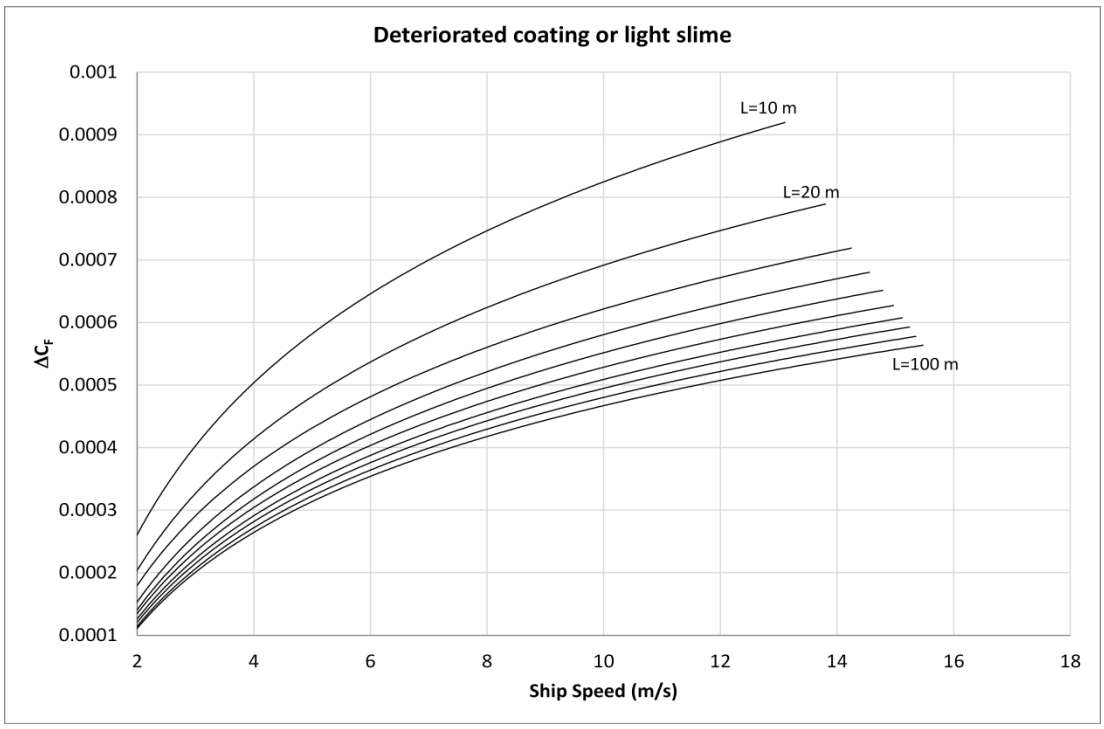

Figure 5.13: Added resistance diagram for ships with a deteriorated coating or light slime condition (L=10-100 m, 10 m increments).

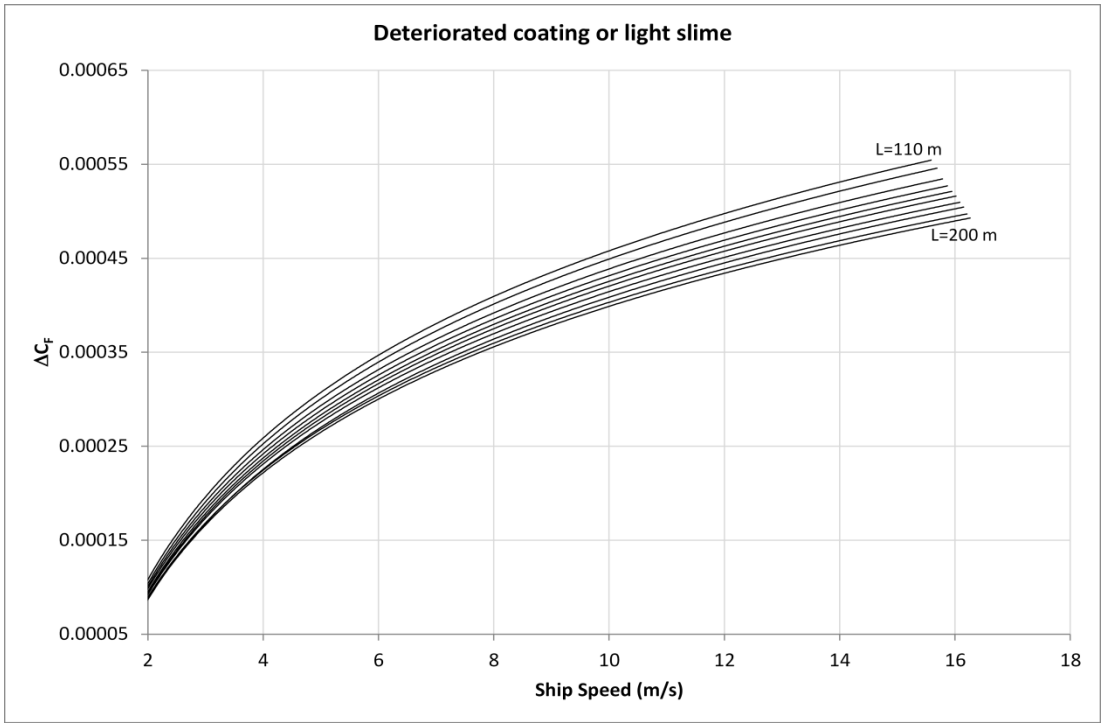

Figure 5.14: Added resistance diagram for ships with a deteriorated coating or light slime condition (L=110-200 m, 10 m increments).

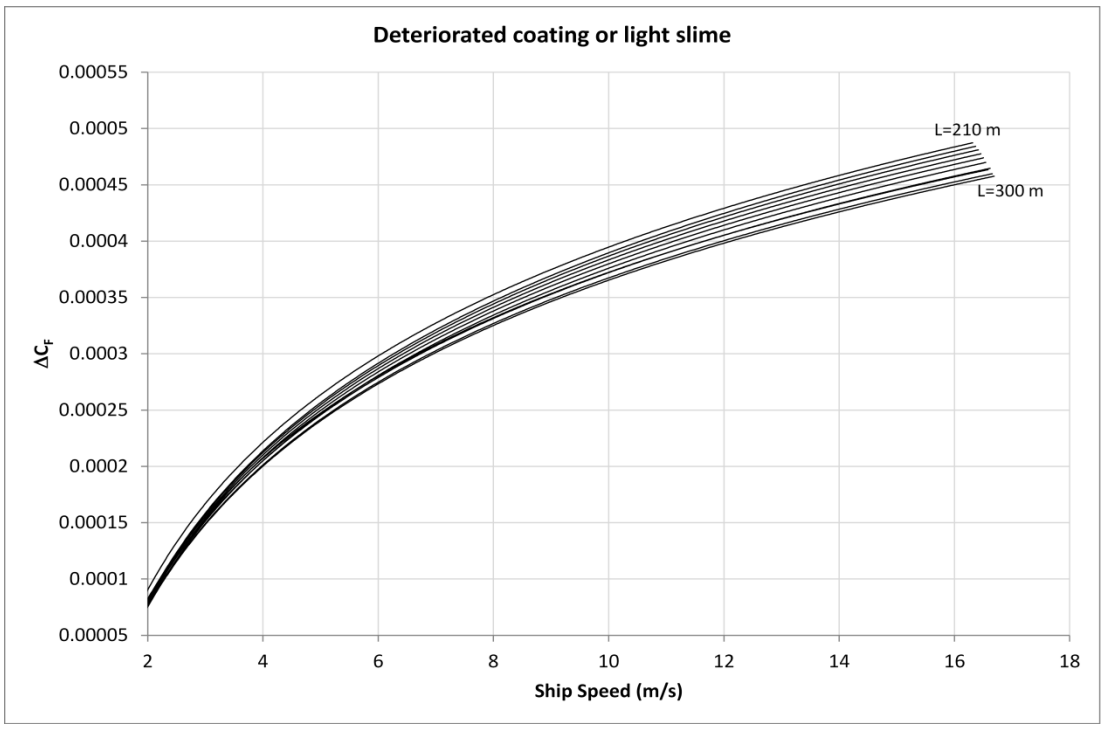

Figure 5.15: Added resistance diagram for ships with a deteriorated coating or light slime condition (L=210-300 m, 10 m increments).

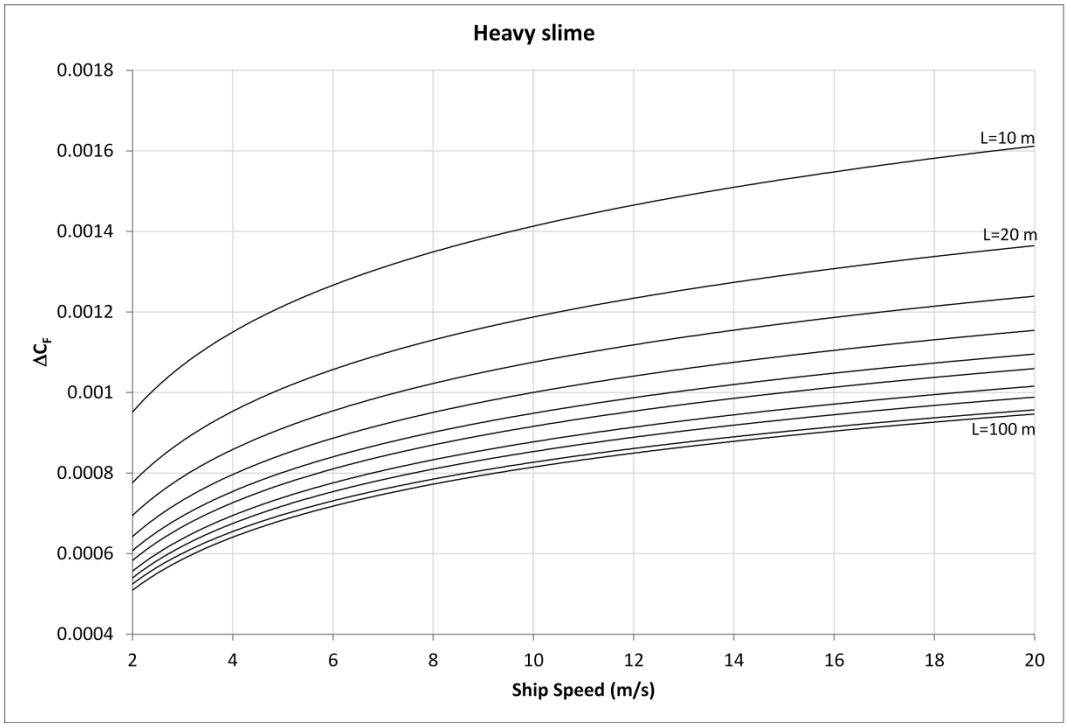

Figure 5.16: Added resistance diagram for ships with heavy slime (L=10-100 m, 10 m increments).

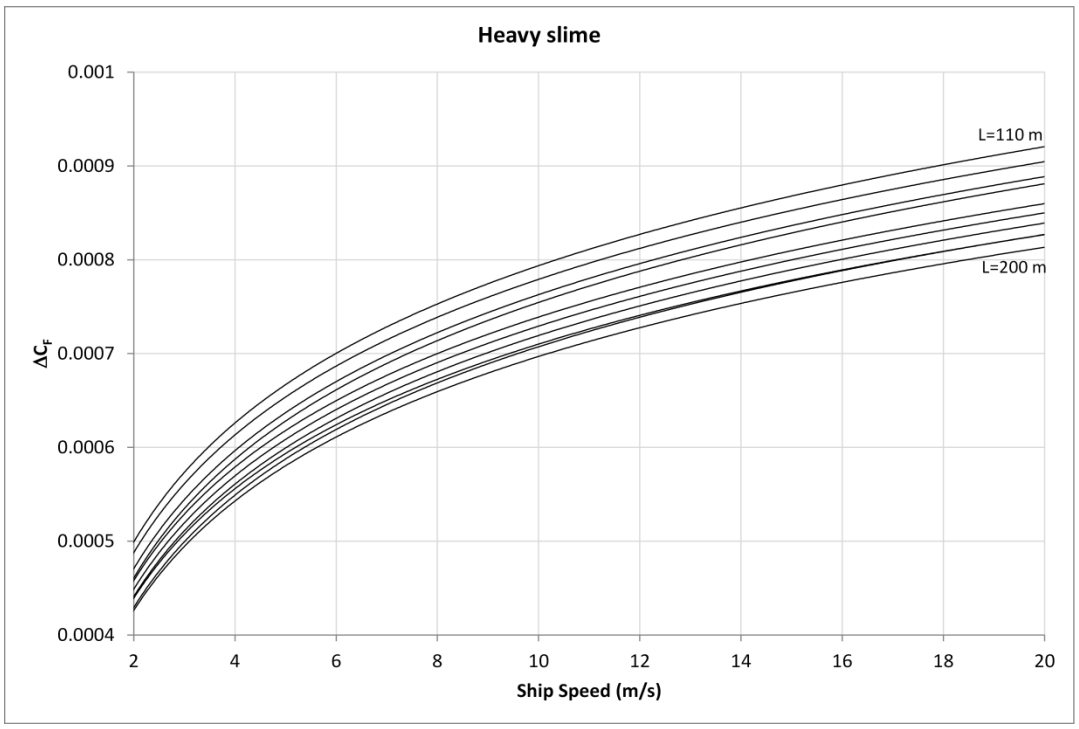

Figure 5.17: Added resistance diagram for ships with heavy slime (L=110-200 m, 10 m increments).

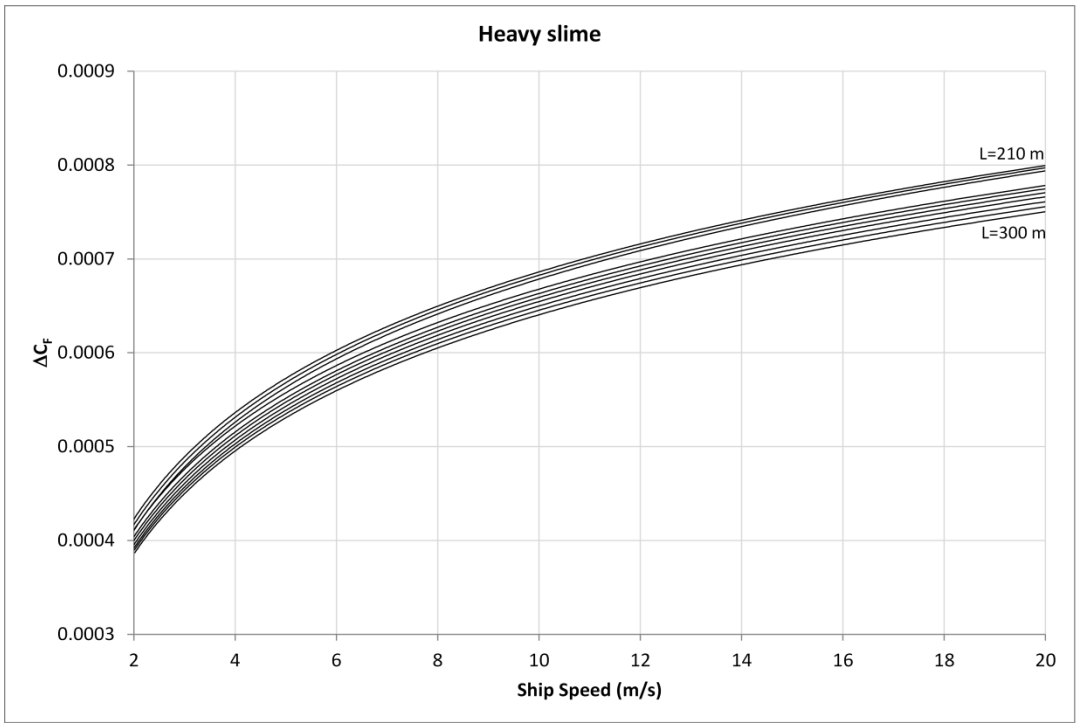

Figure 5.18: Added resistance diagram for ships with heavy slime (L=210-300 m, 10 m increments).

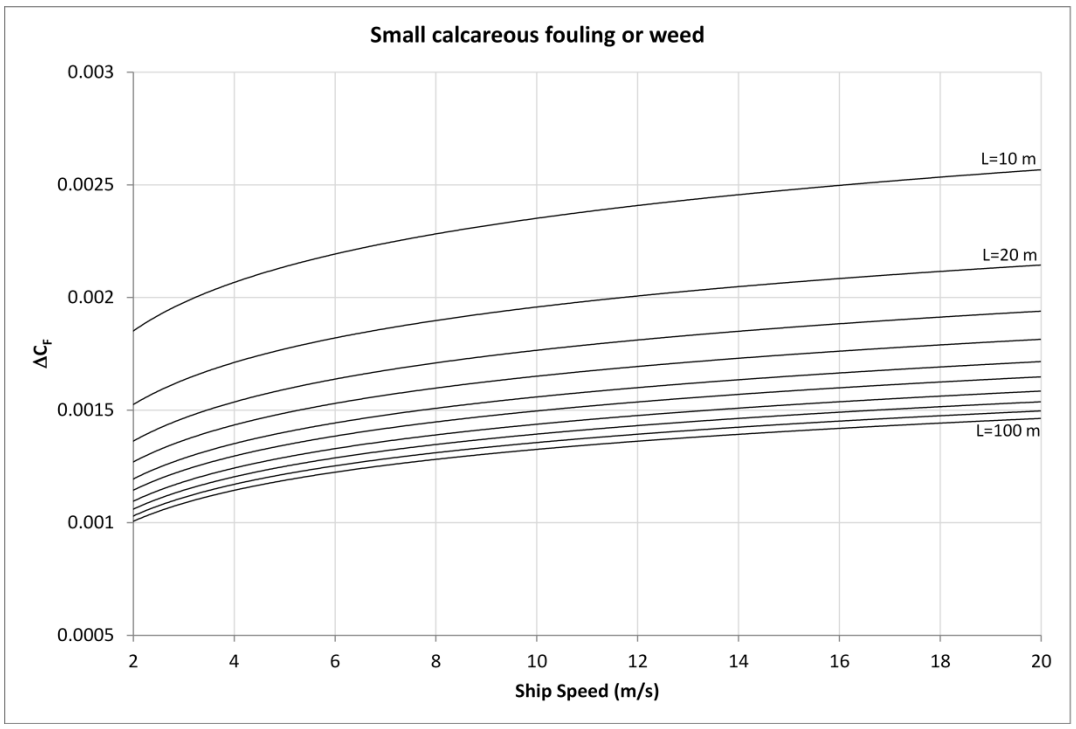

Figure 5.19: Added resistance diagram for ships with small calcareous fouling or weed (L=10-100 m, 10 m increments).

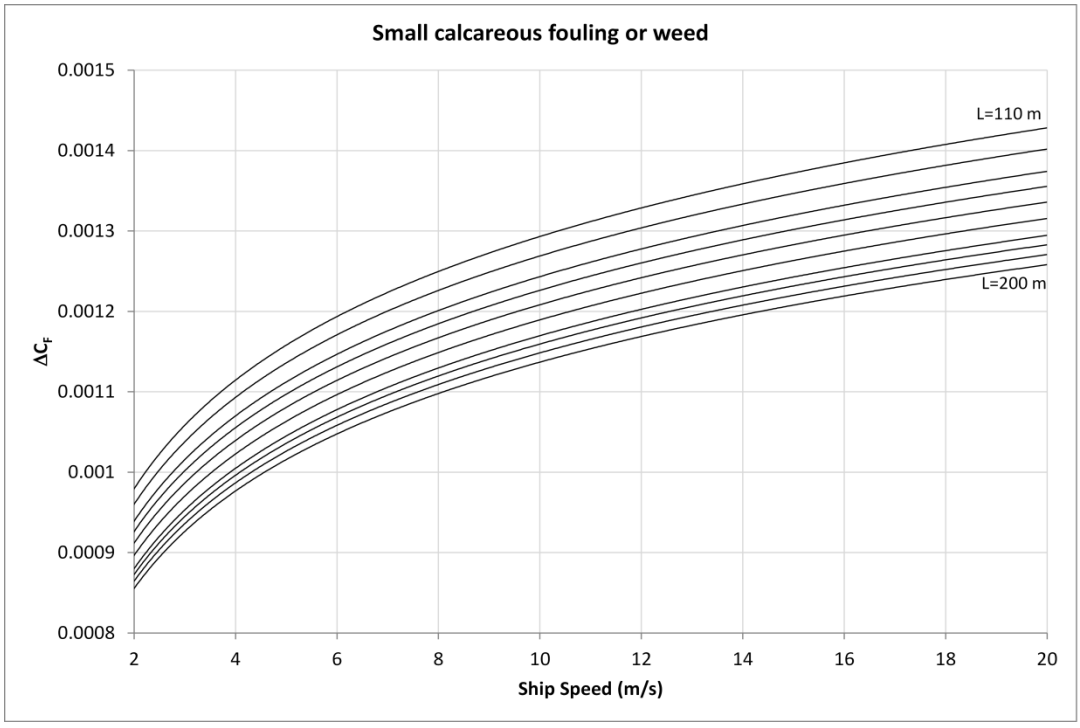

Figure 5.20: Added resistance diagram for ships with small calcareous fouling or weed (L=110-200 m, 10 m increments).

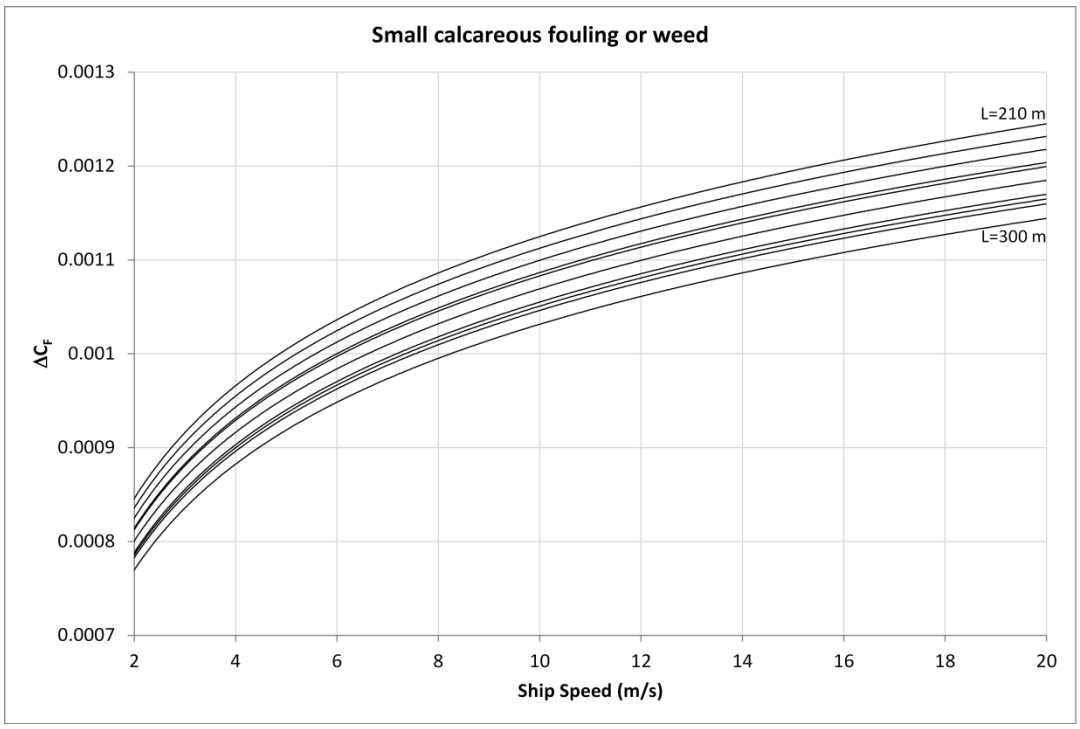

Figure 5.21: Added resistance diagram for ships with small calcareous fouling or weed (L=210-300 m, 10 m increments).

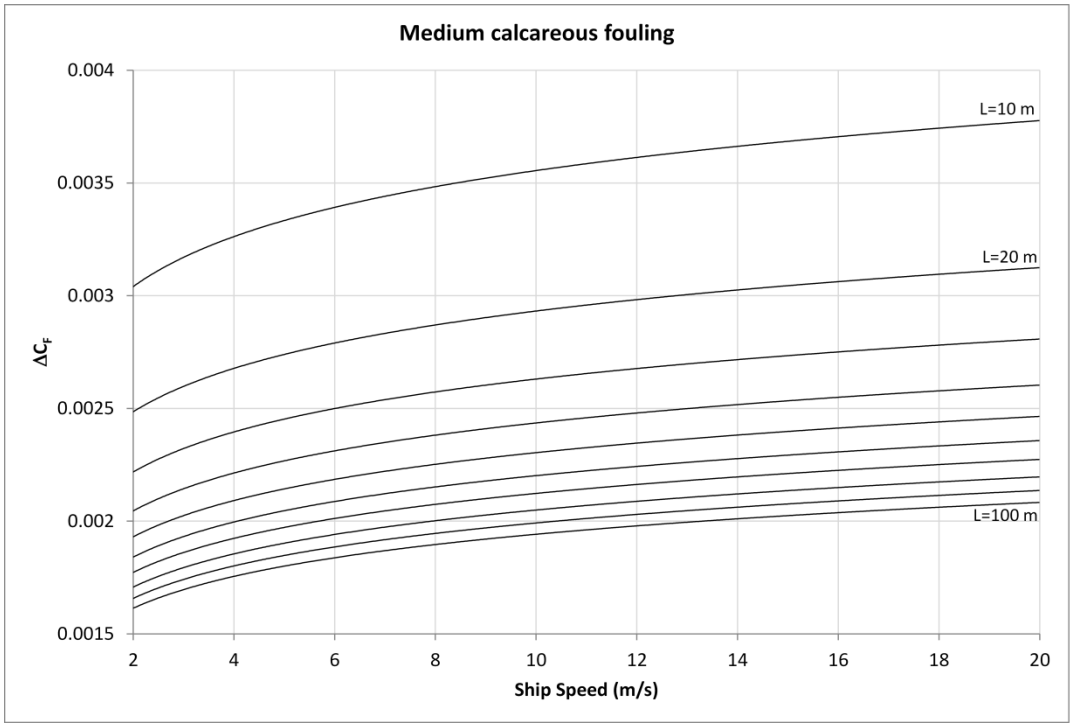

Figure 5.22: Added resistance diagram for ships with medium calcareous fouling (L=10-100 m, 10 m increments).

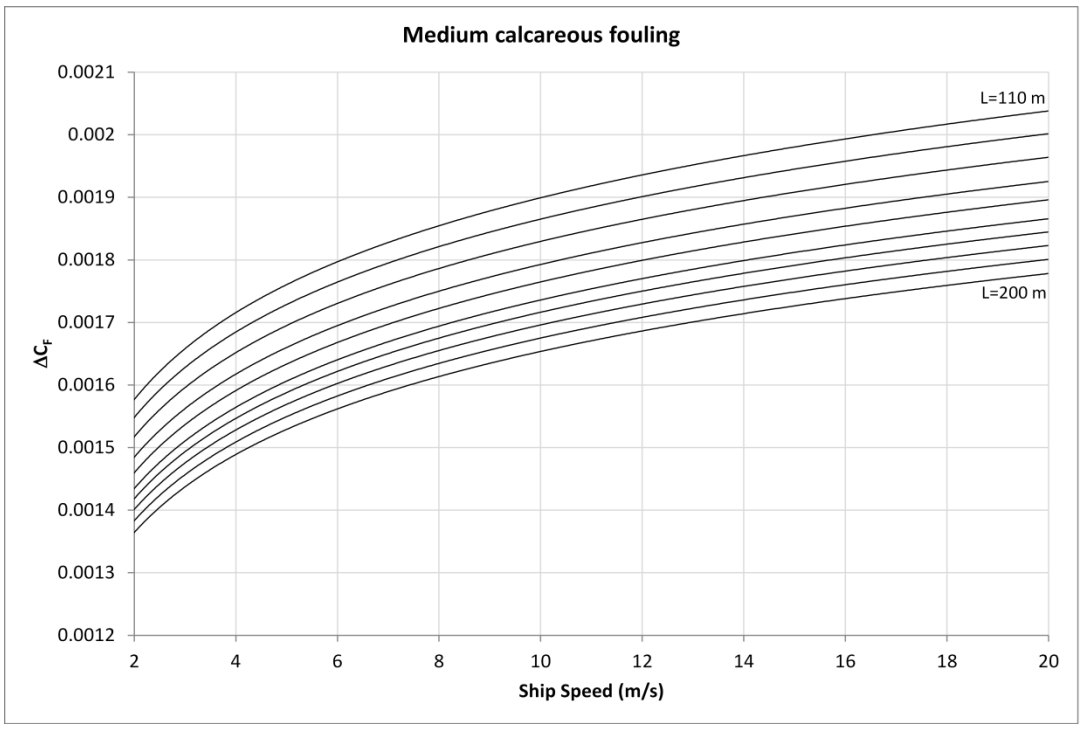

Figure 5.23: Added resistance diagram for ships with medium calcareous fouling (L=110-200 m, 10 m increments).

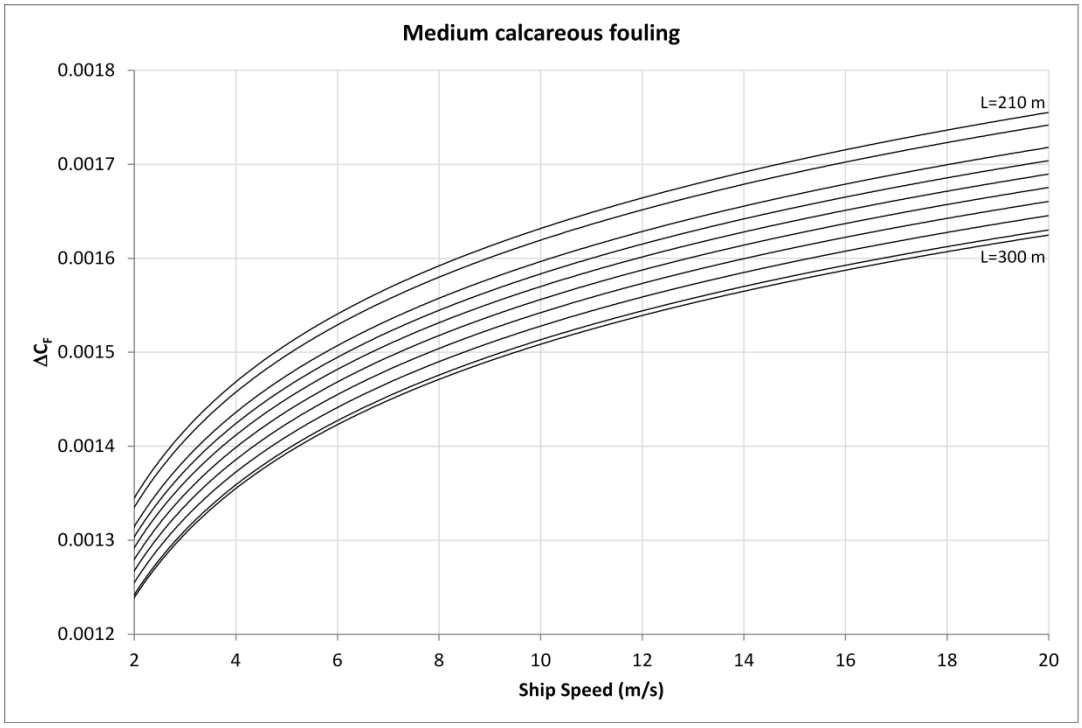

Figure 5.24: Added resistance diagram for ships with medium calcareous fouling (L=210-300 m, 10 m increments).

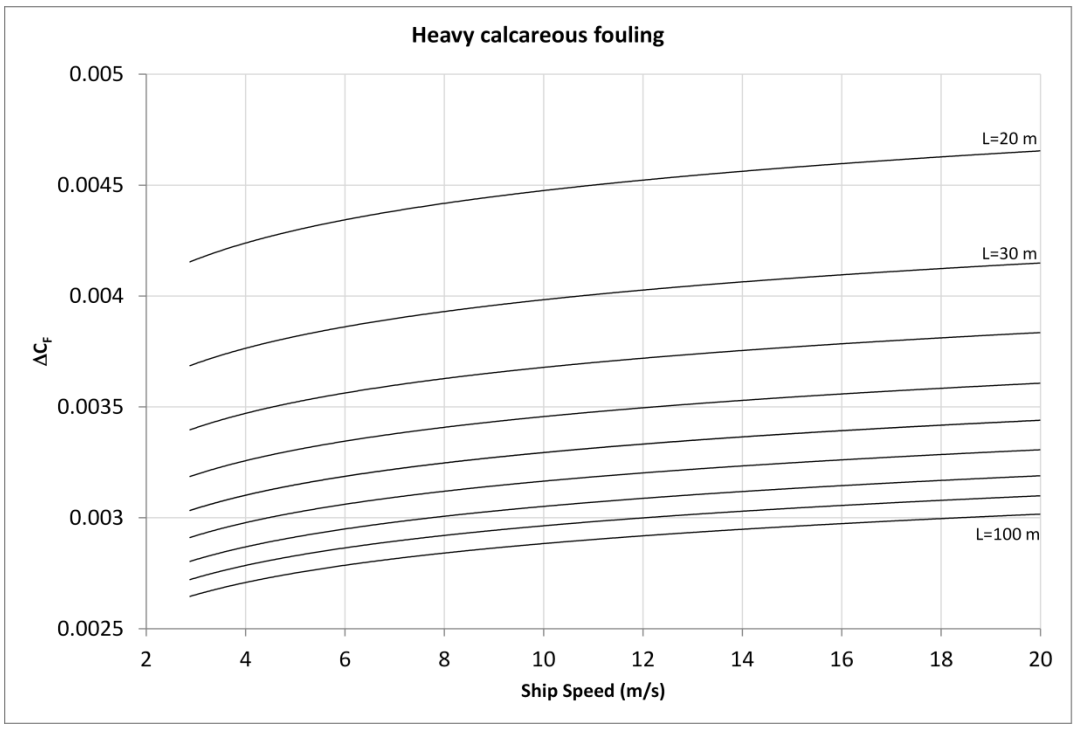

Figure 5.25: Added resistance diagram for ships with heavy calcareous fouling (L=20-100 m, 10 m increments).

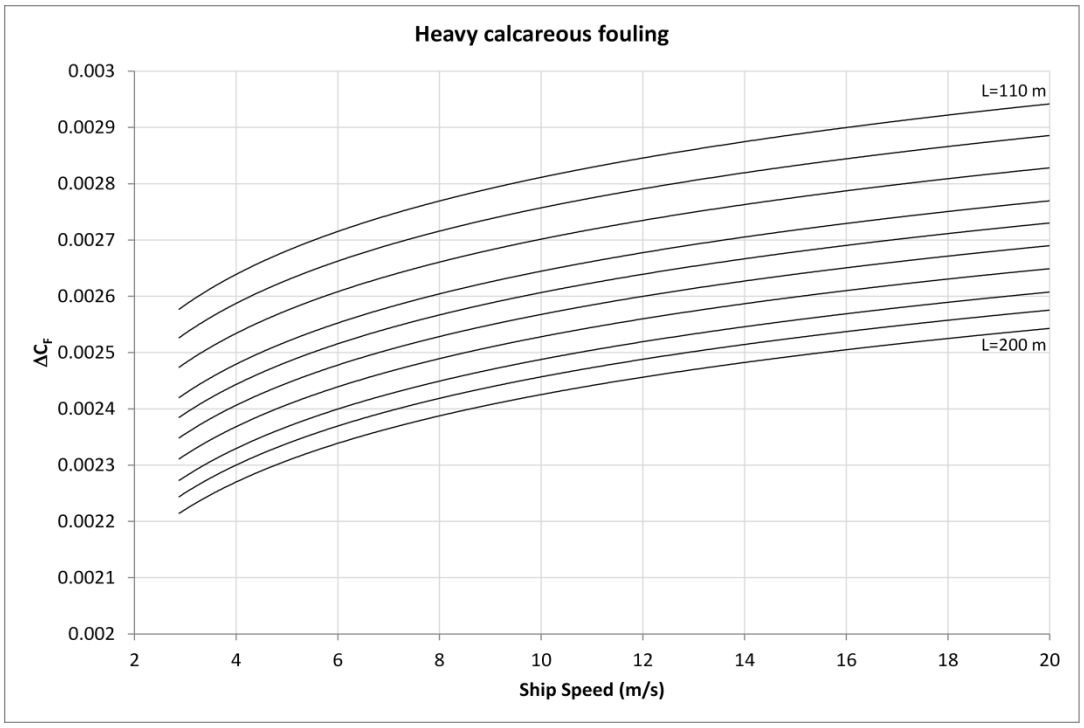

Figure 5.26: Added resistance diagram for ships with heavy calcareous fouling (L=110-200 m, 10 m increments).

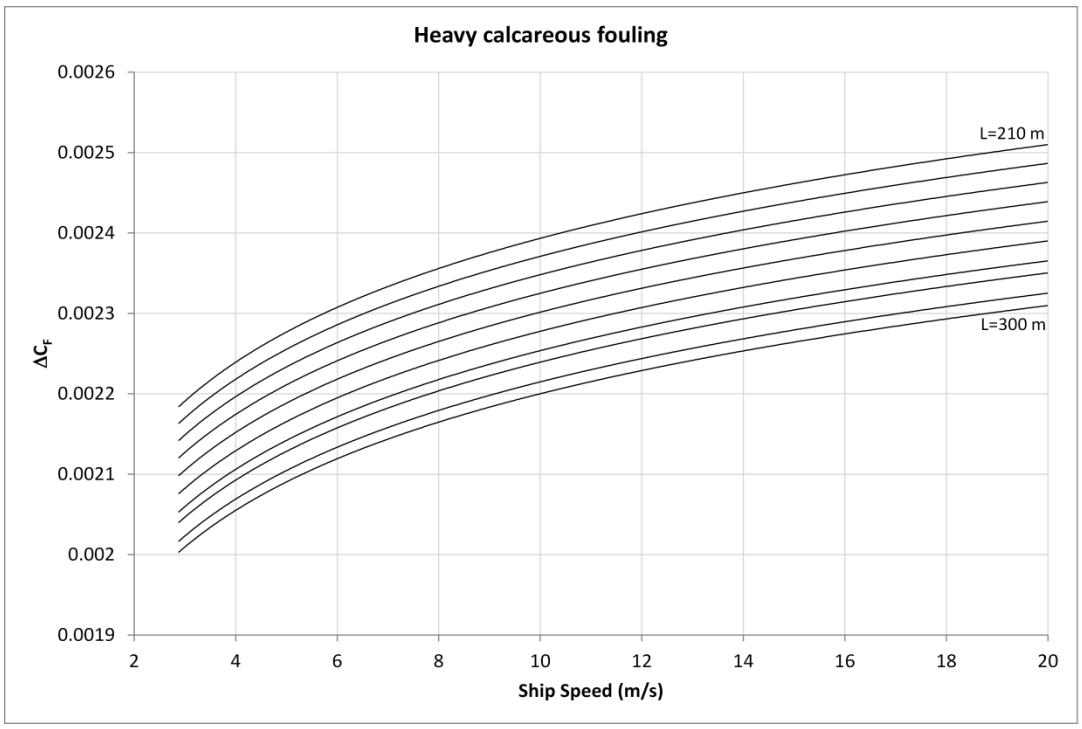

Figure 5.27: Added resistance diagram for ships with heavy calcareous fouling (L=210-300 m, 10 m increments).

It is evidently seen from the above diagrams that the added resistance values increase with increasing speeds. More specifically, at low speeds, the rate of increase in the added frictional resistance coefficients is higher than the rate at higher speeds. As expected, the effect of roughness on the frictional resistance of flat plates varies depending on both the plate length and towing speed. For a given ship speed and surface roughness, a shorter plate will be subjected to a greater degree of frictional resistance per unit area than a longer plate. This observation suggests that the ratio between the roughness height and flat plate length is critical. Interestingly, a lot of variation can be observed between the graphs of the different surface roughness conditions. For example, looking at the surface with the lowest roughness (the as applied AF coating), the added frictional resistance coefficient decreases markedly with increasing plate length between 10 m and 50 m, but for plate lengths of greater than 50 m, the decrease becomes much lower; almost negligible for the highest plate lengths. This is in contrast to a much rougher surface (such as heavy calcareous fouling), where even for the highest plate lengths, a noticeable decrease can still be observed.

It is believed that these diagrams may serve as a simple prediction tool for naval architects and may be used to increase the awareness and emphasise the importance of biofouling mitigation on ship hulls, to ultimately enable more energy efficient ship operations.

5.4.3 Added Resistance and Effective Power of Ships

An increase in the frictional resistance would increase the effective power, P_E, of a ship, which is the necessary power to move a ship through water. P_E is related to the total resistance and ship speed, which is defined by equation (5.4).

$$P_E = R_T V \tag{5.4}$$

If we recall equation (4.2), we can then re-write equation (5.4) as

$$P_E = \frac{1}{2}\rho S C_T V^3 \tag{5.5}$$

The increase in P_E due to the effect of fouling can be expressed by

$$\%\Delta P_E = \frac{C_{T,rough} - C_{T,smooth}}{C_{T,smooth}} \times 100 = \frac{\Delta C_F}{C_{T,smooth}} \times 100 \tag{5.6}$$

similar to that used by Tezdogan et al. (2015). ΔC_F is the added resistance due to surface roughness and can be read from the diagrams given in the previous section. $C_{T,smooth}$ on the other hand, includes other resistance components and the evaluation of this is not the subject of this study. Therefore, other sources were used to obtain the $C_{T,smooth}$ values of ships.

The predictions of the added effective powers of two different ships (a 232.5 m containership (KCS) and a 270 m LNG carrier) were made using the generated diagrams. The $C_{T,smooth}$ values of the KCS were taken from other studies in the literature. The $C_{T,smooth}$ values of the LNG carrier were taken from the report of the experiments that were performed earlier at the Kelvin Hydrodynamics Laboratory at the University of Strathclyde.

During the towing tank tests conducted by Kim et al. (2001), the coefficients of total resistance and residuary resistance for a 1/31.6 scale model of the KCS (Re_{model}=1.4x10^{7}) were found to be 3.557x10^{-3} and 7.250x10^{-4}, respectively, at a model speed corresponding to a full-scale speed of 24 knots. The full scale $C_{T,smooth}$ value was predicted to be 2.075x10^{-3} from the model tests. $C_{T,smooth}$ at a ship speed of 19 knots for the full-scale KCS model was previously predicted to be 1.858x10^{-3} by Tezdogan et al. (2015) through URANS CFD simulations. These values were used to predict the percentage increase in the effective power.

Table 5.9 shows the ΔC_F values of the KCS at ship speeds of 19 and 24 knots, obtained by reading from the diagrams given in the previous section.

Table 5.9: ΔC_F values of the KCS at 19 and 24 knots.

Description of condition	**Speed (knots)**	**ΔC_F (Granville)**
Hydraulically smooth surface	19	-
	24	-
Typical as applied AF coating	19	0.000088
	24	0.000121
Deteriorated coating or light slime	19	0.000369
	24	0.000405
Heavy slime	19	0.000662
	24	0.000698
Small calcareous fouling or weed	19	0.001072
	24	0.001108
Medium calcareous fouling	19	0.001559
	24	0.001594
Heavy calcareous fouling	19	0.002270
	24	0.002304

Table 5.10 and Table 5.11 illustrate the percentage increase in the frictional resistances and effective powers of the KCS at 19 and 24 knots, respectively, calculated using the ΔC_F values given in Table 5.9.

Table 5.10: The increases in the frictional resistance and effective power of the KCS at 19 knots.

Description of condition	% ΔC_F	% ΔP_E
Hydraulically smooth surface	-	-
Typical as applied AF coating	6.3	4.7
Deteriorated coating or light slime	26.6	19.9
Heavy slime	47.8	35.7
Small calcareous fouling or weed	77.4	57.7
Medium calcareous fouling	112.6	83.9
Heavy calcareous fouling	163.9	122.2

Table 5.11: The increases in the frictional resistance and effective power of the KCS at 24 knots.

Description of condition	% ΔC_F	% ΔP_E
Hydraulically smooth surface	-	-
Typical as applied AF coating	9.0	5.8
Deteriorated coating or light slime	30.0	19.5
Heavy slime	51.8	33.6
Small calcareous fouling or weed	82.2	53.4
Medium calcareous fouling	118.3	76.8
Heavy calcareous fouling	171.0	111.0

The results presented in Table 5.10 and Table 5.11 indicate that the increases in C_F of the KCS due to the hull roughness of a typical AF coating are relatively insignificant (6.3% and 9% at 19 knots and 24 knots, respectively), whereas the increases in C_F due to biofouling are predicted to be dramatic, which can lead to a drastic increase in its fuel consumption and hence CO_2 emissions.

As can be seen from Table 5.10, the increases in the frictional resistance and effective power of the KCS due to a deteriorated coating or light slime surface condition at a slow steaming ship speed of 19 knots were predicted to be 26.6% and 19.9%, respectively. These values became 47.8% and 35.7% when calculating the increase in C_F and P_E due to a heavy slime condition. Calcareous fouling causes significant increases in C_F values ranging from ~77% to ~164%, and an increase in P_E values ranging from ~58% to ~122%, depending on the type of calcareous fouling.

Likewise, the increases in the C_F and P_E values of the KCS due to a deteriorated coating or light slime surface condition at ship speeds of 24 knots were predicted to be 30% and 19.5%, respectively, as shown in Table 5.11. The increases in C_F and P_E were predicted to be 51.8% and 33.6% for the heavy slime surface condition. Calcareous fouling causes significant increases in C_F values ranging from ~82% to

~171% and an increase in P_E values ranging from ~53% to ~111%, depending on the type of fouling. Table 5.12 shows the ΔC_F values of the LNG carrier at several speeds, obtained by reading from the diagrams given in the previous section.

Table 5.12: ΔC_F values of the LNG carrier at several speeds.

Description of condition	Speed (knots)	ΔC_F (Granville)
Hydraulically smooth surface	10	-
	12	-
	14	-
	16	-
	18	-
	20	-
Typical as applied AF coating	10	1.99854E-05
	12	3.72348E-05
	14	5.74242E-05
	16	7.77768E-05
	18	9.6947E-05
	20	0.000114051
Deteriorated coating or light slime	10	0.000252247
	12	0.000285395
	14	0.000313334
	16	0.000337342
	18	0.000358681
	20	0.000377916
Heavy slime	10	0.000547250
	12	0.000576868
	14	0.000601831
	16	0.000623282
	18	0.000642348
	20	0.000659535
Small calcareous fouling or weed	10	0.000944627
	12	0.000975116
	14	0.001000813
	16	0.001022896
	18	0.001042523
	20	0.001060215
Medium calcareous fouling	10	0.001428413
	12	0.001459802
	14	0.001486258
	16	0.001508992
	18	0.001529198
	20	0.001547413
Heavy calcareous fouling	10	0.002146307
	12	0.002175935
	14	0.002200907
	16	0.002222366
	18	0.002241439
	20	0.002258632

Table 5.13 - Table 5.18 illustrate the percentage increase in the frictional resistances and effective powers of the LNG carrier at ship speeds of 10, 12, 14, 16, 18 and 20 knots, calculated by using the ΔC_F values given in Table 5.12.

Table 5.13: The increases in the frictional resistance and effective power of the LNG carrier at 10 knots.

Description of condition	% ΔC_F	% ΔP_E
Hydraulically smooth surface	-	-
Typical as applied AF coating	1.4	1.1
Deteriorated coating or light slime	17.3	13.3
Heavy slime	37.5	29.0
Small calcareous fouling or weed	64.7	50.0
Medium calcareous fouling	97.8	75.6
Heavy calcareous fouling	147.0	113.6

Table 5.14: The increases in the frictional resistance and effective power of the LNG carrier at 12 knots.

Description of condition	% ΔC_F	% ΔP_E
Hydraulically smooth surface	-	-
Typical as applied AF coating	2.6	1.8
Deteriorated coating or light slime	20.0	13.8
Heavy slime	40.4	27.9
Small calcareous fouling or weed	68.2	47.2
Medium calcareous fouling	102.1	70.7
Heavy calcareous fouling	152.3	105.4

Table 5.15: The increases in the frictional resistance and effective power of the LNG carrier at 14 knots.

Description of condition	% ΔC_F	% ΔP_E
Hydraulically smooth surface	-	-
Typical as applied AF coating	4.1	2.7
Deteriorated coating or light slime	22.3	15.0
Heavy slime	42.9	28.8
Small calcareous fouling or weed	71.3	47.8
Medium calcareous fouling	105.9	71.0
Heavy calcareous fouling	156.9	105.2

Table 5.16: The increases in the frictional resistance and effective power of the LNG carrier at 16 knots.

Description of condition	% ΔC_F	% ΔP_E
Hydraulically smooth surface	-	-
Typical as applied AF coating	5.6	3.7
Deteriorated coating or light slime	24.4	16.1
Heavy slime	45.1	29.8
Small calcareous fouling or weed	74.1	48.9
Medium calcareous fouling	109.3	72.1
Heavy calcareous fouling	160.9	106.2

Table 5.17: The increases in the frictional resistance and effective power of the LNG carrier at 18 knots.

Description of condition	% ΔC_F	% ΔP_E
Hydraulically smooth surface	-	-
Typical as applied AF coating	7.1	4.6
Deteriorated coating or light slime	26.4	17.2
Heavy slime	47.2	30.8
Small calcareous fouling or weed	76.6	50.0
Medium calcareous fouling	112.4	73.3
Heavy calcareous fouling	164.7	107.5

Table 5.18: The increases in the frictional resistance and effective power of the LNG carrier at 20 knots.

Description of condition	% ΔC_F	% ΔP_E
Hydraulically smooth surface	-	-
Typical as applied AF coating	8.5	5.2
Deteriorated coating or light slime	28.1	17.2
Heavy slime	49.1	30.1
Small calcareous fouling or weed	78.9	48.3
Medium calcareous fouling	115.2	70.5
Heavy calcareous fouling	168.2	102.9

As Table 5.13 - Table 5.18 show, the increases in frictional resistance and effective power become significant when the fouling conditions become severe, as expected. The increases in the effective power of the LNG carrier due to a typical, as applied AF coating were predicted to be 1.1%, 3.7% and 5.2% at ship speeds of 10 knots, 16 knots and 20 knots, respectively, whereas those due to a deteriorated coating or light slime may increase to 13.3%, 16.1% and 17.2%, respectively. The effect of heavy slime on the LNG carrier was calculated to cause an increase in the effective power of 29%, 29.8% and 30.1% at ship speeds of 10, 16 and 20 knots, respectively. The calcareous fouling would increase P_E by ~114%, ~106% and ~103%, at ship speeds of 10, 16 and 20 knots.

5.5 Chapter Summary and Conclusions

Firstly, an in-house prediction code based on the similarity law analysis of Granville (1958) was developed to be able to rapidly and robustly predict the effect of a given roughness on the frictional resistance of full-scale ships.

Following this, the roughness functions and roughness Reynolds numbers of FOUL-X-SPEL paints obtained in Chapter 4 were employed in the code. The added frictional resistance coefficients of flat plates representing a yacht, a tugboat, a cargo

vessel, a handymax tanker, a containership (KCS) and an LNG carrier were then predicted and the added resistance diagrams were generated using these predictions. The advantage of the use of the new FOUL-X-SPEL F0034 over the use of other coatings was evidently shown. It was shown that it improves the frictional resistance by an average of 5.3% with respect to the use of the TBT-free SPC antifouling coating.

Predictions of the effect of a range of representative coating and biofouling conditions were then made using the developed code. The roughness functions of such conditions were assumed to follow the roughness function behaviours of the ones provided by Schultz and Flack (2007) and the fouling conditions were assumed to be represented by the roughness length scales proposed by Schultz (2007). These were employed in the aforementioned in-house code and, using this approach, an extensive database of ΔC_F as functions of fouling conditions, ship lengths and ship speeds was generated. Either logarithmic or polynomial equations were then fitted to the individual ΔC_F values using the least squares method in order to evaluate added resistance diagrams. These diagrams were presented from 10 m to 300 m ship lengths and from slow to high ship speeds for each surface condition.

In their current state, these diagrams can be used to predict the effects of a range of representative coating and fouling conditions defined by Schultz (2007). It is of note that this approach assumes a homogenous distribution of fouling on a ship hull, which may not necessarily be the case on real ship hulls. Therefore, additional results from further immersion tests and experiments considering different types of fouling and their spatial distributions would be beneficial to improve the diagrams. Having said that, the present diagrams may be considered as a leap forward towards a universal model.

The diagrams have a key advantage in that they capture the complex hydrodynamic response of fouling in simple curves which can be implemented in a spreadsheet or a tool for life-cycle cost estimation. The main advantage of the proposed diagrams is that they directly enable the use of surface conditions, ship length and ship speed, rather than having to use hydrodynamic parameters. By using the diagrams, one can easily estimate the added resistance, and hence the fuel penalty, of a ship for a

particular fouling condition. Therefore, it becomes very practical to calculate the effect of a range of representative coating and fouling conditions on frictional resistance.

This chapter not only proposes diagrams but it also provides the algorithm of a prediction procedure showing how to develop such diagrams using the available experimental data. This means that once future experimental data is available, the developed in-house code can be operated again and new diagrams can be developed quickly and easily.

Further research is recommended in order to define the surfaces and roughness functions in more complex ways, such as by considering the spatial distribution of fouling, or its percentage coverage on a hull.

6 A CFD Model for the Frictional Resistance Prediction of Antifouling Coatings

6.1 Introduction

The use of marine antifouling coatings is a common method used to smooth hull surfaces to reduce the frictional resistance and fuel consumption of a ship. Additionally, the use of coatings with a proper cathodic protection system can offer effective corrosion protection (Tezdogan and Demirel, 2014). However, such coatings will have initial surface roughnesses which affect a ship's frictional resistance. A means of assessing the effect of such a coating on frictional resistance would therefore be of great benefit. However, at present, there is no accurate method available to predict the effect of ship roughness due to the use of antifouling coatings (ITTC, 2008b, 2011b).

To the best of this author's knowledge, no specific CFD model exists to predict the effects of a marine antifouling coating's roughness on flow and frictional resistance. The aim of the present study is therefore to fill this gap by employing a modified wall-function in the CFD software. The proposed approach enables the prediction of the frictional resistance coefficients of coated plates for different speeds, using only roughness measurements of the surfaces. This model will also be a solid basis for a CFD model for the prediction of the effect of fouling on frictional resistance.

In this study, the experimental data of Schultz (2004) were used to establish a suitable roughness function model for coatings. The required quantities were evaluated from the experimental data using an indirect method, and a roughness function model and roughness length scale were determined for coatings. This roughness function model was then employed in the wall-function of the CFD software package STAR-CCM+.

Following this, a validation study was performed through CFD simulations of towing tests involving coated plates at three Reynolds numbers ($2.8x10^6$, $4.2x10^6$ and $5.5x10^6$), in a similar manner to the experiments of Schultz (2004), using STAR-CCM+. Frictional resistance coefficients and roughness Reynolds numbers were computed and compared with the experimental data. It should also be borne in mind that CFD simulations performed in this study are similar in part to those performed by Demirel et al. (2013) and Demirel et al. (2014a). However, these were exploratory studies and the simulations were performed at only one towing speed. Additionally, within the present study, improvements were made to the simulations to ensure their reproducibility.

After the validation study, the effects of antifouling coatings on the frictional resistance of a tanker were predicted using the developed CFD model and the results were compared with those obtained using the similarity law scaling procedure, presented in Chapter 5, Section 5.2. A flat plate of length 170m was chosen to represent a handymax tanker. Different types of antifouling coatings were considered at an operational ship speed of 13 knots. The plate was fully submerged since the surface roughness does not affect the wave-making resistance. Frictional resistance coefficients of the plate were evaluated for each case.

This chapter is organised as follows: A determination of the appropriate roughness function model for antifouling coatings is presented in Section 6.2, while a new wall-function formulation is proposed and details of the CFD simulations are covered in Section 6.3. In Section 6.4, the numerical results and the experimental data are compared, and predictions of the increase in the frictional resistance coefficients of a tanker coated with different antifouling coatings are demonstrated. Finally, the results of the study are discussed in Section 6.5, along with recommendations for future avenues of research.

6.2 Roughness Functions

Schultz (2004) conducted towing tests of flat plates coated with different antifouling coatings in order to investigate the initial drag performances of the coatings. He used five antifouling coating systems: Silicone 1, Silicone 2, Ablative Copper, SPC (Self-

Polishing Copolymer) Copper and SPC TBT (Tributyltin). Three control surfaces were also tested: the plates covered with 60-grit and 220-grit sandpapers (SP) and a smooth surface. The frictional resistance coefficients of each test surface were obtained for seven different Reynolds numbers.

Roughness amplitude parameters of all test surfaces are shown in Table 6.1. R_a is the average roughness height, R_q is the root mean square average of the roughness profile ordinates and R_t is the maximum peak to trough roughness height.

Table 6.1: Roughness amplitude parameters for all test surfaces, adapted from Schultz (2004).

Test Surface	R_a (μm)	R_q (μm)	R_t (μm)
Silicone 1	12 ± 2	14 ± 2	66 ± 7
Silicone 2	14 ± 2	17 ± 2	85 ± 8
Ablative Copper	13 ± 1	16 ± 1	83 ± 6
SPC Copper	15 ± 1	18 ± 1	97 ± 10
SPC TBT	20 ± 1	24 ± 2	129 ± 9
60-grit SP	126 ± 5	160 ± 7	983 ± 89
220-grit SP	30 ± 2	38 ± 2	275 ± 17

k^+ and ΔU^+ for the surfaces can be obtained iteratively using (2.36) and (2.37) (Granville, 1987) using the experimental data.

As per Schultz's (2004) suggestion, $0.17R_a$ is chosen as the roughness height for antifouling surfaces, whereas the roughness height for sandpapers is chosen as $0.75R_t$. Figure 6.1 depicts the evaluated roughness functions and roughness Reynolds numbers together with the roughness function models.

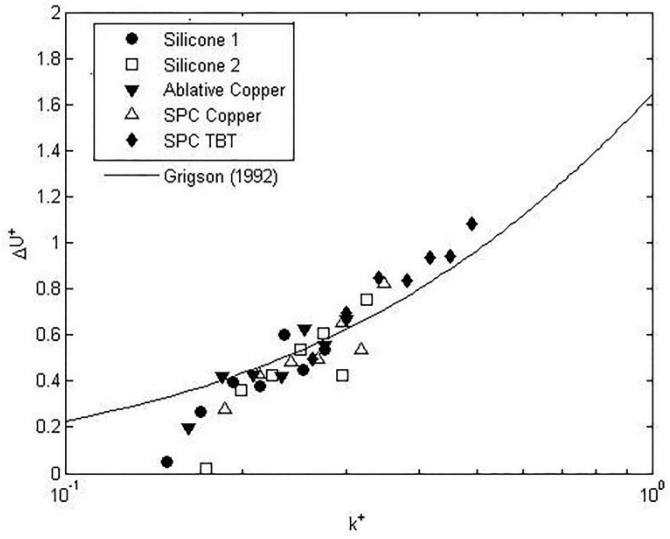

a)

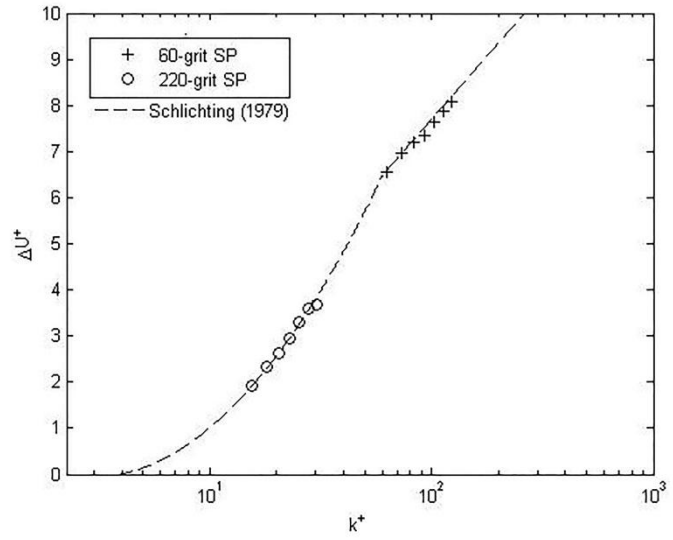

b)

Figure 6.1: Roughness functions vs. roughness Reynolds numbers for a) coatings, b) sandpapers.

It is evident from Figure 6.1 that the roughness functions for antifouling coatings are in good agreement with the Colebrook-type roughness function of Grigson (1992) using $k = 0.17R_a$, and the roughness functions for sandpapers show excellent agreement with Schlichting's (1979) uniform sand roughness function using $k = 0.75R_t$. It should be noted that these roughness heights and roughness function models were proposed by Schultz (2004). A future work may be the investigation of the range of applicability of the selected roughness height for antifouling coatings.

As seen in Figure 6.1, different types of surfaces, such as antifouling coatings and sandpapers, show different roughness function behaviours, meaning different pre-defined roughness function models are appropriate for each type. For this reason, the selected roughness length scales may vary accordingly in order for them to fall on the corresponding model. This means that the roughness function models and roughness heights selected in this study may not necessarily work for other surfaces and other roughness function models.

Although there are other roughness function models which are thought to be more suitable for real engineering surfaces and fouling, such as the inflectional roughness function model described in Schultz and Flack (2007), the monotonic Colebrook-type roughness function of Grigson (1992) is assumed to be appropriate when only antifouling coatings are taken into account.

6.3 Numerical Modelling

6.3.1 Mathematical Formulation

An Unsteady Reynolds-Averaged Navier-Stokes (URANS) method was used to solve the governing equations in this study. These mass and momentum conservation equations were solved by the commercial CFD software STAR-CCM+. The averaged continuity and momentum equations for incompressible flows are given in tensor notation and Cartesian coordinates by (6.1) and (6.2) (Ferziger and Perić, 2002).

$$\frac{\partial\left(\rho\bar{u}_i\right)}{\partial x_i}=0, \tag{6.1}$$

$$\frac{\partial\left(\rho\bar{u}_i\right)}{\partial t}+\frac{\partial}{\partial x_j}\left(\rho\bar{u}_i\bar{u}_j+\rho\overline{u_i'u_j'}\right)=-\frac{\partial\bar{p}}{\partial x_i}+\frac{\partial\bar{\tau}_{ij}}{\partial x_j} \tag{6.2}$$

where ρ is density, $\bar{u}_i$ is the averaged Cartesian components of the velocity vector, $\rho\overline{u_i'u_j'}$ is the Reynolds stresses and p is the mean pressure. $\bar{\tau}_{ij}$ are the mean viscous stress tensor components, as shown in (6.3)

$$\bar{\tau}_{ij}=\mu\left(\frac{\partial\bar{u}_i}{\partial x_j}+\frac{\partial\bar{u}_j}{\partial x_i}\right) \tag{6.3}$$

in which μ is the dynamic viscosity.

The solver uses a finite volume method which discretises the governing equations. A second order convection scheme was used for the momentum equations and a first order temporal discretisation was used. The flow equations were solved in a segregated manner. The continuity and momentum equations were linked with a predictor-corrector approach.

The SST (Shear Stress Transport) k-ω turbulence model was used in order to complete the RANS equations, which blends the k-ω model near the wall and the k-ε

model in the far field. The Volume of Fluid (VOF) method was used to model and position the free surface, in cases where a free surface was present. In this study, the Courant-Frederich-Lewis (CFL) number was always held at values less than unity to ensure numerical stability.

6.3.2 Proposed Wall-Function Approach for Antifouling Coatings

Wall functions are mathematical expressions which are used to link the viscosity affected region between the wall and log-law region (ANSYS, 2011). This approach assumes that the near wall cell lies within the logarithmic region of the boundary layer. The standard wall functions used in this study impose standard wall laws which have discontinuities between the laminar and logarithmic regions. The velocity profiles of standard wall laws are given by (6.4) (CD-ADAPCO, 2014):

$$U^{+} = \begin{cases} U^{+}_{lam} & \rightarrow \quad y^{+} \leq y^{+}_{m} \\ U^{+}_{turb} & \rightarrow \quad y^{+} > y^{+}_{m} \end{cases} \tag{6.4}$$

where U^{+} is the wall-parallel velocity normalised with respect to U_{τ}, y^{+}_{m} is the intersection of the viscous and fully turbulent regions, and the subscripts *lam* and *turb* indicate laminar and turbulent properties, respectively.

Given that roughness causes a downward shift in the velocity distribution in the log-law region, the mean velocity distribution is taken to be equivalent to the turbulent velocity profile from this point onward: $U^{+} = U^{+}_{turb}$. The log-law velocity profile is defined by equation (6.5)

$$U^{+} = \frac{1}{\kappa} \ln(E' y^{+}) \tag{6.5}$$

where

$$E' = \frac{E}{f} \tag{6.6}$$

in which E is the wall function coefficient and f is the roughness coefficient. κ is taken to be 0.42 as suggested by Cebeci and Bradshaw (1977). For smooth flows, f becomes unity, and E was chosen such that (2.6) is satisfied for B = 5.2.

The coefficient f is directly related to the roughness function and its value depends on the flow regime. f is described by (6.7) and (6.8) (CD-ADAPCO, 2014). It is of note that the coefficient f is an expanded version of the expression given by Cebeci and Bradshaw (1977).

$$f = \begin{cases} 1 & \rightarrow \quad k^+ < k_{sm}^+ \\ \left[A\left(\dfrac{k^+ - k_{sm}^+}{k_r^+ - k_{sm}^+} \right) + Ck^+ \right]^a & \rightarrow \quad k_{sm}^+ < k^+ < k_r^+ \\ \mathrm{A} + Ck^+ & \rightarrow \quad k_r^+ < k^+ \end{cases} \tag{6.7}$$

where

$$a = \sin\left[\frac{\pi}{2} \frac{\log(k^+ / k_{sm}^+)}{\log(k_r^+ / k_{sm}^+)} \right] \tag{6.8}$$

k^+_{sm} and k^+_{r} designate smooth and rough roughness Reynolds number limits, respectively, in which the flow is hydraulically smooth for $k^+ < k^+_{\mathrm{sm}}$ and fully rough for $k^+ > k^+_{\mathrm{r}}$. The model used by the software assumes that flow is occurring over uniform, closely packed sand as proposed by Cebeci and Bradshaw (1977), based on Nikuradse's data (1933), using the default values of k^+_{sm}=2.25 and k^+_{r}=90, and the coefficients A=0 and C=0.253.

The proposed model in this study, on the other hand, suggests that the wall law for antifouling coatings satisfies the mean velocity profile given by (6.9).

$$U^+ = \frac{1}{\kappa} \ln\left(\frac{y^+}{1 + k^+} \right) + B \tag{6.9}$$

For this reason, only one roughness function model for coatings is proposed, since the roughness function behaviours of coatings can be represented by one simple

model, as evidenced in Figure 6.1. k^+_{sm} and k^+_r are therefore chosen such that it is almost impossible for k^+ to fall in the first two regimes - k^+ is always greater than k^+_r. The coefficients A and C are then chosen such that the roughness function model matches the Colebrook-type roughness function of Grigson (1992). k=0.17R_a is chosen for the surfaces coated with antifouling coatings.

6.3.3 Geometry and Boundary Conditions

It is necessary to select appropriate boundary conditions for CFD problems, since these boundary conditions directly affect the accurate flow solutions. Two sets of boundary conditions are defined in this study, one for the validation study and the other for the full scale prediction study.

For the validation simulations, no-slip wall boundary conditions were applied to the bottom and wall of the domain because they represent the real bottom and wall of the towing tank used by Schultz (2004). Therefore the corresponding dimensions were chosen accordingly. The plate was also modelled as a no-slip rough wall in order to represent the roughness on the plate. The top of the domain, which represents air, was modelled as a wall with a slip condition applied to it. The two opposite faces at the x-direction of the domain, i.e. the right-hand face and left-hand face and of the domain in the top view, were modelled as a velocity inlet and a pressure outlet, respectively. The symmetry plane, as the name implies, has a symmetry condition. Hence, only half of the plate and control volume were taken into account. This does not significantly affect the computations and it halves the required cell numbers.

For the full scale prediction simulations, it is assumed that the plate is completely submerged in an infinite ocean, since surface roughness only affects skin friction. Therefore, it is only necessary to model a quarter of the plate. The total number of cells and the required computational time is decreased by quartering the problem by means of defining two symmetry planes, with no compromise in accuracy. For this reason, the lower faces, both in the top view and profile view, were modelled as symmetry planes. The boundary conditions of the plate, the left-hand face and right-hand face of the domain in the top view were modelled in a similar manner to those

of the validation simulations The rest was set up to be symmetrical in order to eliminate wall effects to as great a degree as possible.

The dimensions of the plate and the control volume, and the boundary conditions used, are shown in Figure 6.2 for the validation study and in Figure 6.3 for the full scale prediction study. The validation simulations are reproductions of the experiments given by Schultz (2004).

Another critical selection is the positioning of the boundaries, especially the downstream outlet boundary and the upstream inlet boundary. The inlet is placed at one plate length upstream and the outlet boundary is placed at two plate lengths downstream for the full scale predictions, to ensure boundary independent solutions as per the findings of Date and Turnock (1999). The positions of the inlet and outlet boundaries are doubled for the validation study since there is a free surface in this case.

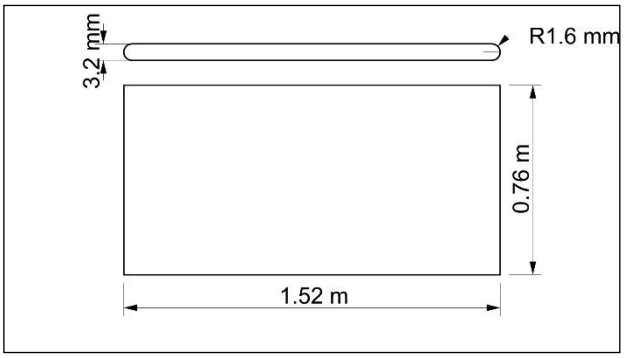

a)

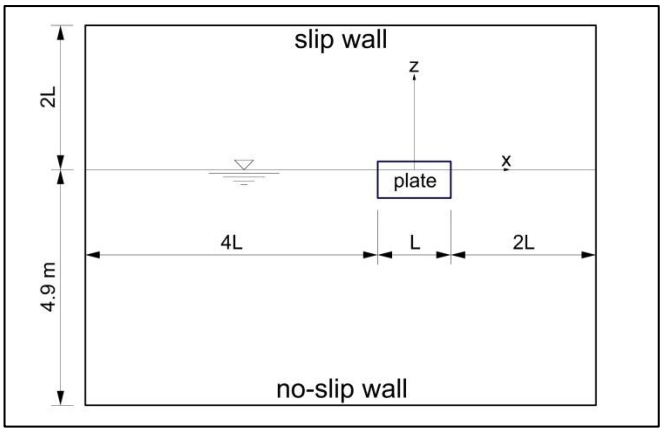

b)

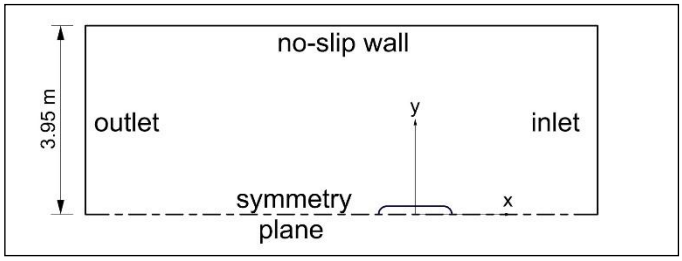

c)

Figure 6.2: a) The plate, **b)** profile view of the domain and **c)** top view of the domain, showing the dimensions and boundary conditions used for the validation study.

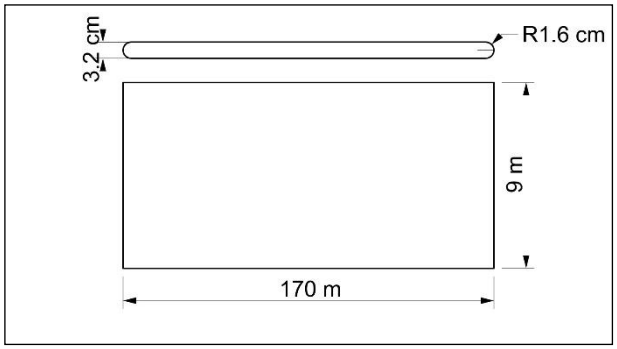

a)

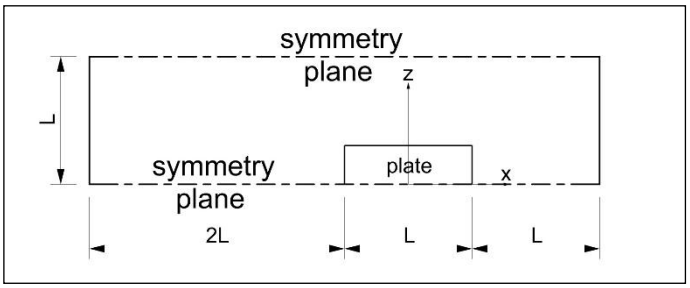

b)

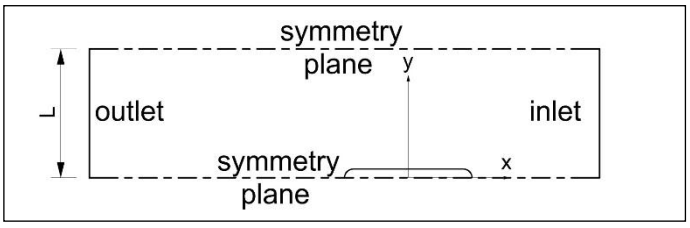

c)

Figure 6.3: a) The plate, **b)** profile view of the domain and **c)** top view of the domain, showing the dimensions and boundary conditions used for the full scale prediction study.

6.3.4 Mesh Generation

A cut-cell grid with prism layer mesh on the walls was generated using the automatic mesh generator in STAR-CCM+. The plate was meshed separately to give a much

finer grid, with additional refinement at the free surface. Refined meshes were generated in the area around the plate, as well as in the wake region, in order to accurately capture the flow properties for the validation study. A special near-wall mesh resolution was applied to all surfaces with the no-slip boundary condition. Details of the near-wall mesh generation are given in the following Section.

A convergence test was carried out in order to obtain grid independent solutions, since the cell numbers are influential on the solution. It is of note that once the mesh independent solution is achieved, further refinement of the mesh does not affect the final solution, though it does affect the solution time. The full details and a discussion of the grid dependence tests are given Section 6.4. As a result of the tests, in total, circa 4 million cells were generated for both the validation and prediction studies.

Figure 6.4 shows cross-sections of the meshed domain whereas Figure 6.5 shows a view of mesh configurations of the plate and the free surface. Figure 6.6 shows cross-sections of the meshed domain of the full scale prediction simulations. It is of note that the figures show the whole sections as if there is no symmetrical boundary owing to the visual transform feature of the software.

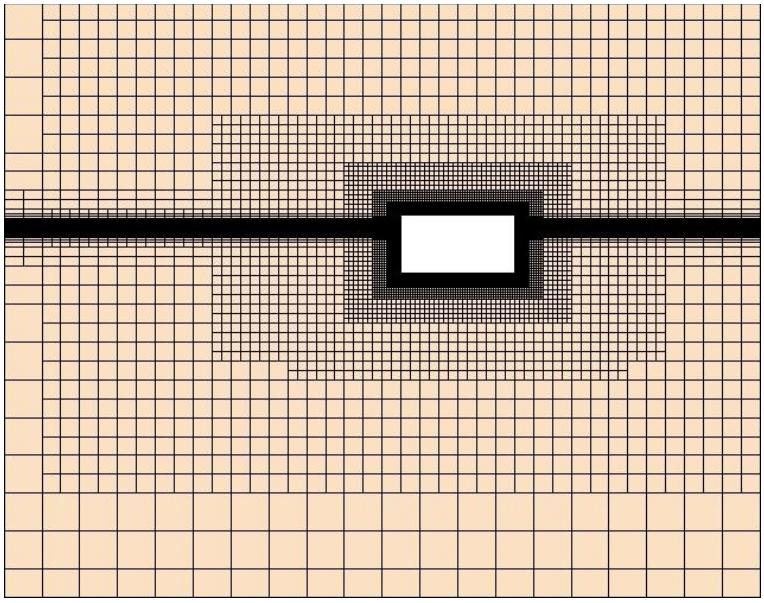

a)

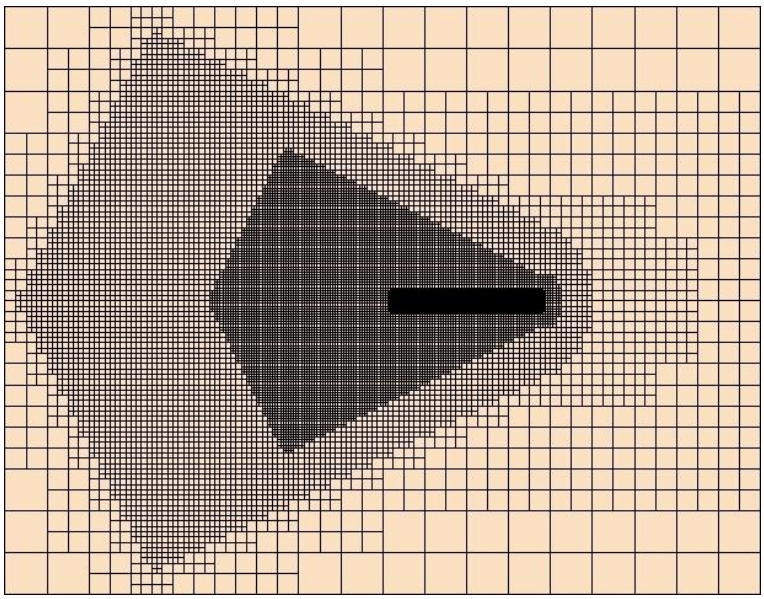

b)

Figure 6.4: a) Profile view cross-section **b)** top view cross-section of the domain.

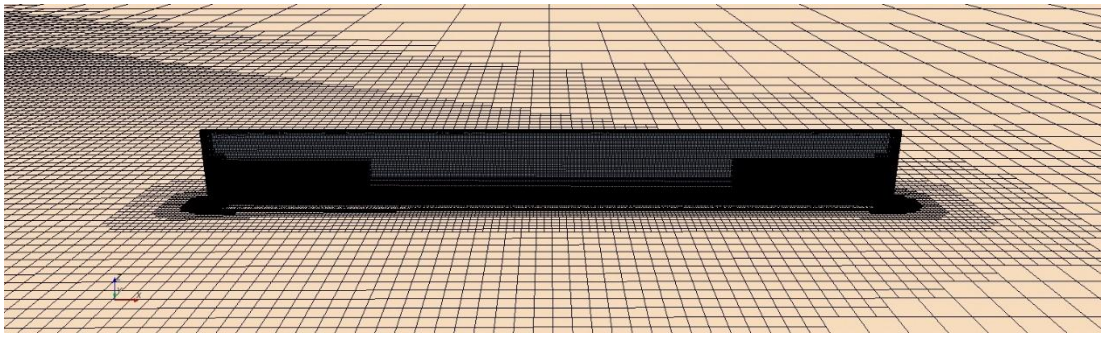

Figure 6.5: Mesh for the plate and free surface.

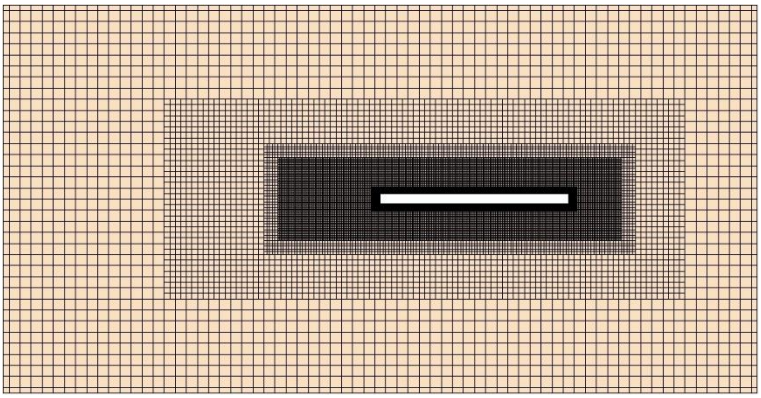

a)

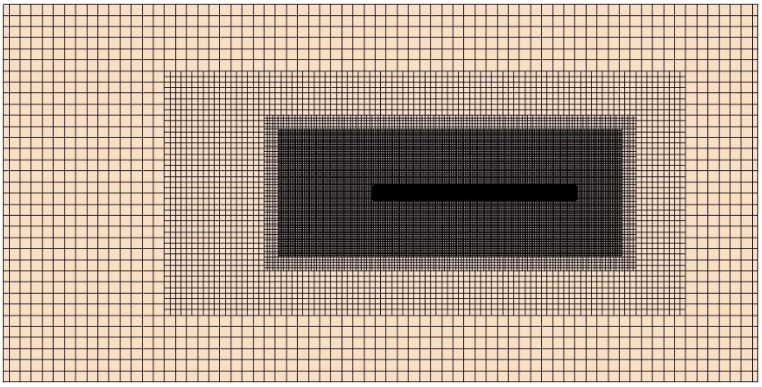

b)

Figure 6.6: a) Profile view cross-section **b)** top view cross-section of the domain.

6.3.4.1 Near-wall mesh generation

An important point is the selection of the prism layer thickness and the number of prism layers, since this represents the boundary layer of the wall. The prism layer thickness and the prism layer number determine the normal distance from the centroid to the wall in wall-adjacent cells. This distance is crucial to capture the gradients in the boundary layer and it should be selected with regards to the roughness height and required y^+ values.

The prism layer thickness on all no-slip walls was set to the corresponding turbulent boundary layer thickness along the flat plate in question for each Reynolds number. Prism layer numbers were selected to ensure that the y^+ value on the plate was maintained at a value greater than 30 in order to use standard wall laws for all Reynolds numbers. It is of note that the same prism layer numbers were used for all Reynolds numbers. In the prism layer mesh generation, a geometric progression with ratio 1.5 was used in all directions. A near wall mesh dependence study was carried out and the details and a discussion of the study are given in the following sub-section. The final y^+ distribution on the smooth surfaces is shown in Figure 6.7 for the validation study and in Figure 6.8 for the full scale prediction study. Only a small portion of the plate is shown in Figure 6.8, as it is 170 m long in total.

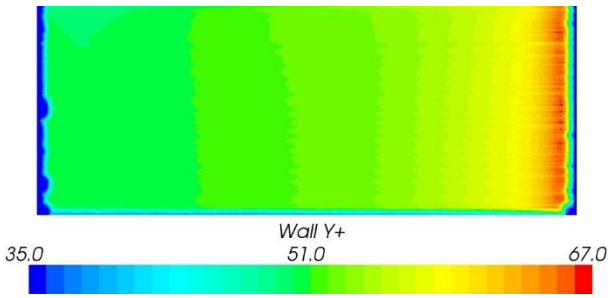

a)

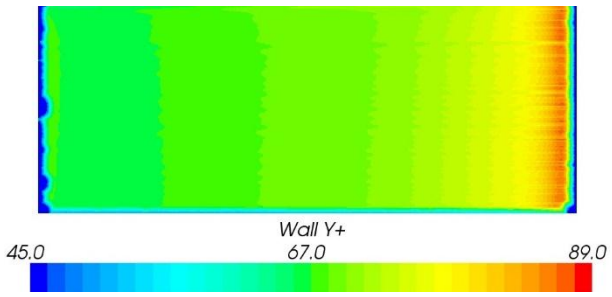

b)

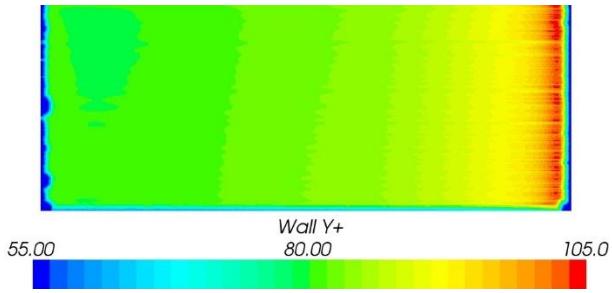

c)

Figure 6.7: y^+ values on the smooth plates at **a)** Re = $2.8x10^6$, **b)** Re = $4.2x10^6$, **c)** Re = $5.5x10^6$.

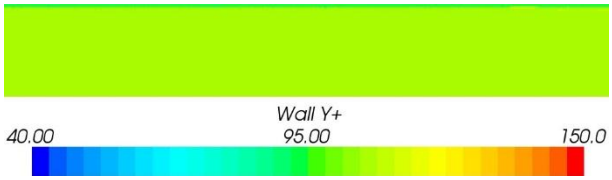

Figure 6.8: y^+ values on the smooth plate at 13 knots.

6.4 Results

6.4.1 Grid Dependence Tests

Systematic studies were performed using the surfaces coated with SPC TBT in order to obtain grid independent solutions for both validation and full scale prediction studies.

Firstly, a near-wall grid dependence study was carried out to determine the effect of y^+ on the calculated C_F values of both the plate operating at Re = $2.8x10^6$, and the plate which represents the tanker operating at 13 knots. To generate each mesh, the distance of the first grid from the rough wall was gradually changed, whilst keeping all other parameters the same. The results from different simulations, each with a different y^+ value, are shown in Table 6.2 for the validation study and in Table 6.3 for the full scale prediction study. The y^+ values listed represent the modes of the y^+ distribution histograms.

Table 6.2: C_F results at different y^+ values for the validation study.

y^+	Total No. of Cells	C_F (CFD)	% Experiment
230	$3.2x10^6$	0.004026	6.42
130	$3.5x10^6$	0.003937	4.08
50	$4x10^6$	0.003776	-0.19
7.5	$4.5x10^6$	0.003494	-7.65

Table 6.3: C_F results at different y^+ values for the full scale prediction study.

y^+	Total No. of Cells	C_F (CFD)
1350	$2.8x10^6$	0.001619
250	$3.6x10^6$	0.001595
110	$4x10^6$	0.001584
75	$4.5x10^6$	0.001580

As demonstrated in Table 6.2, the solution with the y^+ value of 7.5 deviates significantly from the experimental data, as expected, since standard wall laws can be used only if y^+ values are greater than 30. The results presented in Table 6.2 demonstrate that the solution with the y^+ value of 50 has converged fairly well. This resolution was therefore used throughout all cases of the validation study.

It can be seen from Table 6.3 that the solutions with the y^+ values of 110 and 75 converged well, with little variation in the C_F value when using y^+ values of either 110 or 75. On the other hand, the difference in the total number of cells is half a million between these two resolutions. Therefore, the resolution with the y^+ value of 110 was chosen and used throughout all cases of the full scale prediction study.

Having determined the near-wall mesh resolutions, a grid dependence test for the rest of the domain, including the plate itself, was carried out. The rest of the domain was discretised in four different resolutions; coarse, medium, fine and very fine. It is of note that the same refinement ratio was used for both the validation and full-scale prediction study. However, the differences between the total cell numbers of the validation and prediction studies (detailed in Table 6.4 and Table 6.5) occurred due to optimisation property of automatic mesh generator of the software. The frictional resistance coefficients for each mesh configuration were computed and are given in Table 6.4 and Table 6.5.

The solution for the coarse mesh configuration in the validation study did not converge, and showed very large oscillations. This may be due to the weak resolution of the plate geometry, as well as the free surface and wake. From Table 6.4 and Table 6.5 it is evident that the solutions of the fine and very fine meshes converged very well in both the validation and prediction study. Therefore, the fine mesh configuration was selected in all subsequent computations.

Table 6.4: C_F results at different mesh configurations for the validation study.

Mesh configuration	Total No. of Cells	C_F (CFD)	% Experiment
Coarse	$1.5x10^6$	[ ]	[ ]
Medium	$2.5x10^6$	0.003805	0.60
Fine	$4x10^6$	0.003776	-0.19
Very Fine	$6x10^6$	0.003785	0.07

Table 6.5: C_F results at different mesh configurations for the full scale prediction study.

Mesh configuration	Total No. of Cells	C_F (CFD)
Coarse	$1.8x10^6$	0.001574
Medium	$2.5x10^6$	0.001576
Fine	$4x10^6$	0.001584
Very Fine	$5.5x10^6$	0.001584

6.4.2 Validation Study

6.4.2.1 Frictional resistance coefficients

Table 6.6, Table 6.7 and Table 6.8 demonstrate the frictional resistance coefficients computed by CFD and obtained by experiments for five different coatings, as well as a smooth surface, at Re = $2.8x10^6$, Re = $4.2x10^6$ and Re = $5.5x10^6$, respectively.

Table 6.6: Comparison of C_F values at Re = $2.8x10^6$.

Surface	C_F (CFD)	C_F (Experiment)	Difference (%)
Smooth	0.003632	0.003605	0.74
Silicone 1	0.003715	0.003666	1.35
Silicone 2	0.003729	0.003663	1.81
Ablative Copper	0.003722	0.003701	0.58
SPC Copper	0.003736	0.003723	0.35
SPC TBT	0.003776	0.003783	-0.19

Table 6.7: Comparison of C_F values at Re = $4.2x10^6$.

Surface	C_F (CFD)	C_F (Experiment)	Difference (%)
Smooth	0.003411	0.003418	-0.21
Silicone 1	0.003528	0.003499	0.82
Silicone 2	0.003545	0.003540	0.14
Ablative Copper	0.003536	0.003507	0.84
SPC Copper	0.003553	0.003526	0.78
SPC TBT	0.003603	0.003611	-0.23

Table 6.8: Comparison of C_F values at Re = $5.5x10^6$.

Surface	C_F (CFD)	C_F (Experiment)	Difference (%)
Smooth	0.003185	0.003226	-1.26
Silicone 1	0.003460	0.003374	2.54
Silicone 2	0.003481	0.003426	1.60
Ablative Copper	0.003470	0.003401	2.04
SPC Copper	0.003491	0.003438	1.55
SPC TBT	0.003551	0.003500	1.45

As can be seen from Table 6.6, Table 6.7 and Table 6.8, the computed C_F values of the smooth and coated surfaces are in fair agreement with the experimental data. The differences are slightly higher at Re = $5.5x10^6$, though the differences at all of the Reynolds numbers can be considered to be negligible since the experimental

uncertainty in C_F is given as ±5% for Re = $2.8x10^6$ and ±2% for Re = $5.5x10^6$ (Schultz, 2004).

The computed C_F values of the silicone coatings have relatively higher differences from the experimental data at Re = $2.8x10^6$, which is thought to be due to the slight deviation of the roughness functions from the proposed roughness function model at this Reynolds number, as shown in Figure 6.1.

The best agreement between the computed values and the experimental data is achieved at Re = $4.2x10^6$. In this case, the roughness functions at the corresponding Reynolds number correlate remarkably well with the roughness function model given in Figure 6.1.

Although the differences in the roughness amplitude parameters of the coatings are very small, the proposed wall law and CFD model is able to accurately take this effect into account. As expected, the computed C_F values increase with increases in the roughness amplitude parameters, and the frictional resistance coefficients decrease with increasing speed.

6.4.2.2 Roughness Reynolds numbers

Considering equation (2.9), the value of k^+ depends on the friction velocity U_τ. For this reason, the roughness Reynolds numbers are not uniform within the surface, instead varying depending on the location on the plate. Due to the fact that the software is able to obtain the U_τ distribution on the plate in question, a user defined variable, k^+, can be created, and so the distribution of k^+ was evaluated on the plates for each particular case. Histograms were then created using the distribution data. Figure 6.9 shows the k^+ distributions on the plates coated with SPC TBT at three different Reynolds numbers, as an example.

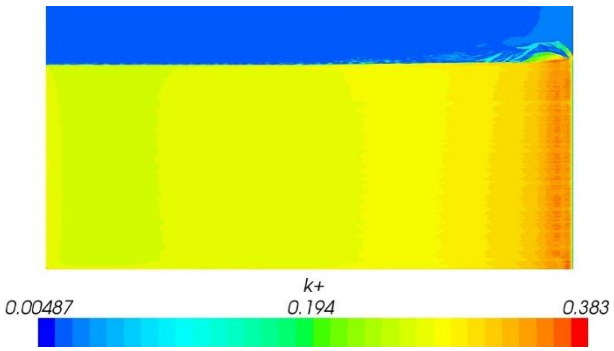

a)

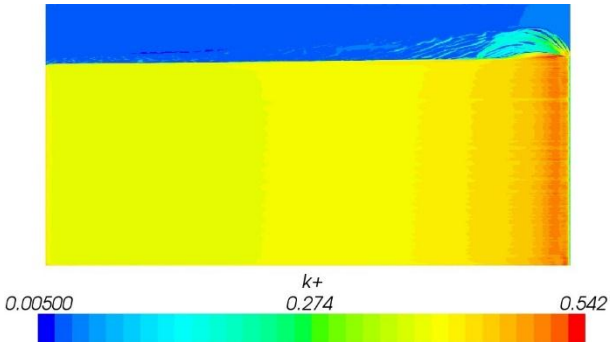

b)

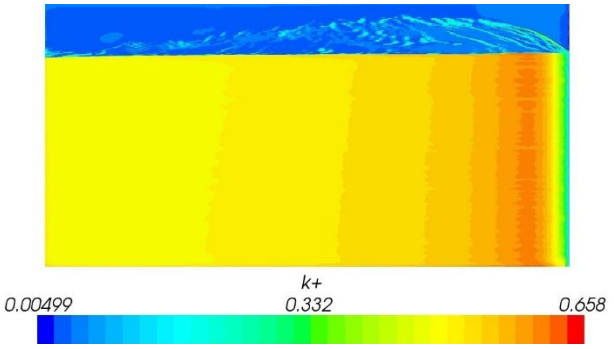

c)

Figure 6.9: k^+ distribution on the plates coated with SPC TBT at a) Re = 2.8×10^6, b) Re = 4.2×10^6, c) Re = 5.5×10^6.

The most frequently occurring roughness Reynolds numbers were obtained from the software and compared with those calculated with Equation (2.36) using the experimental data. The resulting comparisons are shown in Figure 6.10.

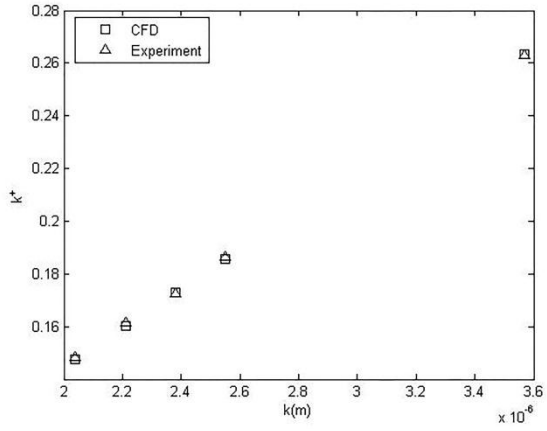

a)

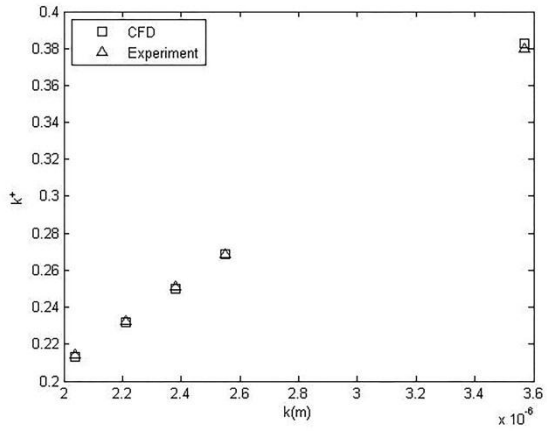

b)

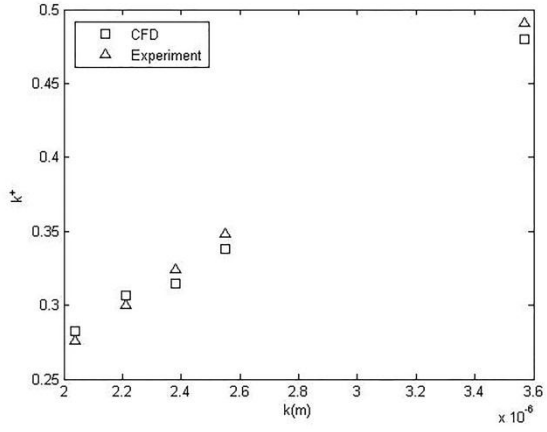

c)

Figure 6.10: Roughness heights vs. roughness Reynolds numbers at a) Re = 2.8×10^6, b) Re = 4.2×10^6 c) Re = 5.5×10^6.

The computed roughness Reynolds numbers showed reasonable agreement with those obtained from the experimental data. The average differences are 0.3%, 0.35% and 2.5% at Re = $2.8x10^6$, Re = $4.2x10^6$ and Re = $5.5x10^6$, respectively. These results prove that the roughness Reynolds numbers can be computed accurately by means of a CFD approach for a given roughness height.

Accurate computation of k^+ values is of paramount importance because the imposed roughness function model provides the required ΔU^+ based on the computed k^+ value, shown in Figure 6.1, leading to the accurate computation of C_F values. The computed k^+ values have relatively higher differences from the experimental data at Re = $5.5x10^6$. This may be one of the reasons for the slight differences between the computed and experimentally obtained C_F values at this speed shown in Table 6.8.

6.4.3 Prediction of C_F values at Full-Scale

Table 6.9 shows the predicted frictional resistance coefficients of a handymax tanker coated with several antifouling coatings at an operational speed of 13 knots using this chapter's proposed CFD method and the similarity law analysis procedure of Granville (1958) presented in Chapter 5, Section 5.2.

Table 6.9: The comparison of C_F values at full scale at 13 knots.

Surface	C_F (CFD)	C_F (Granville)	Difference (%)
Smooth	0.001494	0.0015059	-0.79
Silicone 1	0.001550	0.001564	-0.89
Silicone 2	0.001558	0.001573	-0.95
Ablative Copper	0.001554	0.001568	-0.91
SPC Copper	0.001562	0.001577	-0.92
SPC TBT	0.001585	0.001600	-0.94

It is evident from Table 6.9 that the computed C_F values are in a fair agreement with those obtained using the similarity law scaling procedure of Granville (1958) with differences below 1%.

Table 6.10 gives the percentage increase in frictional resistance coefficients with respect to the smooth condition.

Table 6.10: Predictions of the change in frictional resistance at full scale at 13 knots.

Surface	**% ΔC_F**
Smooth	-
Silicone 1	3.77
Silicone 2	4.32
Ablative Copper	4.05
SPC Copper	4.59
SPC TBT	6.10

As seen in Table 6.10, the percentage increase in the frictional resistance coefficients due to the antifouling coatings' roughness varies between 3.77 and 6.10%. SPC TBT leads to the highest increase in C_F values, as expected, due to its relatively higher roughness amplitude parameters. However, the reader should note that the evaluated C_F values and the percentage increases are due to the initial roughness of the coatings, and the increase in C_F over time varies depending on the duration of sea exposure and the time-dependent drag performance of each coating.

6.5 Chapter Summary and Conclusions

A CFD model for the prediction of the effect of antifouling coatings on frictional resistance has been proposed. The Colebrook-type roughness function of Grigson (1992) was employed in the wall-function of the solver and a validation study was carried out to examine the validity of the proposed model. The frictional resistance coefficients and roughness Reynolds numbers for five antifouling coatings and a smooth surface were computed using CFD simulations. The results of the validation study were in fairly good agreement with the experimental data, with the differences between CFD and experiments ranging from 0.14 – 2.54% for C_F and 0.3 – 2.5% for k^+. It has been shown that surface roughness can be modelled by employing modified wall laws within the wall functions. It may be concluded that the proposed approach is capable of predicting the roughness effects of antifouling coatings on frictional resistance. Hence, the increases in the C_F values of a ship due to different types of antifouling coatings were predicted using the proposed CFD model and compared to the results obtained using the similarity law scaling procedure of Granville (1958).

It should be borne in mind that this study's aim was to propose a robust CFD model, rather than a case-based model, to predict the frictional resistance of antifouling

coatings. For this reason, an appropriate representative roughness function model was employed in spite of the slight discrepancies between the individual roughness function values and the model. The insignificant differences between the computed C_F values and the experimental data are therefore thought to be due to the aforementioned insignificant scatter.

The main advantage of the proposed model is that it enables the use of a simple roughness length scale, according to surface roughness measurements, rather than the equivalent sand-grain roughness height, which is a hydrodynamically obtained parameter.

Additionally, the critical points of the numerical modelling of roughness effects on flow have been highlighted in this chapter. It has also been demonstrated that the existing roughness function model of the CFD software can be modified according to the experimental data and that the effects of different types of roughness on flow can be predicted in this way.

A final point to note is that while CFD may provide accurate results in order to model roughness effects on frictional resistance, experimental data and further study into the correlation between roughness and drag are a necessity for the development of accurate CFD prediction methods.

This approach will be utilised and a new CFD model will be proposed and employed in Chapter 7 to simulate and predict the roughness effects of biofouling on the frictional resistance of flat plates.

7 A CFD Model for the Prediction of the Effect of Biofouling on Frictional Resistance

7.1 Introduction

Current numerical prediction methods are limited by the use of boundary layer similarity law analysis, one example of which was carried out in Chapter 5. This method can only calculate the effect of a given surface roughness on the frictional resistance of a flat plate of ship length. Although this is a reasonable assumption, since the surface roughness is not expected to significantly affect the pressure drag, it is still worth investigating the phenomenon by means of CFD. In addition, a typical CFD work could directly take the effect of surface roughness on the pressure drag of the hull into consideration.

To the best of this author's knowledge, no specific CFD model exists to predict the roughness effect of biofouling on ship frictional resistance. The aim of the present chapter is therefore to fill this gap by employing a modified wall-function in the CFD software package. The proposed approach enables the prediction of the effect of a range of representative coating and biofouling conditions on the frictional resistances of flat plates of ship length for different speeds. Moreover, this CFD model can be used to investigate the effect of biofouling on 3D full-scale hull forms rather than on flat plates.

The main advantage of the proposed model is that it enables the use of a simple roughness length scale to predict the effect of biofouling on a flat plate of ship length, similar to that of Chapter 6 and Demirel et al. (2014b).

In this study, the experimental data of Schultz and Flack (2007) were used to establish a suitable roughness function model for different fouling conditions. Corresponding roughness heights of Schultz (2007) representing different fouling

conditions were used to model the different surfaces. This roughness function model was then employed in the wall-function of the CFD software package STAR-CCM+.

Following this, two typical case studies were performed through CFD simulations of towing tests involving flat plates of length 170 m, representing a handymax tanker, and 232.5 m, representing the Kriso Container Ship (KCS), with different surface conditions at different service speeds. Frictional resistance coefficients were computed and compared with those obtained and presented in Chapter 5. Moreover, the increases in the effective power of the KCS due to such fouling conditions were predicted using the present results and the existing data in the literature.

This chapter is organised as follows: A determination of the appropriate roughness function model for a range of biofouling conditions is presented in Section 7.2, while a new wall-function formulation is proposed and details of the numerical setup are covered in Section 7.3. In Section 7.4, the CFD results and similarity law scaling procedure results are compared, and predictions of the increase in the frictional resistance coefficients of a tanker and a container ship with the mentioned surface conditions are demonstrated. Finally, the results of the study are discussed in Section 7.5, along with recommendations for future avenues of research.

7.2 Roughness Functions

In this chapter's study, the roughness function values of Schultz and Flack (2007) shown in Figure 5.9 (Chapter 5, Section 5.4.1), were used to develop a roughness function model to be employed in the CFD software to represent the coating and fouling conditions given by Schultz (2007), as shown in Table 5.8 (Chapter 5, Section 5.4.1).

An appropriate roughness function model was fitted to the roughness function values of Schultz and Flack (2007), given in (7.1). This roughness function model is presented such that it is in the form of the built-in roughness function model of STAR-CCM+ for application convenience.

$$\Delta U^{+} = \begin{cases} 0 & \rightarrow \quad k^{+} < 3 \\ \frac{1}{\kappa}\ln\left(0.85k^{+}\right)^{\sin\left[\frac{\pi}{2}\frac{\log(k^{+}/3)}{\log(25)}\right]} & \rightarrow \quad 3 < k^{+} < 20 \\ \frac{1}{\kappa}\ln\left(0.26k^{+}\right) & \rightarrow \quad 20 < k^{+} \end{cases} \tag{7.1}$$

Shown for comparison in Figure 7.1 is the roughness function model given in (7.1) together with the roughness functions proposed by Schultz and Flack (2007).

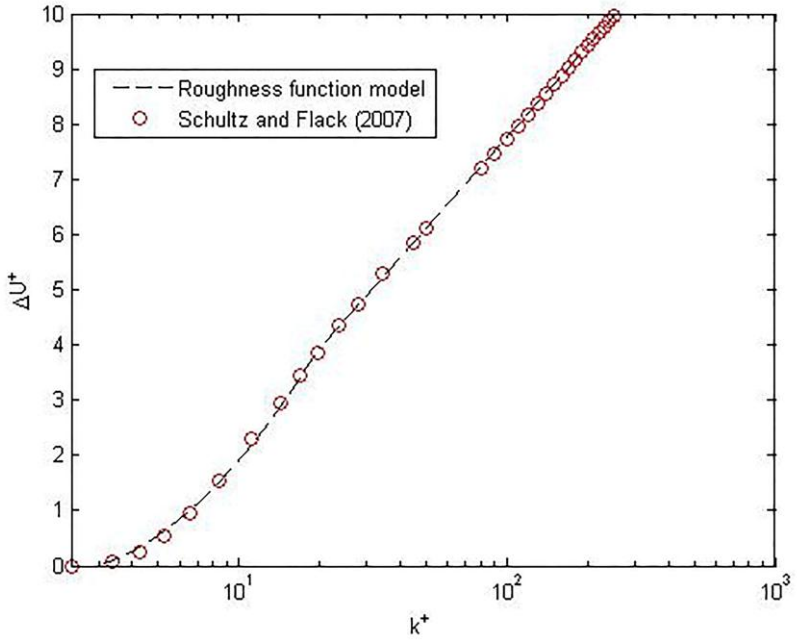

Figure 7.1: Proposed roughness function model together with the roughness functions.

It is evident from Figure 7.1 that there is excellent agreement between the roughness functions and the representative roughness function model. For this reason, the roughness function model given in (7.1) was taken to be an appropriate representative mathematical model for the roughness functions obtained experimentally.

7.3 Numerical Modelling

7.3.1 Mathematical Formulation

An Unsteady Reynolds-Averaged Navier-Stokes (URANS) method was used to solve the governing equations in this study. These mass and momentum conservation equations were solved by the commercial CFD software. The mathematical formulations are identical to those used in Chapter 6. The reader should refer to Chapter 6, Section 6.3.1, for these details. The only difference to mention is that the Volume of Fluid (VOF) method was not used in this chapter's simulations since there is no free surface created in this chapter's CFD modelling.

7.3.2 Proposed Wall-Function Approach for Fouling Conditions

General information about the wall-function approach and the application of roughness functions through wall-functions can be found in Chapter 6, Section 6.3.2.

The proposed model for a range of representative coating and biofouling conditions in this chapter is in a similar form to the built-in wall function of STAR-CCM+ in terms of flow regimes. That is to say, the proposed roughness function model and the wall-law have 3 flow regimes, namely a hydraulically smooth regime, a transitionally rough regime and a fully rough regime, which are similar to those proposed by Cebeci and Bradshaw (1977) based on Nikuradse's data (1933).

In this work, it was intended that the roughness function model given in (7.1) would be employed in the software. However, it was impossible to define these exact formulations due to a limited opportunity with which to trial adjustments of the built-in equations of the software. Referring to (6.7) and (6.8), the coefficients and roughness Reynolds number limits can be adjusted by the user. However, any change made in such parameters would affect the behaviours of the wall-law in both the transitionally and fully rough regimes. Therefore, the use of equation (7.1) can instead be achieved using a two-step method as explained below.

The first step is to arrange the parameters of equations (6.7) and (6.8) such that they satisfy the behaviour of the roughness function model defined by equation (7.1) in

the transitionally rough regime only. In this case, the obtained roughness function model does not match with the roughness function model defined by equation (7.1) in the fully rough regime, as can be seen from Figure 7.2. After the simulations have settled, the roughness Reynolds numbers are checked to determine the flow regime. If the flow regime is the transitionally rough regime, i.e. $3 < k^+ < 20$, the procedure is deemed successful and the results of the simulations are reliable. If the flow regime is in the fully rough regime, the results of the first step are not reliable and the second step would therefore be initiated. The roughness function model modified for the first step, satisfying the roughness function behaviour of Schultz and Flack (2007) in the transitionally rough regime, is shown in Figure 7.2 together with the roughness functions themselves. It is evident from Figure 7.2 that the roughness function model does not satisfy the fully rough regime behaviour of the individual roughness functions.

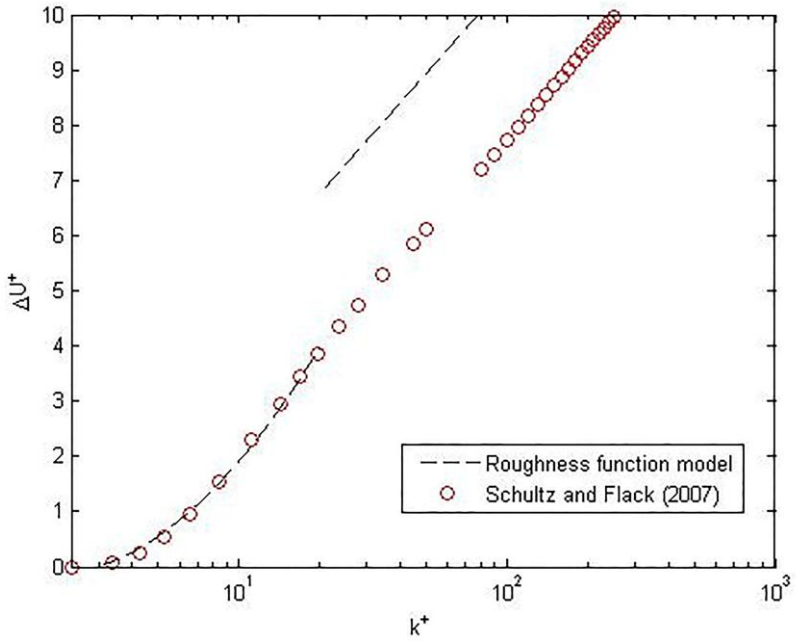

Figure 7.2: The roughness function model modified to satisfy the transitionally rough regime.

The second step involves arranging the parameters of equations (6.7) and (6.8) such that they satisfy the behaviour of the roughness function model defined by equation (7.1) in the fully rough regime only. In this case, the obtained roughness function model does not match with the roughness function model defined by equation (7.1) in the transitionally rough regime, as can be seen from Figure 7.3. The roughness

Reynolds numbers are then re-checked to assess the flow regime. If the flow regime is the fully rough regime, i.e. $k^+ > 20$, the procedure is deemed to be complete and the results of the simulations are reliable. The roughness function model modified for the second step, satisfying the roughness function behaviour of Schultz and Flack (2007) in the fully rough regime, is shown in Figure 7.3 together with the roughness functions themselves. It is evident from Figure 7.3 that the roughness function model does not satisfy the transitionally rough regime behaviour of the individual roughness functions.

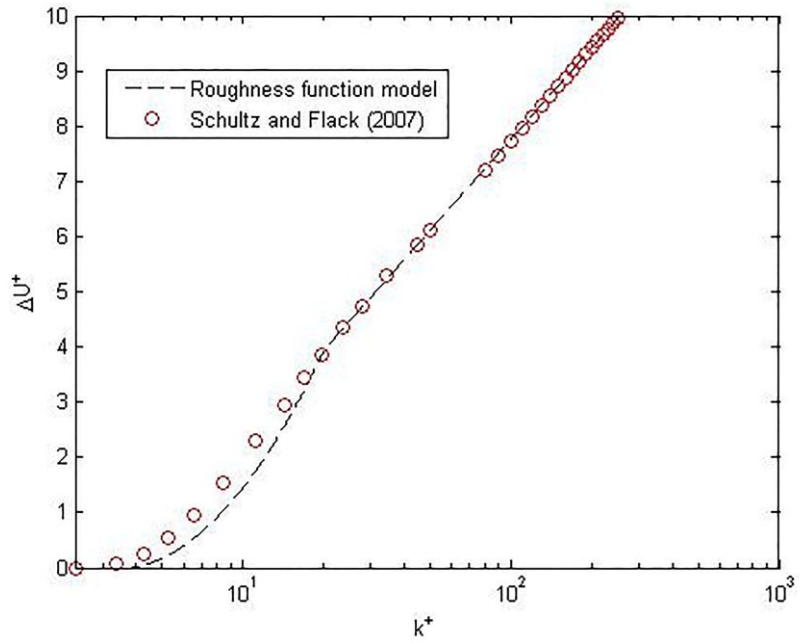

Figure 7.3: The roughness function model modified to satisfy the fully rough regime.

However, it has been understood from this work's exploratory studies that the flow along the plate may be in a transitionally rough regime at some locations, while the flow in certain regions may resemble a fully rough regime. A so-called blended model has therefore been developed to satisfy the behaviours both in the transitionally and fully rough regimes.

Finally, as a result of the discussion above, the most appropriate roughness function model for a range of representative coating and fouling conditions for use in STAR-CCM+ is proposed by equation (7.2).

$$\Delta U^{+} = \begin{cases} 0 & \rightarrow \quad k^{+} < 3 \\ \frac{1}{\kappa}\ln\left(0.26k^{+}\right)^{\sin\left[\frac{\pi}{2}\frac{\log(k^{+}/3)}{\log(5)}\right]} & \rightarrow \quad 3 < k^{+} < 15 \\ \frac{1}{\kappa}\ln\left(0.26k^{+}\right) & \rightarrow \quad 15 < k^{+} \end{cases} \tag{7.2}$$

Shown for comparison in Figure 7.4 is the proposed roughness function model given by (7.2) and roughness functions of Schultz and Flack (2007).

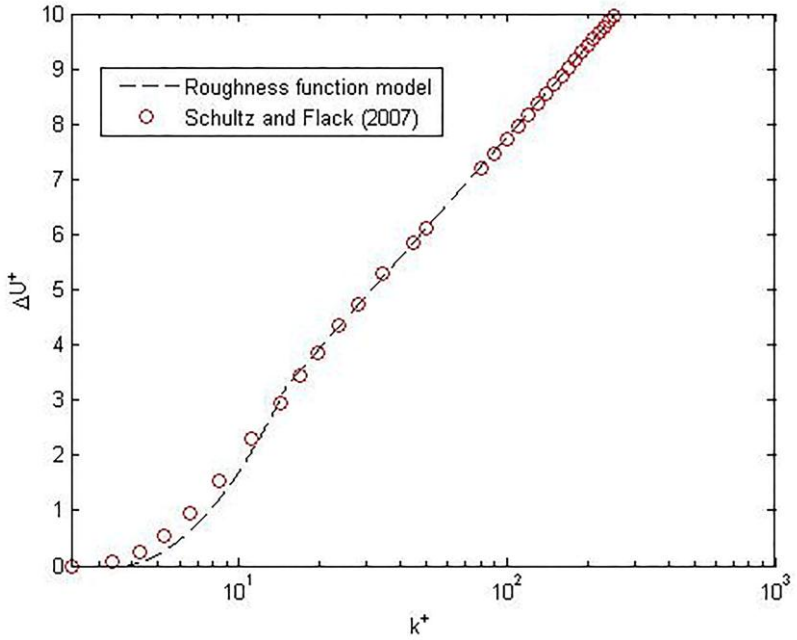

Figure 7.4: The proposed CFD roughness function model together with the roughness functions.

It is evident from Figure 7.4 that an excellent agreement is achieved in the fully rough regime while a reasonable match is obtained in the transitionally rough regime.

7.3.3 Geometry and Boundary Conditions

The boundary conditions of the simulations were chosen to represent the plates being completely submerged in an infinite ocean, with similarity to the full scale prediction simulations presented in Chapter 6. The boundary conditions and the positioning of the boundaries were therefore chosen to be similar to those given in Chapter 6, Section 6.3.3, as shown in Figure 6.3 b) and c).

In addition, the plate geometry representing the tanker in this chapter is the same as the one used in Chapter 6, as illustrated in Figure 6.3 a). The geometry of the plate representing the KCS is shown in Figure 7.5.

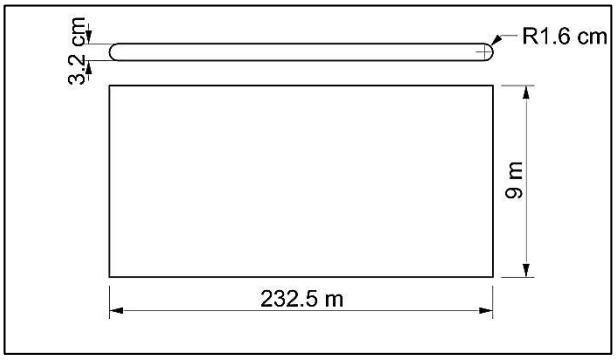

Figure 7.5: The plate representing the KCS.

7.3.4 Mesh Generation

A cut-cell grid with prism layer mesh on the walls was generated using the automatic mesh generator in STAR-CCM+. Additional refinements were applied to give finer grids in the critical regions, such as the area immediately around the plate, the areas around the trailing and leading edges, and the top edge of the plate. The mesh generation was achieved using similar techniques to those explained in Chapter 6, Section 6.3.4. Also, convergence tests were performed to ensure grid-independent mesh configurations, as well as to predict the uncertainty of the CFD simulations.

A special near-wall mesh resolution was applied to all surfaces with no-slip boundary conditions based on the roughness height values corresponding to each fouling condition. For this reason, the near-wall cell numbers varied for some of the fouling conditions. These differences resulted in different total cell numbers. The numbers of the total cells generated are given in Table 7.1 for the tanker and in Table 7.2 for the KCS. Details of the near-wall mesh generation are given in the following section.

Table 7.1: Total cell numbers for the tanker case.

Surface Condition	Cell numbers
k=0, k=30, k=100, k=300	4.23×10^6
k=1000	4×10^6
k=3000	3.44×10^6
k=10000	3.05×10^6

Table 7.2: Total cell numbers for the KCS case.

Surface Condition	Cell numbers
k=0, k=30, k=100, k=300	$5.5x10^6$
k=1000	$5.28x10^6$
k=3000	$4.5x10^6$
k=10000	$4x10^6$

7.3.4.1 Near-wall mesh generation

Near-wall mesh generation must be performed with care since this is directly related to the roughness heights representing fouling conditions. The prism layer thickness and prism layer numbers were, therefore, determined such that y^+ is always higher than 30, and higher than k^+, as per CD-ADAPCO (2014)'s suggestion. Hence, the resulting y^+ values were very high as the k^+ values were high for most of the fouling conditions. The final y^+ distributions are shown for various simulation cases in Figure 7.6 - Figure 7.13, after the solutions have settled. For visual convenience, only a small portion of each plate is shown.

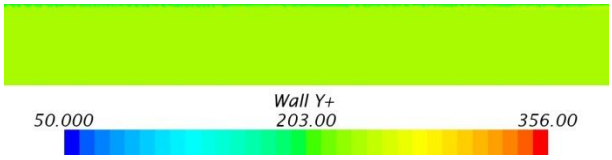

Figure 7.6: y^+ values on the plate representing the KCS in smooth, typical as applied AF coating, deteriorated coating or light slime and heavy slime conditions at 24 knots.

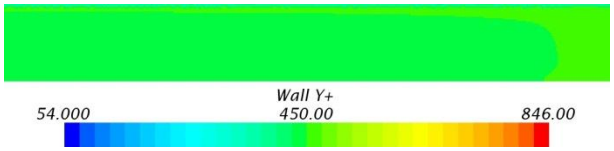

Figure 7.7: y^+ values on the plate representing the KCS in small calcareous fouling or weed conditions at 24 knots.

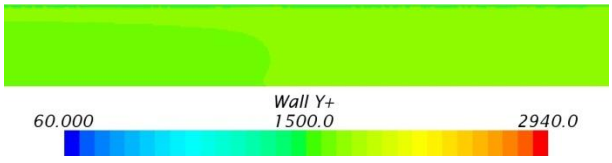

Figure 7.8: y^+ values on the plate representing the KCS in medium calcareous fouling conditions at 24 knots.

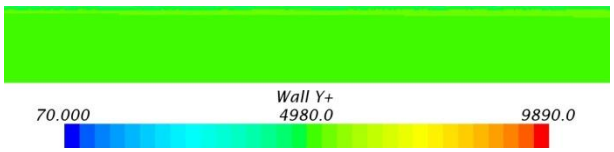

Figure 7.9: y^+ values on the plate representing the KCS in heavy calcareous fouling conditions at 24 knots.

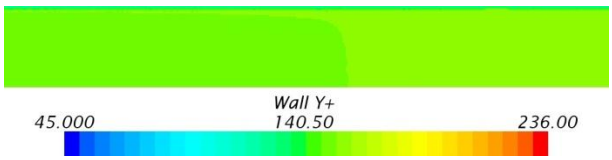

Figure 7.10: y^+ values on the plate representing the tanker in smooth, typical as applied AF coating, deteriorated coating or light slime and heavy slime conditions at 15 knots.

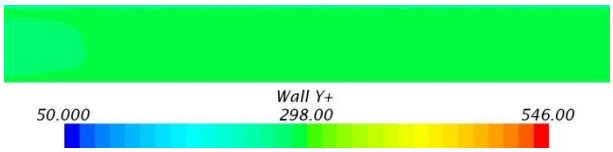

Figure 7.11: y^+ values on the plate representing the tanker in small calcareous fouling or weed conditions at 15 knots.

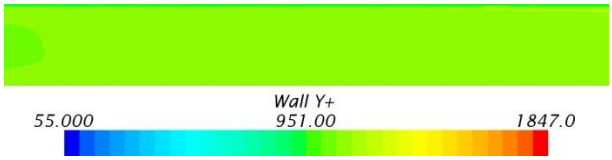

Figure 7.12: y^+ values on the plate representing the tanker in medium calcareous fouling conditions at 15 knots.

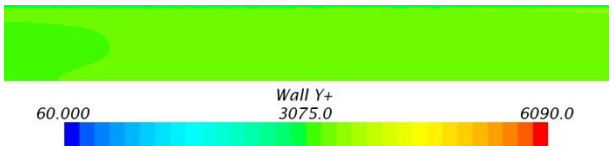

Figure 7.13: y^+ values on the plate representing the tanker in heavy calcareous fouling conditions at 15 knots.

7.4 Results

7.4.1 Grid Dependence Tests

Systematic studies were performed using the surfaces with heavy slime on in order to obtain grid independent solutions and to predict the CFD uncertainties for full scale prediction studies. In order to observe the effect of cell numbers on the key variable, (C_F in this case), the domain was discretised in three different resolutions and the simulations were run for each configuration. The grid refinement factor, *r*, was chosen to be $\sqrt{2}$ as used by Tezdogan et al. (2015).

The frictional resistance coefficients for each mesh configuration were computed and are given in Table 7.3 for the tanker and in Table 7.4 for the KCS.

Table 7.3: C_F results at different mesh configurations for the tanker.

Mesh configuration	Total No. of Cells	C_F (CFD)
Coarse	$1.7x10^6$	0.0020929
Medium	$2.5x10^6$	0.00209312
Fine	$4.2x10^6$	0.0021030

Table 7.4: C_F results at different mesh configurations for the KCS.

Mesh configuration	Total No. of Cells	C_F (CFD)
Coarse	$2.2x10^6$	0.0020086
Medium	$3.3x10^6$	0.0020145
Fine	$5.5x10^6$	0.0020222

From Table 7.3 and Table 7.4 it is evident that the solutions of the fine meshes converged very well. Therefore, the fine mesh configuration was selected in all subsequent computations.

7.4.2 Verification Study

A verification study should be carried out to show the capability of the proposed model and the software for particular calculations. The Grid Convergence Index (GCI) Method based on Richardson extrapolation (Richardson, 1910, Richardson and Gaunt, 1927) was used in this chapter's work for discretisation error estimation as described by Celik et al. (2008).

The apparent order of the method, *p*, is calculated by

$$p = \frac{1}{\ln(r_{21})}\left|\ln\left|\varepsilon_{32}/\varepsilon_{21}\right| + q(p)\right| \tag{7.3}$$

$$q(p) = \ln\left(\frac{r_{21}^{p} - s}{r_{32}^{p} - s}\right) \tag{7.4}$$

$$s = 1 \cdot sign\left(\varepsilon_{32}/\varepsilon_{21}\right) \tag{7.5}$$

where r_{21} and r_{32} are refinement factors, i.e. $\sqrt{2}$ in this study, and $\varepsilon_{32}=\phi_3-\phi_2$, $\varepsilon_{21}=\phi_2-\phi_1$, ϕ_k is the key variable, i.e. C_F in this case, on the k^{th} grid.

The extrapolated values are obtained by

$$\phi_{ext}^{21} = \left(r_{21}^{p}\phi_1 - \phi_2\right)/\left(r_{21}^{p} - 1\right) \tag{7.6}$$

The approximate and extrapolated relative errors are calculated using the following equations, respectively.

$$e_a^{21} = \left|\frac{\phi_1 - \phi_2}{\phi_1}\right| \tag{7.7}$$

$$e_{ext}^{21} = \left|\frac{\phi_{ext}^{12} - \phi_1}{\phi_{ext}^{12}}\right| \tag{7.8}$$

The fine-grid convergence index is calculated by

$$GCI_{fine}^{21} = \frac{1.25e_a^{21}}{r_{21}^{p} - 1} \tag{7.9}$$

These parameters were calculated for C_F values and are presented in Table 7.5 for the tanker and in Table 7.6 for the KCS.

Table 7.5: Calculation of the discretisation error for C_F values of the tanker.

	C_F *(with monotonic convergence)*
r_{21}, r_{32}	$\sqrt{2}$
ϕ_1	0.002103
ϕ_2	0.0020931
ϕ_3	0.0020929
p	10.9779
ϕ_{ext}^{21}	0.0021032
e_a^{21}	0.46981%
e_{ext}^{21}	0.010698%
GCI_{fine}^{21}	0.013374%

Table 7.6: Calculation of the discretisation error for C_F values of the KCS.

	C_F *(with monotonic convergence)*
r_{21}, r_{32}	$\sqrt{2}$
ϕ_1	0.0020222
ϕ_2	0.0020145
ϕ_3	0.0020086
p	0.76829
ϕ_{ext}^{21}	0.0020474
e_a^{21}	0.38077%
e_{ext}^{21}	1.2327%
GCI_{fine}^{21}	1.5601%

As can be seen from Table 7.5 and Table 7.6, insignificant numerical uncertainties (0.0133% for the tanker and 1.56% for the KCS) were estimated for the computed C_F values for both cases.

7.4.3 Prediction of C_F values

Table 7.7 and Table 7.8 show the frictional resistance coefficients of the tanker and the KCS, respectively, obtained for 7 different surface conditions over various ship speeds using this chapter's proposed CFD method in comparison with the similarity law analysis based method carried out in Chapter 5. These tables also include the percentage differences between these two methods.

Table 7.7: Comparison of the C_F values of the tanker at ship speeds of 10, 13 and 15 knots.

Description of condition	Speed (knots)	C_F (CFD)	C_F (Granville)	Difference (%)
Hydraulically smooth surface	10	0.001548	0.001555	-0.45
	13	0.001503	0.001506	-0.20
	15	0.001479	0.001480	-0.06
Typical as applied AF coating	10	0.001583	0.001516	4.45
	13	0.001580	0.001493	5.82
	15	0.001582	0.001485	6.58
Deteriorated coating or light slime	10	0.001809	0.001758	2.93
	13	0.001815	0.001752	3.64
	15	0.001815	0.001752	3.63
Heavy slime	10	0.002103	0.002052	2.51
	13	0.002103	0.002050	2.58
	15	0.002103	0.002049	2.62
Small calcareous fouling or weed	10	0.002507	0.002463	1.77
	13	0.002507	0.002461	1.85
	15	0.002506	0.002459	1.91
Medium calcareous fouling	10	0.003027	0.002952	2.56
	13	0.003027	0.002949	2.66
	15	0.003027	0.002947	2.72
Heavy calcareous fouling	10	0.003766	0.003666	2.74
	13	0.003766	0.003662	2.84
	15	0.003766	0.003659	2.92

Table 7.8: Comparison of the C_F values of the KCS at ship speeds of 19 and 24 knots.

Description of condition	Speed (knots)	C_F (CFD)	C_F (Granville)	Difference (%)
Hydraulically smooth surface	19	0.001386	0.001385	0.08
	24	0.001351	0.001347	0.28
Typical as applied AF coating	19	0.001485	0.001473	0.81
	24	0.001496	0.001469	1.84
Deteriorated coating or light slime	19	0.001750	0.001754	-0.23
	24	0.001750	0.001752	-0.15
Heavy slime	19	0.002022	0.002047	-1.21
	24	0.002022	0.002046	-1.14
Small calcareous fouling or weed	19	0.002401	0.002457	-2.27
	24	0.002401	0.002455	-2.19
Medium calcareous fouling	19	0.002886	0.002944	-1.96
	24	0.002886	0.002941	-1.87
Heavy calcareous fouling	19	0.003578	0.003655	-2.10
	24	0.003571	0.003651	-2.19

It is evident from Table 7.7 and Table 7.8 that the computed C_F values are reasonably consistent with those obtained using the similarity law scaling procedure of Granville (1958). In order to provide a facile illustrative comparison, the C_F values given in Table 7.7 and Table 7.8 are graphically shown in Figure 7.14 - Figure 7.18.

It is not surprising that the C_F value is no longer a function of the Reynolds number once the fully rough regime is reached, as can be seen in Table 7.7 and Table 7.8. These results also support the fact that the CFD model can capture the effect of surface roughness.

The increases in the C_F values of each surface condition with respect to those of a hydraulically smooth surface are listed in Table 7.9 for the tanker and in Table 7.10 for the KCS at different speeds.

Table 7.9: Predictions of the change in frictional resistance for the tanker at 3 different speeds.

Description of condition	**% ΔC_F @ V=10 knots**	**% ΔC_F @ V=13 knots**	**% ΔC_F @ V=15 knots**
Hydraulically smooth surface	-	-	-
Typical as applied AF coating	2.2	5.1	7
Deteriorated coating or light slime	16.8	20.8	22.7
Heavy slime	35.8	39.9	42.2
Small calcareous fouling or weed	61.9	66.8	69.5
Medium calcareous fouling	95.5	101.4	104.7
Heavy calcareous fouling	143.2	150.5	154.6

Table 7.10: Predictions of the change in frictional resistance for the KCS at 2 different speeds.

Description of condition	**% ΔC_F @ V=19 knots**	**% ΔC_F @ V=24 knots**
Hydraulically smooth surface	-	-
Typical as applied AF coating	7.1	10.7
Deteriorated coating or light slime	26.2	29.5
Heavy slime	45.9	49.7
Small calcareous fouling or weed	73.3	77.7
Medium calcareous fouling	108.2	113.6
Heavy calcareous fouling	158.2	164.3

The results presented in Table 7.9 and Table 7.10 indicate that the increases in the C_F values due to the hull roughness of a typical AF coating are relatively insignificant (2.2%, 5.1% and 7% respectively for the tanker and 7.1% and 10.7% for the KCS) compared to those due to biofouling, whereas the increases in the C_F values due to biofouling are predicted to be dramatic, which can lead to a drastic increase in the fuel consumption and hence CO_2 emissions of a ship. It should be borne in mind that

the relatively small increases due to roughness of different marine coatings are still of importance when considering the fuel consumption of a ship.

As can be seen from Table 7.9, the increases in the frictional resistance of the tanker due to a deteriorated coating or light slime surface condition at ship speeds of 10 knots, 13 knots and 15 knots were predicted to be 16.8%, 20.8% and 22.7%, respectively. These values became 35.8%, 39.9% and 42.2% when calculating the increase in the C_F values due to a heavy slime condition. Calcareous fouling causes significant increases in the C_F values ranging from ~62% to ~155% depending on the type of calcareous fouling and ship speed.

Likewise, the increases in the C_F values of the KCS due to a deteriorated coating or light slime surface condition at ship speeds of 19 knots and 24 knots were predicted to be 26.2% and 29.5%, respectively, as shown in Table 7.10. The increases in C_F were predicted to be 45.9% and 49.7% for the heavy slime surface condition. Calcareous fouling causes significant increases in C_F values, ranging from ~73% to ~165%, depending on the type of fouling and speed.

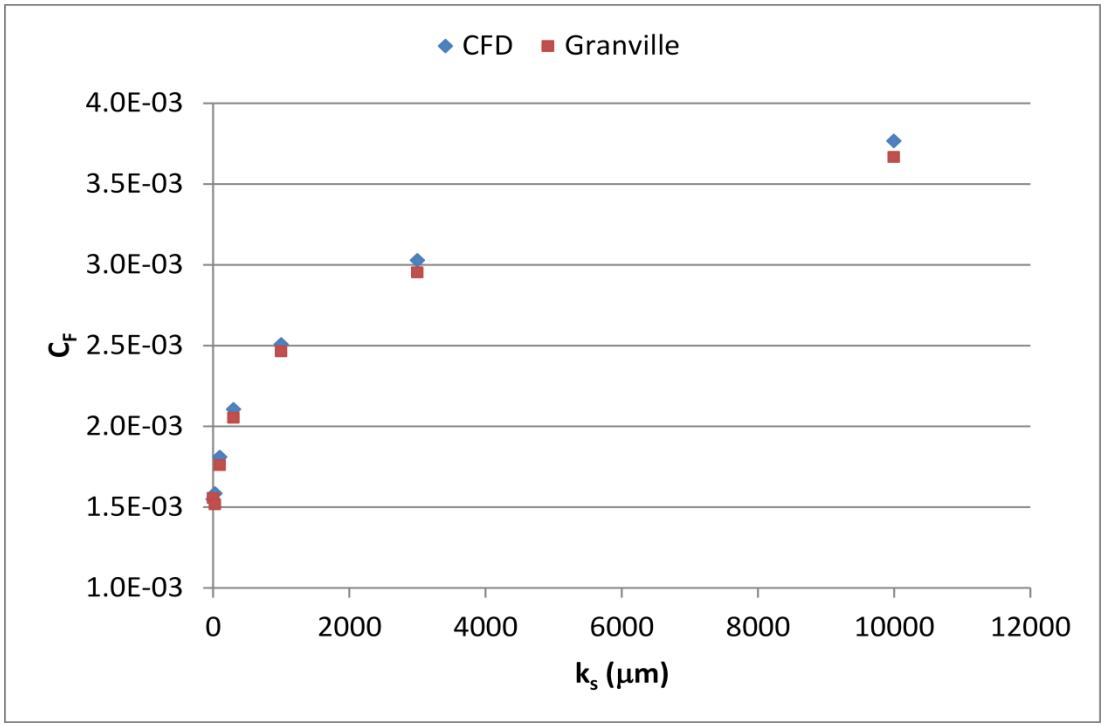

Figure 7.14: Comparison of the C_F values of the tanker at 10 knots for different hull fouling conditions.

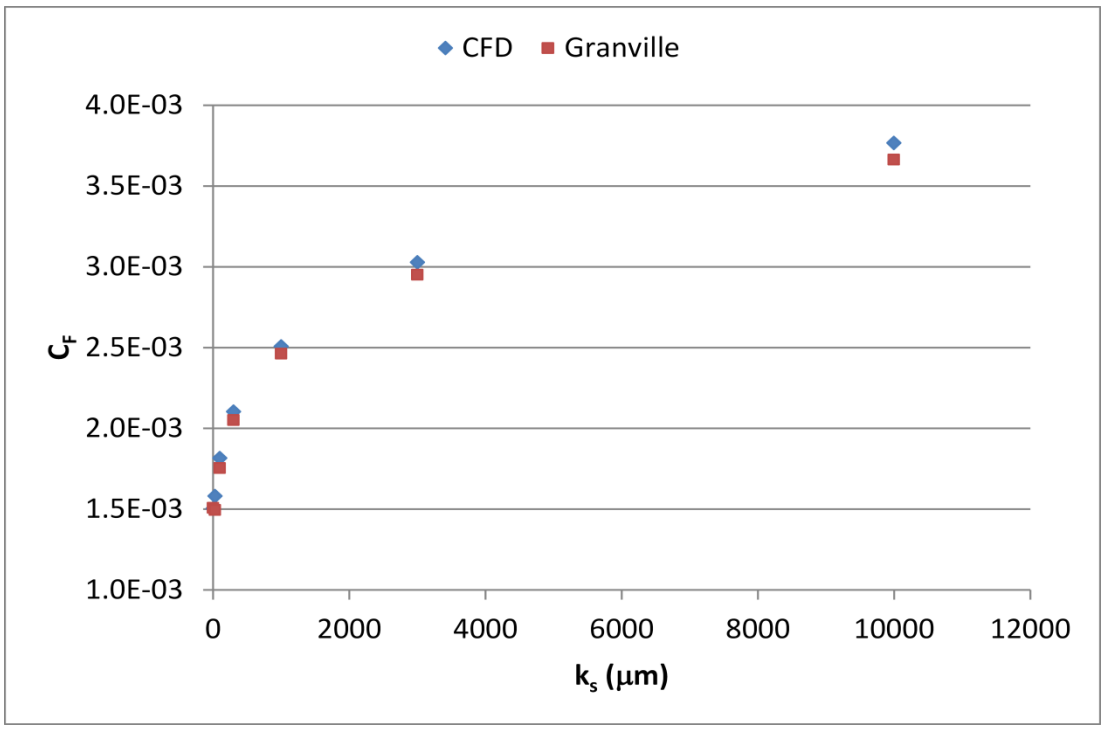

Figure 7.15: Comparison of the C_F values of the tanker at 13 knots for different hull fouling conditions.

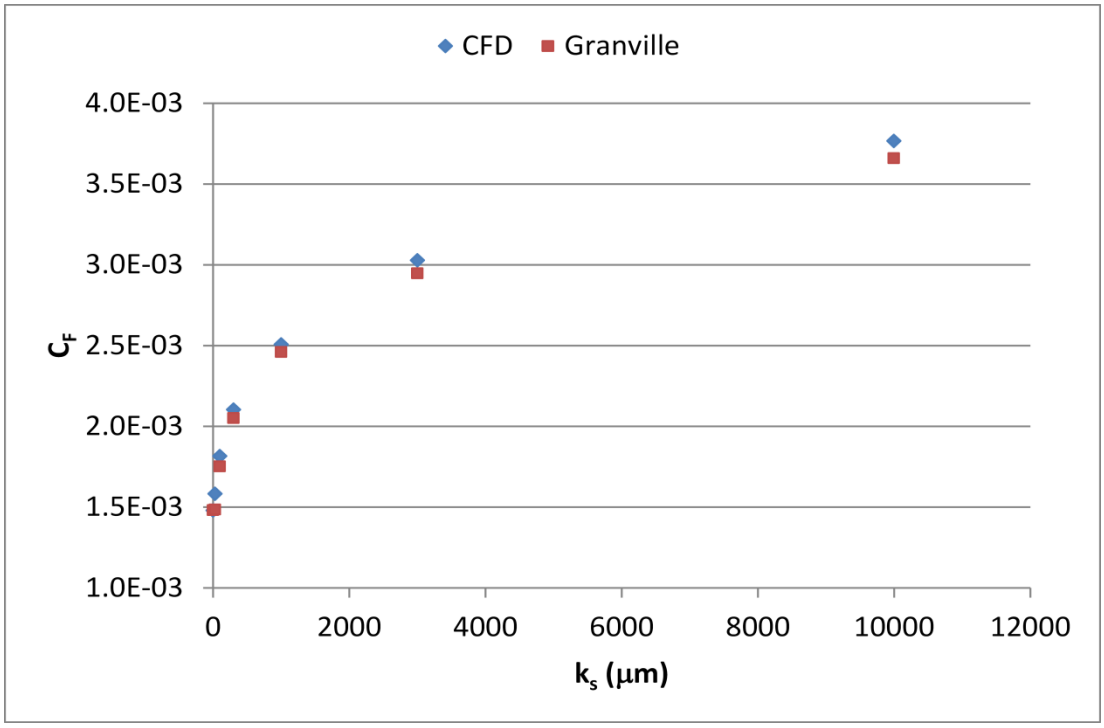

Figure 7.16: Comparison of the C_F values of the tanker at 15 knots for different hull fouling conditions.

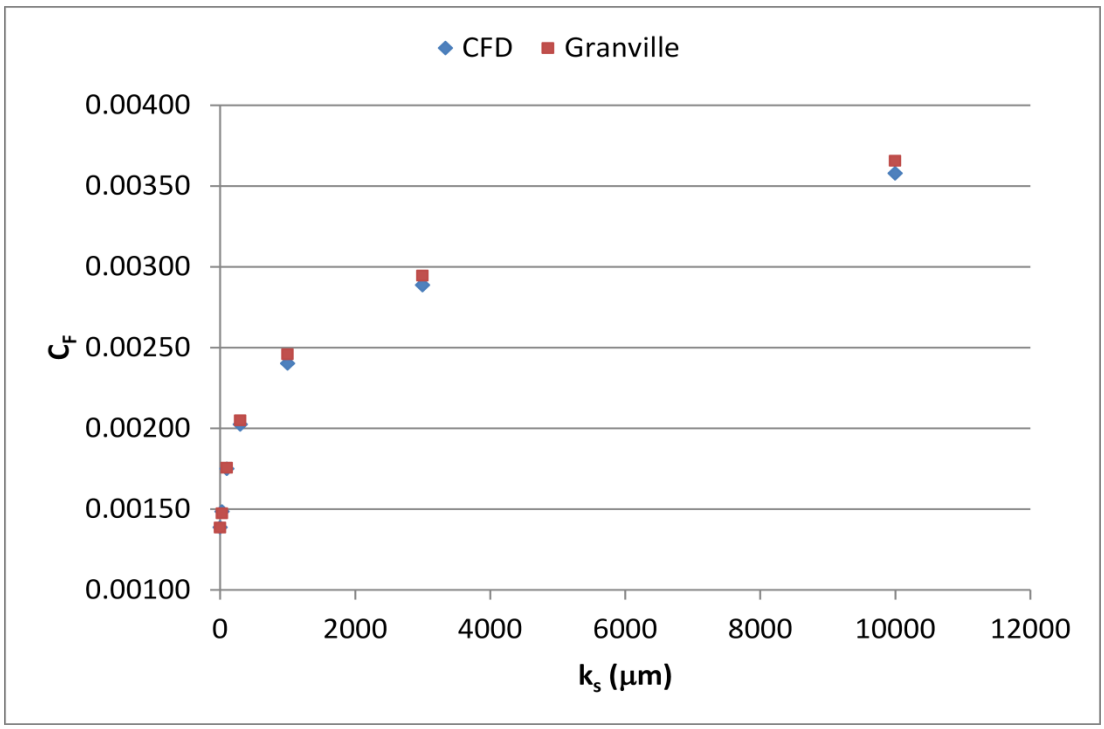

Figure 7.17: Comparison of the C_F values of the KCS at 19 knots for different hull fouling conditions.

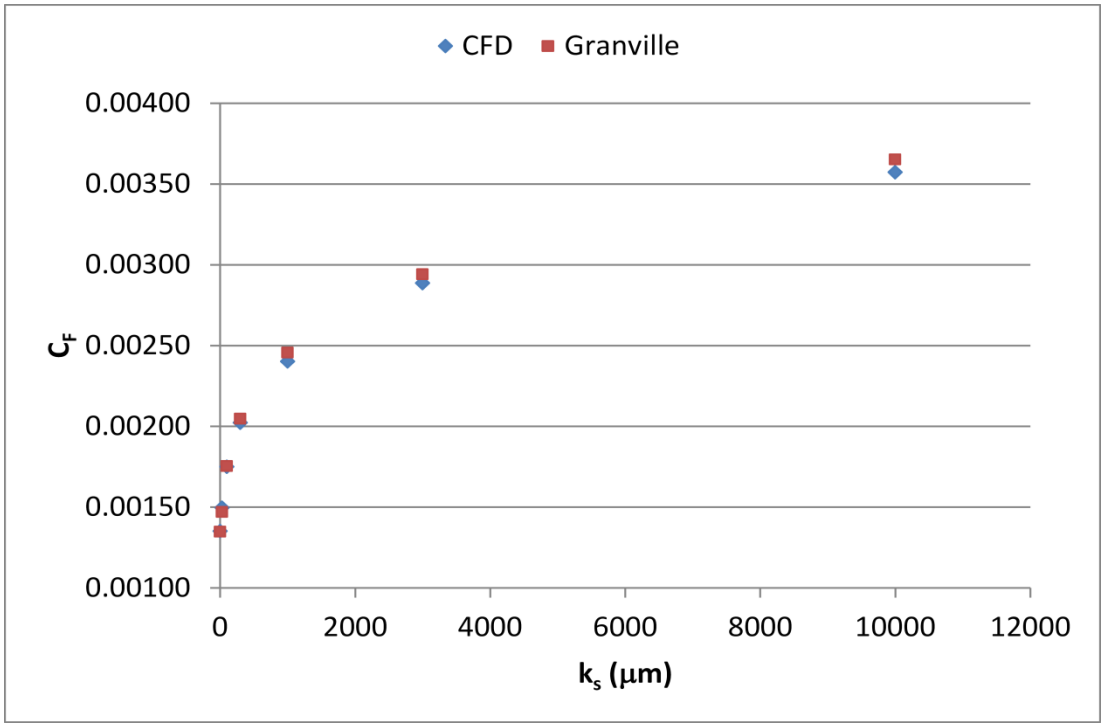

Figure 7.18: Comparison of the C_F values of the KCS at 24 knots for different hull fouling conditions.

Figure 7.19 - Figure 7.23 demonstrate the C_F values obtained using CFD, using bar graphs for various surface conditions at different speeds.

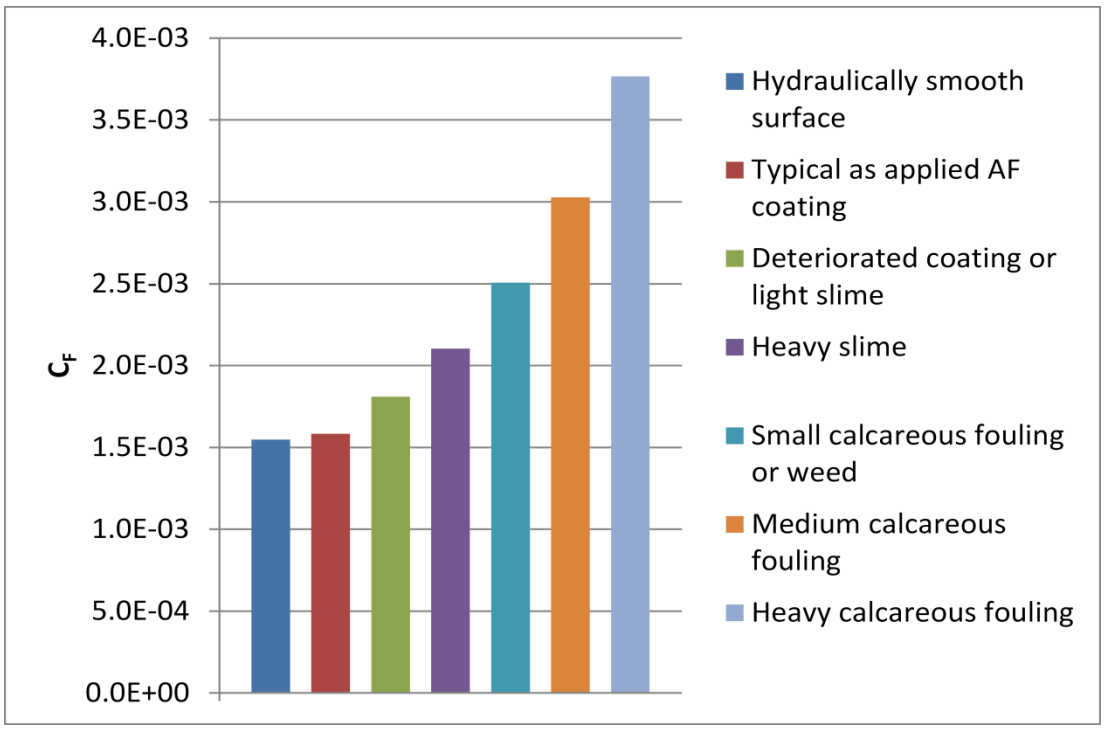

Figure 7.19: C_F values of the tanker for different hull surface conditions at 10 knots.

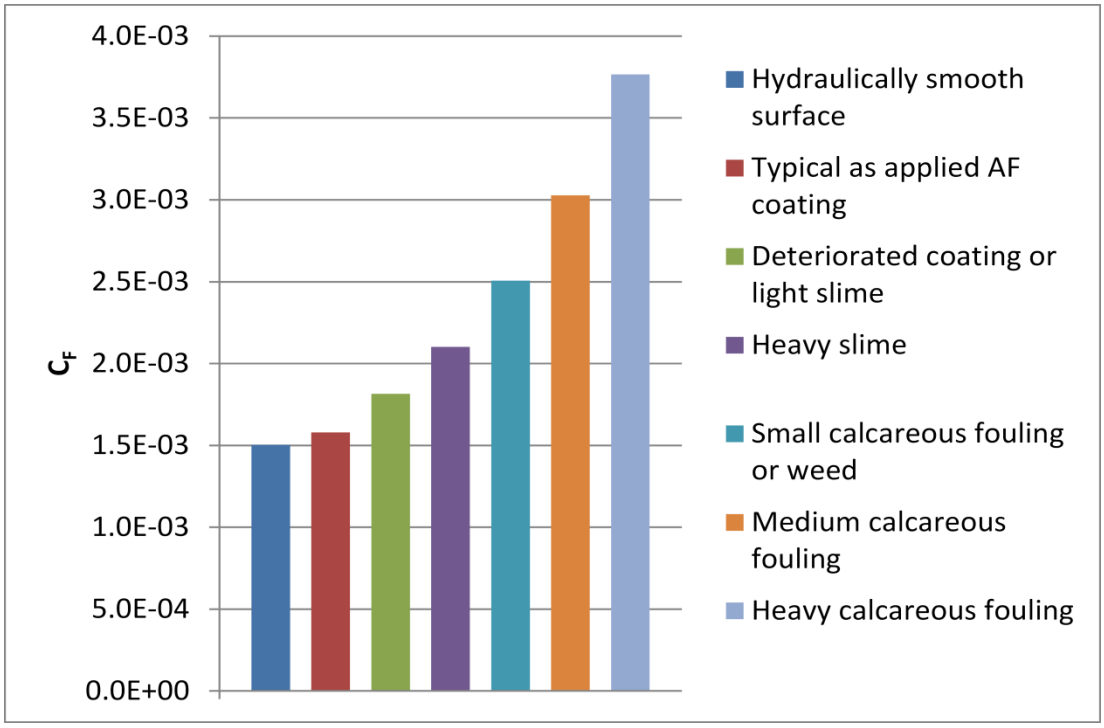

Figure 7.20: C_F values of the tanker for different hull surface conditions at 13 knots.

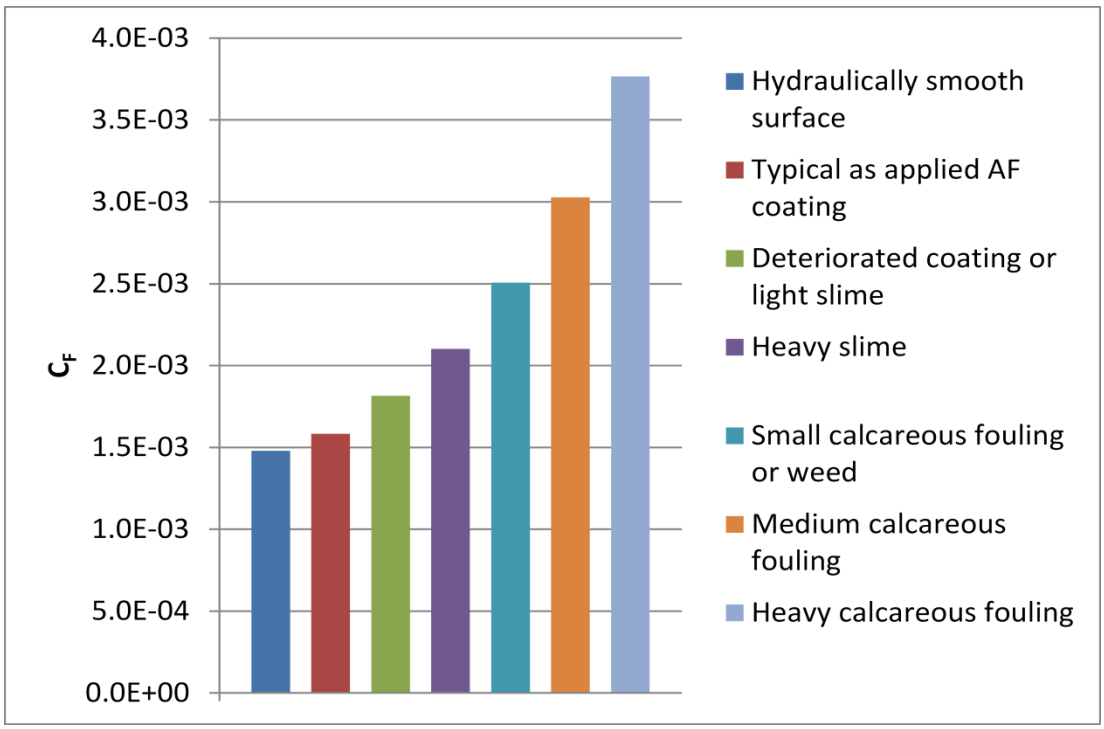

Figure 7.21: C_F values of the tanker for different hull surface conditions at 15 knots.

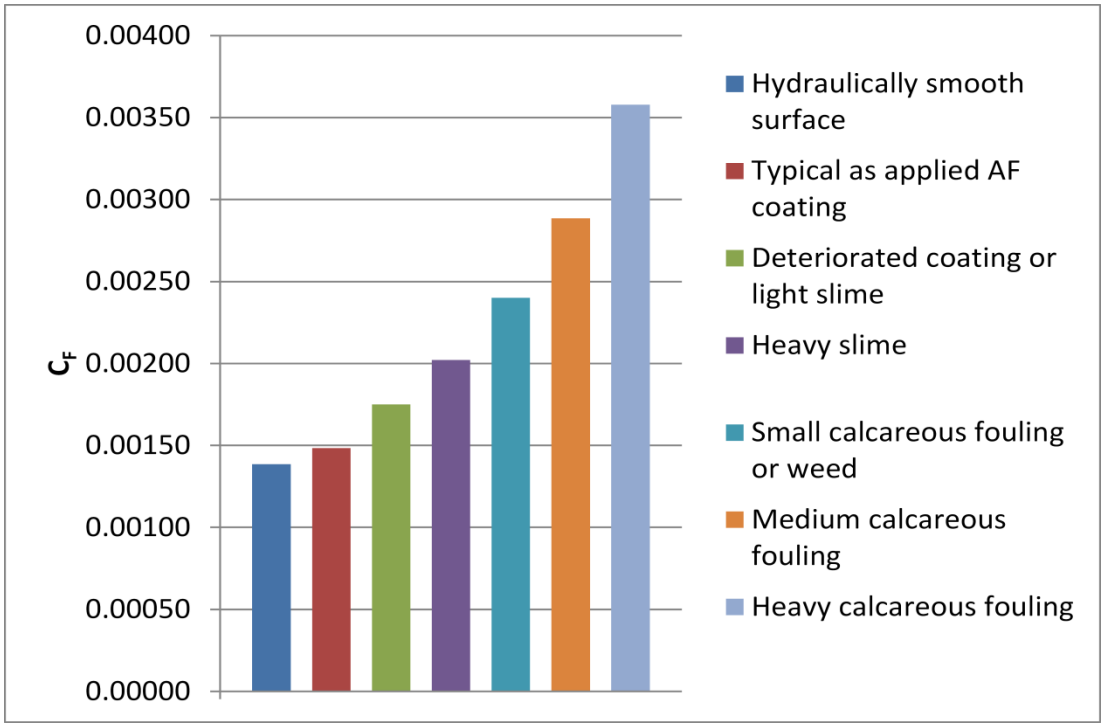

Figure 7.22: C_F values of the KCS for different hull surface conditions at 19 knots.

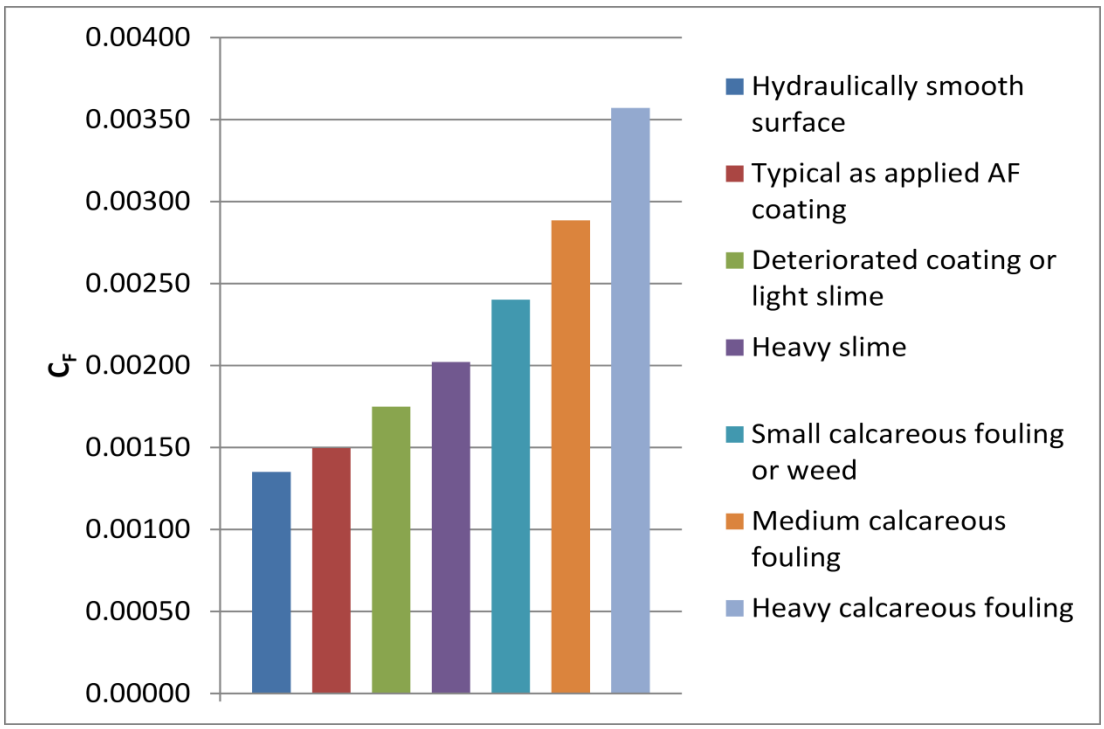

Figure 7.23: C_F values of the KCS for different hull surface conditions at 24 knots.

7.4.4 Increases in the Effective Power of the KCS due to Fouling

The predictions of the increases in the effective power were made using the same formulation described in Chapter 5, Section 5.4.3. The percentage increases in the effective power of the KCS due to different fouling conditions at ship speeds of 19 knots and 24 knots are demonstrated in Figure 7.24 and Figure 7.25, respectively. The results graphically shown in the figures are tabulated in Table 7.11.

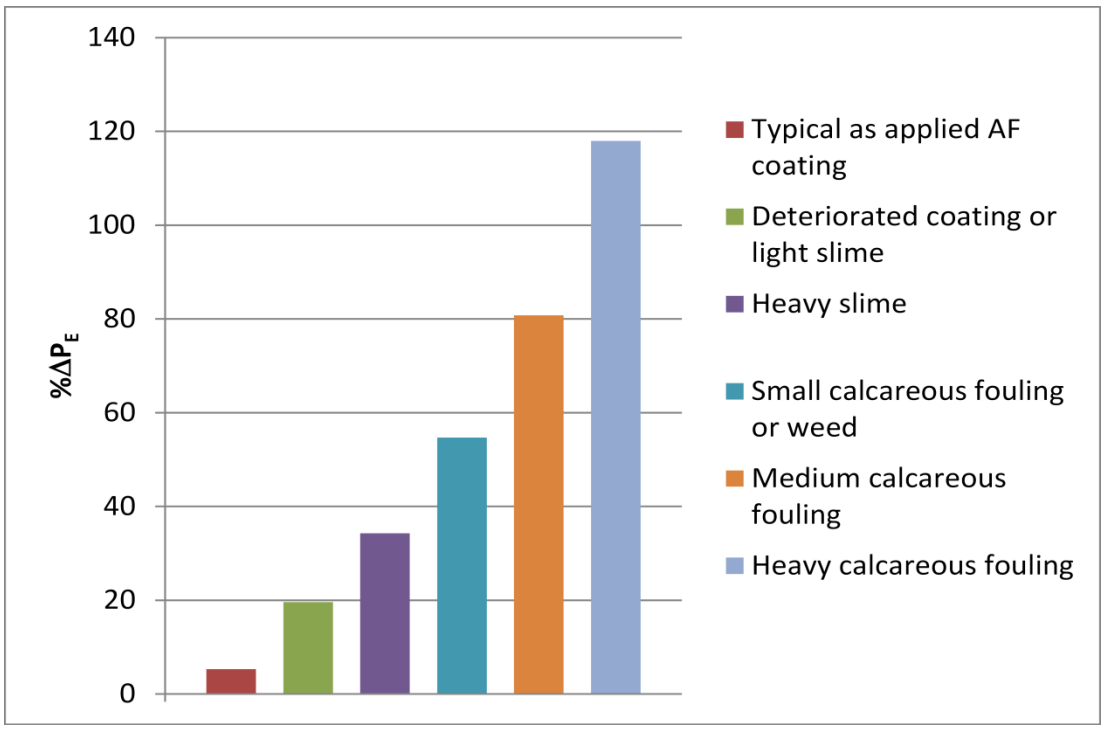

Figure 7.24: Percentage increases in the effective power of the KCS due to different fouling conditions at 19 knots.

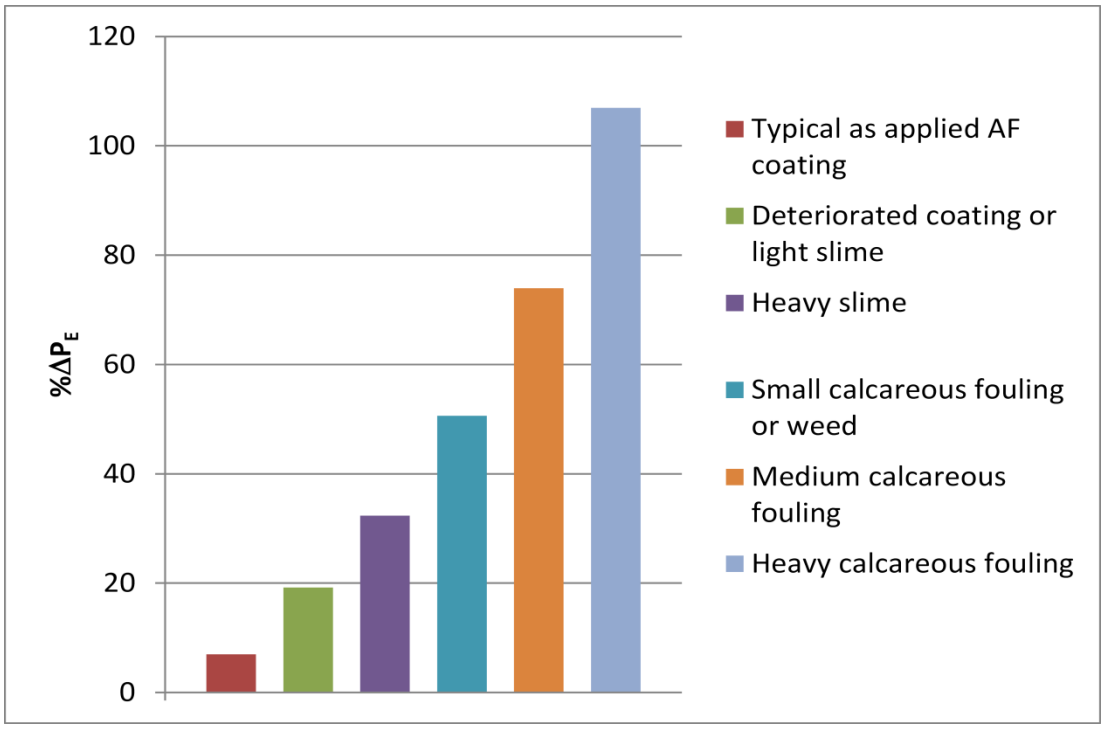

Figure 7.25: Percentage increases in the effective power of the KCS due to different fouling conditions at 24 knots.

Table 7.11: Predictions of the change in the effective power of the KCS at 2 different speeds.

Description of condition	% ΔP_E @ V=19 knots	% ΔP_E @ V=24 knots
Hydraulically smooth surface	-	-
Typical as applied AF coating	5.3	7
Deteriorated coating or light slime	19.6	19.2
Heavy slime	34.3	32.3
Small calcareous fouling or weed	54.7	50.6
Medium calcareous fouling	80.7	74.0
Heavy calcareous fouling	118.0	107.0

As Figure 7.24 and Figure 7.25 jointly show, the increases in effective power become significant when the fouling conditions become severe, as expected. The increases in the effective power of the KCS due to a typical, as applied AF coating were predicted to be 5.3% and 7% at ship speeds of 19 and 24 knots, whereas those due to a deteriorated coating or light slime may increase to 19.6% and 19.2%, respectively. The effect of heavy slime on the KCS hull was calculated to cause an increase in the effective power by 34.3% and 32.3%, at ship speeds of 19 and 24 knots, respectively. The calcareous fouling would increase P_E by 118% and 107%, at ship speeds of 19 and 24 knots.

An interesting point to note is that the effect of a particular fouling condition on the effective power of the KCS is more dominant at lower speeds. This can be attributed to the fact that the contribution of the frictional resistance becomes more important than residuary resistance at lower speeds. In other words, at higher speeds, the wave-making resistance becomes dominant due to wave generation, and the wave-making resistance is not expected to be markedly affected by fouling. Therefore, the effect of a given fouling condition on the total resistance of a ship is expected to be greater at low to moderate speeds than at higher speeds (Schultz, 2007).

7.5 Chapter Summary and Conclusions

A CFD model for the prediction of the effect of biofouling on frictional resistance has been proposed. A new roughness function model, which was developed based on the roughness function values of Schultz and Flack (2007), was proposed and employed in the wall-function of the solver and a series of studies were carried out to predict the effect of a range of representative coating and biofouling conditions on the frictional resistances of flat plates representing a handymax tanker and a

containership (KCS). The resulting C_F values were then compared with those obtained in Chapter 5 using the similarity law procedure of Granville (1958) to examine the applicability of the proposed CFD model. It has been shown that surface roughness can be modelled by employing modified wall-laws within the wall functions. It may be concluded that the proposed approach can be capable of predicting the roughness effect of biofouling on frictional resistance.

It should be borne in mind that this study's aim was to propose a robust CFD model, rather than a case-based model, to predict the frictional resistance of biofouling. For this reason, an appropriate representative roughness function model was employed in spite of the slight discrepancies between the individual roughness function values and the model, especially in the transitionally rough regime. The minor differences between the C_F values obtained by CFD and those obtained using the similarity law procedure of Granville (1958) can be attributed to the aforementioned insignificant scatter.

Without a doubt, these conditions and the roughness functions used in this chapter may not necessarily represent all types of fouling conditions, since the assumptions made are based on the observations made in Schultz (2007) and Schultz (2004). Future pieces of work may be the investigation of the roughness function behaviours of heterogeneous fouling accumulation, as seen on hulls, and an investigation into the range of applicability of the selected roughness length scale for the present conditions.

The applicability of the CFD model and wall function approach proposed in this chapter for the simulation of the effects of surface roughness on ship hulls, rather than on flat plates, will be investigated in Chapter 8.

8 CFD Simulations of the Roughness Effects of Marine Coatings and Biofouling on the Full-Scale KCS Hull

8.1 Introduction

Investigating the roughness effects of marine coatings and biofouling on a ship's resistance is of great importance for determining its performance. As stated earlier, biofouling has adverse effects on the performance of a ship, since it increases the required effective power in order for a ship to reach a certain speed, or it decreases the ship speed for a given effective power.

As discussed in Chapter 2, little effort has been made to perform Unsteady Reynolds-Averaged Navier-Stokes (URANS) CFD simulations of the roughness effects of marine coatings and biofouling on the resistance of a full-scale ship hull, using a specific roughness function model representing different hull surface conditions. Having showed that CFD is a suitable technique with which to predict roughness effects on frictional resistance using flat plates of model-scale and full-scale ship lengths in Chapters 6 and 7, it would be timely to perform unsteady RANS CFD simulations of the roughness effects of marine coatings and biofouling on full-scale ship hulls. The aim of the present study is therefore to fill this gap by employing the CFD model proposed in Chapter 7 to perform such simulations. The proposed approach enables the prediction of the resistance coefficients of full-scale ship hulls bearing a typical coating and a range of fouling conditions.

A full-scale KRISO Container Ship (KCS) hull appended with a rudder was used for all simulations in this chapter due to the existence of available experimental data for comparison purposes, and in order to enable a reasonable comparison with the

outcomes of Chapters 5 and 7. The model was first towed in smooth conditions at a design speed of 24 knots and the resulting resistance coefficient was compared and validated with the experimental data.

Following this, typical parametric case studies were performed at a design speed of 24 knots and a slow steaming speed of 19 knots. These involved changing the surface conditions by employing the roughness function model and corresponding roughness length scales proposed in Chapter 7, to represents a typical coating and a range of fouling conditions, while holding the other parameters constant. Total and frictional resistance coefficients were computed and compared with those obtained and presented in Chapters 5 and 7. Moreover, the increases in the effective power of the KCS due to such surface conditions were predicted using the present results.

This chapter is organised as follows: the employed roughness function model is presented in Section 8.2, while details of the numerical modelling including the geometry, boundary conditions and mesh generation are covered in Section 8.3. In Section 8.4, the present CFD results and those obtained in Chapters 5 and 7 are compared, and a validation and verification study is performed. In addition, predictions of the increase in the resistance coefficients and effective power of the KCS are demonstrated. Finally, the results of the study are discussed in Section 8.5, along with recommendations for future avenues of research.

8.2 Roughness Functions

In this chapter's study, the roughness function model developed in Chapter 7, which was based on the roughness function values of Schultz and Flack (2007), was used to represent a typical as applied coating and a range of fouling conditions. As stated earlier, the considered surface conditions are a hydraulically smooth surface, a typical as applied AF coating, a deteriorated coating or light slime, heavy slime, small calcareous fouling or weed, medium calcareous fouling and heavy calcareous fouling, as explained and classified by Schultz (2007) based on the Naval Ships' Technical Manual (2002). The reader should refer to Chapter 7, Section 7.2 and Chapter 5, Section 5.4.1, for further details.

8.3 Numerical Modelling

A URANS method was used to solve the governing equations in this study. These mass and momentum conservation equations were solved by the commercial CFD software. The mathematical formulations are identical to those used in Chapter 6. The reader should refer to Chapter 6, Section 6.3.1 for these details. It is of note that the ITTC (2011a) recommend the use of $\Delta t = 0.005 \sim 0.01$ L/U, where L is ship length and U is ship speed, for the selection of the time step. However, the time step size of the simulations was set to $\sim 0.0005 L_{BP}/U$, which is ten times lower than the recommendation of the ITTC (2011a), to ensure a reliable solution for such a complex phenomenon.

The general information about the wall-function approach and the application of roughness functions through wall-functions can be found in Chapter 6, Section 6.3.2. The analytical roughness function model given by equation (7.2), which was proposed in Chapter 7, Section 7.3.2, was employed in the CFD software through modifying wall-functions to predict roughness effects on ship resistance.

8.3.1 Geometry and Boundary Conditions

The KRISO Container Ship (KCS) appended with a rudder was used in this chapter's simulations since experimental data for this hull is publicly available and a large body of related CFD studies exist in the literature (e.g. Larsson et al. (2003), Zhang (2010), Castro et al. (2011), Carrica et al. (2011) and Tezdogan et al. (2015)). Additionally, the KCS has a very similar shape to commercial container ships, meaning the results will give an indication of how fouling effects the performance of real commercial container ships.

The principal particulars, body plans and side profiles of the full-scale KCS model are given in Table 8.1 (adapted from Tezdogan et al. (2015) and Kim et al. (2001)), and Figure 8.1 (Kim et al., 2001), respectively.

Table 8.1: Principal particulars of the KCS, adapted from Tezdogan et al. (2015) and Kim et al. (2001).

Length between the perpendiculars (L_{BP})	230.0 m
Length of waterline (L_{WL})	232.5 m
Beam at waterline (B_{WL})	32.2 m
Depth (D)	19.0 m
Design draft (T)	10.8 m
Wetted surface area	9498 m^2
Displacement (∇)	52030 m^3
Block coefficient (C_B)	0.6505
Design Speed	24 knots
Froude number (Fr)	0.26

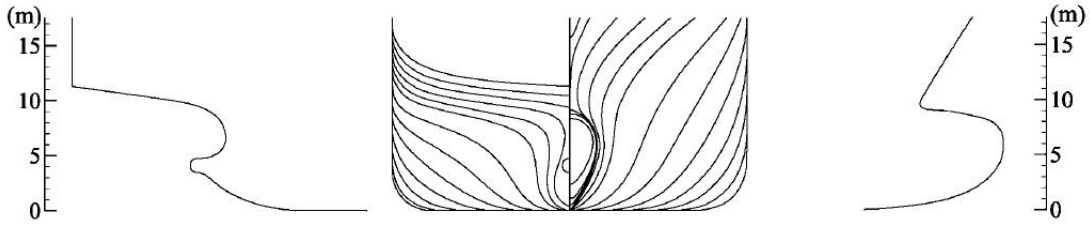

Figure 8.1: Body plan and side profiles of the KCS model (Kim et al., 2001).

The boundary conditions of the simulations were chosen to represent the full-scale KCS model being towed in a deep water condition. Figure 8.2 depicts an overview of the domain with the KCS model and the selected boundary conditions.

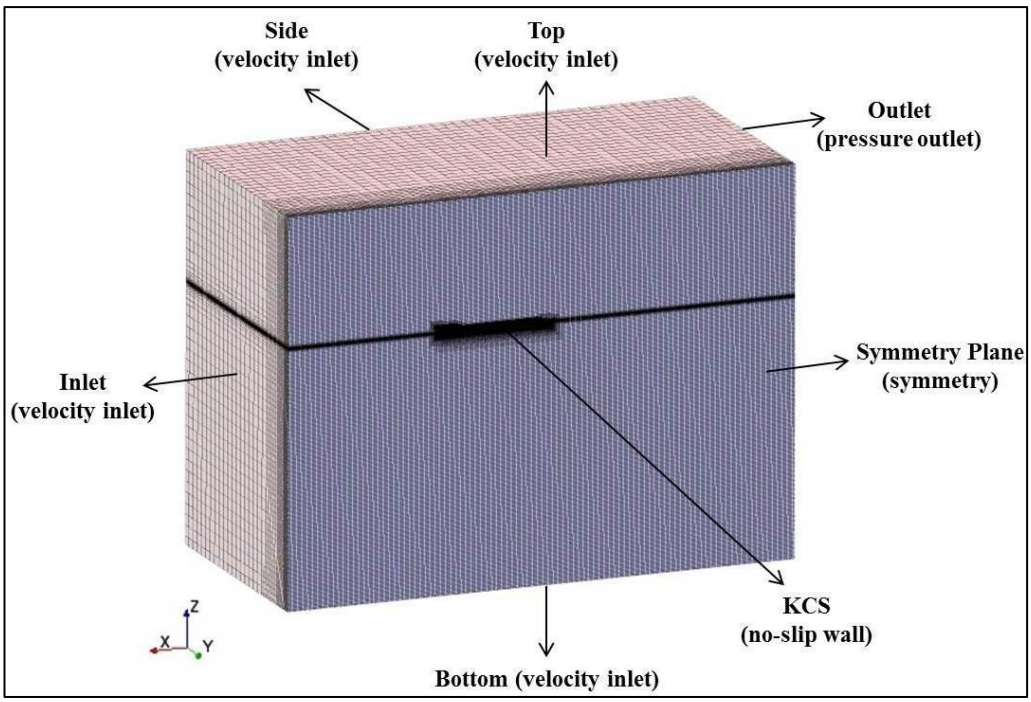

Figure 8.2: An overview of the domain with the selected boundary conditions.

The two opposite faces at the x-direction of the domain, i.e. the left-hand face (positive x-direction) and right-hand face (negative x-direction) of the domain in the top view were modelled as a velocity inlet and a pressure outlet, respectively. A symmetry plane was used to halve the required cell numbers and to reduce the computational demand since this does not significantly affect the computations. A velocity inlet boundary condition was set to the top, bottom and side (the negative y-direction) boundaries. It should be kept in mind that the initial flow velocity at all inlet conditions was set to the velocity of the flat wave, i.e. a ship speed of 24 knots, in the negative x-direction. The selection of the velocity inlet for the top and side of the domain therefore enables the flow at the top and side of the domain to be parallel to the outlet boundary, which prevents reflections from these boundaries. In addition, the representation of the deep water and infinite air conditions was facilitated by the use of a velocity inlet boundary condition for the top and bottom boundaries. As expected, the KCS hull itself has a no-slip rough wall condition to represent the roughness on the hull.

Another critical selection is the positioning of the boundaries, especially the downstream outlet boundary and the upstream inlet boundary. The inlet is placed at ~$1.5L_{BP}$ lengths upstream and the outlet boundary is placed at ~$2.5L_{BP}$ lengths downstream, to ensure boundary independent solutions are produced. Similarly, the top is located at ~$1.5L_{BP}$ and the bottom and the side are positioned at ~$2.5L_{BP}$ away from the KCS hull. It is of note that the selection of these boundary conditions and the positioning of the boundaries were made based on the recommendations and applications reported in CD-ADAPCO (2014). The locations of the boundaries are shown in Figure 8.3.

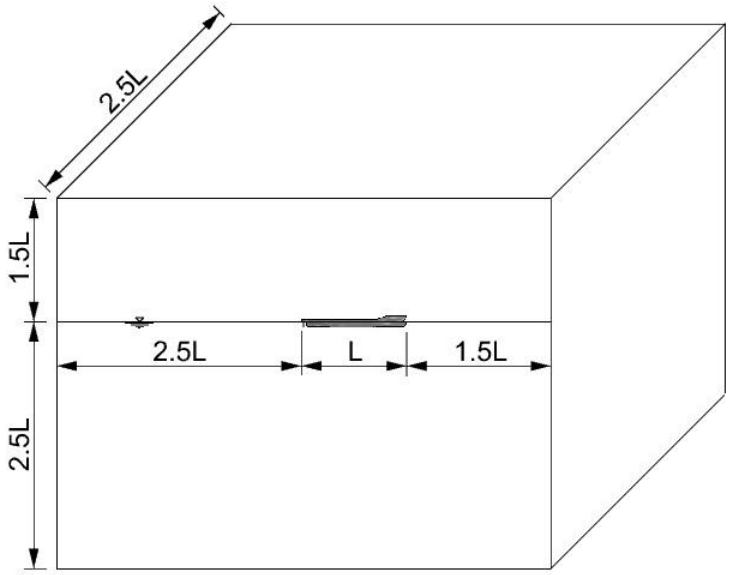

Figure 8.3: The positions of the boundaries (L: length of the ship between perpendiculars).

It should be noted that the VOF wave damping capability of the software was applied to the outlet and all velocity inlet boundaries, namely the inlet, bottom, top and side, with a damping length equal to ~1L_{BP}, to prevent reflections from these boundaries.

8.3.2 Mesh generation

A cut-cell grid with prism layer mesh on the walls was generated using the automatic mesh generator in STAR-CCM+. Additional refinements were applied to give finer grids in the critical regions, such as the area immediately around the hull and rudder, the area where the bow encounters the free surface, the area where water breaks with the hull stern, and the area in the wake generated by the ship. The mesh generation was achieved using similar techniques to those explained in Chapter 6, Section 6.3.4. Also, convergence tests were performed to ensure grid-independent mesh configurations, as well as to predict the numerical uncertainty of the CFD simulations.

A special near-wall mesh resolution was applied to surfaces with no-slip boundary conditions based on the roughness height values corresponding to each fouling condition. For this reason, the near-wall cell numbers varied for some of the fouling conditions. These differences resulted in different total cell numbers. The numbers of

the total cells generated are given in Table 8.2. Details of the near-wall mesh generation are given in the following section.

Table 8.2: Total cell numbers.

Surface Condition	Cell numbers
k=0, k=30, k=100, k=300	4.09×10^6
k=1000	4.00×10^6
k=3000	3.70×10^6
k=10000	3.58×10^6

Figure 8.4 shows cross-sections of the meshed domain whereas Figure 8.5 shows the volume mesh on the KCS hull and rudder. It is of note that, from this point onward, the figures show the whole sections as if there is no symmetrical boundary, owing to the visual transform feature of the software.

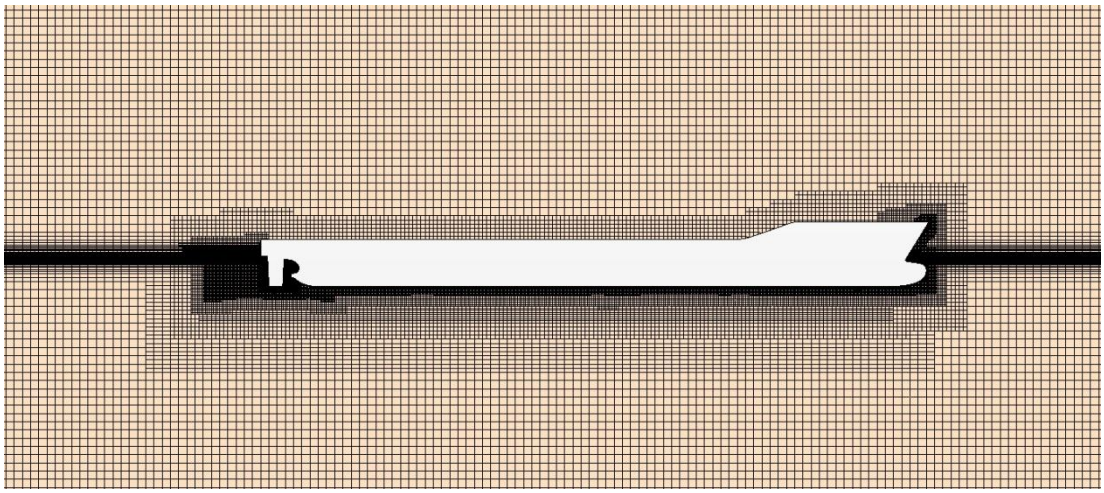

a)

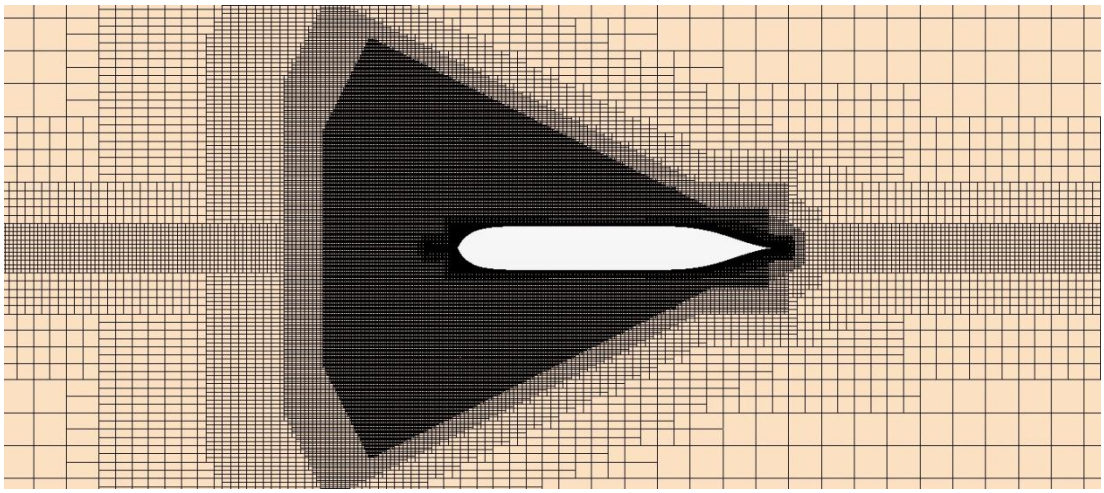

b)

Figure 8.4: a) Profile view cross-section **b)** top view cross-section of the domain.

Figure 8.4 demonstrates the cross-section from the centreline of the hull and the free surface and shows only a portion of the cross-sections for visual convenience, since the domain is rather large. The refinements to capture the free surface and Kelvin wake are clearly visible in Figure 8.4.

Figure 8.5 clearly shows the effects of additional refinements on the KCS hull and rudder, especially the ones applied to the free surface, bow and stern regions.

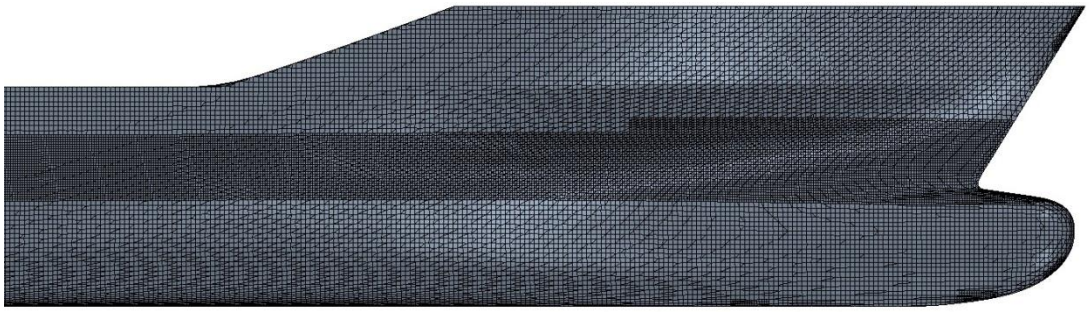

a)

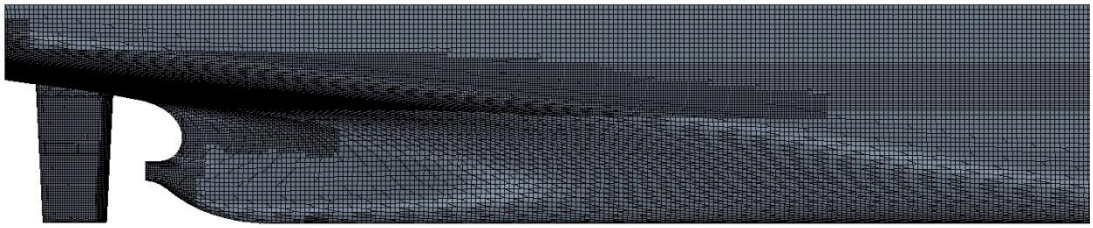

b)

Figure 8.5: Volume meshes on the **a)** bow, **b)** stern of the KCS hull and rudder.

8.3.2.1 Near-wall Mesh Generation

Near-wall grids on the hull are of vital importance because these are directly related to the hull roughness due to marine coatings and biofouling. The prism layer thickness and prism layer numbers were therefore determined such that y^+ is always higher than k^+, as per CD-ADAPCO (2014)'s suggestion. Hence, the resulting y^+ values were very high, as the k^+ values were high for most of the fouling conditions. The final y^+ distributions at a speed of 24 knots are shown for various simulation cases in Figure 8.6 - Figure 8.9, after the solutions have settled.

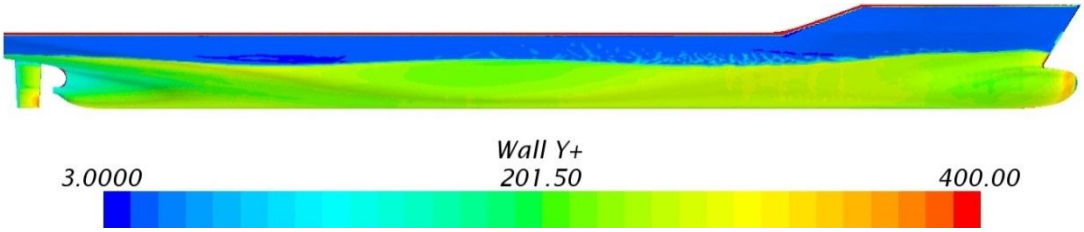

Figure 8.6: y^+ values on the KCS in smooth, typical as applied AF coating, deteriorated coating or light slime and heavy slime conditions at 24 knots.

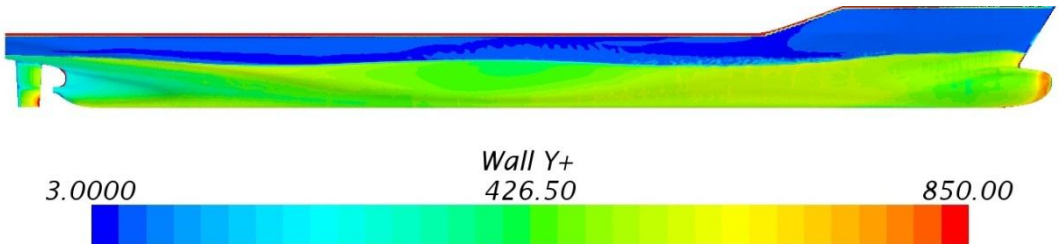

Figure 8.7: y^+ values on the KCS in small calcareous fouling or weed conditions at 24 knots.

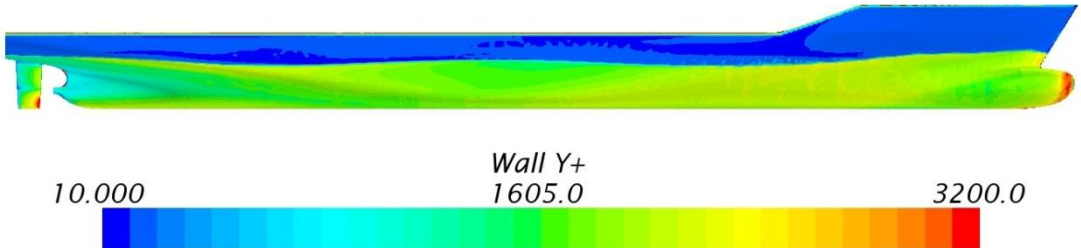

Figure 8.8: y^+ values on the KCS in medium calcareous fouling conditions at 24 knots.

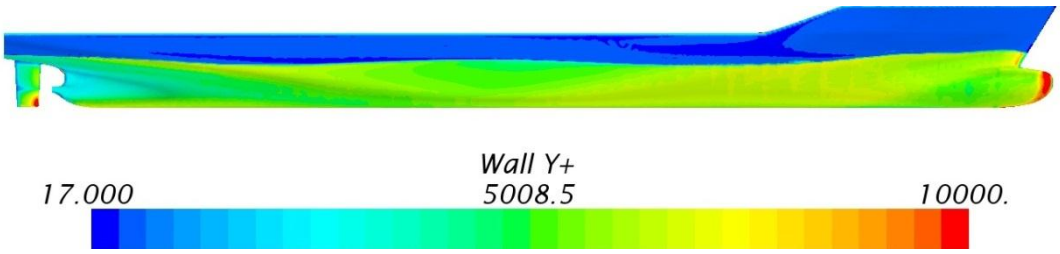

Figure 8.9: y^+ values on the KCS in heavy calcareous fouling conditions at 24 knots.

8.4 Results

8.4.1 Grid Dependence Tests

Systematic studies were performed using the KCS hull appended with a rudder with a smooth surface condition, in order to obtain grid independent solutions and to predict the CFD uncertainty, as was performed in Chapter 7. In order to observe the effect of cell numbers on the key variable (C_T in this case), the domain was discretised in three different resolutions and the simulations were run for each configuration. The grid refinement factor, *r*, was chosen to be $\sqrt{2}$, as in Chapter 7.

The frictional resistance coefficients for each mesh configuration were computed at a design speed of 24 knots and are given in Table 8.3.

Table 8.3: C_F results at different mesh configurations for the KCS at 24 knots.

Mesh configuration	Total No. of Cells	C_T (CFD)	% Experiment
Coarse	1.07×10^6	0.002120	2.30
Medium	2.04×10^6	0.002113	1.94
Fine	4.09×10^6	0.002097	1.17

From Table 8.3 it is evident that the solution of the fine mesh converged very well. Therefore, the fine mesh configuration was selected in all subsequent computations.

8.4.2 Validation and Verification

8.4.2.1 Validation Study

The available experimental data for the KCS was used to validate the CFD approach using the smooth condition. During the towing tank tests conducted by Kim et al. (2001), the residuary resistance coefficient for a 1/31.6 scale model of the KCS was found to be 7.250×10^{-4}, at the corresponding model speed for the full-scale speed of 24 knots (Fr = 0.26). Given that the residuary resistance is a function of Froude number, the residuary resistance coefficient of the full-scale KCS model is assumed to be the same ($C_R = 7.250 \times 10^{-4}$) and the full-scale frictional resistance coefficient, C_F, is calculated to be 1.347×10^{-3}, using the "ITTC 1957 model-ship correlation line", given by equation (2.25) at the corresponding Reynolds number. The total resistance

coefficient of the full-scale KCS model is therefore predicted to be 2.0725×10^{-3} (see equation (4.3)).

Table 8.3 demonstrates the total resistance coefficients computed by CFD and obtained using the experimental data of Kim et al. (2001), at a ship speed of 24 knots. As can be seen from Table 8.3, the computed total resistance coefficient, C_T, is in excellent agreement with the experimental data, with a difference of only ~1.17%. This CFD approach can therefore be claimed to be validated and can be used for further investigations. This model was therefore used throughout all the cases.

The residuary resistance coefficient, C_R, of the full-scale KCS model at a ship speed of 24 knots is assumed to be 7.250×10^{-4}, which was experimentally found by Kim et al. (2001), based on the major assumption which proposes that the residuary resistance is not markedly affected by surface roughness. The residuary resistance coefficients of all cases are therefore assumed to be 7.250×10^{-4}, and the difference between the computed total resistance coefficients and the residuary resistance coefficient were taken to be the frictional resistance coefficients for each case. It is of note that all numerical errors and uncertainties (given as 1.17% in Table 8.3) were therefore attributed to the differences in C_F values computed by the CFD method and by using the ITTC 1957 friction line.

The frictional resistance coefficients of the KCS calculated by this method and calculated using the ITTC 1957 friction line are compared in Table 8.4.

Table 8.4: Comparison of C_F values at 24 knots.

C_F (CFD)	C_F (ITTC 1957)	Difference (%)
0.001372	0.001347	1.80%

As can be seen from Table 8.4, the difference is only 1.8%. This method was therefore used throughout all cases to calculate the frictional resistance coefficients.

8.4.2.2 Verification Study

Having validated the present CFD approach, a verification study was carried out to identify the numerical uncertainty using the Grid Convergence Index (GCI) Method based on Richardson extrapolation (Richardson (1910), Richardson and Gaunt

(1927)) was used in this chapter's work for discretisation error estimation as described by Celik et al. (2008). The reader should refer to Chapter 7, Section 7.4.2 for further details of the verification study.

The described parameters were calculated for C_T values at 24 knots and are presented in Table 8.5. As can be seen from Table 8.5, insignificant numerical uncertainty (~0.7418%) was estimated for the computed C_T value.

Table 8.5: Calculation of the discretisation error for C_T values.

	C_F *(with monotonic convergence)*
r_{21}, r_{32}	$\sqrt{2}$
ϕ_1	0.002097
ϕ_2	0.002113
ϕ_3	0.002120
p	2.3853
ϕ_{ext}^{21}	0.0020846
e_a^{21}	0.76299%
e_{ext}^{21}	0.59698%
GCI_{fine}^{21}	0.7418%

8.4.3 Prediction of Drag Coefficients and Increases in the Effective Power

Table 8.6 and Table 8.7 show the predicted total resistance coefficients of the KCS hull obtained for 7 different surface conditions at ship speeds of 24 knots and 19 knots, respectively. They also give the percentage increase in resistance coefficients, and hence effective power, P_E, with respect to the smooth condition. The increases in C_T and P_E tabulated in Table 8.6 and Table 8.7 are graphically shown in Figure 8.10 and Figure 8.11.

Table 8.6: The computed C_T values at full scale at 24 knots.

Description of condition	**C_T (CFD)**	**Increase in C_T, P_E (%)**
Hydraulically smooth surface	0.002097	-
Typical as applied AF coating	0.002245	7.07
Deteriorated coating or light slime	0.002476	18.1
Heavy slime	0.002742	30.76
Small calcareous fouling or weed	0.003127	49.14
Medium calcareous fouling	0.003619	72.62
Heavy calcareous fouling	0.004351	107.52

Table 8.7: The computed C_T values at full scale at 19 knots.

Description of condition	C_T (CFD)	Increase in C_T, P_E (%)
Hydraulically smooth surface	0.001803	-
Typical as applied AF coating	0.001911	5.95
Deteriorated coating or light slime	0.002187	21.25
Heavy slime	0.002471	37.00
Small calcareous fouling or weed	0.002876	59.47
Medium calcareous fouling	0.003393	88.17
Heavy calcareous fouling	0.004163	130.86

As Table 8.6, Table 8.7, Figure 8.10 and Figure 8.11 jointly show, the increases in the total resistance coefficient and effective power become significant when the fouling conditions become severe, as expected. The increases in the C_T and P_E of the KCS due to a typical, as applied AF coating were predicted to be 7.07% and 5.95% whereas those due to a deteriorated coating or light slime may increase to 18.1% and 21.25% at ship speeds of 24 knots and 19 knots, respectively. The effect of heavy slime on the KCS hull was calculated to cause an increase in the C_T and P_E of 30.76% at 24 knots and 37% at 19 knots. The calcareous fouling would increase P_E by up to 107.52% at 24 knots and 130.86% at 19 knots.

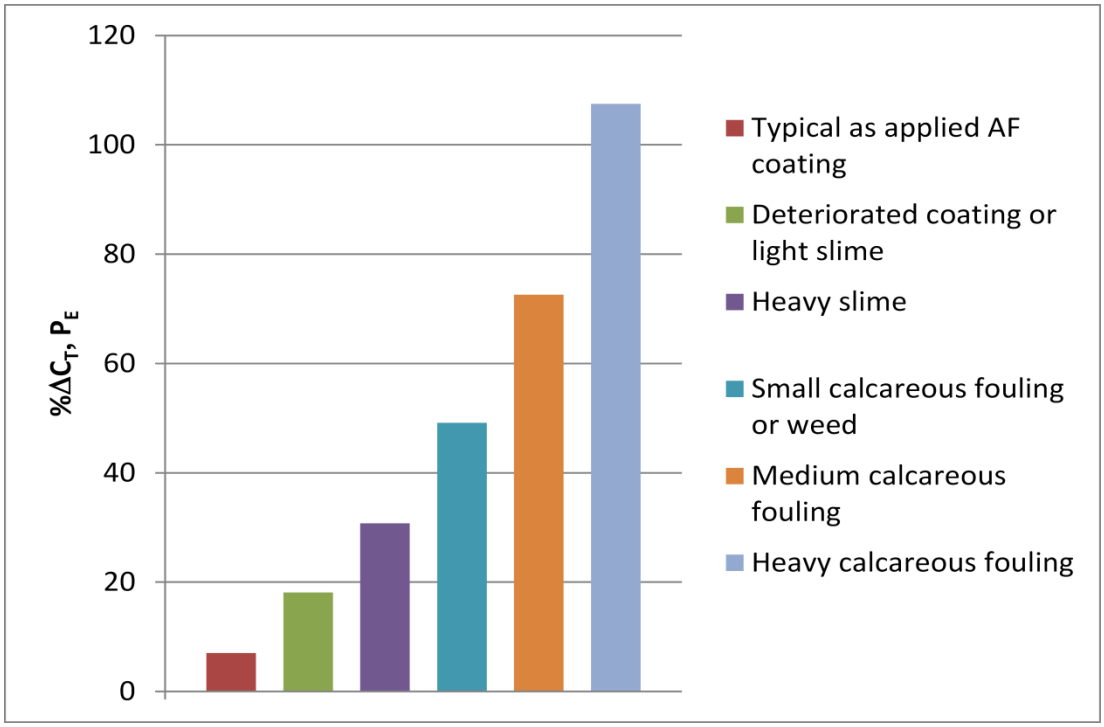

Figure 8.10: Percentage increase in the effective power of the KCS due to different fouling conditions at 24 knots.

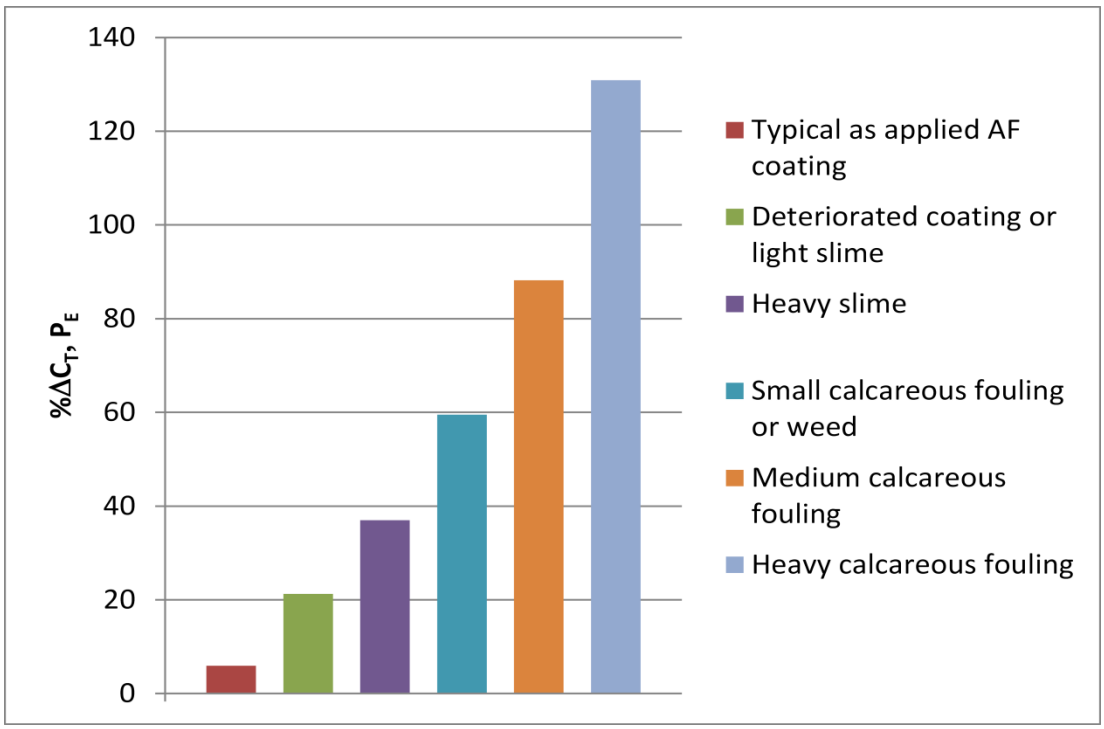

Figure 8.11: Percentage increase in the effective power of the KCS due to different fouling conditions at 19 knots.

Table 8.8 and Table 8.9 illustrate the C_F values of each surface condition and the percentage increases with respect to a smooth condition at ship speeds of 24 knots and 19 knots, while these increases are graphically shown in Figure 8.12 and Figure 8.13.

Table 8.8: The computed C_F values at full scale at 24 knots.

Description of condition	**C_F (CFD)**	**% ΔC_F**
Hydraulically smooth surface	0.001372	-
Typical as applied AF coating	0.001520	10.82
Deteriorated coating or light slime	0.001751	27.67
Heavy slime	0.002017	47.03
Small calcareous fouling or weed	0.002402	75.12
Medium calcareous fouling	0.002894	111.00
Heavy calcareous fouling	0.003626	164.36

Table 8.9: The computed C_F values at full scale at 19 knots.

Description of condition	C_F (CFD)	% ΔC_F
Hydraulically smooth surface	0.001385*	-
Typical as applied AF coating	0.001492	7.75
Deteriorated coating or light slime	0.001768	27.67
Heavy slime	0.002052	48.19
Small calcareous fouling or weed	0.002457	77.44
Medium calcareous fouling	0.002975	114.82
Heavy calcareous fouling	0.003745	170.41

*ITTC 1957 friction line

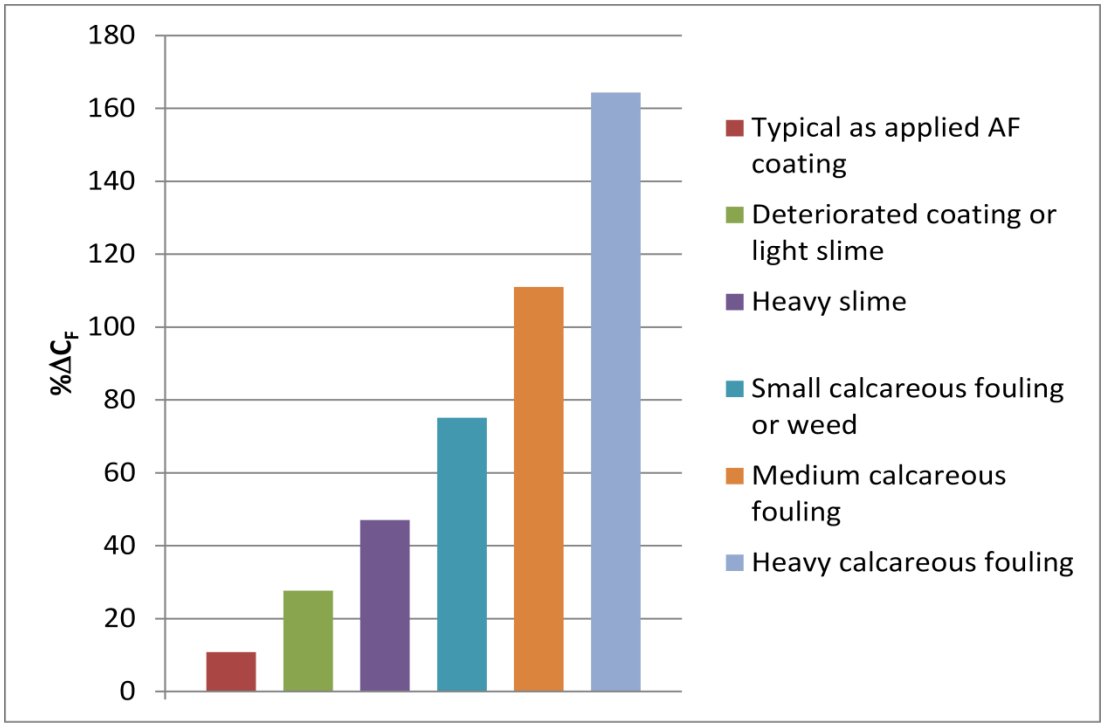

Figure 8.12: Percentage increase in the frictional resistance coefficient of the KCS due to different fouling conditions at 24 knots.

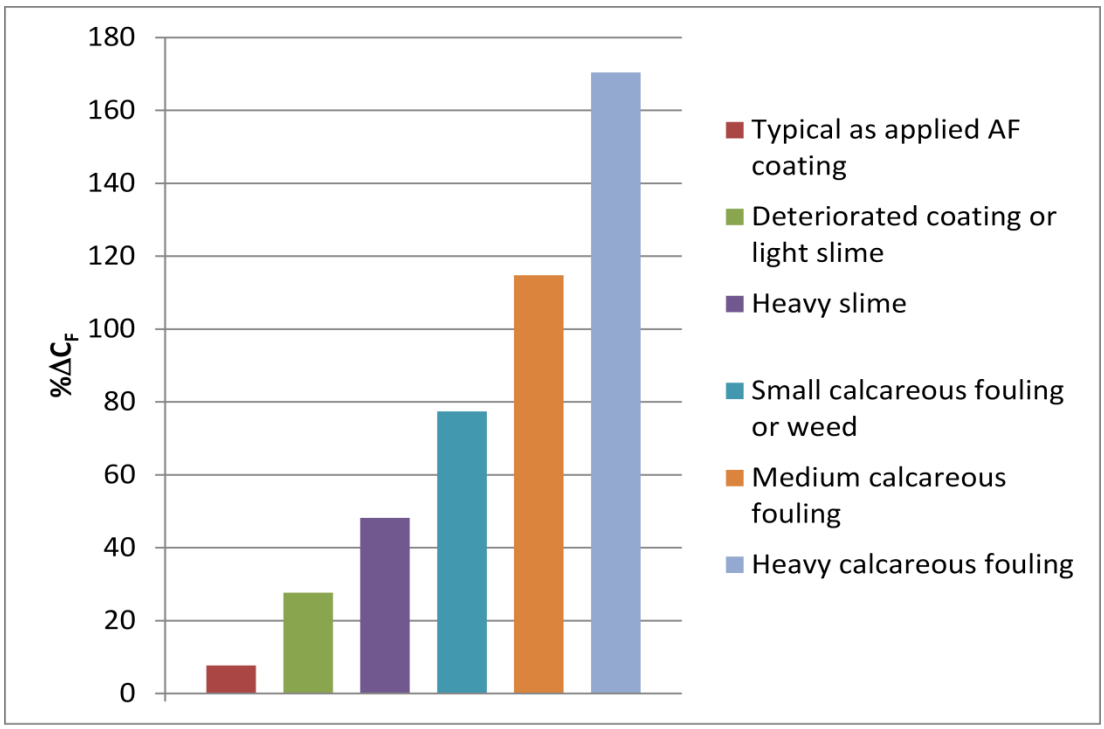

Figure 8.13: Percentage increase in the frictional resistance coefficient of the KCS due to different fouling conditions at 19 knots.

It is of note that the frictional resistance coefficient, C_F, of the full-scale KCS model at a ship speed of 19 knots for the smooth condition was calculated to be 1.385×10^{-3}, using the ITTC 1957 friction line. The residuary resistance coefficient, C_R, was calculated by subtracting this C_F from the total resistance coefficient, C_T. Based on the major assumption which proposes that the residuary resistance is not markedly affected by surface roughness, the residuary resistance coefficients of all cases are assumed to be 4.18×10^{-4}, and the difference between the computed total resistance coefficients and the residuary resistance coefficient were taken to be the frictional resistance coefficients for each case (see equations (4.4), (4.5) and (4.6)).

The results presented in Table 8.8, Table 8.9, Figure 8.12 and Figure 8.13 indicate that the increases in C_F due to the hull roughness of a typical AF coating are relatively insignificant (10.82% at 24 knots and 7.75% at 19 knots) compared to those due to biofouling, whereas the increases in C_F due to biofouling are predicted to be dramatic, which would likely lead to a drastic increase in the fuel consumption and hence CO_2 emissions. The increase in the frictional resistance of the KCS due to a deteriorated coating or light slime surface condition was predicted to be 27.67% at

a ship speed of 24 knots and to be 27.67% at a ship speed of 19 knots. These values became 47.03% and 48.19% when calculating the increase in C_F due to a heavy slime condition. Calcareous fouling causes significant increases in C_F values, ranging from ~75% to ~164% at 24 knots and ~77% to ~170% at 19 knots, depending on the type of calcareous fouling and ship speed.

8.4.4 Comparison of the methods

Having performed prediction studies using both flat plates representing the KCS, in Chapters 5 and 7, and the full-scale KCS model itself in the present chapter, it would be interesting to compare these different methods. Therefore, the following tables and figures aim to compare and discuss the results obtained using different techniques. These techniques are the current, 3D full-scale CFD simulations of the KCS hull (referred to as 'CFD-KCS hull'), flat plate CFD simulations performed in Chapter 7 (referred to as 'CFD-Flat plate') and the similarity law scaling procedure of Granville (1958) performed in Chapter 5 (referred to as 'Granville').

Table 8.10 and Table 8.11 show the frictional resistance coefficients of the KCS obtained for 7 different surface conditions, at ship speeds of 24 knots and 19 knots, using the different methods explained above. They also include the percentage differences between the results. The increases in the frictional resistance of the KCS due to different surface conditions, predicted using the different techniques, are demonstrated in Table 8.12 and Figure 8.14 for 24 knots and in Table 8.13 and Figure 8.15 for 19 knots.

It is interesting to note that the C_F values obtained at a ship speed of 24 knots (Table 8.10) in the present chapter are slightly higher than those obtained in Chapter 7 (with the exception of heavy slime), and slightly lower than those obtained in Chapter 5, with the exception of the unfouled conditions, i.e. the hydraulically smooth surface and typical as applied AF coating.

The C_F values obtained at a ship speed of 19 knots (Table 8.11) in the present chapter are slightly higher than those obtained in Chapter 5 and 7 (with the exception of the hydraulically smooth surface).

Table 8.14, Figure 8.16, Table 8.15 and Figure 8.17 demonstrate and compare the increases in the total resistances and hence in the effective power of the KCS due to different surface conditions, predicted in the present chapter, Chapter 5 and Chapter 7 at a design speed of 24 knots and at a slow steaming speed of 19 knots, respectively.

Table 8.10: Comparison of the computed C_F values using different methods at full scale at 24 knots.

Description of condition	C_F			%Differences with respect to	
	CFD-KCS hull	CFD-Flat plate	Granville	CFD-Flat plate	Granville
Hydraulically smooth surface	0.001372	0.001351	0.001347	1.53	1.83
Typical as applied AF coating	0.001520	0.001496	0.001469	1.60	3.47
Deteriorated coating or light slime	0.001751	0.001750	0.001752	0.07	-0.04
Heavy slime	0.002017	0.002022	0.002046	-0.26	-1.43
Small calcareous fouling or weed	0.002402	0.002401	0.002455	0.04	-2.16
Medium calcareous fouling	0.002894	0.002886	0.002941	0.29	-1.59
Heavy calcareous fouling	0.003626	0.003571	0.003651	1.54	-0.68

Table 8.11: Comparison of the computed C_F values using different methods at full scale at 19 knots.

Description of condition	C_F			%Differences with respect to	
	CFD-KCS hull	CFD-Flat plate	Granville	CFD-Flat plate	Granville
Hydraulically smooth surface	0.001385	0.001386	0.001385	-0.08	-0.009
Typical as applied AF coating	0.001492	0.001485	0.001473	0.48	1.30
Deteriorated coating or light slime	0.001768	0.001750	0.001754	1.03	0.80
Heavy slime	0.002052	0.002022	0.002047	1.49	0.25
Small calcareous fouling or weed	0.002457	0.002401	0.002457	2.35	0.015
Medium calcareous fouling	0.002975	0.002886	0.002944	3.08	1.05
Heavy calcareous fouling	0.003745	0.003578	0.003655	4.66	2.45

Table 8.12: Comparison of the computed % ΔC_F values using different methods at full scale at 24 knots.

Description of condition	% ΔC_F		
	CFD-KCS hull	CFD-Flat plate	Granville
Hydraulically smooth surface	-	-	-
Typical as applied AF coating	10.8	10.7	9
Deteriorated coating or light slime	27.67	29.5	30
Heavy slime	47.03	49.7	51.8
Small calcareous fouling or weed	75.12	77.7	82.2
Medium calcareous fouling	111.00	113.6	118.3
Heavy calcareous fouling	164.36	164.3	171.0

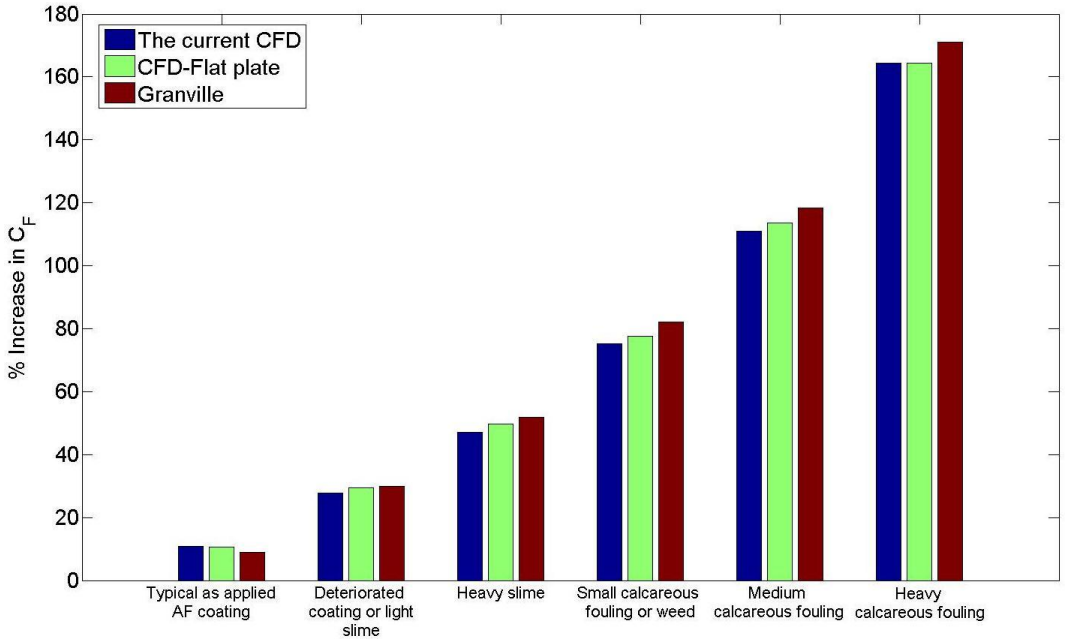

Figure 8.14: Estimation of the percentage increase in the frictional resistance of the KCS due to different surface conditions at 24 knots.

Table 8.13: Comparison of the computed % ΔC_F values using different methods at full scale at 19 knots.

Description of condition	% ΔC_F		
	CFD-KCS hull	CFD-Flat plate	Granville
Hydraulically smooth surface	-	-	-
Typical as applied AF coating	7.75	7.1	6.3
Deteriorated coating or light slime	27.67	26.2	26.6
Heavy slime	48.19	45.9	47.8
Small calcareous fouling or weed	77.44	73.3	77.4
Medium calcareous fouling	114.82	108.2	118.3
Heavy calcareous fouling	170.41	158.2	163.9

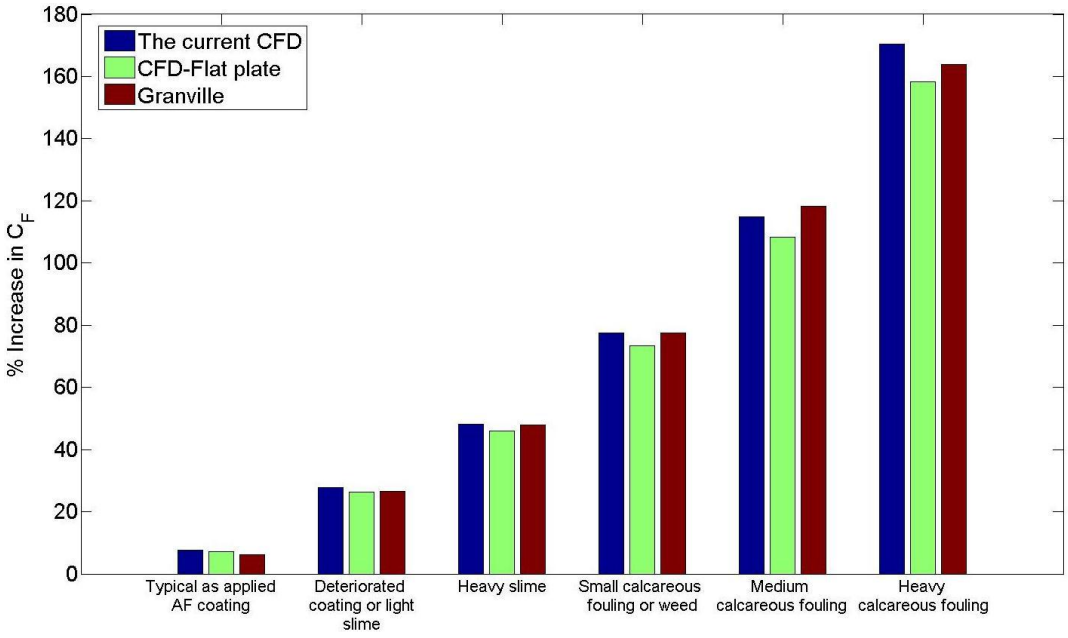

Figure 8.15: Estimation of the percentage increase in the frictional resistance of the KCS due to different surface conditions at 19 knots.

Table 8.14: Comparison of the computed % ΔC_T, ΔP_E values using different methods at full scale at 24 knots.

Description of condition	**% ΔC_T, ΔP_E**		
	CFD-KCS hull	**CFD-Flat plate**	**Granville**
Hydraulically smooth surface	-	-	-
Typical as applied AF coating	7.07	7	5.8
Deteriorated coating or light slime	18.1	19.2	19.5
Heavy slime	30.76	32.3	33.6
Small calcareous fouling or weed	49.14	50.6	53.4
Medium calcareous fouling	72.62	74.0	76.8
Heavy calcareous fouling	107.52	107.0	111.0

Table 8.15: Comparison of the computed % ΔC_T, ΔP_E values using different methods at full scale at 19 knots.

Description of condition	**% ΔC_T, ΔP_E**		
	CFD-KCS hull	**CFD-Flat plate**	**Granville**
Hydraulically smooth surface	-	-	-
Typical as applied AF coating	5.95	5.3	4.7
Deteriorated coating or light slime	21.25	19.6	19.9
Heavy slime	37.00	34.3	35.7
Small calcareous fouling or weed	59.47	54.7	57.7
Medium calcareous fouling	88.17	80.7	76.8
Heavy calcareous fouling	130.86	118.0	122.2

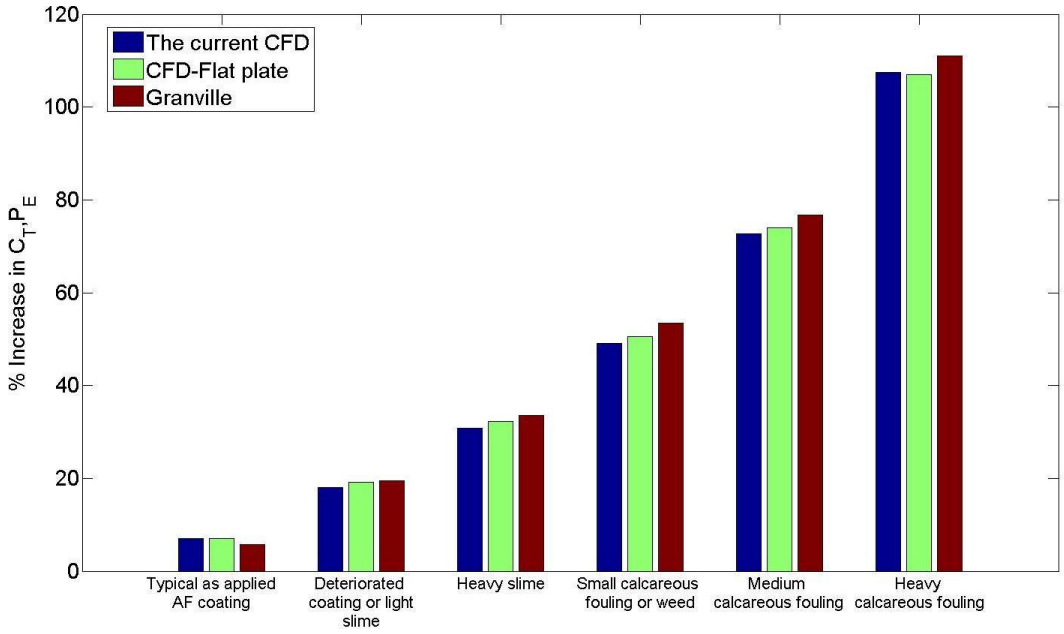

Figure 8.16: Estimation of the percentage increase in the resistance and effective power of the KCS due to different surface conditions at 24 knots.

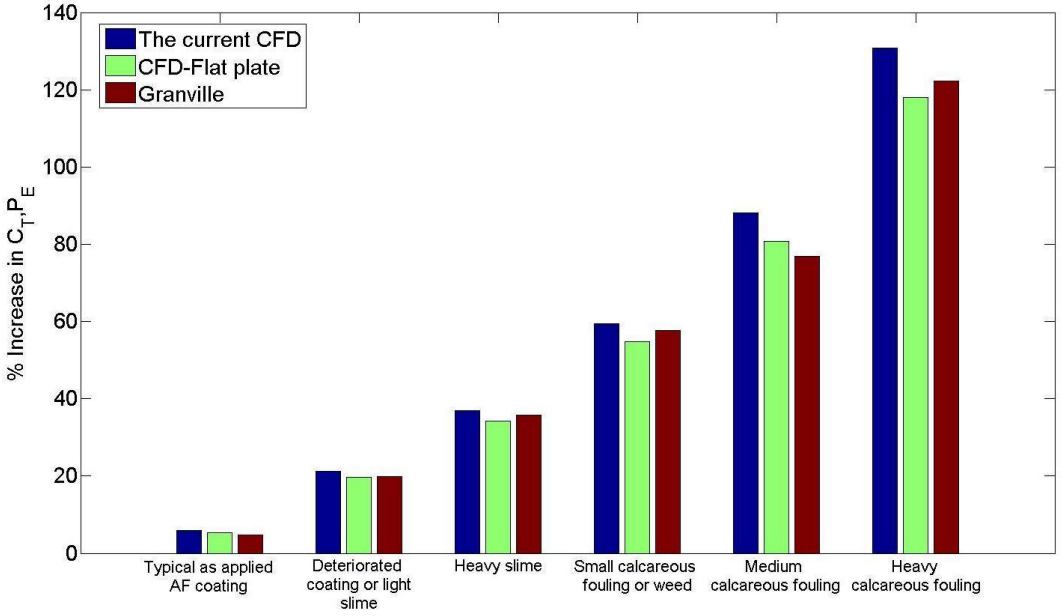

Figure 8.17: Estimation of the percentage increase in the resistance and effective power of the KCS due to different surface conditions at 19 knots.

8.5 Chapter Summary and Conclusions

The roughness function model proposed in Chapter 7 was employed in the wall-function of the solver and unsteady RANS simulations were carried out to predict the effect of a typical as applied coating and different biofouling conditions on the resistance of the full-scale KCS model appended with a rudder. This enabled the related objectives to be achieved by comparing the present chapter's '3D hull' approach with the 'flat plate' approach of Chapters 5 and 7.

Firstly, the total and frictional resistance values of the full-scale KCS model were obtained at a ship speed of 24 knots and compared with the experimental data of Kim et al. (2001) and the "ITTC 1957 model-ship correlation line" given by equation (2.25), respectively, for validation and verification purposes. It was shown that the total resistance coefficient was over-predicted by 1.17% compared to the related towing tank results and the frictional resistance coefficient was over-predicted by 1.80% compared to the ITTC 1957 friction line, with a numerical uncertainty of ~0.74%. Following this, roughness effects of a typical AF coating and different fouling conditions on the resistance of the full-scale KCS model were predicted at a design speed of 24 knots and a slow steaming speed of 19 knots. The increases in the effective power of the full-scale KCS hull were predicted to be 7.07% at a ship speed of 24 knots and 5.95% at a ship speed of 19 knots for a typical as applied AF coating, 18.1% at 24 knots and 21.25% at 19 knots for a deteriorated coating or light slime condition and 30.76% at 24 knots and 37% at 19 knots for a heavy slime condition. These values altered to 49.14%, 72.62% and 107.52% at 24 knots and 59.47%, 88.17% and 130.86% at 19 knots for small calcareous fouling or weed, medium calcareous fouling and heavy calcareous fouling, respectively.

The resulting C_F values and the increases in the drag coefficients were then compared with those obtained in Chapter 7 using flat-plate CFD simulations and with those obtained in Chapter 5 using the similarity law procedure of Granville (1958). The results suggest that the present approach can predict the roughness effects of biofouling on the resistance of a 3D full-scale ship. In other words, the applicability of the wall-function approach to simulate the surface roughness on ship hulls, rather than on flat plates, was shown.

Having shown the applicability of the wall-function approach to account for the roughness effects of AF coatings and biofouling on full-scale 3D ship hulls, this approach can be used to simulate this effect on more complex structures such as on self-propelled ships with a rotating propeller.

It is important to note that the application of the proposed wall-functions does not cause any additional run-time for a typical towing test simulation. In addition, this method is not expected to cause any additional run-time for a typical self-propulsion or seakeeping simulation. The main advantage of the proposed approach is that it enables the prediction of the effect of a typical coating and different biofouling conditions on the resistance of a ship under the effect of a rotating propeller or under the effect of a dynamic fluid-body interaction, which is not possible using the similarity law scaling procedure. Therefore, this approach stands as a practical prediction method for both academia and industry.

9 Discussion

9.1 Introduction

This chapter presents a discussion on the work performed within this thesis. Firstly, the achievement of specific research aims and objectives is discussed in Section 9.2, addressing each specific objective given earlier. Afterwards, the novelties and contributions to the field within this PhD study are listed in Section 9.3 and a general discussion is made on the difficulties encountered and important points to note, in Section 9.4.

9.2 Achievement of Research Aims and Objectives

The main aim of this PhD was described in Chapter 1 as being to model the roughness effects of marine coatings and biofouling on ship frictional resistance and fuel consumption. This ultimate aim was achieved by performing novel studies within each chapter and combining them to form one complete model.

The first specific objective listed in Chapter 1 was as follows:

- *To review the literature on modelling the roughness effects of marine coatings and biofouling on frictional resistance and to define the gaps in the literature.*

Chapter 2 addressed this aim by presenting an extensive critical review on the subjects covered in this thesis, including a discussion on the historical cornerstones of the research into ship frictional resistance with a focus on hull roughness, investigations into the effects of hull roughness on ship resistance and the determination of roughness functions.

The following objectives were achieved in Chapter 4:

- *To determine the roughness functions of several marine coatings, including the new FOUL-X-SPEL paints and control surfaces, using Granville's (1987) overall method.*

- *To compare the resistance characteristics of such coatings with an uncoated ship hull condition, rather than with only a smooth surface.*

Six different flat plates with different surface conditions were towed and the frictional drag coefficients were computed. These surface conditions are as follows:

- Reference Plate (sanded and polished)
- Hempel's Antifouling Olympic+ 72950 (FoulXSpel 2)
- New FOUL-X-SPEL Polyurethane system with an immobilised biocide (F0037)
- New FOUL-X-SPEL Silicone system with an immobilised biocide (F0034)
- Hempasil X3 87500 (FoulXSpel 1)
- Grit-blasted surface (Hull)

Following this, roughness functions were evaluated using an indirect method. Using this method, the drag characteristics of the paints and control surfaces were obtained. The as applied drag performance of each surface was compared with others. The advantage or disadvantage of the use of marine coatings over an uncoated ship hull condition was demonstrated.

The following objectives were achieved in Chapter 5:

- *To predict the effects of FOUL-X-SPEL paints on full-scale ship frictional resistance.*

- *To develop an in-house code based on the similarity law scaling for the prediction of the roughness effect on skin friction.*

- *To generate added resistance diagrams to predict the increases in the frictional resistance coefficients and effective powers of ships due to the use of marine coatings and biofouling conditions.*

In the beginning of Chapter 5, an in-house prediction code based on the similarity law scaling was developed to be able to predict a given roughness effect on any

arbitrary body. The drag characteristics were then employed in the code and the effects of several coatings, including the novel FOUL-X-SPEL paints, on ship frictional resistance were predicted. The advantage of the use of F0034 over the use of other coatings was clearly highlighted using the predictions made in Chapter 5, based on the results of the experiments conducted in Chapter 4. Following this, roughness functions and roughness Reynolds numbers from the literature were employed in the code, which enabled large numbers of predictions of the effects of a range of coating and fouling conditions on ship frictional resistances at various ship speeds. Using this extensive database, added resistance diagrams were generated and proposed. These diagrams may be easily used by naval architects in the early stages of ship design to predict the powering penalties of the use of coatings and due to biofouling accumulated on hulls.

The following objectives were achieved in Chapter 6:

- *To investigate and show the applicability of a CFD method for the simulation of surface roughness by means of employing modified wall-functions.*

- *To develop and propose a CFD model which enables the prediction of the effect of antifouling coatings on frictional resistance.*

- *To outline details of CFD simulations of resistance tests on coated plates in a towing tank.*

Several exploratory studies were performed and the applicability of CFD methods for the simulation of surface roughness was shown. It was observed that this can successfully be achieved using wall-functions. Hence, the experimentally obtained roughness function models were employed in the wall-function of the software and predictions were made. A CFD-based URANS model for the frictional resistance prediction of antifouling coatings was proposed. CFD simulations of resistance tests on coated plates in a towing tank were performed and important points were outlined.

The following objective was achieved in Chapter 7:

- *To develop and propose a CFD model which enables the prediction of the effect of biofouling on frictional resistance.*

Having demonstrated the suitability of the CFD method for frictional resistance predictions as functions of roughness, a new roughness function model was proposed and employed in the CFD software. A new CFD-based URANS model for the prediction of the effect of biofouling on frictional resistance was developed and proposed.

The following objectives were achieved in Chapter 8:

- *To investigate the applicability of the wall function approach of CFD to simulate the surface roughness on ship hulls, rather than on flat plates, and to show that it is a suitable method with which to predict the roughness effects of marine coatings and biofouling on 3D full-scale ships.*

- *To perform unsteady RANS CFD simulations of the roughness effects of marine coatings and biofouling on the full-scale KCS hull, and hence investigate such effects on the total resistance and effective power of the KCS.*

Having demonstrated the applicability of the CFD models proposed in Chapters 7 and 8 by comparing the results with experimental data and the results obtained in Chapter 6, unsteady RANS towing simulations of the full-scale KCS hypothetically coated with a typical AF coating and covered with different fouling conditions were performed. It was shown that the proposed wall-function approach is capable of predicting the roughness effects of marine coatings and biofouling on the resistances of 3D full-scale ships.

9.3 Novelties and Contributions to the Field

The main novelties achieved within this PhD study are given as follows:

- To the best of this author's knowledge, this is the first time that a fully nonlinear URANS CFD method has been proposed to model the roughness effects of marine coatings and biofouling on the resistance of a 3D full-scale ship. This can be considered as an alternative method to similarity law scaling procedure, which uses the flat plate approach.

This was achieved by employing a new roughness function model, which represents a typical coating and a range of biofouling conditions, through the modification of the built-in wall-function of the CFD software.

- To the best of this author's knowledge, this is the first time that added resistance diagrams have been proposed to predict the roughness effects of marine coatings and biofouling on the frictional resistance of flat plates of ship lengths. This can be used as a practical tool for designers and engineers to be able to assess and estimate the added resistance and hence the fuel penalty of a ship, for a particular fouling condition at a specific speed.

This was achieved by developing an in-house code based on the similarity law scaling procedure. This enabled an extensive database to be constructed, containing added resistance values due to different surface conditions.

Other main contributions to the field within this PhD study are listed below:

- The roughness functions of two new-generation commercial marine coatings, two novel FOUL-X-SPEL paints and a grit-blasted surface representing a bare ship hull were determined and provided.

- The resistance characteristics of such coatings were compared with an uncoated ship hull condition, rather than with only a smooth surface.

- An in-house code was developed based on the similarity law scaling for the prediction of the roughness effect on the skin friction of flat plates. The

algorithm of a prediction procedure showing how to develop such diagrams using the available experimental data was provided.

- The effects of FOUL-X-SPEL paints on full-scale ship frictional resistance were predicted and the importance of the type of marine coatings in the as applied condition was demonstrated.

- Two CFD models were developed and proposed for the prediction of the roughness effects of marine coatings and biofouling on the frictional resistances of flat plates of ship lengths.

- The applicability of CFD methods for the simulation of surface roughness by means of employing modified wall-functions were evidently shown by comparing the results obtained using the proposed CFD models with those obtained using the similarity law scaling procedure and experimental data.

- Unsteady RANS CFD simulations of the roughness effects of marine coatings and biofouling on the full-scale KCS hull were performed using the proposed CFD models and hence such effects on the total resistance and effective power of the KCS were investigated.

- The applicability of the wall function approach of CFD to simulate the surface roughness on ship hulls, rather than on flat plates, was demonstrated and it was shown that it is a suitable method with which to predict the roughness effects of marine coatings and biofouling on 3D full-scale ships.

9.4 General Discussion

This work was built on two pillars: the experimental determination of the drag characteristics of coatings, and the predictions of roughness effects on full-scale ship frictional resistance.

It was clearly shown in Chapter 4 that the overall (towed plate) method can be used to determine the drag characteristics of surfaces. As expected, some difficulties were experienced during these experiments. Firstly, the alignment of the flat plate is of vital importance since poor alignment would create side forces and the zero-pressure gradient condition would not be met. The alignment procedure was therefore very difficult and time consuming during the experiments. It is suggested that the alignment should be done using an additional transducer which measures the side forces, and that the plate should be towed repeatedly at slow speeds for alignment until the side forces are effectively zero. Following this, the plate should be towed at the highest speed and the side forces should be checked. Once the alignment is set, no alterations should be made to the set-up. A disadvantage of the overall method may be the limited maximum Reynolds number. Given that the maximum speed is constant, longer plates may be used to increase the maximum Reynolds number so that a wider range of roughness functions and roughness Reynolds numbers can be obtained.

In Chapter 5, the similarity law scaling was used as the prediction method. The only real assumption of the method is that the outer layer similarity holds in the mean velocity profiles for smooth and rough-wall boundary layers. That is to say, the velocity-defect profiles collapse to a single curve in the outer layer. The studies in the literature show that this is indeed the case as long as the roughness height is not a large fraction of the boundary layer thickness. A weakness of the method might be attributed to the assumption of one single roughness Reynolds number and roughness function for a given speed and surface condition. This is definitely not the case in reality, as the friction velocity varies along flat plates. Another important subject is that this method can only predict the skin friction of flat plates. That is to say, the roughness effect on pressure drag cannot be predicted by this method and this leads the user to have an assumption that pressure drag is not affected by the surface roughness. This is a reasonable assumption as this effect is expected to be negligible. However, it is worth investigating the roughness effect on the total resistance. The advantage of this method is that once the prediction code is ready, it is very easy and fast to define and change the inputs in order to obtain results.

It was clearly shown in Chapters 6, 7 and 8 that CFD can be used for simulating roughness effects on the frictional resistance of flat plates and on the resistance of full-scale 3D ship hulls and that different types of roughness can be defined by modifying the wall-function of the software. This means that the CFD method can be used to predict the effects of such roughness on the frictional resistances of any arbitrary body without being obliged to conduct further experiments, once the relationship between the roughness functions and roughness Reynolds numbers of each surface is known. Having said that, experimental data is still a necessity for the development of accurate CFD prediction methods. Some difficulties were experienced while carrying out the CFD work presented in this thesis. Each case using the CFD method required a tailored treatment, such as the definition and location of the boundaries, mesh configuration and selection of the time-step. Several exploratory studies were therefore required to define the best configuration to obtain reasonable results. On the one hand, generating a very fine mesh would increase the accuracy of the results; on the other hand it would dramatically increase the run time. For this reason, a reasonable compromise was required to avoid overly-long run times. This compromise was achieved by performing grid-dependence studies.

It is known that CFD simulations require much longer run-times compared to the use of the similarity law scaling procedure. The longer run-times of CFD simulations are not due to the application of roughness function models. Employing new roughness function models by modifying wall-functions does not therefore cause any additional run-time to the CFD simulations. That is to say, the run-time of CFD simulations of any arbitrary body with any surface roughness would be literally identical to those of CFD simulations of the same body with an otherwise smooth surface condition. It should be noted that the CFD simulations presented in this thesis could not have been performed without using the supercomputing facilities of the University of Strathclyde.

Another important issue was the definition of the roughness functions in the software. The built-in roughness function model was in the form of the roughness functions of the uniform, closely packed sand roughness of Nikuradse (1933). For this reason, it was not possible to define any exact mathematical formulations and

hence some approximations were made, especially in Chapter 7. Having said that, these were reasonable approximations that would not significantly affect the results or the validity of the proposed models.

Another issue to be discussed is the selection of roughness function models representing the roughness function behaviours of the coatings and biofouling conditions. In Chapter 6, a Colebrook-type roughness function model was chosen to represent the coatings in question, based on the experimental results, and a good agreement was achieved with the experiments. However, the systematic departure of the roughness functions against roughness Reynolds numbers below this roughness function model at low roughness Reynolds numbers might indicate that a roughness function model somewhere between the monotonic Colebrook and the inflectional Nikuradse type roughness functions may be a better fit for real engineering surfaces. That is to say, the use of a Colebrook-type roughness function model may lead to overestimation of roughness functions and roughness Reynolds numbers, and hence frictional resistances, at low roughness Reynolds numbers for a given roughness length scale. In Chapter 7, a roughness function model which shows an inflectional behaviour was therefore chosen, as suggested by Schultz (2007). It is of note that the roughness function models chosen in the present study were based on the experimental data available in the literature and they may not necessarily work for other surfaces or every kind of coating or fouling condition. This debate is, however, beyond the aim of this study since the main aim of the present study is not to define correlations between surfaces and roughness functions.

9.5 Chapter Summary

In this chapter, a summary of the achievement of the research aims and objectives has been presented along with a general discussion focusing on the difficulties experienced when performing the work. The state-of-the art contributions to the field were clearly demonstrated.

10 Conclusions and Recommendations

10.1 Introduction

This chapter presents conclusions on the work performed within this thesis and recommendations for future research.

10.2 Conclusions

The majority of the studies in the literature focus on the roughness effects of coatings and biofouling on the turbulent boundary layer and/or skin friction of lab-scale plates. This fundamental information is essential from a scientific point of view; however it may be inconclusive on a vital question from a practical point of view: *"How might the roughness of coatings and biofouling be related to full-scale ship resistance and powering?"* The answers to this question were sought in this research, and novel contributions were made to the state-of-the-art knowledge.

This thesis set out to model the roughness effects of marine coatings and biofouling on ship frictional resistance. It should be kept in mind that this study did not aim to correlate the surface characteristics of coatings or biofouling to roughness functions and drag; instead it aimed to relate a given roughness effect to full-scale ship frictional resistance. It has presented a means of determining the drag characteristics of several new-generation coatings, proposed goal-based added resistance prediction diagrams and two CFD-based URANS models to predict these effects, and presented CFD simulations of the roughness effects of marine coatings and biofouling on the full-scale KCS hull.

It was evidently seen in Chapter 4 that even the roughness of as applied marine coatings greatly influences the frictional resistance through towing tests of flat plates coated with such coatings. New-generation silicone-based coatings showed superior performance compared to SPC systems, especially at higher speeds. It was seen that

F0034 showed the best drag performance among all the test surfaces. An important point to note is that the roughness function behaviours of the new-generation silicone-based commercial paint and newly developed novel FOUL-X-SPEL paints tend to decrease with increasing speeds after a certain speed. The application of these coatings improved the resistance characteristics of an uncoated ship hull condition, whereas the SPC system worsened the drag characteristics of it. The conducted experiments provided knowledge of the roughness functions and roughness function behaviours of the commercial new-generation and novel coatings developed within the FOUL-X-SPEL Project, and demonstrated the importance of the roughness effects of as applied marine coatings on frictional resistance.

The first attempt to relate roughness effects to ship frictional resistance was made in Chapter 5 using a well-known similarity law scaling procedure. This enables the prediction of the effects of the coatings used in Chapter 4 on full-scale ship frictional resistance. In other words, the evaluated roughness effects of coatings on lab-scale flat plates were extrapolated to several full-scale flat plates of ship sizes. It was shown that the type of coating remarkably affected the full-scale ship frictional resistance.

Another outcome of this chapter was the goal-based added resistance diagrams for the prediction of the effects of a range of coating and fouling conditions on the frictional resistance. These diagrams were generated using experimental data from the literature using the same methodology. The main advantage of the proposed diagrams is that they directly enable the use of surface conditions, ship length and ship speed, rather than having to use hydrodynamic parameters. It is therefore believed that these diagrams will serve as a practical prediction tool for designers, engineers and students to be able to assess and estimate the added resistance, and hence fuel penalty, of a ship for a particular fouling condition at a specific speed. Having said that, these diagrams were generated using roughness functions obtained under several assumptions and they therefore cannot be expected to characterise all types of fouling conditions.

In Chapter 6, a CFD model for the frictional resistance prediction of antifouling coatings was proposed. A roughness function model representing several coatings

from the literature was employed in the CFD software and then CFD simulations of the experiments given in the literature were performed. The results showed that even very small differences in surface roughness can be predicted by the use of modified wall-functions and a CFD method. The main advantage of the proposed model is that it enables the use of a simple roughness length scale, according to the surface roughness measurements, rather than the equivalent sand-grain roughness height, which is a hydrodynamically obtained parameter. It should be kept in mind that this roughness length scale was based on the available experimental data and may not be appropriate for other types of coatings.

In Chapter 7, a CFD model for the prediction of the effect of biofouling on frictional resistance was proposed. A roughness function model was developed by fitting a curve to the roughness functions used in Chapter 5; this was then employed in the CFD software. The results were compared with those computed in Chapter 5. The main advantage of the proposed model is that it enables the use of a simple roughness length scale to predict the effect of biofouling on a flat plate of ship length.

The CFD models presented in this study have advantages over the similarity law scaling presented in Chapter 5, in that they move towards more realistic modelling of roughness effects. The dynamic changes in friction velocity along a flat plate can be taken into account using a CFD method, contrary to the similarity law scaling procedure. Having showed the applicability of the CFD models using flat plates in Chapter 6 and Chapter 7, these models can be used to predict the roughness effects of coatings and biofouling on ship hulls, propellers or any arbitrary body, rather than solely on flat plates.

In Chapter 8, unsteady RANS CFD simulations of the roughness effects of marine coatings and biofouling on the resistance of the full-scale KCS hull appended with a rudder were performed, employing the roughness function model proposed in Chapter 7. The results were compared with the results obtained in Chapters 7 and 5, and it was shown that the wall function approach of CFD to simulate the surface roughness on ship hulls, rather than on flat plates, is a suitable method with which to predict the roughness effects of marine coatings and biofouling on 3D full-scale

ships. It is important to note that employing the roughness function model by modifying the wall-functions does not lead to any additional run-time for typical towing, self-propulsion or seakeeping simulations of the full-scale ships. Employing the proposed CFD approach for a typical self-propulsion and/or sekaeeping simulation of a full-scale ship would therefore enable the user to directly assess the roughness effects of marine coatings and biofouling on ship resistance and delivered power.

This author believes that this study has shown the applicability of the CFD-based method to investigate the roughness effects of marine coatings and biofouling on ship frictional resistance. It is also thought that the use of such a CFD method will be a leap forward towards practical investigations of these effects on ship powering, along with the fundamental experimental research in the field.

10.3 Recommendations for Future Research

1. In Chapter 4, Rt_{50} values of each coating were measured with a hull roughness gauge and therefore only Rt_{50} was used as the roughness length scale. A piece of future work might be to measure additional roughness parameters using an optical measurement so that the effect of surface texture can be taken into account.

2. The drag characterisation of coatings was made using the overall (towed plate) method in Chapter 4. The towing tank facility has a limited maximum towing speed which leads to a lack of data for high speeds. It would therefore be beneficial to evaluate the roughness functions of such surfaces through turbulent boundary layer measurements or the rotating disk method in order to evaluate the roughness function behaviour at higher speeds.

3. A future work may be the determination of the roughness functions of surfaces covered with fouling, by conducting further experiments. Either naturally fouled surfaces, or surfaces covered with artificial fouling organisms, such as barnacles or slime, could be used for the experiments.

4. In Chapter 5, the added resistance diagrams were generated based on the assumption that the roughness functions of such conditions follow the roughness function behaviours of the ones provided by Schultz and Flack (2007) and the fouling conditions were represented by the roughness length scales proposed by Schultz (2007). Therefore, these conditions cannot be expected to define all possible conditions. Further experimental studies should be performed to characterise different fouling conditions in terms of roughness functions. Once new relationships are obtained, they can be employed in the prediction code and new diagrams can be generated.

5. In Chapters 6, 7 and 8, the roughness functions were employed using modified wall-functions in the CFD software. Alternative ways of employing the roughness function in the CFD software, such as by using turbulence models and field functions, should be further investigated. This may enable users to directly use the experimentally obtained models without compromising on accuracy.

6. A comparison of the CFD predictions for a coated or fouled surface using a standard CFD approach and the proposed CFD approach in this thesis can be made.

7. The proposed CFD models can easily be applied to full-scale self-propulsion simulations of ships. The effect of hull roughness on the delivered power of a ship might be investigated using the proposed approach.

8. The effect of fouling on propeller performance can be investigated using the proposed CFD approach.

References

ABS. 2011. *Surveyor* [Online]. Available: http://www.eagle.org/eagleExternalPortalWEB/ShowProperty/BEA%20Repository/News%20&%20Events/Publications/Quarterly/Surveyor/2011/Surveyor_2011Fall 14/07/2013].

Acharya, M., Bornstein, J. & Escudier, M. P. 1986. Turbulent boundary layers on rough surfaces. *Experiments in Fluids,* 4**,** 33-47.

Alzieu, C. L., Sanjuan, J., Deltreil, J. P. & Borel, M. 1986. Tin contamination in Arcachon Bay: Effects on oyster shell anomalies. *Marine Pollution Bulletin,* 17**,** 494-498.

AMBIO. 2005. *AMBIO: Advanced nanostructured surfaces for the control of biofouling* [Online]. http://www.birmingham.ac.uk/generic/ambio/index.aspx.

Anderson, C., Atlar, M., Callow, M., Candries, M. & Townsin, R. The development of foul-release coatings for seagoing vessels. Proceedings of the Institute of Marine Engineering, Science and Technology. Part B, Journal of Marine Design and Operations, 2003. Institute of Marine Engineering, Science and Technology, 11-23.

Anderson, J. D. 2005. Ludwig Prandtl's boundary layer. *Physics Today 58 (12), 42* [Online].

Andrewartha, J., Perkins, K., Sargison, J., Osborn, J., Walker, G., Henderson, A. & Hallegraeff, G. 2010. Drag force and surface roughness measurements on freshwater biofouled surfaces. *Biofouling,* 26**,** 487-496.

ANSYS 2011. FLUENT Theory Guide, Release 14.

Antonia, R. A. & Krogstad, P. Å. 2001. Turbulence structure in boundary layers over different types of surface roughness. *Fluid Dynamics Research,* 28**,** 139-157.

Antonia, R. A. & Luxton, R. E. 1971. The response of a turbulent boundary layer to a step change in surface roughness Part 1. Smooth to rough. *Journal of Fluid Mechanics,* 48**,** 721-761.

Antonia, R. A. & Luxton, R. E. 1972. The response of a turbulent boundary layer to a step change in surface roughness. Part 2. Rough-to-smooth. *Journal of Fluid Mechanics,* 53**,** 737-757.

Apsley, D. 2007. CFD Calculation of Turbulent Flow with Arbitrary Wall Roughness. *Flow, Turbulence and Combustion,* 78**,** 153-175.

Atlar, M. An update on marine antifoulings. 25th ITTC Group Discussions 3 – Global Warming and Impact on ITTC Activities, Fukuoka, 2008.

Atlar, M., Ünal, B., Ünal, U. O., Politis, G., Martinelli, E., Galli, G., Davies, C. & Williams, D. 2012. An experimental investigation of the frictional drag characteristics of nanostructured and fluorinated fouling-release coatings using an axisymmetric body. *Biofouling,* 29**,** 39-52.

Aupoix, B. 2007. A general strategy to extend turbulence models to rough surfaces: application to Smith's k-L model. *Journal of Fluids Engineering,* 129**,** 1245-1254.

Bandyopadhyay, P. R. 1987. Rough-wall turbulent boundary layers in the transition regime. *Journal of Fluid Mechanics,* 180**,** 231-266.

Benson, J., Ebert, J. & Beery, T. 1938. Investigation in the NACA tank of the effect of immersion in salt water on the resistance of plates coated with different shipbottom paints. *NACA Memorandum Report C&R C-S19-1(3).*

Blasius, H. 1908. Grenzschichten in Fliissigkeiten mit kleiner Reibung. *Zeitschrift fur Mathematik und Physik,* band 56.

Bowden, B. & Davison, N. 1974. Resistance increments due to hull roughness associated with form factor extrapolation methods. *NPL Ship Division Report TM 380*.

BYEFOULING. 2013. *BYEFOULING: Low-toxic cost-efficient environment-friendly antifouling materials* [Online]. http://cordis.europa.eu/project/rcn/110983_en.html.

Candries, M. 2001. *Drag, boundary-layer and roughness characteristics of marine surfaces coated with antifoulings.* PhD Thesis, University of Newcastle upon Tyne.

Candries, M. & Atlar, M. 2004. Experimental Investigation of the Turbulent Boundary Layer of Surfaces Coated With Marine Antifoulings. *Journal of Fluids Engineering,* 127**,** 219-232.

Candries, M., Atlar, M. & Anderson, C. Low-energy surfaces on high-speed craft. 2nd International EuroConference on High-Performing Marine Vehicles (HIPER'01), 2001a Hamburg. 119-127.

Candries, M., Atlar, M. & Anderson, C. 2003a. Estimating the impact of new-generation antifoulings on ship performance: the presence of slime. *Journal of Marine Engineering & Technology,* 2**,** 13-22.

Candries, M., Atlar, M., Guerrero, A. & Anderson, C. Lower frictional resistance characteristics of foul release systems. 8th International Symposium on Practical Design of Ships and other Floating Structures (PRADS 2001), 2001b Shanghai.

Candries, M., Atlar, M., Mesbahi, E. & Pazouki, K. 2003b. The Measurement of the Drag Characteristics of Tin-free Self-polishing Co-polymers and Fouling Release Coatings Using a Rotor Apparatus. *Biofouling,* 19**,** 27-36.

Carrica, P. M., Fu, H. & Stern, F. 2011. Computations of self-propulsion free to sink and trim and of motions in head waves of the KRISO Container Ship (KCS) model. *Applied Ocean Research,* 33**,** 309-320.

Castro, A. M., Carrica, P. M. & Stern, F. 2011. Full scale self-propulsion computations using discretized propeller for the KRISO container ship KCS. *Computers & Fluids,* 51**,** 35-47.

CD-ADAPCO 2014. User Guide STAR-CCM+, Version 9.02.011.

Cebeci, T. & Bradshaw, P. 1977. *Momentum Transfer in Boundary Layers*, Hemisphere Publishing Corporation/McGraw-Hill.

Cebeci, T. & Chang, K. C. 1978. Calculation of incompressible rough-wall boundary-layer flows. *AIAA Journal,* 16**,** 730-735.

Celik, I. B., Ghia, U., Roache, P. J., Freitas, C. J., Coleman, H. & Raad, P. E. 2008. Procedure for estimation and reporting of uncertainty due to discretization in CFD applications. *Journal of Fluids Engineering-Transactions of the ASME,* 130**,** 078001-1-4.

Chambers, L. D., Stokes, K. R., Walsh, F. C. & Wood, R. J. K. 2006. Modern approaches to marine antifouling coatings. *Surface and Coatings Technology,* 201**,** 3642-3652.

Champ, M. A. 2003. Economic and environmental impacts on ports and harbors from the convention to ban harmful marine anti-fouling systems. *Marine Pollution Bulletin,* 46**,** 935-940.

Charnley, M., Textor, M. & Acikgoz, C. 2011. Designed polymer structures with antifouling–antimicrobial properties. *Reactive and Functional Polymers,* 71**,** 329-334.

Christoph, G. H. & Pletcher, R. H. 1983. Prediction of rough-wall skin friction and heat transfer. *AIAA Journal,* 21**,** 509-515.

Clauser, F. H. 1954. Turbulent Boundary Layers in Adverse Pressure Gradients. *Journal of the Aeronautical Sciences,* 21**,** 91-108.

Colebrook, C. F. 1939. Turbulent Flow in Pipes, with particular reference to the Transition Region between the Smooth and Rough Pipe Laws. *Journal of Civil Engineers,* 11**,** 133-157.

Colebrook, C. F. & White, C. M. 1937. Experiments with Fluid Friction in Roughened Pipes. *Proceedings of the Royal Society of London. Series A, Mathematical and Physical Sciences,* 161**,** 367-381.

Coleman, H. W. & Steele, W. G. 1999. *Experimentation and Uncertainty Analysis for Engineers*, Wiley.

Coles, D. 1956. The law of the wake in the turbulent boundary layer. *Journal of Fluid Mechanics,* 1**,** 191-226.

Corbett, J. J., Winebrake, J. J., Comer, B. & Green, E. 2011. Energy and GHG emissions savings analysis of fluoropolymer foul release hull coating. *Energy and Environmental Research Associates, LLC* [Online]. Available: http://www.theengineer.co.uk/Journals/1/Files/2011/2/21/20110215b%20International%20Paint%20Report.pdf.

Cortana. 2013. *Description of Drag* [Online]. Available: http://www.cortana.com/Drag_Description.htm [Accessed 24th November 2013].

Couch, R. B. 1951. *Preliminary report of friction plane resistance tests of anti-fouling ship bottom paints,* David Taylor Model Basin Report 789.

Dafforn, K. A., Lewis, J. A. & Johnston, E. L. 2011. Antifouling strategies: History and regulation, ecological impacts and mitigation. *Marine Pollution Bulletin,* 62**,** 453-465.

Date, J. C. & Turnock, S. R. 1999. A study into the techniques needed to accurately predict skin friction using RANS solvers with validation against Froude's historical flat plate experimental data. Southampton, UK: University of Southampton.

Demirel, Y. K., Khorasanchi, M., Turan, O. & Incecik, A. A parametric study: Hull roughness effect on ship frictional resistance. RINA, Royal Institution of Naval Architects - International Conference on Marine Coatings, 2013. 21-28.

Demirel, Y. K., Khorasanchi, M., Turan, O. & Incecik, A. CFD approach to resistance prediction as a function of roughness. Transport Research Arena Conference 2014, 14 - 17 April 2014 2014a Paris/France.

Demirel, Y. K., Khorasanchi, M., Turan, O., Incecik, A. & Schultz, M. P. 2014b. A CFD model for the frictional resistance prediction of antifouling coatings. *Ocean Engineering,* 89**,** 21-31.

Denny, M. E. 1951. BSRA Resistance Experiments on the Lucy Ashton: Part I : Full-Scale Measurements. *Trans. RINA*, 93**,** 40-57.

Eça, L. & Hoekstra, M. 2011. Numerical aspects of including wall roughness effects in the SST k–ω eddy-viscosity turbulence model. *Computers & Fluids,* 40**,** 299-314.

Ferziger, J. H. & Perić, M. 2002. *Computational methods for fluid dynamics*, Springer Berlin.

Flack, K. A. & Schultz, M. P. 2010. Review of Hydraulic Roughness Scales in the Fully Rough Regime. *Journal of Fluids Engineering,* 132**,** 041203-041203.

Flack, K. A., Schultz, M. P. & Connelly, J. S. 2007. Examination of a critical roughness height for outer layer similarity. *Physics of Fluids (1994-present),* 19**,** -.

Flack, K. A., Schultz, M. P. & Shapiro, T. A. 2005. Experimental support for Townsend's Reynolds number similarity hypothesis on rough walls. *Physics of Fluids (1994-present)*, 17**,** -.

FOUL-X-SPEL. 2011. *FOUL-X-SPEL : Environmentally friendly antifouling technology to optimise the energy efficiency of ships* [Online]. http://www.foulxspel-antifouling.com/.

Froude, W. 1872. Experiments on the surface-friction experienced by a plane moving through water. *British Association for the Advancement of Science.* The Collected Papers of William Froude, Institution of Naval Architects, 1955.

Froude, W. 1874. *Report to the Lords Commissioners of the Admiralty on Experiments for the Determination of the Frictional Resistance of Water on a Surface, Under Various Conditions, Performed at Chelston Cross, Under the Authority of Their Lordships,* 44th Report by the British Association for the Advancement of Science.

Gebers, F. 1919. Das Aehnlichkeitsgesetz bei im Wasser geradlinig fortbewegter Platten. *Schiffbau,* 22.

George, W. K. 2007. *Is there a universal log law for turbulent wall-bounded flows?*

Ghani, M. A., Karim, K. & Milani, K. 2010. Experimental investigation of the drag characteristics of different ship hull coating with using rotor apparatus. *Jurnal Mekanikal,* 31**,** 92-102.

Gibbs, P. & Bryan, G. 1986. Reproductive failure in populations of the dog-whelk, Nucella lapillus, caused by imposex induced by tributyltin from antifouling paints. *Journal of the Marine Biological Association of the United Kingdom,* 66**,** 767-777.

Granville, P. S. 1958. The frictional resistance and turbulent boundary layer of rough surfaces. *Journal of ship research,* 2**,** 52-74.

Granville, P. S. 1977. Drag and turbulent boundary layer of flat plates at low Reynolds numbers. *Journal of Ship Research,* 21**,** 30-39.

Granville, P. S. 1978. Similarity-law characterization methods for arbitrary hydrodynamic roughnesses. *Final Report Naval Ship Research and Development Center, Bethesda, MD. Ship Performance Dept.,* 1.

Granville, P. S. 1982. Drag-Characterization Method for Arbitrarily Rough Surfaces by Means of Rotating Disks. *Journal of Fluids Engineering,* 104**,** 373-377.

Granville, P. S. 1985. Mixing-length formulations for turbulent boundary layers over arbitrarily rough surfaces. *Journal of Ship Research,* 29**,** 223-233.

Granville, P. S. 1987. Three indirect methods for the drag characterization of arbitrarily rough surfaces on flat plates. *Journal of Ship Research,* 31**,** 70-77.

Grégoire, G., Favre-Marinet, M. & Amand, F. J. S. 2003. Modeling of turbulent fluid flow over a rough wall with or without suction. *Journal of Fluids Engineering,* 125**,** 636-642.

Grigson, C. 1983. The drag coefficients of a range of ship surfaces II. *RINA,* 125**,** 183-198.

Grigson, C. 1985a. The drag at ship scale of planes having any quality of roughness. *Journal of Ship Research,* 29**,** 94-104.

Grigson, C. Velocity loss functions of rough surfaces in intermediate flow. Proceedings of the 2nd International Symposium on Ship Viscous Resistance, 1985b Gothenburg.

Grigson, C. 1992. Drag losses of new ships caused by hull finish. *Journal of Ship Research,* 36**,** 182-196.

Hama, F. R. 1954. Boundary-layer characteristics for smooth and rough surfaces. *SNAME Transactions,* 62**,** 333-351.

Haslbeck, E. G. & Bohlander, G. 1992. Microbial biofilm effects on drag-lab and field. *1992 Ship Production Symposium Proceedings, SNAME.*

Hughes, G. 1952. Frictional resistance of smooth plane surfaces in turbulent flow. *Trans. INA,* 94.

Hughes, G. 1954. Friction and form resistance in turbulent flow and a proposed formulation for use in model and ship correlation. *Trans. INA,* 96.

Hundley, L. & Tate, C. 1980. Hull-fouling studies and ship powering trial results on seven FF 1052 class ships. *D W Taylor Naval Ship Research and Development Center Report # DTNSRDC-80/027. 111 p.*

IMO. 2001. International convention on control of harmful anti-fouling systems on ships.

IMO. 2009a. MEPC 59/4/15, Prevention of air pollution from ships, Energy Efficiency Operational Indicator (EEOI)

IMO 2009b. Second IMO GHG Study.

IMO. 2012. Annex 9, Resolution MEPC.213(63), 2012 Guidelines for the development of a Ship Energy Efficiency Management Plan (SEEMP).

IMO. 2014. Annex 5, Resolution MEPC.245(66), 2014 Guidelines on the method of calculation of the attained Energy Efficiency Design Index (EEDI) for new ships.

Ioselevich, V. A. & Pilipenko, V. N. 1974. Logarithmic velocity profile for flow of a weak polymer solution near a rough surface. *Soviet Physics Doklady,* 18**,** 790.

ITTC 1987. Report of the Powering Performance Committee. Proceedings of the 18th ITTC.

ITTC 1990. Report of the Powering Performance Committee. Proceedings of the 19th ITTC.

ITTC. The Resistance Committee - Final Report and Recommendations to the 23rd ITTC. Proceedings of the 23rd ITTC - Volume III, 2002a.

ITTC 2002b. Uncertainty Analysis, Example for Resistance Test. *ITTC Recommended Procedures and Guidelines, Procedure 7.5-02-02-02, Revision 01.*

ITTC 2008a. The Specialist Committee on Powering Performance Prediction – Final report and recommendations to the 25th ITTC. Proceedings of 25th ITTC – Volume II

ITTC 2008b. Testing and Extrapolation Methods, Propulsion, Performance, Predicting Powering Margins. *ITTC Recommended Procedures and Guidelines, Procedure 7.5-02-03-01.5, Revision 01.*

ITTC 2011a. Practical Guidelines for Ship CFD Application. *ITTC Recommended Procedures and Guidelines, Procedure 7.5-03-02-03, Revision 01.*

ITTC. Specialist Committee on Surface Treatment – Final report and recommendations to the 26th ITTC. Proceedings of 26th ITTC – Volume II 2011b.

ITTC 2014a. Resistance Committee – Final report and recommendations to the 27th ITTC. Proceedings of 27th ITTC – Volume I.

ITTC 2014b. Specialist Committee on Performance of Ships in Service – Final report and recommendations to the 27th ITTC. Proceedings of 27th ITTC – Volume II.

Izaguirre-Alza, P., Pérez-Rojas, L. & Núñez-Basáñez, J. F. 2010. Drag reduction through special paints coated on the hull. *International Conference on Ship Drag Reduction SMOOTH-SHIPS.* Istanbul, Turkey.

Jiménez, J. 2004. Turbulent flows over rough walls. *Annual Review of Fluid Mechanics,* 36**,** 173-196.

Kauczynski, W. & Walderhaug, H. Effect of paint roughness on the skin friction of ships. 3rd Int. Cong. of the Int. Maritime Assoc. of the E. Mediterranean, 1983 Athens.

Kawashima, H., Makino, M., Fukasawa, R., Takeshi, H., Kawaguchi, Y., Tuji, Y., Iwamoto, K., Motozawa, M., Masuda, H. & Mieno, H. Effect of geometric roughness parameters on turbulent frictional resistance. Conference Proceedings of the Japan Society of Naval Architects and Ocean Engineers, 2012.

Keirsbulck, L., Labraga, L., Mazouz, A. & Tournier, C. 2002. Surface roughness effects on turbulent boundary layer structures. *Journal of fluids engineering,* 124**,** 127-135.

Kempf, G. 1929. Results Obtained in Measuring Frictional Resistance. *Trans. INA,* 71.

Kempf, G. 1937. On the effect of roughness on the resistance of ships. *Trans INA,* 79**,** 109-119.

Khor, Y. S. & Xiao, Q. 2011. CFD simulations of the effects of fouling and antifouling. *Ocean Engineering,* 38**,** 1065-1079.

Kim, W. J., Van, S. H. & Kim, D. H. 2001. Measurement of flows around modern commercial ship models. *Experiments in Fluids,* 31**,** 567-578.

Klebanoff, P. S. & Diehl, Z. W. 1951. Some features of artificially thickened fully developed turbulent boundary layers with zero pressure gradient. NACA TN 2475.

Krogstad, P.-A. 1991. Modification of the van Driest damping function to include the effects of surface roughness. *AIAA Journal,* 29**,** 888-894.

Krogstad, P.-Å., Antonia, R. & Browne, L. 1992. Comparison between rough-and smooth-wall turbulent boundary layers. *Journal of Fluid Mechanics,* 245**,** 599-617.

Krogstad, P. Å. & Antonia, R. A. 1999. Surface roughness effects in turbulent boundary layers. *Experiments in Fluids,* 27**,** 450-460.

Kunkel, G. J. & Marusic, I. 2006. Study of the near-wall-turbulent region of the high-Reynolds-number boundary layer using an atmospheric flow. *Journal of Fluid Mechanics,* 548**,** 375-402.

Lackenby, H. 1962. The Thirty-Fourth Thomas Lowe Gray Lecture: Resistance of Ships, with Special Reference to Skin Friction and Hull Surface Condition. *Proceedings of the Institution of Mechanical Engineers,* 176**,** 981-1014.

Lakehal, D. 1999. Computation of turbulent shear flows over rough-walled circular cylinders. *Journal of Wind Engineering and Industrial Aerodynamics,* 80**,** 47-68.

Larsson, L. & Baba, E. 1996. Ship resistance and flow computations. *In:* OHKUSU, M. (ed.) *Advances in Marine Hydrodynamics.*

Larsson, L., Stern, F. & Bertram, V. 2003. Benchmarking of computational fluid dynamics for ship flows: the Gothenburg 2000 workshop. *Journal of Ship Research,* 47**,** 63-81.

LEAF. 2012. *LEAF: Low emission antifouling coatings based on the novel discovered post settlement penetration triggered antifouling* [Online]. http://leaf-antifouling.eu/.

Leer-Andersen, M. & Larsson, L. 2003. An experimental/numerical approach for evaluating skin friction on full-scale ships with surface roughness. *Journal of Marine Science and Technology,* 8**,** 26-36.

Lewis, J. A. Marine biofouling and its prevention on underwater surfaces. Materials Forum, 1998. 41-61.

Lewkowicz, A. & Das, D. 1986. Turbulent boundary layers on rough surfaces with and without a pliable overlayer: a simulation of marine fouling. *International Shipbuilding Progress,* 33**,** 174-186.

Lewkowicz, A. & Musker, A. The surface roughness and turbulent wall friction on ships. Int. Symp. on Ship Viscous Resistance, 1978 SSPA, Gothenburg. Papers 10 and 11.

Lewthwaite, J., Molland, A. & Thomas, K. 1985. An investigation into the variation of ship skin frictional resistance with fouling. *Transactions of Royal Institution of Naval Architects,* 127**,** 269-284.

Ligrani, P. M. & Moffat, R. J. 1986. Structure of transitionally rough and fully rough turbulent boundary layers. *Journal of Fluid Mechanics,* 162**,** 69-98.

Loeb, G., Laster, D. & Gracik, T. 1984. The influence of microbial fouling films on hydrodynamic drag of rotating discs. *In:* COSTLOW, J. D. & TIPPER, R. (eds.) *Marine Biodeterioration: An Interdisciplinary Study.* Naval Institute Press, Annapolis, MD.

McEntee, W. 1915. Variation of frictional resistance of ships with condition of wetted surface. *Trans. Soc. Nav. Arch. Mar. Eng.,* 24**,** 37-42.

McKeon, B., Li, J., Jiang, W., Morrison, J. & Smits, A. 2004. Further observations on the mean velocity distribution in fully developed pipe flow. *Journal of Fluid Mechanics,* 501**,** 135-147.

Mieno, H. An experimental study for friction resistance of ship hull sprayed with paints. Conference Proceedings of the Japan Society of Naval Architects and Ocean Engineers, 2012.

Millikan, C. M. A critical discussion of turbulent flows in channels and circular tubes. Proceedings of the International Congress for Applied Mechanics, 1938 Cambridge, MA. 386–392.

Milne, A. Roughness and drag from the marine paint chemist's viewpoint. Marine Roughness and Drag Workshop, 1990 London.

Mirabedini, S. M., Pazoki, S., Esfandeh, M., Mohseni, M. & Akbari, Z. 2006. Comparison of drag characteristics of self-polishing co-polymers and silicone foul release coatings: A study of wettability and surface roughness. *Progress in Organic Coatings,* 57**,** 421-429.

Munk, T. Fuel conservation through managing hull resistance. Motorship Propulsion Conference, 2006 Copenhagen.

Musker, A. 1981. Universal roughness functions for naturally-occurring surfaces. *Transactions of Canadian Society of Mechanical Engineers,* 1**,** 1-6.

Musker, A. & Lewkowicz, A. The effect of ship hull roughness on the development of turbulent boundary layers. Proceedings of International Symposium on Ship Viscous Resistance, 1978 Gothenburgh.

Nakato, M., Onoghi, H., Himeno, Y., Tanaka, I. & Suzuki, T. Resistance increase due to surface roughness. 15th Symp. on Naval Hydrodynamics, 1984 Hamburg. 45-59.

Naval Ships' Technical Manual 2002. Waterborne underwater hull cleaning of navy ships. S9086-CQ-STM-010/CH-081R5. . *Naval Sea Systems Command*.

Nikuradse, J. 1933. *Laws of flow in rough pipes*, NACA Technical Memorandum 1292.

Okay, O. S. Antifouling içeren gemi boyalarının uluslararası kurallar çerçevesinde kirletici etkilerinin incelenmesi. TMMOB, Gemi Mühendisliği Odası, Gemi Mühendisliği ve Sanayimiz Sempozyumu, 24-25 December 2004 Istanbul, Turkey.

Okuno, T., Lewkowicz, A. & Nicholson, K. Roughness effects on a slender hull. Proceedings of the 2nd International Symposium on Ship Viscous Resistance, 1985 SSPA, Gothenburg. Paper 20.

Patel, V. C. 1998. Perspective: Flow at high reynolds number and over rough surfaces—Achilles heel of CFD. *Journal of Fluids Engineering,* 120**,** 434-444.

Perry, A. & Li, J. D. 1990. Experimental support for the attached-eddy hypothesis in zero-pressure-gradient turbulent boundary layers. *Journal of Fluid Mechanics,* 218**,** 405-438.

Perry, A. E., Schofield, W. H. & Joubert, P. N. 1969. Rough wall turbulent boundary layers. *Journal of Fluid Mechanics,* 37**,** 383-413.

Prandtl, L. 1921. *Ergebnisse der Aerodynamischen Versuchsanstalt zu Goettingen*, Abhandlungen aus dem Aerodynamischen Institut, Aachen.

Prandtl, L. 1927. *Ergebnisse der Aerodynamischen Versuchsanstalt zu Goettingen*, III Lieferung.

Prandtl, L. 1932. *Ergebnisse der Aerodynamischen Versuchsanstalt zu Goettingen*, IV Lieferung.

RAEng. 2013. *Future Ship Powering Options* [Online]. Available: http://www.raeng.org.uk/publications/reports/future-ship-powering-options 01/12/2013].

Raupach, M., Antonia, R. & Rajagopalan, S. 1991. Rough-wall turbulent boundary layers. *Applied Mechanics Reviews,* 44**,** 1-25.

Richardson, L. F. 1910. The approximate arithmetical solution by finite differences of physical problems involving differential equations, with an application to the stresses in a masonry dam. *Transactions of the Royal Society of London. Series A,* 210**,** 307-357.

Richardson, L. F. & Gaunt, J. A. 1927. The deferred approach to the limit. *Philosophical Transactions of the Royal Society of London. Series A,* 226**,** 299-361.

Schlichting, H. 1979. *Boundary Layer Theory, 7th ed.*, McGraw-Hill, New York.

Schoenherr, K. E. 1932. Resistances of flat surfaces moving through a fluid. *Transactions of SNAME,* 40**,** 279-313.

Schubauer, G. B. & Tchen, C. M. 1961. *Turbulent flow*, Princeton University Press, New Jersey, USA.

Schultz, M. P. 1998. *The Effect of Biofilms on Turbulent Boundary Layer Structure.* PhD Thesis, Florida Institute of Technology.

Schultz, M. P. 2000. Turbulent Boundary Layers on Surfaces Covered With Filamentous Algae. *Journal of Fluids Engineering,* 122**,** 357-363.

Schultz, M. P. 2002. The relationship between frictional resistance and roughness for surfaces smoothed by sanding. *Journal of fluids engineering,* 124**,** 492-499.

Schultz, M. P. 2004. Frictional resistance of antifouling coating systems. *Journal of fluids engineering,* 126**,** 1039-1047.

Schultz, M. P. 2007. Effects of coating roughness and biofouling on ship resistance and powering. *Biofouling,* 23**,** 331-341.

Schultz, M. P. 2014. Personal communication.

Schultz, M. P., Bendick, J. A., Holm, E. R. & Hertel, W. M. 2011. Economic impact of biofouling on a naval surface ship. *Biofouling,* 27**,** 87-98.

Schultz, M. P. & Flack, K. 2007. The rough-wall turbulent boundary layer from the hydraulically smooth to the fully rough regime. *Journal of Fluid Mechanics,* 580**,** 381-405.

Schultz, M. P. & Flack, K. A. 2003. Turbulent boundary layers over surfaces smoothed by sanding. *Journal of Fluids Engineering,* 125**,** 863-870.

Schultz, M. P. & Flack, K. A. 2005. Outer layer similarity in fully rough turbulent boundary layers. *Experiments in Fluids,* 38**,** 328-340.

Schultz, M. P. & Myers, A. 2003. Comparison of three roughness function determination methods. *Experiments in Fluids,* 35**,** 372-379.

Schultz, M. P. & Swain, G. 1999. The effect of biofilms on turbulent boundary layers. *Journal of Fluids Engineering,* 121**,** 44-51.

Schultz, M. P. & Swain, G. W. 2000. The influence of biofilms on skin friction drag. *Biofouling,* 15**,** 129-139.

SEAFRONT. 2014. *SEAFRONT: Synergistic fouling control technologies* [Online]. http://cordis.europa.eu/project/rcn/111293_en.html.

Shapiro, T. A. 2004. The effect of surface roughness on hydrodynamic drag and turbulence. USNA Trident Scholar project report; no. 327.

Shockling, M. A., Allen, J. J. & Smits, A. J. 2006. Roughness effects in turbulent pipe flow. *Journal of Fluid Mechanics,* 564**,** 267-285.

Suga, K., Craft, T. J. & Iacovides, H. 2006. An analytical wall-function for turbulent flows and heat transfer over rough walls. *International Journal of Heat and Fluid Flow,* 27**,** 852-866.

Swain, G. W., Kovach, B., Touzot, A., Casse, F. & Kavanagh, C. J. 2007. Measuring the Performance of Today's Antifouling Coatings. *Journal of Ship Production,* 23**,** 164-170.

Tachie, M., Bergstrom, D. & Balachandar, R. 2000. Rough wall turbulent boundary layers in shallow open channel flow. *Journal of Fluids Engineering,* 122**,** 533-541.

Tanaka, H., Toda, Y., Higo, K. & Yamashita, K. 2003. Influence of Surface Properties of Coatings to Frictional Resistance. *Journal of the Kansai Society of Naval Architects* 239.

Taylan, M. An overview: effect of roughness and coatings on ship resistance. International Conference on Ship Drag Reduction SMOOTH-SHIPS, 2010 Istanbul, Turkey.

Tezdogan, T. & Demirel, Y. K. 2014. An overview of marine corrosion protection with a focus on cathodic protection and coatings. *Brodogradnja*, 65**,** 49-59.

Tezdogan, T., Demirel, Y. K., Kellett, P., Khorasanchi, M., Incecik, A. & Turan, O. 2015. Full-scale unsteady RANS CFD simulations of ship behaviour and performance in head seas due to slow steaming. *Ocean Engineering*, 97**,** 186-206.

Todd, F. 1951. *Skin friction resistance and the effects of surface roughness*, Transactions SNAME.

Townsend, A. A. 1976. *The structure of turbulent shear flow, 2nd edition,* Cambridge, UK, Cambridge University Press.

Townsin, R., Byrne, D., Svensen, T. & Milne, A. 1981. Estimating the technical and economic penalties of hull and propeller roughness. *Trans. SNAME,* 89**,** 295-318.

Townsin, R. & Dey, S. The correlation of roughness drag with surface characteristics. Proceedings of the RINA International Workshop on Marine Roughness and Drag, 1990.

Townsin, R. L. 2003. The Ship Hull Fouling Penalty. *Biofouling*, 19**,** 9-15.

TQC. 2014. *Hull Roughness Gauge* [Online]. http://www.tqc.eu/en/products/article/hull-roughness-gauge. [Accessed 09.06.2014.

Ünal, B. 2012. *Effect of surface roughness on the turbulent boundary layer due to marine coatings.* PhD Thesis, Istanbul Technical University.

Ünal, U., Ünal, B. & Atlar, M. 2012. Turbulent boundary layer measurements over flat surfaces coated by nanostructured marine antifoulings. *Experiments in Fluids*, 52**,** 1431-1448.

UNFCCC. *Kyoto Protocol* [Online]. http://unfccc.int/kyoto_protocol/items/2830.php. [Accessed 04 / 05 / 2015].

Usta, O. & Korkut, E. A study for the effect of surface roughness on resistance characteristics of flat plates. RINA, Royal Institution of Naval Architects - International Conference on Marine Coatings, 2013.

van Manen, J. D. & van Oossanen, P. 1988. Resistance. *In:* LEWIS, E. V. (ed.) *Principles of Naval Architecture. Second Revision.* Volume II: Resistance, Propulsion and Vibration. The Society of Naval Architects and Marine Engineers, Jersey City, NJ.

Van Rompay, B. 2012. *Surface Treated Composites White Book*, Tahoka Press.

Wahl, M. 1989. Marine epibiosis. I. Fouling and antifouling: some basic aspects. *Marine Ecology Progress Series,* 58**,** 175-189.

Watanabe, S., Nagamatsu, N., Yokoo, K. & Kawakami, Y. 1969. The augmentation in frictional resistance due to slime. *J. Kansai Soc. Nav. Arc.,* 131**,** 45-51.

Weinell, C. E., Olsen, K. N., Christoffersen, M. W. & Kiil, S. 2003. Experimental Study of Drag Resistance Using a Laboratory Scale Rotary Set-up. *Biofouling,* 19**,** 45-51.

Woods Hole Oceanographic Institution 1952. *Marine Fouling and Its Prevention,* Annapolis, Maryland, United States Naval Institute.

Yaglom, A. M. 1979. Similarity laws for constant-pressure and pressure-gradient turbulent wall flows. *Annual Review of Fluid Mechanics,* 11**,** 505-540.

Yokoi, K. 2004. On the influence of ship's bottom fouling upon speed performance. *Bulletin of Toyama National College of Maritime Technology*.

Yokoo, K., Tarao, T., Sasajima, H., Ogewa, A. & Nakato, M. Roughness of hull surface and its effect on hull friction. Ship Res. Inst., 1966 Tokyo. Paper 17.

Zagarola, M. V. & Smits, A. J. 1998. Mean-flow scaling of turbulent pipe flow. *Journal of Fluid Mechanics,* 373**,** 33-79.

Zhang, Z.-r. 2010. Verification and validation for RANS simulation of KCS container ship without/with propeller. *Journal of Hydrodynamics, Ser. B,* 22**,** 932-939.

Research Outputs

The following publications were generated throughout the timespan of the PhD studies related to this thesis.

Journal papers (SCI / SCI Expanded):

1. **Demirel, Y. K.**, Khorasanchi, M., Turan, O., Incecik, A., Schultz, M. P., 2014. A CFD model for the frictional resistance prediction of antifouling coatings. *Ocean Engineering*, 89, 21-31. http://dx.doi.org/10.1016/j.oceaneng.2014.07.017
2. Tezdogan, T., **Demirel, Y.K.**, 2014. An overview of marine corrosion protection with a focus on cathodic protection and coatings. *Brodogradnja/Shipbuilding*, 65 (2), 49-59. http://hrcak.srce.hr/123461?lang=en
3. Tezdogan, T., **Demirel, Y.K.**, Kellett P., Khorasanchi, M, Incecik, A., Turan, O., 2015. Full-scale unsteady RANS CFD simulations of ship behaviour and performance in head seas due to slow steaming. *Ocean Engineering*, 97, 186-206. http://dx.doi.org/10.1016/j.oceaneng.2015.01.011

Conference papers:

1. **Demirel, Y.K.**, Khorasanchi, M., Turan, O., Incecik, A., 2013. A parametric study: Hull roughness effect on ship frictional resistance. In: Proceedings of the International Conference on Marine Coatings, RINA, 18 April 2013. London, UK, pp.21–28.
2. **Demirel, Y.K.**, Khorasanchi, M., Turan, O., Incecik, A., 2013. On the importance of antifouling coatings regarding ship resistance and powering. In: Proceedings of the 3rd International Conference on Technologies, Operations, Logistics and Modelling for Low Carbon Shipping, 9 - 10 September 2013. London, UK.
3. Tezdogan, T., **Demirel, Y.K.**, Mortola, G., Incecik, A., Turan, O., Khalid, H., 2013. Chapter 31. Operability analysis of a high speed car/passenger ferry. In: Soares, C.G., Pena, F.L. (Eds.) Developments in Maritime Transportation and Exploitation of Sea Resources. pp. 273-281. http://dx.doi.org/10.1201/b15813-36.

4. **Demirel, Y.K.**, Khorasanchi, M., Turan, O., Incecik, A., 2014. CFD approach to resistance prediction as a function of roughness. In: Proceedings of Transport Research Arena Conference 2014, 14 - 17 April 2014. Paris La Défense, France.
5. Tezdogan, T., **Demirel, Y.K.**, Incecik, A., Turan, O., 2014. Hydrodynamics of heaving twin cylinders in a free surface using an unsteady-RANS method. In: Proceedings of International Conference on Maritime Technology. 7 - 9 July, 2014. Glasgow, UK.
6. Mizzi, K., **Demirel, Y.K.**, Banks, C., Turan, O., Kaklis, P., 2014. PBCF design optimisation and propulsion efficiency impact. In: Proceedings of the International Conference on Influence of EEDI on Ship Design, RINA, 24 – 25 September 2014. London, UK.
7. Mizzi, K., Kellett P., **Demirel, Y.K.**, Martin, R., Turan, O., 2015. HPC and CFD in the marine industry: past, present and future. In: Proceedings of Exascale Applications and Software Conference (EASC 2015), 21 – 23 April 2015. Edinburgh, UK.

Project Reports:

1. **Demirel, Y.K.**, Khorasanchi, M., Turan, O., 2013. Report on resistance prediction in function of roughness using CFD approach. EU FP7 FOUL-X-SPEL Project Report, Deliverable 5.2.
2. **Demirel, Y.K.**, Turan, O., 2014. Report on basin hydrodynamic tests. EU FP7 FOUL-X-SPEL Project Report, Deliverable 7.3.
3. **Demirel, Y.K.**, Jayanta, M., Turan, O., 2014. Effect of hull roughness on ship performance and new hull roughness prediction method. EU FP7 FOUL-X-SPEL Project Report, Deliverable 8.1.
4. **Demirel, Y.K.**, Jayanta, M., Turan, O., 2014. New model for energy and environmental efficiency. EU FP7 FOUL-X-SPEL Project Report, Deliverable 8.2.
5. **Demirel, Y.K.**, Jayanta, M., Turan, O., 2014. Life cycle assessment and cost benefit analysis and environmental impact assessment of new paints. EU FP7 FOUL-X-SPEL Project Report, Deliverable 8.3.

6. **Demirel, Y.K.**, Jayanta, M., Turan, O., 2014. Techno-economic feasibility study. EU FP7 FOUL-X-SPEL Project Report, Deliverable 11.1.
7. **Demirel, Y.K.**, Turan, O., 2014. Guidelines for surface treatment, coating application and inspection, surveying. EU FP7 FOUL-X-SPEL Project Report, Deliverable 11.2.

Abstracts / Conference Presentations:

1. **Demirel, Y.K.**, 2013. A CFD approach on the effects of fouling and antifouling coatings on resistance. In: Proceedings of 4th UK MTPC 2013, 11 – 12 June, 2013, pp. 11-12, London, UK.
2. **Demirel, Y.K.**, Khorasanchi, M., Turan, O. and Incecik, A., 2013. New horizons in marine antifouling coatings. (Presentation only). International Conference on Marine Coatings, 18 April 2013. London, UK.
3. **Demirel, Y.K.**, Khorasanchi, M., Turan, O., Incecik, A., 2014. Prediction of the effect of hull fouling on ship resistance using CFD. 17th International Congress on Marine Corrosion and Fouling (ICMCF), 6 - 10 July 2014. Singapore.

Posters:

1. **Demirel, Y.K**., Turan, O. and Incecik, A., 2014. Prediction of the effects of hull fouling and antifoulings on ship resistance. 11th Annual Green Ship Technology Conference 2014, 18-20 March 2014, Oslo, Norway.